Transmembrane Cell Signaling by Targeted Ultrasound Contrast Agents in Cancer Therapy

A Thesis

Submitted to the Faculty

of

Drexel University

by

Lauren Jablonowski

in partial fulfillment of the

requirements for the degree

of

Doctor of Philosophy in Biomedical Engineering

May 2016

Dedications

To Steve,

with love and thanks

To Mom, Dad, and Kevin,

for everything

Acknowledgements

First and foremost, I would like to thank my advisor Dr. Margaret Wheatley for her guidance, enthusiasm, and genuine care and support. This thesis would not have been possible without her help and support over the past 5 years.

I would also like to thank all of my committee members: Dr. Flemming Forsberg, Dr. John Eisenbrey, Dr. Adrian Shieh, and Dr. Fred Allen for their collaboration, guidance, and feedback.

Thanks to all of my previous and current labmates, especially Nutte Tarn Teraphongphom, Averie Palovcak, James Andorko, Brian Oeffinger, Rawan Shraim, David Brown, Nicholas Daroshefski, Mi Thant Mon Soe, Reva Street, Tim Hoang, Rebecca Sheridan, Stephen Zachariah, Jaap Patel, Matthew Chin, and Skye Miller. Special thanks to Michael Cochran and Nicola Francis for their support and advice.

I would also like to share my sincerest gratitude to the BIOMED staff, especially Natalia Broz, Lisa Williams, Danielle Crocker, Laurie Lenz, and Caryn Glaser, who have always been there when I have needed anything, and have been a constant source of friendship and support. Special thanks to Dolores Conover for help with the cell studies and support, I am very grateful.

Finally, I would like to thank all of my family and friends for their love, support, and encouragement throughout my journey. Thank you especially to my parents, John and Diane, and my brother Kevin, for your constant support and love throughout my life. To Steven Delaney, thank you for your love, encouragement, and understanding. Special thanks to Jaimie Dougherty, David Alfego, Nicholas Pashos, and Jonathan Neafsey for your friendship, love, support, and all-around awesomeness.

Table of Contents

List of Tables

List of Figures

List of Abbreviations

DI water: Deionized water

DMSO: Dimethyl sulfoxide

Dox: Doxorubicin

EPR Effect: Enhanced permeation and retention effect

FDA: Food and drug administration (USA)

IPA: Isopropyl alcohol

MI: Mechanical index

MW: Molecular weight

n-Sh: Nanoshard

PEG: Polyethylene glycol

PBS: Phosphate buffered saline

PDI: Polydispersity index

PLA: Poly (lactic acid)

PRF: Pulse repetition frequency

PVA: Poly (vinyl alcohol)

SEAM: Standard error about the mean

SEM: Scanning electron microscopy

TRAIL: Tumor necrosis factor-related apoptosis inducing ligand

US: Ultrasound

UCA: Ultrasound contrast agent

w/(o/w): Water-oil-in water double emulsion

List of Variables Used

z: Acoustic impedance (N s/m^3)

ρ: Density (kg/m^3)

c: Speed of sound in a medium (m/s)

R: Reflection coefficient (no units)

P: Pressure (N/m^2)

γ: Bubble surface tension (N/m)

r: Bubble radius (μm)

t: time (s)

D: Diffusion coefficient of the gas in liquid (m^2/s)

R_{shell}: Resistance of the shell to gas permeation (s/m)

σ: Scattering cross section (m^2)

I: Intensity (N s^{-1} m^{-1})

d: Distance from the transducer to the ultrasound contrast agent (m)

K: Wavenumber (1/m)

k: Compressibility (m^2/N)

S_T: Shell thickness (m)

E: Young's Modulus (N/m^2)

ν: Poisson's ratio (no units)

F_r: Acoustic radiation force (N)

Pa: peak applied acoustic pressure (N/m^2)

δ: Damping coefficient (no units)

$ω_0$: Resonant frequency of the ultrasound contrast agent (1/s)

Abstract

Transmembrane Cell Signaling by Targeted Ultrasound Contrast Agents in Cancer Therapy

Lauren Jablonowski

Margaret A. Wheatley, PhD

In 2016, over 1.68 million people in the United States are expected to be diagnosed with cancer, with approximately 35% of these cases resulting in death making cancer the second most common cause of death in the US [1]. Specifically, the American Cancer Society predicts that approximately 250,000 new breast cancer cases will be diagnosed in 2016, with approximately 16% of these cases resulting in death [1]. While significant progress has been made in the field of cancer treatment, many therapy regimes still rely heavily on the systemic administration of toxic chemotherapeutic agents. Most clinically used chemotherapeutic drugs are non-specific and as a result are highly toxic to both cancerous and non-cancerous tissues, leading to dangerous side effects and overall low treatment efficacy.

Ultrasound contrast agents (UCA) have emerged as a drug delivery vehicle to overcome these challenges, consisting of a small (<6μm) gas bubble stabilized within a lipid, protein, or polymer microcapsule shell that can be injected intravenously and pass freely through the capillaries. Upon entering the focused ultrasound beam, the UCA gas core rapidly expands and contracts, a phenomenon known as cavitation, and ultimately ruptures producing drug-loaded particles (up to 400nm) that can exit the vasculature, embed in the target tissue, and provide localized drug release. Our lab has previously developed hollow polymeric microspheres that encapsulated doxorubicin (Dox) within the polylactic acid (PLA) shell [2, 3]. These Dox-loaded UCA have been shown to

exhibit high echogenicity, and also shatter into nanoshards (n-Sh) of less than 400nm, when exposed to ultrasound [4]. When evaluated in an *in vivo* rat hepatocellular carcinoma model, we found these n-Sh were able to effectively exit the vasculature and deliver Dox to tumor tissue [5]. However, elevated Dox levels were also observed in the healthy liver and spleen tissues, suggesting immune recognition and uptake of circulating agents and n-Sh.

Here we describe the development of non-immunogenic, functionalized PLA UCA for use in targeted breast cancer therapy. We believe that the use of a targeting ligand in conjunction with polyethylene glycol (PEG) will help to shield the UCA from immune recognition and improve the treatment efficacy at the target site. For ultrasound (US) imaging with polymeric contrast agents, it is necessary to modify the shell to create "stealth" microbubbles but without these modifications sacrificing the agent's ability to interact with the focused US beam. We hypothesize that addition of the classic immune shielding molecule PEG to a polylactide (PLA) microbubble shell will affect the acoustic and physical properties of the resulting agents.

In an effort to determine the best formulation to achieve a balance between stealth and acoustic activity, we compared two PEGylation techniques; addition of increasing amounts of PEG-PLA copolymer and employing incorporation of a PEG lipid (LipidPEG) into the shell. Loss of acoustic enhancement occurred in a dose-dependent manner for both types of PEGylated agents (loss of signal occurred at >5 wt% PEG-PLA and >1 wt% LipidPEG), while immune activation was also reduced in a dose-dependent manner for the PEG-PLA agents. This study shows that the balance between acoustic behavior and improved immune avoidance was scalable and successful to different

degrees with both PEGylation methods, and was best achieved using for PEG-PLA at 5 wt% and for LipidPEG at 1 wt%.

The added advantage to the use of the targeting ligand, specifically tumor necrosis factor-related apoptosis inducing ligand (TRAIL), is that it also induces tumor cell death upon binding to the cell surface receptors DR4 and DR5 and initiating a transmembrane apoptosis signal. Healthy cells possess decoy receptors (DcR1 and DcR2) that cannot process the apoptotic signal, therefore being protected from non-specific binding. Additionally, the UCA were designed to co-encapsulate the chemotherapeutic drug doxorubicin (Dox) that can be released from the polymer shell in response to US focused at the tumor site, shielding healthy tissues from the toxic substance while also increasing the potency and efficiency of treatment to the tumor tissue. The ability of the ligand to cause cell death was tested against ligand-sensitive MDA-MB-231 human breast adenocarcinoma cells and ligand-resistant MCF7 human breast adenocarcinoma cells, comparing the efficacy of the microbubble formulations. It is believed that co-administration of Dox to cancer cells that are normally resistant to TRAIL increases the expression of death receptors on the cell surface, sensitizing the cell to TRAIL and improving its efficacy. For the MDA-MB-231 cells, cell viability was reduced by approximately 25-50% (52.84±11.65% to 76.34±3.25% live cells) upon incubation with the TRAIL-ligated US-generated nanoshards, and was further reduced to approximately 40-80% (20.32±6.91% to 64.19±2.68% live cells) with the addition of doxorubicin compared to TRAIL alone. TRAIL-resistant MCF7 cells showed little apoptotic response to TRAIL-ligated nanoshards (93.44±2.88% to 98.18±1.04% live cells); however, co-administration of doxorubicin increased apoptosis and reduced cell viability

(37.37±5.39% to 67.78±3.98% live cells), supporting the sensitization effect of the drug. Healthy MCF-12A human breast epithelial cells were also tested, to confirm the selective targeting and apoptotic activity of TRAIL to cancer cells and not healthy cells. These cells exhibited from 90.64±2.54% to 97.46±0.62% cell viability when incubated with TRAIL-ligated nanoshards, confirming their insensitivity to TRAIL-induced death. However, cell viability was greatly decreased (44.73±15.26% to 68.79±6.89% live cells) when also exposed to doxorubicin, demonstrating the toxic effects of the chemotherapeutic agent on surrounding healthy cells during systemic treatment.

Overall, this work has resulted in the production of effective ultrasound-triggered, non-immunogenic, targeted drug delivery agents for potential use in cancer therapy. This platform has many advantages over the systemic administration of chemotherapeutic drugs, and represents a promising treatment to better serve the population with breast cancer, and solid cancerous tumors as a whole.

1. INTRODUCTION

1.1 Problem Statement

In 2016, over 1.68 million people in the United States are expected to be diagnosed with cancer, with approximately 35% of these cases resulting in death making cancer the second most common cause of death in the US [1]. Specifically, the American Cancer Society predicts that approximately 250,000 new breast cancer cases will be diagnosed in 2016, with approximately 16% of these cases resulting in death [1]. While significant progress has been made in the field of cancer treatment, many therapy regimes still rely heavily on the systemic administration of toxic chemotherapeutic agents. Most clinically used chemotherapeutic drugs are non-specific and as a result are highly toxic to both cancerous and non-cancerous tissues, leading to dangerous side effects and overall low treatment efficacy. Additionally, there are many challenges associated with treatment of solid cancerous tumors that further reduce the efficacy of systemic chemotherapy including high interstitial pressures, high cell density, unusual tumor tissue and extracellular matrix composition, an absence of supporting lymphatic drainage structures, and reliance on passive targeting through the Enhanced Permeability and Retention (EPR) effect [6-9]. However, reliance on EPR is limited by slow accumulation (up to 6 hours), inconsistent degrees of tumor vessel permeability, and is precluded entirely in some tumors [10, 11].

Ultrasound contrast agents (UCA) have emerged as a drug delivery vehicle to overcome these challenges, consisting of a small (<6μm) gas bubble stabilized within a lipid, protein, or polymer microcapsule shell that can be injected intravenously and pass

freely through the capillaries. Much research has been focused on the development of drug-loaded UCA, which can interact with an ultrasound beam focused at a point of interest to trigger localized drug delivery. Upon entering the focused ultrasound beam, the UCA gas core rapidly expands and contracts, a phenomenon known as cavitation, and ultimately ruptures producing drug-loaded particles (up to 400nm) that can exit the vasculature, embed in the target tissue, and provide localized drug release. Our lab has previously developed hollow polymeric microspheres that encapsulated doxorubicin (Dox) within the polylactic acid (PLA) shell [2, 3]. These Dox-loaded UCA have been shown to exhibit high echogenicity, and also shatter into nanoshards (n-Sh) of less than 400nm, when exposed to ultrasound [4]. When evaluated in an *in vivo* rat hepatocellular carcinoma model, we found these n-Sh were able to effectively exit the vasculature and deliver Dox to tumor tissue [5]. However, elevated Dox levels were also observed in the healthy liver and spleen tissues, suggesting immune recognition and uptake of circulating agents and n-Sh.

Here we describe the development of non-immunogenic, functionalized PLA UCA for use in targeted breast cancer therapy. We believe that the use of a targeting ligand in conjunction with polyethylene glycol (PEG) will help to shield the UCA from immune recognition and improve the treatment efficacy at the target site. The added advantage to the use of the targeting ligand, specifically tumor necrosis factor-related apoptosis inducing ligand (TRAIL), is that it also induces tumor cell death upon binding to the cell surface receptor and initiating a transmembrane apoptosis signal. Healthy cells possess decoy receptors that cannot process the apoptotic signal, therefore being protected from non-specific binding. As such, this platform has many advantages over the

systemic administration of chemotherapeutic drugs, and represents a promising treatment to better serve the population with breast cancer.

1.2 Thesis Objectives

The overall goal of this research is the development of a multi-functional PEGylated UCA that is loaded with TRAIL for targeting cancer cells and inducing apoptosis as well as Dox chemotherapeutic to allow for local, sustained treatment within the tumor interstitial. A strategy comprised of the following three specific aims was used to reach these goals.

Specific Aim 1: Develop and characterize polymeric UCA functionalized with TRAIL, without compromising the ability to produce n-Sh upon interaction with diagnostic ultrasound. This study served as a "proof of concept" to establish the feasibility of decorating the UCA surface with TRAIL molecules to produce functional agents that exhibit apoptotic activity against susceptible cells while retaining the ability to interact with diagnostic ultrasound. This was achieved by pursuing maleimide TRAIL-ligation to the UCA surface and evaluating the resulting agent for its acoustic and apoptotic behavior against MDA-MB-231 breast cancer cells. Our hypothesis is that TRAIL ligation does not inhibit UCA inertial cavitation and shattering into n-Sh when the agents are exposed to a focused ultrasound beam. We also hypothesize that the TRAIL molecule will remain attached to the polymeric surface upon cavitation and shattering into n-Sh, and that it will retain its apoptotic activity toward susceptible cells after ligation.

Specific Aim 2: Develop and characterize non-immunogenic PEGylated polymeric UCA, without compromising the acoustic properties and cavitation ability of the UCA. We have previously found that native PLA UCA collected in the healthy liver and spleen in an *in vivo* rat hepatocellular carcinoma model, suggesting that these agents were being sequestered from circulation by the immune system without reaching the intended target [5]. Therefore, our objective is to modify the native UCA to include PEG along the polymeric shell surface, in an effort to circumvent opsonization and immune response to the circulating agent. Two methods of PEGylation are investigated in this thesis; one method evaluating the use of a co-polymer as the shell material, and the other method evaluating the use of lipid-anchored PEG molecules extending from the UCA surface. We hypothesize that PEGylation will not significantly affect the UCA shell properties, thus allowing for acoustically-triggered n-Sh production in an *in vitro* ultrasound environment. We also hypothesize that PEGylation will reduce the agent immunogenicity, as measured against C3 complement protein activation. At the conclusion of this aim, we determined that 5 wt% PEG-PLA co-polymer and 1 wt% LipidPEG represented the most viable PEGylated agents for continued investigation into targeting, drug loading, and drug delivery capabilities.

Specific Aim 3: Functionalize PEGylated UCA for targeted cancer therapy with TRAIL ligation to the UCA surface and encapsulate Dox within the UCA shell to increase target sensitivity against breast cancer models. The work in this aim focused on the attachment of TRAIL to the UCA surface to target and induce apoptosis in susceptible cancer cells, as well as the co-encapsulation of Dox within the polymeric

shell to further sensitize TRAIL-resistant cells and synergistically act with TRAIL to induce tumor cell death. It is hypothesized that the TRAIL molecule retains its apoptotic activity when attached to the UCA surface and PEG molecules, and that this attachment is not detrimental to the acoustic behavior of the functionalized agents. We also hypothesize that the co-encapsulation of Dox will provide a sustained, local release of the chemotherapeutic to improve the treatment efficacy and further sensitize cells to the apoptotic action of TRAIL. These functionalized agents were evaluated against TRAIL-sensitive MDA-MB-231 breast adenocarcinoma cells, TRAIL-resistant MCF-7 breast adenocarcinoma cells, and TRAIL-negative MCF-12A healthy breast epithelial cells. Additionally, the agents were evaluated for Dox release during cavitation into n-Sh to determine any burst release effects as well as from the resulting n-Sh to determine the long-term release profile.

2. BACKGROUND AND LITERATURE REVIEW

2.1 Cancer and Cancer Therapies

Cancer is a broad term that is used to describe a group of diseases characterized by uncontrolled cell division that can invade other tissues. Cancer results from a change in cell differentiation, accumulating mutations in the genes involved in regulating cell division. Genetic mutations can occur from DNA damage due to radiation, microbes and viruses, toxins, inherited mutations, certain lifestyle concerns (obesity, poor diet, lack of exercise), immune conditions, or chronic inflammation. Left unchecked, cancerous cells can multiply, spread through the blood and lymphatic systems causing metastases, and eventually lead to death if not controlled. Cancer is the second leading cause of death in the United States, exceeded only by heart disease. According to the American Cancer Society, almost 1.7 million people in the United States are expected to be diagnosed with new cancer cases in 2016, with over 590,000 deaths expected from cancer [1].

2.1.1 Breast Cancer

While the platforms designed and discussed in this thesis are expected to be useful in the treatment of a variety of cancers, a breast cancer model is used for proof of principle. In 2016, breast cancer is projected to be the most common type of cancer diagnosed in women in the United States, with over 246,000 new cases expected to be diagnosed [1]. For women diagnosed with localized breast cancer that has not spread to lymph nodes or other tissues outside the breast, the five-year survival rate can be as high as 99%; however, 5-year survival rates drop to 85% when cancer spreads to regional, or nearby, lymph nodes, and further drops to 26% if cancer spreads to distant lymph nodes or tissues. The overall survival rates 5, 10, and 15 years following diagnosis are 89%,

83%, and 78% respectively. Despite relatively high survival rates, breast cancer is still projected to be the second leading cause of cancer deaths in women in the United States after lung cancer, with over 40,000 deaths expected in 2016 [1]. Common chemotherapeutic drugs for the treatment of breast cancer include anthracyclines such as doxorubicin (Dox) [12, 13], making these drugs excellent candidates for encapsulation into microbubbles for ultrasound-triggered drug delivery.

2.1.2 Solid Tumor Biology, Architecture, and Treatment

Solid tumors develop in a large percentage of cancers (approximately 85% of all cases), with close to 50% of these cases leading to metastases and death [14]. Tumorigenesis, the transformation of normal cells into cancer cells, is initiated by a combination of mutational activation of oncogenes together with mutational inactivation of tumor suppressor genes within a cell, leading to aberrant cell division [15]. Mutated cells continue to divide as a small avascular nodule (1-2mm) until reaching a steady state of balance between apoptosis and cell division [16]. Similar to healthy cells, cancerous cells require oxygen and nutrient supply to support metabolism making it necessary for tumor cells to access the vascular system through formation of a new blood supply through angiogenesis [17]. Angiogenesis in healthy tissues is a highly regulated process, but disproportionate production of angiogenic growth factors such as vascular endothelial growth factor as well as inhibitors such as thrombospondin-1 in the tumor environment lead to abnormal vascular development that varies from tumor to tumor [17-19]. Tumor angiogenic vessels can be comprised of cancer cells and abnormal endothelial cells, contributing to their irregularity [20]. These vessels are also chaotic in nature, ranging in diameter from 10-200μm and lacking traditional features such as basement membrane,

functional pericytes for constriction, arterioles, capillaries, and venules [17, 20, 21]. These physiological differences together with rapid development result in highly permeable “leaky” vessels, with endothelial gaps ranging from 100-1000nm and averaging approximately 700nm [22]. Studies have shown that tumors possess a characteristic pore cutoff size ranging from 380-780nm, with the size of these pores increasing with stage and malignancy [6, 23-25].

Increased vascular permeability causes an increase in the osmotic pressure of the tumor interstitium, due to outflow of proteins and other molecules from the vascular pores [26]. In normal tissues, this pressure would be dissipated by a system of lymphatic vessels collecting the outflow and transporting it back into the vascular system; however, many tumors lack lymphatic vessels causing accumulation within the tumor interstitium [9, 11, 26, 27]. While these high pressures (up to 18mmHg) reduce the transport of large molecules and drugs from the blood to the tumor, the lack of lymphatic drainage can allow small particles to accumulate in the interstitia in a phenomenon known as the Enhanced Permeability and Retention (EPR) effect [9, 26, 28]. Several studies have focused on exploiting the EPR effect for chemotherapeutic delivery, aiming to encapsulate drug within delivery vessels small enough to pass freely through the leaky tumor vasculature allowing for accumulation and delivery to the tumor tissue [6, 8, 10, 29]. However, reliance on the EPR effect is limited by slow accumulation (up to 6 hours) and inconsistent degrees of tumor vessel permeability, and is precluded entirely in some tumors that do not exhibit an EPR effect [8-11].

There are a number of factors that inhibit direct drug delivery to solid tumors, including irregular vasculature, uneven blood flow, and high interstitial pressures [11, 23,

30]. As such, primary options for cancer treatment include chemotherapy, radiation and ablation treatment, and surgical removal.

Chemotherapy is one of the most common methods of cancer treatment, applicable to a variety of cancer types. Chemotherapy treatment involves systemic injection and circulation of drugs, often toxic, that attack rapidly dividing cells such as cancer cells. However, most chemotherapy drugs are non-selective, and patients receiving treatment often experience strong negative side effects, such as lowered resistance to infection, anemia, increased bleeding, dehydration, alopecia/hair loss, nausea, fatigue, and pain. Another concern with traditional chemotherapy is systemic toxicity, causing complications such as collateral damage to heart, liver, and kidney tissues. Treatment efficacy is often limited due to the low doses administered to control these dangerous side effects, further reducing the potency and efficiency at the tumor site. Doxorubicin, the drug evaluated in this thesis, is a commonly used chemotherapy drug that will be discussed in more detail later in this chapter.

Development of localized treatments, such as 3D confocal radiation therapy, have greatly improved cancer treatment with radiation. Recent developments have not yet been able to mitigate the side effects of these treatments, which include hair loss, damage to healthy tissue, nausea, and vomiting. Additionally, deep tumors are difficult to treat with radiation, as attenuation through tissue and positioning behind other organs or tissues limit the ability to reach the region of interest. In some cancers, radiation has been shown to only relieve symptoms with no improvement to survival rates [31]. Tumor ablation is also very limited in applications, only being considered viable for very small tumors ($\leq$ 1cc) that are accessible by the probe, and is limited by high recurrence rates [32, 33].

One of the more invasive cancer treatments is surgical tumor removal, and is limited by ability to reach the tumor without significant damage to surrounding tissues and organs. Recurrence rates can be high for surgical resection, especially if cancer cells have metastasized and spread to other areas of the body. Many times, surgical removal is followed by radiation and/or chemotherapy to help reduce the chance of recurrence and improve survival rates.

2.1.3 Current Treatment for Breast Cancer

Breast cancer treatment often depends on the stage of the disease and tumor characteristics. Among the treatment options discussed in the preceding section, breast cancer treatment usually involves surgical intervention by way of removing the tumor and its surrounding tissue (lumpectomy) or removal of the entire breast (mastectomy). Surgical removal is often combined with radiation therapy, hormone therapy, or chemotherapy. Recurrence is decreased when lumpectomy is combined with radiation therapy, and 20-year survival rates are similar to those of patients who underwent mastectomy without additional radiation [34]. These findings represent a great advantage for breast cancer patients, allowing them to undergo a less invasive surgery and to retain their breast tissue and improve their self-image and emotional state during and following treatment.

When radiation therapy is utilized, ionizing radiation is focused at the tumor site with an external beam of X-rays or gamma rays. The radiation creates free radicals that damage the cancer cell DNA in the hopes of inhibiting proliferation, leading to cell death through apoptosis or necrosis [35]. Even though state-of-the-art technology is used to create 3D maps of the tumor area for highly-controlled dose, radiation therapy still causes

DNA damage to healthy cells in the area surrounding the region of interest, especially the skin cells that the beam must pass through to reach the tumor.

Chemotherapy is often co-administered with surgical removal, both before and after surgery to help kill any metastatic cells that have spread beyond the region of interest. Common drugs used to treat breast cancer include Dox, docetaxel, paclitaxel, and 5 fluorouracil (5FU), and these drugs are often administered in combination to help improve survival rates up to 38% for patients receiving combination therapy [12, 13].

2.1.4 Doxorubicin and TRAIL

While the platforms developed and discussed in this thesis are not drug specific, the main focus is on delivery of Dox as it is widely used as a cancer chemotherapeutic. As a member of the anthracycline class of drugs, Dox (brand names Adriamycin®, Rubex®, Doxil®) is a hydrophilic compound with a molecular weight of 543 Daltons and consists of an aglycone ring covalently bound to an amino sugar, as shown in Figure 2.1 [36].

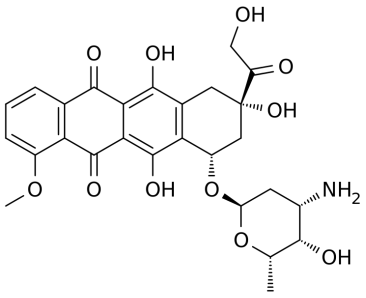

Figure 2.1: Chemical structure of doxorubicin.

Dox is effective against cancer cells via two main mechanisms of action: intercalation of the aglycone ring between DNA base pairs and inhibition of topoisomerase II. As a result of intercalation, Dox blocks DNA synthesis and transcription, limiting cell replication. In normal cell division, topoisomerase II assists DNA transcription by creating transient breaks in the DNA strands that allow the double helix to untwist and then resealing the untwisted DNA strands without any sequence changes. When Dox inhibits this enzyme by forming a complex between the amino sugar, DNA, and topoisomerase II, DNA cannot be resealed thus stopping any replication [37, 38].

As stated previously, Dox has been used to treat various cancer types, including liver, breast, ovarian, esophageal, endometrial, and lung tumors [39, 40]. However, systemic administration of Dox results in side effects including hair loss, nausea, leukopenia, myelosuppression, and neutropenia, most of which are temporary during the duration of treatment. One of the more serious risks associated with Dox treatment is cardiotoxicity, as the generation of free radicals from administration can cause dilative cardiomyopathy and congestive heart failure (CHF) [37, 40]. Congestive heart failure risk is dependent on cumulative Dox dose, with 4% of patients developing CHF when cumulative dose reaches 500mg/m^2 and 36% of patients developing CHF when cumulative dose exceeds 600mg/m^2 [40].

Another treatment associated with cancer therapy is receptor-specific ligands to induce anti-cancer action, and this thesis specifically investigates tumor necrosis factor-related apoptosis inducing ligand (TRAIL). TRAIL can act as both a targeting and therapeutic entity, selectively binding to specific cell surface receptors on cancer cells

that signal apoptosis upon this binding, but do not induce apoptosis in healthy cells. TRAIL induces apoptosis in tumor cells by binding to death receptors TRAIL-R1 (DR4) and TRAIL-R2 (DR5). Activation of DR4 and DR5 causes induction of an apoptotic signal from the membrane through the cytoplasm to the nucleus, resulting in cell death [41-44]. An advantage of TRAIL over other similar ligands, such as tumor necrosis factor (TNF) and Fas ligand (FasL), is that TRAIL is non-toxic to healthy cells, which do not express DR4 and DR5 receptors but instead express DcR1 and DcR2 decoy receptors that lack the transmembrane signaling component [42, 44, 45]. All four receptors have been shown to exhibit high affinity for TRAIL binding in several cancer types [46]. For example, evaluation of tumor tissue from colon cancer patients revealed that 92% of tumors expressed DR4 and 87% expressed DR5 [47]. In clinical trials, however, TRAIL has performed below expectations, with two mechanisms suggested to be the cause. First, bioavailability may be diminished due to non-productive binding to decoy receptors, limiting productive binding to DR4 and DR5 [48]. Secondly, some cancer cells are resistant to TRAIL-induced apoptosis, limiting efficacy. Several studies have investigated methods of overcoming this resistance, identifying compounds such as proteasome inhibitors and other drugs, including Dox, that can potentiate the apoptotic activity of TRAIL [49-54].

TRAIL acts by inducing apoptosis in cancer cells, which is a process of programmed cell death characterized by chromatin condensation, DNA fragmentation, membrane blebbing, and cell shrinkage, and plays critical roles in homeostatic maintenance [55]. Apoptosis occurs through extrinsic and intrinsic pathways, with a

caspase cascade that cleaves regulatory and structural molecules to cause cell death as the final step in each pathway (Figure 2.2).

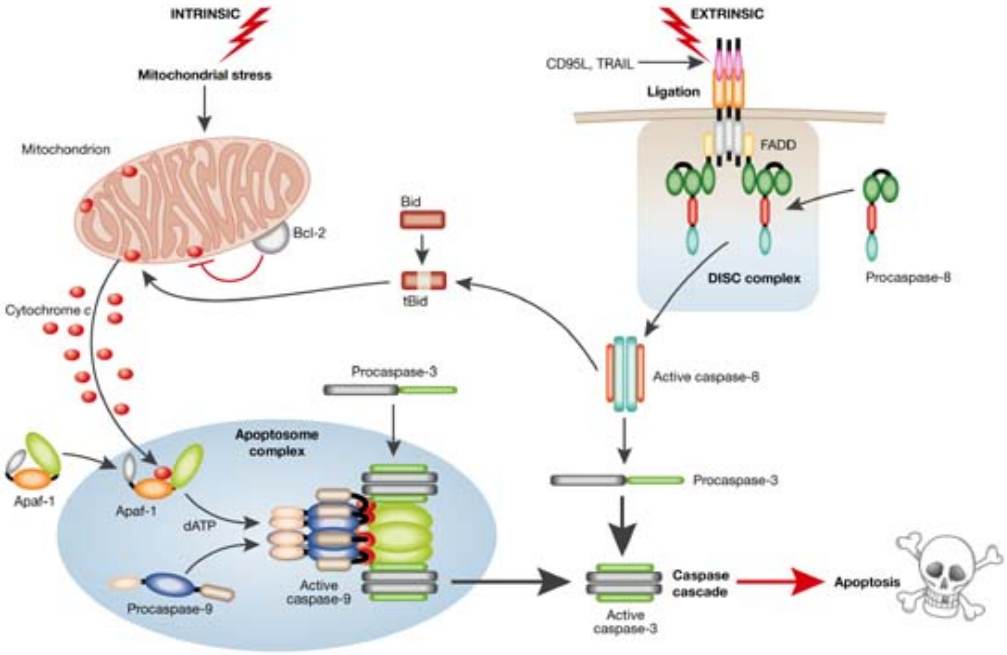

Figure 2.2: Apoptosis: the 'extrinsic' and 'intrinsic' pathways to caspase activation. Reprinted with permission from [56].

The extrinsic pathway, also known as the death receptor (DR) pathway, is induced by extracellular agents such as TRAIL, TNF, and FasL through activation of specific DRs expressed on the cell membrane. When their specific ligands bind and form dimer/trimer complexes, DRs recruit adaptor molecules such as caspase-8 and caspase-10 to further transmit the death-induction signal [55, 56]. The intrinsic apoptotic mechanism acts by perturbing the mitochondrial membrane, relying on release of apoptogenic factors for activation [56]. Both the extrinsic and intrinsic pathways activate caspase cascades,

which are responsible for inducing the morphological and biochemical changes associated with apoptotic cellular phenotype [56].

2.1.5 Targeted Drug Delivery in Cancer

Effectiveness of systemic cancer treatment is limited by lack of sensitivity and selectiveness of most anticancer drugs, resulting in undesirable side effects and significant toxicity to healthy tissues. Targeted drug delivery in cancer therapy refers to a system that delivers therapeutic concentrations of drug to the intended tumor cells (target) while reducing systemic exposure, limiting uptake by healthy cells, and improving the overall therapeutic index [57]. Drug carriers, such as liposomes, dendrimers, nanoparticles, microspheres, or polymer-drug conjugates are common targeted drug delivery systems used for cancer treatment [58]. These particles must either rely on passive targeting through the EPR effect, or be actively targeted to cells of interest through cell markers such as integrins and monoclonal antibodies. Carriers can also be designed to be environmentally responsive, triggered to release drugs at the region of interest in response to changes in pH or temperature, or through external stimuli such as heat, light, magnetic fields, or ultrasound waves [59-61]. A PEGylated liposomal Dox-carrying agent, Doxil® (Johnson & Johnson, Langhorne, PA), is an FDA-approved drug carrier that has been demonstrated to reduce cardiotoxicity and systemic side effects while also improving survival rates [62]. Studies such as this provided preliminary evidence that drug encapsulation can help reduce systemic side effects while still providing effective drug delivery at the target site. As a result, many research efforts have focused on development of drug-loaded microspheres as more efficient drug delivery vehicles.

2.2 Ultrasound and Contrast Agents

Ultrasound (US) has become one of the most widely used imaging modalities in diagnostic imaging. Some of the advantages of US are that it is non-invasive, non-ionizing, less expensive than other imaging modalities, portable, and provides real-time imaging [63]. Imaging sensitivity can be improved with the use of ultrasound contrast agents (UCA), which are injectable bubbles that increase the impedance mismatch and enhance the US image.

2.2.1 Ultrasound

Ultrasound is characterized by the transmission of a short cyclic pressure (sound) wave from a transducer through the body. As these acoustic waves pass through the tissue, some of the energy is lost to attenuation caused by scattering and friction. Attenuation can be estimated by:

$$Attenuation = \alpha L f \qquad \text{(Eq. 1)}$$

where α is the attenuation coefficient (assumed to be 0.3dB/MHz cm^{-1} along the beam axis for most soft tissue), L is the transmission distance (cm), and f is the transmission frequency (MHz).

When transmitted waves passing through the tissues reach a boundary with an impedance mismatch, some of the energy is reflected back to the transducer while the remaining energy continues to pass through the tissue until it encounters another boundary or is absorbed by the body. Reflected waves are used to generate images. The acoustic impedance (Z) of a material is defined as:

$$Z = \rho c \qquad \text{(Eq. 2)}$$

where ρ is the density of the material (kg/m^3) and c is the speed of sound in that material (m/s). The reflection coefficient (R) describes the degree of reflection exhibited by an US wave when passing from one medium to a second medium. The reflection coefficient of an acoustic wave passing through two media is defined as:

$$R = \left(\frac{z_2 - z_1}{z_2 + z_1}\right)^2 \quad \text{(Eq. 3)}$$

where z is the acoustic impedance (kg/m^{2}s). An R value of 1 signifies 100% wave reflection, while an R value of 0 signifies 100% transmission of the wave.

Some characteristics used to describe an acoustic signal, which can be selected by the sonographer, include its center frequency in MHz, pressure amplitude or peak negative (rarefactional) pressure (PNP) in Pa, pulse length in seconds, pulse repetition frequency in Hz, duty cycle, and intensity in W/cm^2. The intensity (I) of a continuous wave is defined as:

$$I = \frac{PNP^2}{2Z} = \frac{P_{RMS}^2}{Z} \quad \text{(Eq. 4)}$$

where P_{RMS} (Pa) is the root mean square of the pressure wave. For pulsed US, wave intensity can also be described as the spatial peak temporal average intensity I_{SPTA} (W/cm^2) and the spatial peak pulse average intensity I_{SPPA} (W/cm^2), which are defined as:

$$I_{SPTA} = I \times DC \quad \text{(Eq. 5)}$$

$$I_{SPPA} = I \quad \text{(Eq. 6)}$$

where DC is the duty cycle of the acoustic wave [64]. The current FDA recommendations for diagnostic ultrasound suggest a derated maximum I_{STPA} of 0.72 W/cm^2 and an I_{SPPA} of 190 W/cm^2 [64].

Clinical US, administered to patients, is also described by a safety index, mechanical index (MI), that relates to the risk of non-thermal damage to the tissue. MI is an empirical factor that is standardized across all medical transducers and US systems, and is defined by:

$$MI = \frac{PNP}{\sqrt{F^C}} \qquad \text{(Eq. 7)}$$

where PNP is the peak negative pressure (MPa) of the US wave, and F^C is the center frequency (MHz) of the US wave [65, 66]. The maximum allowable MI for clinical use on humans is 1.9 by current FDA standards.

2.2.2 Ultrasound Contrast Agents

The numerous advantages of US imaging have led to various research efforts focused on developing technology to expand the range of imaging applications while also improving the overall imaging quality. For example, cardiac imaging has been improved by introducing small stabilized gas bubbles, known as contrast agents, into the blood stream to enhance tissue delineation [67]. Broadly, ultrasound contrast agents (UCA) are gas-filled microbubbles that can be injected intravenously to provide an impedance mismatch (increasing contrast by at least 20dB) [68, 69]. These microbubbles reflect US due to the acoustic impedance mismatch between air and water, or in the body the blood to gas interface (Eq. 3). Air is considered a "perfect" reflector of US waves in blood and tissue, as the reflection coefficient for a boundary between air (Z_{air} = 415 Pa*s/m) and water (Z_{water} = 1.49 x 10^6 Pa*s/m) is nearly 1 at 20°C, 1 atm, and 20dB, indicating that almost all energy is reflected back to the transducer [70]. The strong signal generated by microbubbles results from the difference in compressibility between a gas bubble and the

surrounding tissue (~20,000x greater than tissue), allowing the microbubbles to resonate and reflect an US signal roughly 1,000 times greater than a gas microbubble of the same diameter in a rigid shell [71].

Understanding how UCA will behave in circulation and under insonation are important considerations to determine the type and dosage of UCA to use, as well as the appropriate US imaging parameters for optimal visualization. Various *in vitro* models have been used to predict how UCA will function *in vivo*. Here we will briefly discuss three main UCA characterization categories: UCA stability, backscattering radius, and resonant frequency.

The encapsulated gas bubble within the UCA must be stabilized to prevent diffusion of the gas into the solution when suspended in solution. UCA stability can be determined by exposing suspended agents to intermittent US scanning over a set period of time, either *in vitro* or *in vivo*, and comparing normalized enhancement values. Many research efforts have focused on modeling gas diffusion through the stabilized UCA, resulting in the Epstein-Plesset model with modifications to account for shell resistance:

$$\frac{\delta r}{\delta t} = \frac{-L}{\left(\frac{r}{D}\right)+R_{Shell}}\left(\frac{\frac{1+2\gamma}{P_F r-C}}{\frac{1+3\gamma}{4P_F r}}\right) \qquad \text{(Eq. 8)}$$

where t is time, r is UCA radius, L is Ostwald's coefficient, D is the diffusion coefficient of the gas in liquid, R_{Shell} is the resistance of the shell to gas permeation, and C is the ratio of concentration of dissolved gas to its saturated concentration, γ is bubble surface tension, and P_F is hydrostatic fluid pressure [72, 73]. Based on this model, the presence of a stabilizing shell reduces the rate of bubble shrinkage over time, due to the reduction of surface tension and gas diffusion that comes with shell encapsulation.

UCA expand and contract as the acoustic wave passes through it, in a phenomenon known as cavitation. The degree to which the agent expands and contracts is proportional to the pressure rarefaction and compression of the sound wave, respectively. Microbubble backscattering radius, or scattering cross-section, can be modeled empirically with the following equation, under the assumption that the product of US wavenumber and radius scatterer value is much less than one:

$$\sigma = \frac{I_S \times 4\pi \times d^2}{I_0} \qquad \text{(Eq. 9)}$$

where σ represents the scattering cross-section, I_0 represents the applied wave intensity, I_S is the scattering intensity, and *d* represents the distance between the UCA and the transducer. Backscattering area describes how well a contrast agent reflects US waves, and provides an indication of how effectively a UCA will provide acoustic enhancement. It is important to note that the UCA scattering cross-section can be orders of magnitude larger than the physical area of the UCA itself [74]. A more precise calculation of scattering cross-section taking into account the adiabatic compressibility and density of the UCA and surrounding fluid can be performed with the following equation:

$$\sigma = \frac{4\pi r^6 K^4}{9}\left[\left(\frac{\kappa_s - \kappa_f}{\kappa_f}\right)^2 + \frac{1}{3}\left(\frac{\rho_s - \rho_f}{2\rho_s + \rho_f}\right)^2\right] \qquad \text{(Eq. 10)}$$

where *K* represents the wavenumber, κ_s is the scatterer compressibility, κ_f is the fluid compressibility, ρ_s represents the scatterer density, ρ_f represents the fluid density, and *r* is the UCA radius. Scattering cross-section is sensitive to insonation parameters, increasing with frequency (wavenumber) to the fourth power, and UCA characteristics, increasing

with radius to the sixth power, both having great importance to the overall effectiveness of the UCA to provide acoustic enhancement.

UCA backscatter and scattering cross-section are maximized when UCA can oscillate at harmonics, or its resonant frequency. The resonant frequency of a free bubble is modeled with the following equation:

$$f_0 = \frac{6500}{2r} \qquad \text{(Eq. 11)}$$

where f_0 is the frequency (kHz) and r is the radius of the free bubble (μm) [75]. Models have also been developed to estimate the natural frequency of encapsulated gas bubbles, taking into account elastic compression modulus (χ) and harmonics, such as this equation by Marmottant:

$$f_0 \approx \frac{1}{2\pi R_0}\sqrt{\frac{1}{\rho}\left(3kp_0 - \frac{2\gamma(R_0)}{R_0}(3k-1) + \frac{4\chi}{R_0}\right)} \qquad \text{(Eq. 12)}$$

where R_0 is the microbubble radius, γ is microbubble surface tension, ρ is the liquid density, p_0 is pressure, and k is the polytropic gas exponent [76, 77]. This model demonstrates that resonant frequency increases as Young's Modulus of the UCA increases. Resonance also affects scattering cross-section, increasing backscattering area up to three orders of magnitude over the actual cross section of a free bubble, as shown in the following model by Anderson and Hamilton:

$$\sigma = \frac{4\pi r^2}{\left[\left(\frac{f_0}{f}\right)^2 - 1\right]^2 + \left(\frac{f_0}{f}\right)^4 \delta^2} \qquad \text{(Eq. 13)}$$

where δ represents the bubble shell damping coefficient [74, 78, 79]. UCA performance can be optimized with a solid understanding of the stability, backscattering radius, and

resonant frequency of the agents for proper use. Empirical calculations can be used to estimate these properties during agent design, but they can also be determined experimentally for thorough agent evaluation and characterization.

2.2.3 Existing Ultrasound Contrast Agents

UCA have been developed using a variety of materials and gases. An ideal UCA would provide a high degree of acoustic enhancement, be non-toxic, be injected intravenously, have a diameter of 6μm or less to pass freely through the capillary bed, and have appropriate stability to withstand the duration of an US examination [79]. Initial attempts involved agitation of a saline or sugar solution, but these free air bubbles were highly unstable and often filtered by the lungs upon administration [80]. This instability is due to the pressure difference (ΔP) across the gas to blood interface, which can be determined using the LaPlace equation:

$$\Delta P = P_G - P_F = \frac{2\gamma}{r} \qquad \text{(Eq. 14)}$$

where P_G is the gas pressure within the microbubble (N/m^2), P_F is the hydrostatic fluid pressure (N/m^2), γ is the bubble surface tension (N/m), and *r* is the radius of the microbubble (m). For a free air bubble of radius 2μm, ΔP is approximately 1bar making it highly unstable in solution [80]. Based on these calculations, the majority of research to develop UCA has focused on creation of gas bubbles encapsulated within an outer shell for added stability.

Over the last few decades, many iterations of UCA have been developed with various combinations of gases (i.e. air, sulfur hexafluoride (SF6), and oxygen) and shell materials (i.e. synthetic polymers, proteins, phospholipids, and surfactants) with mixed

success [69, 81, 82]. Currently, only three UCA (Optison, Definity, and Lumason) are FDA-approved for use in the United States. Optison contrast agents (GE Healthcare, approved 1997) are human albumin-stabilized perfluorocarbon (C_3F_8) gas bubbles, while Definity (Lantheus Medical Imaging, approved 2001) is a phospholipid-stabilized, PEGylated C_3F_8 microbubble. Lumason contrast agents, formerly known as SonoVue, (Bracco Diagnostics, approved 2014 (heart) and 2016 (liver)) are lipid microspheres filled with sulfur hexafluoride (SF_6), and are approved for use in echocardiograms and liver imaging. SonoVue contrast agents (Bracco Diagnostics) have been approved for use in Europe, South America, and China, and are comprised of an SF_6 core encapsulated within a phospholipid shell containing PEG4000, non-PEGylated lipids, and palmitic acid.

2.2.4 Polymer Ultrasound Contrast Agents

Polymer-shelled UCA have also been developed and investigated, however no polymeric UCA have been approved for clinical use in humans in the United States as of 2015. Initial efforts involved the use of natural polymers, such as alginate and collagen, but have since largely transitioned to synthetic polymers such as poly(lactic-co-glycolic) acid (PLGA) and poly(lactic acid) (PLA). Synthetic polymer UCA fabrication generally involves emulsification of an ammonium acetate or ammonium bicarbonate solution (aqueous phase) with the polymeric solution (organic phase) followed by spray drying or lyophilization [83-86].

The polymeric UCA that have been developed in the Wheatley Lab are fabricated using a water in oil in water (w/o/w) double emulsion process to create an air-filled microbubble stabilized by a PLA shell with residual poly(vinyl alcohol) (PVA) [3, 87-

90]. The resulting UCA have an average diameter of 1-2μm, with a shell thickness of 100-200nm (10% of diameter), have been shown to provide an acoustic enhancement of over 20dB at 5MHz *in vitro* and *in vivo*, and are stable enough to withstand the duration of a typical US examination (15-20 minutes) [87-89, 91].

PLA (Figure 2.3) is a logical choice for our UCA shell material, since it is biodegradable, its breakdown product (lactic acid) is a natural body metabolite, and it is FDA approved for clinical use in injectable devices. Important material properties of PLA that enhance its candidacy as UCA shell material and a drug delivery vehicle are its Young's Modulus (350-2800MPa), glass transition temperature (45-65°C), and density (1210-1430kg/m^3) [92].

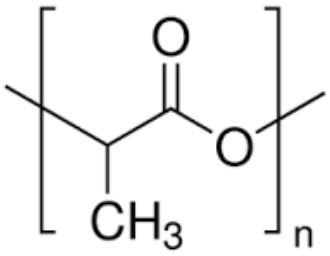

Figure 2.3: Chemical structure of poly(lactic acid) repeating unit.

Polymeric UCA have been shown to withstand higher US pressures than lipid-based UCA, with studies showing tolerance of over 0.54MPa higher PNP levels than phospholipid agents [93]. Polymeric agents also have increased shell volume compared to lipid-based agents, suggesting that polymeric agents can encapsulate higher drug payloads within the shell for therapeutic applications.

2.2.5 Ultrasound-induced Contrast Agent Action

Aside from US image enhancement, UCA can be used to cause physiological effects for therapeutic applications as a result of their unique interaction with and response to acoustic waves. As discussed previously, the highly compressible gas core of UCA cavitates when exposed to the rarefaction and compression of a pulsed acoustic pressure wave [94]. At moderate US intensities (lower MI, 0.1-0.3), UCA undergo stable cavitation, where the encapsulated gas bubble will oscillate around the resonant diameter, vibrating millions of times per second with a velocity up to 700m/s [95, 96]. At higher US intensities (higher MI, 0.3-0.5), UCA undergo inertial cavitation characterized by rapid expansion in the rarefaction phase followed by rapid collapse due to inertia of the surrounding fluid during the compression phase [96]. This violent bubble collapse can create local physiological effects such as microstreaming, mechanical shock waves, microjets, free radical generation, and temperatures as high as 5000K [97]. As the bubble collapses against a boundary, fluid away from the boundary will be focused and accelerated through the bubble, forming a liquid jet in the direction of the boundary that can travel over 20μm with an average velocity of roughly 80m/s and pressures up to 60MPa [94, 98]. These microjets have been shown to be capable of penetrating the cell membrane, in a phenomenon known as sonoporation [99]. Research efforts are being pursued to exploit this cell permeabilization ability for drug delivery and gene therapy.

2.2.6 Blood Vessel Permeability and Radiation Force

Sonoporation is not only limited to cell membranes, but has also been used to increase vascular permeability. US triggering of UCA has been shown to create gaps in artificial endothelia and cell monolayers under *in vitro* conditions [100]. Further studies

have demonstrated formation of discrete extravasation points in skeletal muscle in response to insonation (1MHz, 0.75MPa, pulse length 100μs) of Optison UCA flowing through capillaries, and that nanoparticles 100nm in diameter can escape through these pores [101]. Additionally, capillary rupture and cell death can be correlated with the MI used while imaging in these studies [102]. In this second study and another similar study, research shows that red blood cells, polymer microspheres up to 500nm in diameter, and Opticell fragments exhibited extravasation from the US-cavitation induced capillary rupture [102, 103]. However, other groups have demonstrated that US-induced increased in capillary permeability is transient, with permeability returning to near normal levels approximately 60 minutes after completion of insonation until healed through platelet activation [104, 105].

Since sonoporation is most effective when the UCA is against the boundary of the vessel wall, harnessing the radiation forces on the cavitating UCA help maximize the capillary rupture and extravasation potential. When placed in an acoustic field, UCA experience directional radiation force in response to the pressure gradient generated by acoustic waves passing through a medium. The primary radiation force UCA experience is directed away from the transducer, and is defined as:

$$F_r = \frac{2\pi P_a^2 r}{\varrho c \delta w_0}\left[\frac{D}{T}\right] \qquad \text{(Eq. 14)}$$

where *Pa* represent the peak applied acoustic pressure, *r* is the UCA radius, δ is the damping coefficient, ϱ is the medium density, w_0 is the angular resonance frequency of the UCA, and [D/T] is the US duty cycle [106]. Dayton et al. also developed an equation to describe the primary radiation force averaged over an acoustic cycle:

$$F = \frac{DC(P^2R_0)}{\rho cf} \frac{\left(\frac{\delta f_r}{f}\right)}{\left[\left(\frac{f_r}{f}\right)^2 - 1\right]^2 + \left(\frac{\delta f_r}{f}\right)^2} \quad \text{(Eq. 15)}$$

where δ is the total damping coefficient, f_r is the UCA resonance frequency, f is the driving US wave frequency, and R0 is the initial UCA radius [107]. When the resonance frequency of the UCA and US frequency used for insonation are the same, the force equation can be simplified to:

$$F = \frac{DC(P^2R_0)}{\rho cf\delta} \quad \text{(Eq. 16)}$$

This group went to use high-speed photography to show that radiation forces can move microbubbles up to 5μm during a single 20 cycle pulse (2.25MHz, 380kPa) at an average velocity of 500mm/s [108]. This same group went on to demonstrate deposition of fluorescent nanoparticles attached to phospholipid UCA onto a biotin-coated cellulose tube surface using radiation forces [109].

Radiation force is not only dependent on the intensity of the applied US wave, but also on the size of the particle with forces exerted decreasing as particle size decreases. Smaller particles are also characterized by higher resonance frequencies, causing lower radiation forces to be exhibited by these particles. Additionally, the US-reflective UCA core plays a critical role in driving particles with radiation forces. Studies have shown that radiation forces on solid particles in the micron-nanometer range were significantly lower than those observed on gas-filled particles [110]. UCA in solution under insonation are also susceptible to secondary Bjerknes forces as a results of the US-induced oscillations causing attraction between particles. However, these forces are generally very small (0.5pN at a separation distance of 200μm, 2MHz insonation at 122kPa and PRF

10Hz) compared to radiation forces (0.9nM at the same parameters) [106]. These forces can be harnessed and exploited to improve delivery efficacy of drug-loaded, polymer-shelled, micron-sized UCA.

2.2.7 Ultrasound-triggered Targeted Drug Delivery

The physiological effects induced by US insonation have been used in a variety of ways for targeted drug delivery, both with and without the use of contrast agents. Studies have demonstrated increased cytotoxicity and drug retention at the tumor site when exposed to therapeutic US (up to a 3-fold increase for Dox) compared to cells that were not insonated [111, 112]. Increased cytotoxicity is likely due to increased cell uptake of drug in response to US-induced increases in cell membrane permeability [112].

These therapeutic benefits of combining chemotherapy with US insonation become even more clear and significant when UCA are also utilized in drug delivery. Several groups have demonstrated enhanced drug uptake, cytotoxicity, and tumor suppression when UCA are co-administered with chemotherapy drugs such as Dox and bleomycin in the presence of US, compared to groups receiving drug and US without UCA and groups receiving drug only [113, 114]. Other studies have shown that small molecules, such as genes and peptides, can be effectively delivered to the intracellular space when administered with UCA and focused insonation causing cavitation-induced permeability [115-117].

Drugs have also been loaded into UCA for drug delivery without systemic administration of free drug, aiming to increase bioavailability at the tumor site while sparing healthy tissues from collateral damage from exposure to the toxic drug. This treatment modality uses US pressures to induce inertial cavitation and UCA destruction,

resulting in drug release localized to the region of interest. Several studies have investigated the development of lipid-based, drug-loaded UCA, demonstrating successful drug release in response to exposure to US. For example, Lentacker et al. loaded Dox-filled, nano-sized liposomes to the surface of a phospholipid-shelled UCA (total loading roughly 3.25 x 10^{-8} μgDox/bubble) and showed significantly more cytotoxicity when UCA were triggered with US *in vitro* (1MHz, I= 2W/cm^2) [118]. Similarly, Huang et al. demonstrated that calcein was successfully released from phospholipid liposomes when exposed to a 1MHz transducer [119]. As an alternative to thin-walled lipid-based UCA, a good deal of research is being directed toward the development of polymer-shelled UCA where the thicker shell (100-400nm) can increase drug loading and ultimately improve targeted, US-driven drug delivery. As an example, the gas core can be partially replaced with hexadecane oil loaded with lipophilic drugs that can release from the UCA when the polymeric shell is cracked by cavitational destruction in response to US exposure [120]. Additionally, drugs encapsulated within the UCA shell can undergo sustained release as the surrounding polymer hydrolyzes, providing prolonged treatment times. However, lipid-based UCA for drug delivery currently dominate the literature, due to their ease of fabrication, immediate release profile, and commercial availability. Nonetheless, the increased shell stability, potential for increased drug loading, and sustained release of encapsulated drug from polymer-shelled UCA warrants further investigation for targeted drug delivery applications.

Specifically to the polymeric UCA created in the Wheatley lab, we have reported on encapsulation of Dox within the air-filled PLA shell, the presence of which has been visualized using confocal microscopy [2, 3]. The double emulsion (w/o/w) preparation

method used to fabricate our PLA-shelled UCA is versatile for encapsulation of drugs or other species for US-guided delivery, since species can be incorporated into either the organic or aqueous phase [2, 4, 121, 122]. Dox-loaded PLA UCA have shown significant greater cytotoxic effects on cancer cells *in vitro* when triggered with US, compared to non-insonated controls [121]. In a separate study, insonation of these resulted in significant particle size reduction (below 400nm), likely due to shell fragmentation into nanoshards (n-Sh) induced by inertial cavitation [4]. Promising *in vivo* studies in a rat hepatocellular carcinoma model demonstrated extravasation potential of these US-generated n-Sh in addition to effective delivery of Dox to tumor tissue, resulting in measureable tumor stasis [5]. However, elevated Dox levels were also observed in the spleen and healthy liver, indicating mononuclear phagocyte system (MPS) involvement [123-127]. Based on these results, we hypothesize that intact MB and/or n-Sh that were not taken up into the tumor were recognized by the immune system while circulating through the blood stream and thus accumulated in the spleen and healthy liver. Therefore, the major focus of this thesis is to develop drug-loaded UCA that can avoid recognition and removal by the immune system, improving delivery to the target site while protecting susceptible organs and tissues.

2.3 Immune Considerations with Drug Delivery in Cancer

Many of the side effects associated with chemotherapy drug administration involve an immune component, especially inflammation and damage to the liver, spleen, and kidneys. Systemically-injected drug, whether freely administered or encapsulated within a drug carrier, can be recognized as a foreign body in the blood stream and

removed from circulation by the components of the immune system. The most relevant immune components to the platform investigated in this thesis are discussed below.

2.3.1 Mononuclear Phagocyte System

A major factor that has limited efficacy and success of most injectable drug delivery vehicles has been immune recognition through the mononuclear phagocyte system (MPS) and its rapid detection and removal of injected particles from the blood stream. The MPS is comprised of a group of highly phagocytic mononuclear cells, such as macrophages in tissues and monocytes in blood [128]. Macrophages are responsible for clearing the blood, lymph, and tissues of particles, microorganisms, and dead cells, essentially acting as the cleaning system. The MPS acts by recognizing foreign objects circulating in the blood stream and removing these objects within minutes through the spleen and liver, through processes known as opsonization and phagocytosis respectively [125, 129-131]. In terms of response to injected drug delivery agents, removal by the MPS reduces the amount of drug available for delivery to the region of interest, while also causing a buildup of the toxic drug in the liver and spleen. When these particles are exposed to blood flow, opsonization is activated as proteins such as immunoglobulins and complement proteins adsorb to the particle surface and subsequently bind to macrophages of the MPS eventually leading to phagocytosis of the injected particle before ever reaching the target site [132, 133].

2.3.2 Complement System

The complement system is a group of blood proteins responsible for facilitating opsonization and phagocytosis of foreign bodies to maintain host defense and inflammation [129, 134, 135]. Complement activation leads to a cascade of enzymatic

reactions ultimately resulting in formation of anaphylatoxins that can induce chemoattraction and cell death [135]. There are three different complement activation pathways, classical, alternate, and lectin, which all converge at complement protein C3 activation and eventually lead to the formation of the membrane attack complex. The classical complement pathway is activated when immunoglobulins IgG and IgM bind to pathogens or other foreign bodies in the blood. Recognition of carbohydrates, lipids, and proteins found on foreign bodies by C3b protein triggers activation of the alternate complement pathway, while the lectin pathway is activated when mannose binding lectin binds to surfaces on yeast, bacteria, parasites, or viruses [135]. When C3, the most abundant complement protein in the blood, is activated in forms cleavage products C3a and C3b which are two of the main regulators of the complement system. While C3a is mainly associated with facilitating the inflammatory response, C3b identifies foreign bodies, adsorbs to their surface, and signals their opsonization [136]. Immunogenicity evaluations in this work will focus on activation of the C3 complement protein as an indicator of immune activation.

2.3.3 Polyethylene Glycol

Many strategies for avoiding immune activation and uptake have been investigated, including particle size, chemical makeup, and surface coating. Particle surface characteristics play a large role in determining which proteins will adsorb to the surface and how quickly they will adsorb. When designing “stealth” particles that can evade the immune system, hydrophobic and ionic interactions that can drive protein adsorption are major factors to consider; for example, highly charged particles have been

shown to activate more complement proteins and more rapidly bind opsonins than neutral particles [133, 137].

In an effort to prevent opsonization and complement activation, particles can be modified to become “invisible” to monocytes and macrophages. One of the most common methods of circumventing MPS and complement recognition is surface modification with polyethylene glycol (PEG) [132, 137-144]. PEG is more effective at immune shielding than other polymers because it is highly hydrophilic, neutral in charge, flexible, and usually non-immunogenic [133, 145, 146]. Additionally, PEG is FDA-approved, inexpensive, and easily modified, making it an excellent candidate for conjugation to various lipids and polymers for immune shielding. Surface coating with PEG has been shown to extend particle circulation times by reducing protein adsorption; however, PEG chain length and density must be optimized to the particular agent in order to create a “brush” that prevents protein adsorption through steric hindrance without creating entanglement within the chains [130, 137, 140, 145, 147].

In addition to shielding particles from immune recognition, several studies describe PEGylation of TRAIL for increased circulation time [141, 148]. One study in particular investigated the sustained release of PEGylated and non-PEGylated TRAIL following encapsulation within PLGA microspheres [149]. PEGylated TRAIL exhibited sustained release from the microspheres over a period of 15 days, while non-PEGylated TRAIL exhibited a burst release from the microspheres and was completely cleared from the plasma within 3 days[149]. Studies such as this form a good basis for the PEG-TRAIL complexes investigated in this thesis.

3. MATERIALS AND METHODS

3.1 Materials

3.1.1 UCA Fabrication Materials

Polylactic acid (PLA) 100 DL 7E, MW 118kDa, Lot# LX00414-119 was purchased from Evonik Lakeshore Biomaterials (Birmingham, AL). Polyethylene glycol-polylactic acid (PEG-PLA) co-polymer 100 DL mPEG 5000 6CE, 67 mol% PLA, 33 mol% PEG, MW 69kDa, was purchased from Evonik (Essen, Germany). 1,2-distearoyl-*sn*-glycero-3-phosphoethanolamine-N-[carboxy(polyethylene glycol)-2000] (LipidPEG), MW 2.8kDa, and 1,2-distearoyl-*sn*-glycero-3-phosphoethanolamine-N-[carboxyfluorescein(polyethylene glycol)-2000] were purchased from Avanti Polar Lipids (Alabaster, AL). Ammonium carbamate and camphor were purchased from Sigma-Aldrich (St. Louis, MO). Poly(vinyl alcohol) (PVA), MW 25kDa, 88 mol% hydrolyzed, was purchased from Polysciences (Warrington, PA). Methylene chloride (MeCl), isopropyl alcohol (IPA), and hexanes were purchased from Fisher Scientific (Pittsburgh, PA).

3.1.2 Cells and Cell Culture Materials

Human breast adenocarcinoma cell lines MDA-MB-231 and MCF7, human breast epithelial cell line MCF-12A, human epidermal growth factor, cholera toxin, Tryspin-EDTA 1x, USDA-tested fetal bovine serum (FBS), Eagle's Minimum Essential Medium (EMEM), Ham's F12 medium, horse serum, and bovine insulin were purchased from American Type Culture Collection (ATCC) (Manassas, VA). Dulbecco's Modified Eagle's Medium (DMEM) with L-glutamine, sodium pyruvate, and 4.5g/L glucose, an antibiotic solution (10,000 units penicillin and 10mg streptomycin per mL) and

hydrocortisone were purchased from Sigma-Aldrich (St. Louis, MO). Phosphate buffered saline (PBS) was purchased from Fisher Scientific (Pittsburgh, PA). Accutase cell detachment solution, FITC Annexin V Apoptosis Detection Kit II, FITC Annexin V, and propidium iodide (PI) were purchased from BD Biosciences (Franklin Lakes, NJ). Live/dead cytotoxicity assay was purchased from Invitrogen (Waltham, MA).

3.1.3 Other Materials

Doxorubicin HCl (Dox) was purchased from Tecoland (Irvine, CA). Dimethyl sulfoxide (DMSO), acetone, glacial acetic acid, phosphate buffered saline (PBS), N-beta-maleimidopropionic acid hydrazide (BMPH), 2-(*N*-morpholino)ethanesulfonic acid (MES), thioglycolic acid and lab consumables were purchased from Fisher Scientific (Pittsburgh, PA). Tumor necrosis factor-related apoptosis inducing ligand (TRAIL), expressed in *E. coli*, MW 19.6kDa, *n*-hydrosulfosuccinimide (NHS), and N-(3-dimethylaminopropyl)-N'-ethylcarbodiimide hydrochloride (EDC) were purchased from Sigma-Aldrich (St. Louis, MO). Ethanol (200 proof) was purchased from Decon Laboratories (King of Prussia, PA). Human complement-preserved serum was purchased from Valley Biomedical (Winchester, VA). Human C3 ELISA Kit (catalog #550499) was purchased from BD Biosciences (Franklin Lakes, NJ). Pierce LAL Chromogenic Endotoxin Quantitation Kit (catalog #88282) was purchased from Life Technologies (Carlsbad, CA).

3.2 Methods

3.2.1 Contrast Agent Fabrication

UCA were prepared using the water/oil/water (w/o/w) emulsion process that has been well-established in our lab previously [88]. Briefly, 10mL of methylene chloride, 0.05g camphor, and 0.5g PLA were added to a 50mL beaker, and stirred for 15 minutes to ensure that all of the polymer had dissolved. Then, 1mL of 0.4M ammonium carbamate solution was added to the organic phase and sonicated with 110W applied power (Misonix XL2020 CL4 tapped horn probe with 0.5" tip, Farmingdale, NY) on ice for 30 seconds, with 1 second pauses between 3 second pulses. The first w/o emulsion was then added to 50mL of 5% w/v PVA solution kept at 4°C, and homogenized (Brinkman PT 3100 homogenizer with a Polytron PT-3020/2 saw tooth probe, Westbury, NY) at 9500rpm for 5 minutes to create the second emulsion. After homogenizing, 100mL of 2% v/v isopropanol (IPA) was added, and the solution stirred at 375rpm for 90 minutes at room temperature to evaporate off the organic material. The remaining UCA solution was centrifuged at 5000rpm (~2600g) for 5 minutes, and the pellet was collected and washed three times with hexane to remove any remaining organic material. After allowing the residual hexane to evaporate in the fume hood for 20 minutes, the UCA were washed with deionized (DI) water. The particles were then flash frozen in liquid nitrogen and lyophilized for 48 hours using a Virtis Benchtop freeze drier (Gardiner, NY) with the chambers exposed to room temperature and a pressure of 10-30μbar. The aqueous core material and camphor from the polymer shell were sublimated during lyophilization to create a porous polymer shell encapsulating a void, resulting in the formation of air-filled hollow microcapsules when exposed to the atmosphere.

3.2.2 Fabrication Modifications for UCA Functionalization

3.2.2.1 TRAIL Ligation via Maleimide Chemistry

Once the UCA were formed, TRAIL was ligated to the UCA surface using a maleimide reaction [150, 151] with a BMPH spacer arm of 0.81nm in length, using EDC and NHS to activate and catalyze the reactions (Figure 3.1).

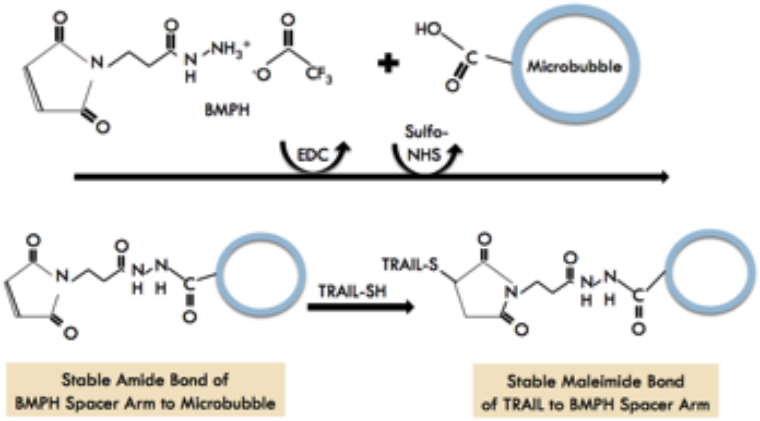

Figure 3.1: Maleimide reaction to bind TRAIL to the UCA surface.

Briefly, 60mg of UCA were suspended in 4mL of 0.1M MES buffer (pH 5.2), while the solutions for crosslinking were prepared (14.86mg BMPH in 1mL DI water, 19.17mg EDC in 1mL DI water, and 12mg NHS in 1mL DI water). These solutions were added to the UCA suspension, which was then shaken end over end at room temperature for 30 minutes. Activated UCA were then centrifuged at 5000rpm (~2600g) for 5 minutes and washed with DI water to remove unreacted EDC. The UCA were then resuspended in a solution of 1.2µg TRAIL in 4mL phosphate buffered saline (PBS), and shaken end over end at room temperature for 90 minutes. The crosslinking was stopped by adding 50µL

thioglycolic acid to the solution and shaking end over end for 10 minutes. TRAIL-ligated UCA (TRAIL-UCA) were then centrifuged (5000rpm for 5 minutes), washed 3 times with DI water, flash frozen in liquid nitrogen, and lyophilized for 48 hours. In preliminary studies, a control group was created following the ligation procedure, but without the use of BMPH, EDC, and NHS (non-linker control), to account for the possibility that observed effects were from TRAIL that was only adsorbed to the surface rather than covalently linked. Such adsorbed TRAIL would be easily eluted when contacted with cell cultures, releasing free TRAIL.

3.2.2.2 PEGylation via PEG-PLA Co-polymer

For PEGylated MB using the co-polymer method, an aliquot of 500mg polymer was proportionally comprised of PEG-PLA and PLA by weight, at concentrations of 1, 2, 5, 10, and 15 wt% (mg PEG-PLA/mg PLA). These polymers were mixed while dissolving in MeCl before the first emulsion, and the standard UCA fabrication procedure was followed to produce PEGylated agents.

3.2.2.3 PEGylation via Lipid Anchoring

For PEGylated MB using the LipidPEG method, 1,2-distearoyl-sn-glycero-3-phosphoethanolamine-n-[carboxy(polyethylene glycol)2000] (LipidPEG), in powder form, was added to the PLA solution at concentrations of 0.2, 1, and 2 wt% (mg LipidPEG/mg PLA) prior to the first emulsion. Agents were then produced following the standard UCA fabrication procedure.

3.2.2.4 Doxorubicin Encapsulation

UCA loaded with Dox were generated by modifying the standard UCA fabrication procedure to dissolve 15mg (3% w/w) of the chemotherapeutic agent in the polymer solution before the primary emulsion, then proceeding with the standard procedure. This Dox loading procedure was followed for all agents that encapsulated the chemotherapeutic, regardless of PEGylation method.

3.2.2.5 TRAIL Ligation to LipidPEG Molecules

TRAIL was attached to LipidPEG by modifying the maleimide chemistry technique used to ligate TRAIL to the UCA surface. Five milligrams of LipidPEG was suspended in 5mL MES buffer while crosslinking solutions were prepared (95.85mg EDC in 5mL DI water and 60mg NHS in 5mL DI water). These 5mL crosslinking solutions were added LipidPEG suspension, and the resulting solutions were shaken end over end for 30 minutes at room temperature to prepare the carboxy end group on the LipidPEG for crosslinking with TRAIL. After 30 minutes, 6 μg of TRAIL was added to the solution, which was then shaken end-over-end for 90 minutes at room temperature. The crosslinking reaction was stopped by adding 250 μL thioglycolic acid to the solution at the end of the 90 minutes. After 10 minutes, the solution was poured into Spectra/Por 7 dialysis tubing (1kDa MW cutoff, 24.4mm diameter, Cole Parmer #132104, Vernon Hills, IL) and stirred in 3L DI water for 6 hours, changing the DI water every 2 hours, to remove the salts. The dialyzed LipidPEG-TRAIL solution was then flash frozen with liquid nitrogen, frozen at -20°C overnight, and lyophilized for 48 hours.

3.2.3 Characterization of UCA

3.2.3.1 Acoustic Testing *in vitro*

Acoustic Tank Testing of Dose and Time Response

Acoustic testing was performed *in vitro* to determine the ability of the UCA to interact with a focused ultrasound beam to provide enhancement as well as to measure the stability of the agent during insonation. The custom-built *in vitro* acoustic setup used for this testing is shown in Figure 3.2.

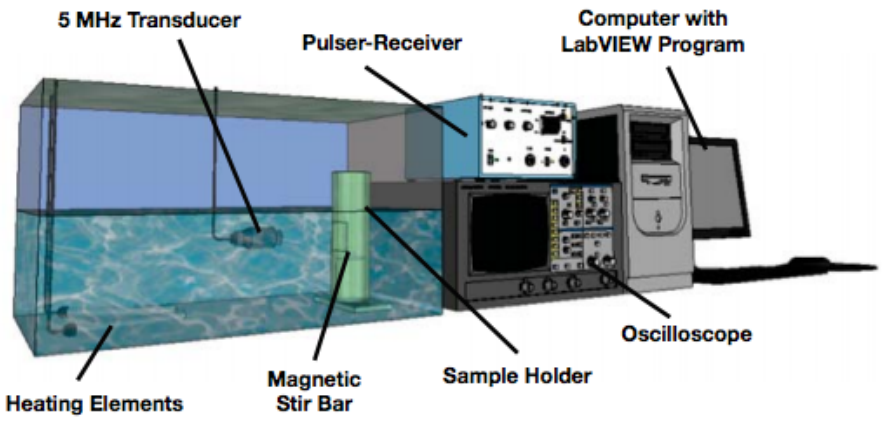

Figure 3.2: Custom built acoustic setup for in vitro testing. Rendering courtesy of Nutte Tarn Teraphongphom.

Dose and time response tests were performed using a 5 MHz, 12.7mm diameter, single element ultrasound transducer (Panametrics, Waltham, MA) spherically focused at a length of 50.8mm, 6dB bandwidth of 91%, submerged in a 37°C water bath and focused through the acoustically transparent window of an acrylic sample holder holding 50mL of 1x PBS at 37°C (pH 7.4) continuously stirred on a magnetic stir plate. The cover of the water bath was fitted with an x-y-z positioning system (Edmund Scientific, Barrington,

NJ) to hold and position the ultrasonic transducer. The transducer was connected to a Panametrics 5072 pulser/receiver (Waltham, MA) to generate an acoustic pulse with a pulse repetition frequency (PRF) of 100Hz and pulse length of 1μs (duty cycle 0.01). The reflected signal from the UCA was detected with the transducer and amplified 40dB before being read by an oscilloscope (Lecroy 9350A Chestnut Ridge, NY). Data acquisition and processing was performed using LabView 7 Express (National Instruments, Austin, TX).

Acoustic backscattering enhancement was measured to determine the ability of the agent to respond to ultrasound for imaging sensitivity and drug delivery applications. A cumulative dose response of acoustic enhancement was performed by suspending 3mg of dry UCA in 800μL 1x PBS and briefly vortexing and then adding 20μL of the UCA suspension to the sample vessel every 30 seconds and measuring the acoustic backscatter signal at each time point. A PRF of 100Hz and peak negative pressure amplitude of 0.45MPa (energy level 1) was used for these studies. The acoustic backscattering enhancement is defined as

$$Enhancement = 20\log_{10}\left[\frac{rms[UCA]}{rms[Blank]}\right] \qquad \text{(Eq. 17)}$$

where rms[UCA] represents the root mean square of the backscatter signal measured from the UCA and rms[Blank] represents the root mean square of the backscatter signal measured from the PBS solution alone prior to injection of UCA. All values were based on an average of three readings from five individual samples (15 readings, n=5).

Stability of the UCA in the presence of ultrasound was measured to determine the effect of these pressures on the shell stability and to determine whether the agents would last for the duration of a typical imaging session in a medical clinic (using 15 minutes as

a benchmark length of imaging time). A dosage on the linear rise portion of the dose response curve (generally 4μg/mL) of UCA was added to 50mL of 1x PBS at 37°C and continuously stirred and insonated at a peak negative pressure of 0.45MPa (energy level 1) with a PRF of 100Hz. Enhancement was measured immediately following injection and every minute for a total of 15 minutes, and was then normalized with respect to the initial enhancement. Detailed protocols for these tests are included in Appendix A.

Flow Phantom Imaging

All UCA samples were evaluated with a clinical ultrasound scanner (used for imaging of patients in a hospital setting) and a tissue mimicking flow phantom at Thomas Jefferson University with the assistance of Dr. John Eisenbrey. Imaging was performed with an ACUSON S3000 Ultrasound System HELX™ Evolution equipped with a 9L4 probe (Siemens, Erlangen, Germany) operated under nonlinear contrast imaging mode with dual contrast/grayscale imaging. A concentration of $1.0x10^7$ UCA in 800mL 1x PBS was circulated through a tissue mimicking flow phantom (ATS Laboratories, model 524, Bridgeport, CT) with a 6mm diameter vessel embedded at a depth of 2cm in urethane rubber using a peristaltic pump at 350mL/minute. Dual non-linear contrast mode and fundamental B-mode images were captured pre-injection, at time of injection, and every 5 minutes post injection for a total of 20 minutes.

3.2.3.2 Characterization of Nanoshard (n-Sh) Behavior

All agents were evaluated for the potential to generate n-Sh by performing ultrasound triggering in the acoustic tank setup described previously (Figure 3.2). Ten milligrams of dry UCA was suspended in 50mL 1x PBS at 37°C and continuously stirred.

The sample was insonated at 5MHz with the transducer described previously, at a PRF of 100Hz and a peak negative pressure of 0.94MPa (energy level 4). US-generated particles were collected after 15 minutes of insonation for size evaluation with dynamic light scattering in a Malvern Nano ZetaSizer (Worcestershire, United Kingdom), described in detail in the Size and Zeta Potential Measurements section. All experiments were completed in triplicate and are reported as average peak particle size by number.

UCA were also evaluated for the potential to extravasate as a result of cavitation with an *in vitro* model of the leaky tumor vasculature using Corning Transwell inserts with a 24mm diameter polyester membrane containing 400nm pores with a density of $4x10^6$ pores/cm^2 (Lowell, MA). Inserts were modified by placing clear adhesive tape over the openings in the sides of the inserts to allow for higher fluid levels, which helped reduce the chances of creating a standing wave during insonation. An insert was placed into a 6 well plate containing a suspension of 3mg dry UCA in 3mL 1x PBS at 37°C. Three milliliters of 1x PBS was then added to the upper compartment of the insert, and the plate was suspended on the surface of the DI water in the acoustic tank. The 5MHz spherically focused transducer was oriented to insonate from below the plate at a length of 50.8mm from the membrane surface so that the beam would be focused at this point. A rubber stopper was placed above the insonated well to serve as an acoustic absorber to minimize reflected energy at the air-liquid interface. A schematic of this testing setup is shown in Figure 3.3.

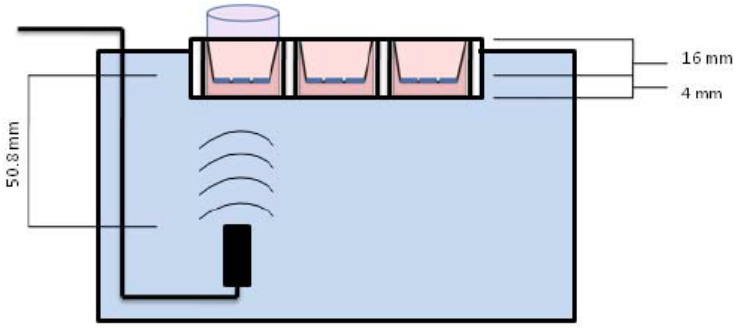

Figure 3.3: Schematic of extravasation testing setup showing Transwell insert (light pink) and well plate (dark pink), with transducer and acoustic absorber. Schematic courtesy of Dr. John Eisenbrey [87].

The sample was insonated for 20 minutes with a peak negative pressure of 0.94MPa (energy level 4) and a PRF of 5000Hz. At the end of the 20 minutes, a 1mL sample was taken from the top chamber, placed into a plastic cuvette and assessed for particle size using a ZetaSizer with dynamic light scattering. For Dox-loaded samples, 200µL samples were taken from the top chamber at 0, 5, 10, 15, and 20 minutes and fluorescence was read in a Tecan fluorimeter (λ_{ex} 495nm, λ_{em} 585nm). Dox concentration was then calculated based on a standard curve and expressed as the amount present above the membrane. All tests were performed in triplicate, and control tests were performed without ultrasound.

3.2.3.3 Resonant Frequency Measurements

Given the multiple modifications made to the UCA shell, it is important to understand the effect of these modification on the resonance and cavitation activity of the resulting UCA. It is important that the UCA are insonated at a frequency that matches their resonance to best harness their ability to serve as contrast agents and ultrasound-

triggered drug delivery agents. To determine the resonant frequency, a pulse-echo setup was employed with a custom-built sample holder, equipped with an acoustically transparent window and an air-backed metallic reflector, holding 250mL of 1x PBS at 37°C and stirred continuously. This sample holder was submerged in the DI water bath held at 37°C, and a single element, 12.7mm diameter, unfocused transducer (both 5MHz and 10 MHz were used) was positioned to transmit through the acoustically transparent window (Panametrics, Waltham, MA). The 5MHz transducer had a -6dB bandwidth of 91% and a pulse length of 1.2mm, and the 10MHz transducer bandwidth was 65% with a pulse length of 0.75mm. A schematic of this setup is shown in Figure 3.4.

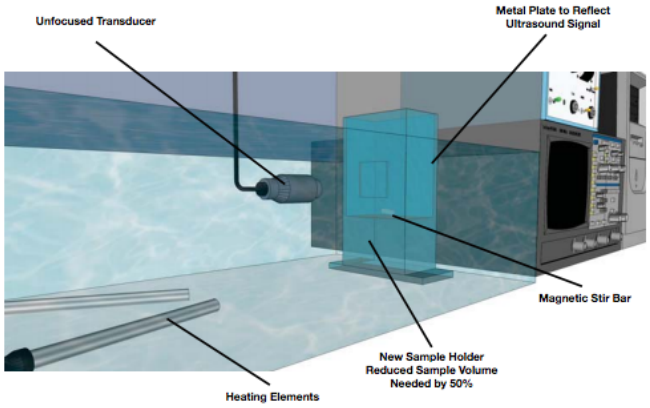

Figure 3.4: Schematic of resonant frequency testing setup. Rendering courtesy of Nutte Tarn Teraphongphom.

The Panametrics model 5072 pulser/receiver was used to pulse the transducers at a PRF of 100Hz, gain of 0dB, peak negative pressure of 0.45MPa (energy level 1), damping level of 3, and mode 1 for pulse-echo. The signals were received and visualized with an Agilent Technologies InfiniiVision MSO-X 2014A digital oscilloscope (Agilent,

Santa Clara, CA). The signals were converted to Fast Fourier Transforms (FFT) using the Math function of the oscilloscope. Data was acquired by collecting 250 samples of the baseline signal (1x PBS) and the signal after addition of 15mg UCA to a final concentration of 0.06mg/mL PBS. Resonant frequency was determined similarly to calculations by de Jong [152, 153] (Equation 18), where $FFT_{baseline}$ represents the transform of the signal before agent was added, $FFT_{attenuated}$ represents the transform of the signal after the agent was added, and D represents the distance from the acoustic window (6cm).

$$Attenuation = \frac{(FFT_{baseline} - FFT_{attenuated})}{D} \quad \text{(Eq. 18)}$$

Samples were tested in triplicate for both the 5MHz and 10MHz transducers. The attenuated signals were analyzed using OriginPro 8 software (OriginLab, Northampton, MA), using the smoothing filter with 20 points to smooth out noise signals. Final processed data from both the 5MHz and 10MHz transducers were plotted together with attenuation (dB/cm) against frequency (MHz) according to the appropriate bandwidth ranges for the transducers. Resonant frequency was determined as the frequency at which attenuation reaches a minimum point on the curve. A more detailed protocol for this testing is included in Appendix A.

3.2.3.4 Size and Zeta Potential Measurements

Particle size distribution and zeta potential (ζ) measurements were performed using a Malvern Nano ZetaSizer (Worcestershire, United Kingdom) to assess the UCA population average diameter and surface charge of the agents. For particle sizing, 1mg of dry UCA was suspended in 1.5mL DI water by vortexing for 10 seconds, transferred to a

clear plastic cuvette, and measured in triplicate at room temperature. The peak particle size by number was recorded and reported as an average. The polydispersity index (PDI) was also recorded as an indication of size distribution for the population. Zeta potential was measured by suspending 1mg dry UCA in 1mL DI water, loading the suspension into a Malvern Zeta Capillary Cuvette, and reading in triplicate at room temperature. Detailed protocols for these tests are included in Appendix A.

3.2.3.5 Scanning Electron Microscopy

Scanning electron microscope (SEM) images were taken with a Philips FEI XL30 Environmental SEM (Hillsboro, OR) to assess the MB surface morphology. One milligram of dried UCA was gently fixed onto an aluminum stub using conductive adhesive tape and sputter coated with platinum-palladium for 40 seconds using a Denton Desk-II sputtering system (Denton Vacuum, Moorestown, NJ). Imaging was performed under hi-vac conditions, at an average of $7x10^{-6}$ mbar vacuum pressure. Images were taken at varying magnifications at an accelerating voltage of 5.0kV, working distance of 11mm, and spot size of 3. Three images are taken from a random location on each SEM stub holding the UCA sample. All SEM imaging and sample preparation was performed at the Drexel University Centralized Research Facility Materials Characterization Lab.

3.2.3.6 Drug Encapsulation Measurements

Amounts of encapsulated Dox were determined by dissolving 2mg of dry Dox-loaded UCA in 2mL DMSO by vortexing for 30 seconds. Fluorescence of the solution was then read in triplicate using a Tecan fluorimeter (Männedorf, Switzerland) at an

excitation wavelength of 495nm and an emission wavelength of 585nm. Dox concentration was then calculated based on a standard curve of known amounts of Dox in DMSO and reported as an average. Encapsulation efficiency was determined using Equation 19:

$$Encapsulation\ Efficiency = \frac{Final\ Dox\ Concentration}{Loading\ Dox\ Concentration} \quad \text{(Eq. 19)}$$

Encapsulation of Dox within the UCA shell was also visualized with confocal microscopy with assistance from Nutte Tarn Teraphongphom. Confocal microscopy was performed using an Olympus IX81 microscope equipped with Olympus Fluorview 1.7b software (Olympus, Tokyo, Japan). One milligram of dry UCA was suspended in 1mL 1x PBS by vortexing, and a droplet of the solution was placed onto a glass microscope slide. The UCA were observed at 100x magnification with the use of microscope oil immersion.

3.2.3.7 Drug Release *in vitro*

Initial drug release from Dox-loaded UCA, commonly known as burst release effect, was measured for each type of agent by suspending 10mg of dry UCA in 50mL of 1x PBS at 37°C while stirring. This was performed both with and without the presence of a focused ultrasound beam to determine any difference in release behavior. One milliliter of the solution was removed immediately after suspension and every two minutes for 20 minutes while stirring. Immediately after sampling, samples were centrifuged at 7500g for 2 minutes to pellet the polymer. A 200μL sample of the supernatant was read in triplicate using a Tecan fluorimeter at an excitation wavelength of 495nm and an emission wavelength of 585nm. Free Dox concentration was then calculated using a

calibration curve of known amounts of Dox in PBS, and expressed as a percent of total concentration encapsulated within the UCA.

Long-term release profiles of Dox encapsulated within UCA were measured to determine the potential for sustained drug release over time, both with and without exposure to US. Samples were weighed to have a UCA concentration equivalent to that of 6mg unloaded native 100% PLA UCA and were suspended in 50mL of 1x PBS at 37°C. The insonated group was then continuously stirred while insonated for 20 minutes in the same setup used for the dose and time response testing at 0.94 MPa peak negative pressure (Energy Level 4) and a PRF of 5000Hz. Following insonation samples were transferred to 50mL centrifuge tubes and rotated end-over-end in an incubator at 37°C. Non-insonated samples were suspended in PBS directly in the 50mL centrifuge tubes. For Dox measurement, samples were centrifuged at 48,000g for 20 minutes (SorvallWX Ultra80 Ultracentrifuge, AH-629 rotor, Thermo Electron Corp, Waltham, MA). The supernatant was collected for measurement, and the pellet was resuspended in 50mL fresh 1x PBS to maintain sink conditions. Resuspended samples were then returned to the rotator in the incubator until the next reading. Samples of 200μL from the collected supernatant were measured for Dox release by reading fluorescence using a Tecan Fluorimeter at an excitation wavelength of 495nm and an emission wavelength of 585nm. Measurements were taken at 1hr, 2hr, 4hr, 6hr, 8hr, 12hr, 24hr, 36hr, 48hr, 72hr, 96hr, 120hr, 144hr, and 168hr after initial suspension. Concentrations of released Dox were determined in triplicate using a standard curve of known amounts of Dox in 1x PBS.

3.2.3.8 LipidPEG Quantification

PEG loading via lipid anchoring into the MB polymeric shell was quantified using a PEG lipid conjugated with a carboxyfluorescein (CF) tag (1,2-distearoyl-sn-glycero-3-phosphoethanolamine-n-[carboxyfluorescein(polyethylene glycol)2000] incorporated into the polymer solution prior to the first emulsion at a concentration of 1 wt%. A 1mg sample of the resulting UCA was dissolved in DMSO and read in triplicate with a Tecan Fluorimeter (λ_{ex} 485nm, λ_{em} 523nm) and compared against a standard curve of CF-tagged LipidPEG. Anchoring of CF-tagged LipidPEG within the UCA shell was also visualized with confocal microscopy with assistance from Nutte Tarn Teraphongphom, as described previously.

3.2.3.9 UCA Counting

UCA counting was performed using a BD Accuri C6 flow cytometer (BD Biosciences, Franklin Lakes, NJ). Dried UCA were suspended in DI water at a concentration of 20µg UCA/mL DI water. An aliquot of 0.5mL of the diluted UCA solution was added to a round-bottomed 2mL Eppendorf tube, along with 10µL of UV CountBright absolute counting beads (Life Technologies, Carlsbad, CA). Counting beads and UCA were separated using Forward Scatter A and Phycoerythrun-A filters. A detailed protocol for this test is included in Appendix A.

3.2.3.10 Immunogenicity Evaluations

C3 complement activation was determined by modifying a procedure performed by Borden and colleagues to the properties of our microbubbles [140, 154]. All testing

was performed under sterile conditions with certified sterile endotoxin-free materials. One milligram UCA were exposed to UV light for 60 minutes for sterilization prior to testing. UV-irradiated UCA were suspended in a solution of 1.5mL PBS with 1mL human complement-preserved serum and shaken end over end at room temperature for 30min. This suspension was then centrifuged at 300g for 3min to precipitate the MB, and the supernatant was collected for C3a activation analysis and diluted 1:5 with 20mM EDTA. The amount of activated C3a per MB species was assayed using a Human C3 ELISA kit using the manufacturer's instructions. Absorbance was read at 570nm with a Tecan Fluorimeter in triplicate and C3a activation reported as an average.

Samples were evaluated for endotoxin contamination using a Pierce LAL Chromogenic Endotoxin Quantitation Kit. All testing was performed under sterile conditions with certified sterile endotoxin-free materials. One milligram UCA were exposed to UV light for 60 minutes to inhibit biological activity and for sterilization. UV-irradiated UCA were suspended in 25mL endotoxin-free water for testing. The endotoxin quantitation assay was performed using the manufacturer's instructions. Absorbance was read at 405nm with a Tecan Fluorimeter in triplicate and endotoxin concentration was reported as an average.

3.2.4 *In vitro* Evaluation of UCA Against Breast Cancer Cells

3.2.4.1 Cell Culture Techniques

MDA-MB-231 human breast adenocarcinoma cells were grown in DMEM medium with L-glutamine, sodium pyruvate, and 4.5 g/L glucose supplemented with 10% (v/v) fetal bovine serum (FBS) and 1% (v/v) antibiotic (Penicillin/Streptomycin). MCF7 human breast adenocarcinoma cells were grown in EMEM medium supplemented with

10% (v/v) FBS and 0.01 mg/mL human recombinant insulin. MCF-12A human breast epithelial cells were grown in a 1:1 mixture of DMEM and Ham's F12 media supplemented with 20 ng/mL human epidermal growth factor, 100 ng/mL cholera toxin, 0.01 mg/mL bovine insulin, 500 ng/mL hydrocortisone, and 5% (v/v) horse serum. All three populations of cells were maintained in a humidified incubator at 37°C with a 5% CO_2 atmosphere.

3.2.4.2 Treatment and Evaluation Techniques

Cells were plated in 6-well plates at a concentration of $0.6x10^5$ cells per well, and grown to 70-80% confluency for testing. Cells were treated with 1.5mg of UCA or n-Sh species suspended in 3mL of the appropriate medium, as explained in Table 3.1.

Table 3.1: Cell treatments arranges by type of UCA shell material and functionalization.

No Treatment	100% PLA UCA	100% PLA n-Sh	5% PEG-PLA UCA	5% PEG-PLA n-Sh	1% LipidPEG UCA	1% LipidPEG n-Sh
Free Dox	100% PLA UCA	100% PLA n-Sh	5% PEG-PLA UCA	5% PEG-PLA n-Sh	1% LipidPEG UCA	1% LipidPEG n-Sh
Free TRAIL	100% PLA UCA + Free Dox	100% PLA n-Sh + Free Dox	5% PEG-PLA UCA + Free Dox	5% PEG-PLA n-Sh + Free Dox	1% LipidPEG UCA + Free Dox	1% LipidPEG n-Sh + Free Dox
Free Dox + Free TRAIL	100% PLA UCA + Free TRAIL	100% PLA n-Sh + Free TRAIL	5% PEG-PLA UCA + Free TRAIL	5% PEG-PLA n-Sh + Free TRAIL	1% LipidPEG UCA + Free TRAIL	1% LipidPEG n-Sh + Free TRAIL
	100% PLA UCA + Free Dox + Free TRAIL	100% PLA n-Sh + Free Dox + Free TRAIL	5% PEG-PLA UCA + Free Dox + Free TRAIL	5% PEG-PLA n-Sh + Free Dox + Free TRAIL	1% LipidPEG UCA + Free Dox + Free TRAIL	1% LipidPEG n-Sh + Free Dox + Free TRAIL
	Dox-loaded 100% PLA UCA	Dox-loaded 100% PLA n-Sh	Dox-loaded 5% PEG-PLA UCA	Dox-loaded 5% PEG-PLA n-Sh	Dox-loaded 1% LipidPEG UCA	Dox-loaded 1% LipidPEG n-Sh
	TRAIL-loaded 100% PLA UCA	TRAIL-loaded 100% PLA n-Sh	TRAIL-loaded 5% PEG-PLA UCA	TRAIL-loaded 5% PEG-PLA n-Sh	TRAIL-loaded 1% LipidPEG UCA	TRAIL-loaded 1% LipidPEG n-Sh
	TRAIL-loaded 100% PLA UCA + Free Dox	TRAIL-loaded 100% PLA n-Sh + Free Dox	TRAIL-loaded 5% PEG-PLA UCA + Free Dox	TRAIL-loaded 5% PEG-PLA n-Sh + Free Dox	TRAIL-loaded 1% LipidPEG UCA + Free Dox	TRAIL-loaded 1% LipidPEG n-Sh + Free Dox
	Dox- and TRAIL-loaded 100% PLA UCA	Dox- and TRAIL-loaded 100% PLA n-Sh	Dox- and TRAIL-loaded 5% PEG-PLA UCA	Dox- and TRAIL-loaded 5% PEG-PLA n-Sh	Dox- and TRAIL-loaded 1% LipidPEG UCA	Dox- and TRAIL-loaded 1% LipidPEG n-Sh

Free Dox was added at a concentration of 1μM per well, and free TRAIL was added at a concentration of 100ng/well. For treatment, n-Sh were prepared by insonating UCA as described previously for a period of 20 minutes at a peak negative pressure of 0.94MPa (energy level 4) and a PRF of 100Hz. The resulting particles were then frozen at -20°C overnight and lyophilized for 48 hours to obtain the post-insonation n-Sh. Both the UCA and n-Sh were irradiated under UV light for 60 minutes for sterilization.

Growth media was removed from the cells to be replaced by the treatment media. Treatments were applied to the cells, which were then incubated in a humidified incubator at 37°C with a 5% CO_2 atmosphere for 24 hours. After 24 hours, the treatment media was removed from the wells and the cells were washed with 1mL of 1x PBS at room temperature. The treatment media and PBS wash solutions were discarded, as they contained mostly microbubbles and n-Sh that would obscure the flow cytometry readings. Once washed, the cells were incubated at 37°C with 1mL of Accutase cell detachment solution for 20 minutes. The detached cells were then collected, and the wells were washed with 1mL 1x PBS at room temperature. Both the Accutase solution and PBS wash were combined in a 2mL round-bottom Eppendorf tube, and the cells were centrifuged at 4000rpm at 4°C for 7 minutes to collect the cell pellet. The cells were washed in 1mL cold PBS and centrifuged at 4000rpm at 4°C for 7 minutes. After the final wash, the cell pellet was then suspended in 200μL of cold 1x annexin binding buffer, and 5μL FITC annexin V and 5μL propidium iodide were added to this solution. The cell suspension was incubated in the dark at room temperature for 15 minutes, when an additional 200μL of cold 1x annexin binding buffer was added to stop staining.

Cell fates were quantified using a BD Accuri C6 flow cytometer calibrated for multi-color analysis of stained cells. Cells suspensions were evaluated by sampling for 2 minutes at fast fluidics (66µL/min), followed by a 30 second wash of the sampling needle with DI water and plate agitation between each sample. Tests were performed in triplicate, and results were reported as an average of the cell population for each cell fate. An additional round of cell testing was performed to acquire fluorescent images of the cell fates. The treatment procedure was followed as explained previously, but cells were washed three times with 1x PBS in the wells, and then stained with Alexa Fluor 488 annexin V for apoptotic cells, red-fluorescent propidium iodide for dead cells, and Hoescht blue for live cells. Early apoptotic cells are positive for annexin V (green) only, while late apoptotic and necrotic cells are positive for both annexin V and PI (red and green). Live cells are positive for Hoescht (blue) only. Apoptosis was qualitatively assessed visually with fluorescent microscopy using an EVOS FL Cell Imaging System (Thermo Fisher Scientific, Waltham, MA).

3.2.5 Statistical Analysis

All data are expressed as a mean value ± standard error of the mean calculated with Microsoft Excel (Microsoft Corporation, Redmond, WA). Statistically significant differences for multiple groups were determined using a one-way ANOVA with Bonferroni correction for multiple comparisons and Tukey's multiple comparison post-test when appropriate. These tests were used to determine significance for the acoustic evaluations, immunogenic assays, and cell viability results. Differences were evaluated across all groups, and also within each group for more robust analysis. Statistical

significance between individual groups for pre- and post-US size comparison was determined using a matched pairs Student's t-test. All statistical testing was done using Prism 7 (GraphPad, San Diego, CA) using α=0.05 significance level. Error bars were displayed as standard error about the mean (SEAM).

4. RESULTS AND DISCUSSION

4.1 Development and Characterization of a TRAIL-Ligated UCA

This study serves as a feasibility study for the functionalization of PLA microbubbles with tumor necrosis factor-related apoptosis inducing ligand (TRAIL) and the ability of these agents to interact with US for targeting and therapeutic applications. Building upon previous studies with TRAIL and microbubbles, we were specifically interested in determining the effect of TRAIL ligation on the acoustic behavior of the UCA, as well as the effect of insonation and cavitation on the apoptotic activity of TRAIL.

4.1.1 Effects of TRAIL Ligation on Acoustic Enhancement and Stability

To assess whether the agents retained their function as contrast agents, acoustic enhancement and stability were assessed. The cumulative dose response results are shown in Figure 4.1A, where a 5-8 decibel (dB) reduction in maximum enhancement at a value of 12μg/mL is seen in the TRAIL-UCA groups when compared to blank PLA controls at the same dose, suggesting that UCA shell properties are altered during maleimide attachment of TRAIL.

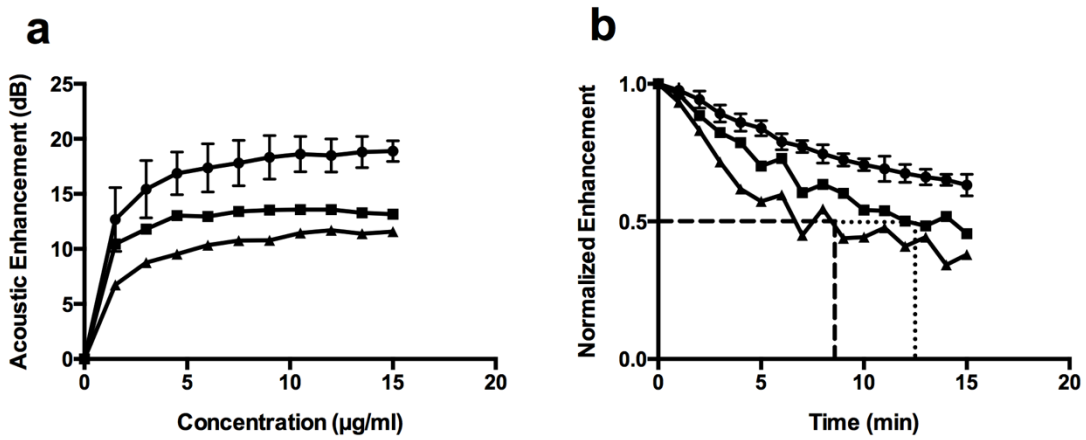

Figure 4.1: Acoustic evaluation of UCA. a) Cumulative acoustic enhancement of each agent, 15µg/ml doses added and read every 30 seconds, with cumulative enhancement reported in dB. b) Acoustic stability of each agent, normalized to 1, with readings taken every minute, dotted lines indicate half-life of agent. ▣ Blank PLA (n=3), ● Non-linker TRAIL-UCA (n=1), ⏏ Ligated TRAIL-UCA (n=1). Error bars = SEAM.

Despite this modification-induced reduction, both test groups were still able to reflect a clinically-relevant US signal as judged by our previous *in vivo* work [89], suggesting that TRAIL-UCA are still effective contrast agents. In fact, Figure 4.1B suggests that the process of TRAIL ligation may actually enhance acoustically-triggered n-Sh production, since the stability in the US beam is reduced for these groups compared to the blank PLA control. The acoustic half-life, or time until the enhancement signal is halved, is assumed to be due to UCA rupture. For comparison, this half-life was approximately 9 minutes for the ligated TRAIL-UCA and approximately 12 minutes for the surface adsorbed TRAIL-UCA, whereas the half-life of the control blank UCA is greater than 15 minutes. However, there is not a large enough difference between the ligated UCA and non-linker controls ($p>0.05$) to suggest that the ligation itself has a large effect on the UCA shell properties.

Overall, these results suggest that the aqueous environment to which the UCA are exposed during TRAIL attachment modifies the UCA structure, likely due to swelling and hydrolysis of the PLA. As shown by Proikakis and colleagues, the nature and pH of aqueous buffer has a significant effect on the swelling behavior of solid PLA tablets, which can be even more disruptive to the shell structure of hollow PLA microbubbles during TRAIL ligation and subsequent lyophilization [155]. The results also indicate that the agents are still capable of functioning as contrast agents that shatter when exposed to US. The larger dose that is required to reach maximum enhancement for TRAIL-UCA is probably due to the fact that a portion of the UCA are destroyed or rendered less echogenic during the ligation process, resulting in a lower concentration of intact UCA.

4.1.2 Effects of TRAIL Ligation on Surface Morphology and UCA Size

TRAIL-UCA and unmodified blank UCA were characterized by evaluating surface morphology and average diameter before and after modification. As shown in Figure 4.2, SEM images demonstrate that TRAIL attachment does not significantly affect surface morphology as pre- and post-ligation images show smooth, spherical UCA.

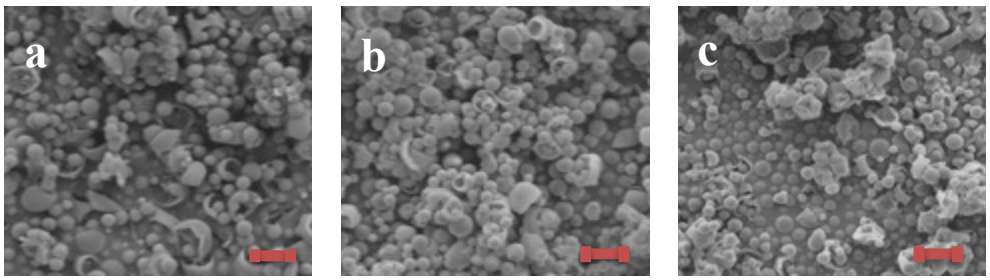

Figure 4.2: SEM images of UCA. a) Pre-ligation blank UCA. b) Ligated TRAIL-UCA. c) Non-linker control TRAIL-UCA. Accelerating voltage 5kV, spot size 3, magnification 2500x, scale bar 4μm.

Additionally, these SEM images were used to measure UCA diameter, and the results are shown in Figure 4.3. While the average diameter of blank UCA (1.055±0.060μm) and non-linker TRAIL-UCA (0.999±0.066μm) were nearly identical, the SEM images indicate a shift in the size distribution for the non-linker controls. The average diameter of TRAIL-ligated UCA (1.190±0.072μm) was significantly larger than the controls (p=0.0642).

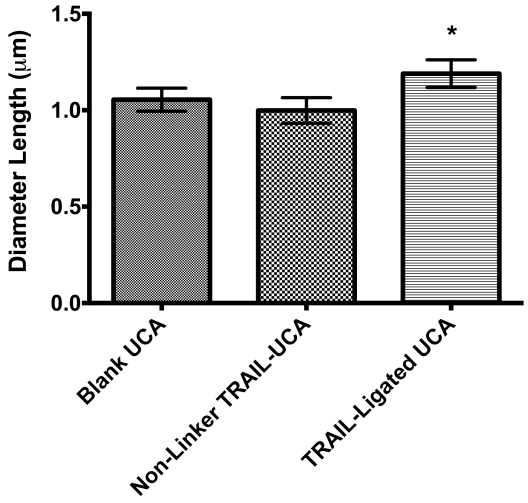

Figure 4.3: Average UCA diameter, as measured from SEM images. *p=0.0642.

These changes in size can be expected, due to structural modifications, especially swelling and hydrolysis, being made to the UCA shell during the ligation process [155]. Nonetheless, all of these agents are within the desired 1-2μm range [88] for average diameter, and are therefore acceptable for these experiments. Characterization of these agents determined that they would be considered viable based on our design constraints, allowing progression into *in vitro* cell studies.

4.1.3 *In vitro* Tumoricidal Activity of TRAIL-UCA

To evaluate these agents for potential use in targeted cancer therapy, we used a human breast cancer cell line, MDA-MB-231, which is known to be apoptotically sensitive to TRAIL. As a control population, we also used 3T3 fibroblasts to represent TRAIL-insensitive non-cancerous cells. Cell fates were determined with a live/dead assay, fluorescent microscopy, and counted using customized macros in NIH Image J.

Cells were treated with modified cell culture media consisting of the appropriate intact UCA or n-Sh population suspended in the medium (Table 4.1). The treatment groups were: intact non-linker TRAIL-UCA, non-linker n-Sh after 30 minutes of insonation, intact ligated TRAIL-UCA, and ligated n-Sh after 30 minutes of insonation. The control groups were: no treatment (negative control), intact blank PLA UCA (1mg, negative control), and free TRAIL (10ng, positive control representing the maximum TRAIL concentration used in the ligation step).

Table 4.1 Treatment groups for in vitro cell studies, both TRAIL-sensitive and TRAIL-resistant cell lines.

Negative Controls	Positive Controls	Test Group 1	Test Group 2
No Treatment	Free TRAIL	Intact Non-linker UCA	Intact TRAIL-ligated UCA
Intact Blank UCA		Non-linker n-Sh (30 mins insonation)	TRAIL-ligated n-Sh (30 mins insonation)

The live/dead assay results for the MDA-MB-231 breast cancer cells are shown in Figure 4.4. As expected, there is little cell death in both negative controls (Figure 4.4A – no treatment, 2.299±0.347% cell death, and Fig. Figure 4.4B – intact blank UCA, 0.519±0.216% cell death), while a visibly large degree of cell death (32.820±0.796%) is evident in the free TRAIL positive control (Figure 4.4C). Cell death is characterized by both the red stained cells and the large black patches, which corresponds to areas where dead cells detached from the plate, with subsequent loss due to washing. For the ligated TRAIL groups, the live/dead assay indicates cell death for both intact UCA (8.296±0.169%, Figure 4.4D) and n-Sh (38.420±0.020%, Figure 4.4E). Figure 4.4 clearly shows that the ligated TRAIL n-Sh were much more effective in inducing cell death in these susceptible cells. In fact, TRAIL-ligated n-Sh induced significantly more cell death than the intact TRAIL-UCA ($p<0.0001$). Additionally, cell death induced by TRAIL-ligated n-Sh is significantly greater than treatment with free TRAIL ($p<0.0001$). However, since the images show large areas where dead cells detached and were lost during washing and staining steps, this result could be even more significant. In agreement with our expectations, we saw little cell death in both control non-linker groups (Figure 4.4F – intact non-linker UCA, 2.397±0.299%, and Figure 4.4G – non-linker n-Sh, 2.020±1.358%), which is not significantly different from the no treatment group ($p=0.8502$ and $p=0.8608$, respectively). The non-linker control group results indicate that the observed cell death effects are not incidental events due to release of physically adhered TRAIL, and that the active TRAIL molecules are those that are ligated to the UCA surface.

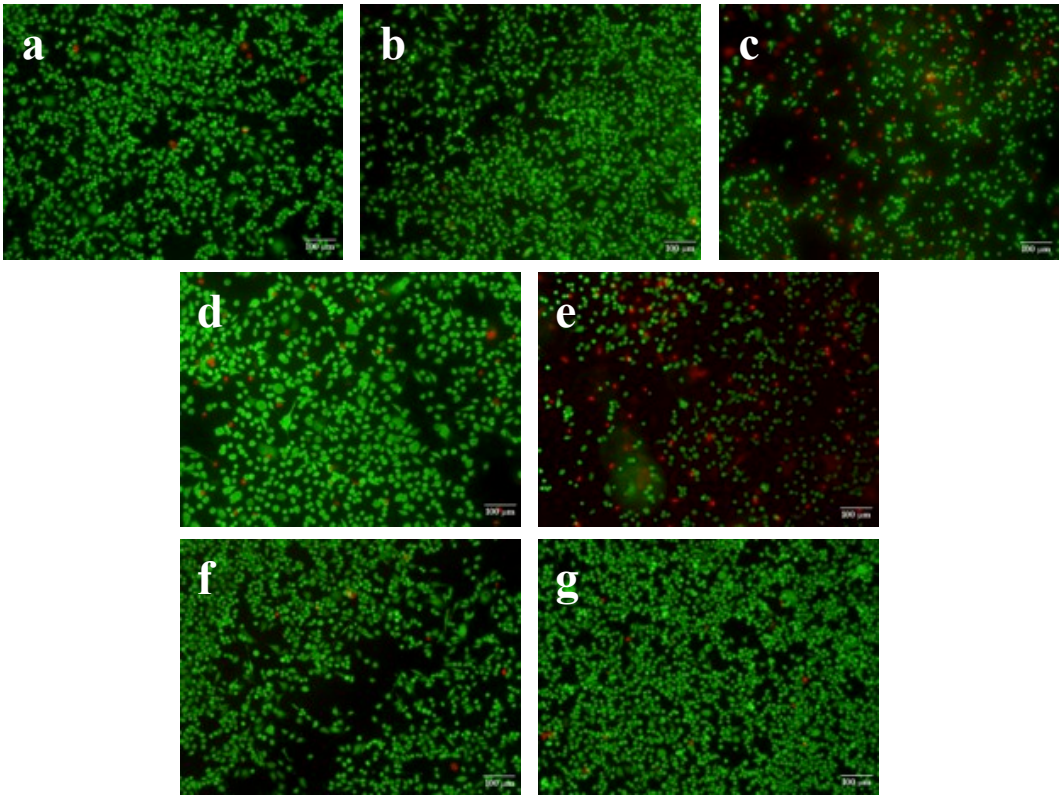

Figure 4.4: Fluorescent images of MDA-MB-231 human breast cancer cells under various treatments. Green indicates live cells, red indicates dead cells, scale bar 100µm. a) no treatment (negative control), b) intact blank PLA UCA (negative control), c) free TRAIL (positive control), d) intact ligated TRAIL-UCA, e) ligated n-Sh, g) intact non-linker TRAIL-UCA, and g) non-linker n-Sh.

On the other hand, very little cell death is observed in the TRAIL-insensitive 3T3 fibroblasts, as expected (Figure 4.5). 3T3 fibroblast cell were grown to 30% confluence, and after treatment very few, if any, red-stained dead cells are visible in any of the test groups. For comparison, the free TRAIL group (C) also shows very few dead cells, indicating that TRAIL has no effect on non-sensitive healthy cells. All 3T3 fibroblast samples exhibited less than 3% cell death in images collected (Table 4.2). In all of these

samples, the dark patches represent areas that were never populated with cells, and did not change throughout the experiment.

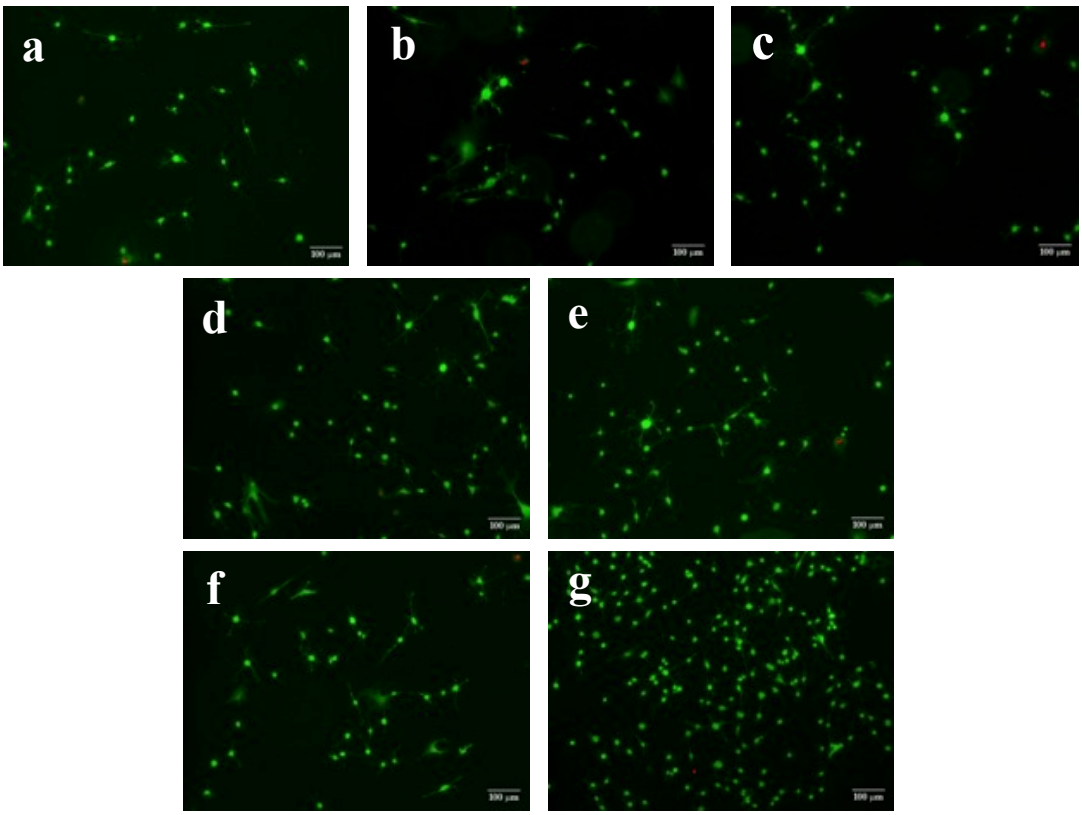

Figure 4.5: Fluorescent images of 3T3 fibroblasts under various treatments. Green indicates live cells, red indicates dead cells, scale bar 100µm. a) no treatment (negative control), b) intact blank PLA UCA (negative control), c) free TRAIL (positive control), d) intact ligated TRAIL-UCA, e) ligated n-Sh, f) intact non-linker TRAIL-UCA, and g) non-linker n-Sh.

Table 4.2: Cell death percentages for 3T3 fibroblast cells.

	Cell Death (%)
No Treatment (Negative Control)	1.742±0.076%
Intact Blank PLA UCA (Negative Control)	2.548±0.016%
Free TRAIL (Positive Control)	1.669±0.056%
Intact Ligated TRAIL-UCA	2.753±0.051%
Ligated TRAIL n-Sh	0.799±0.041%
Intact Non-linker TRAIL-UCA	1.106±0.031%
Non-linker TRAIL n-Sh	0.659±0.267%

For comparison, Figure 4.6 shows cytotoxicity of the TRAIL-ligated treatments and control groups against both cell types.

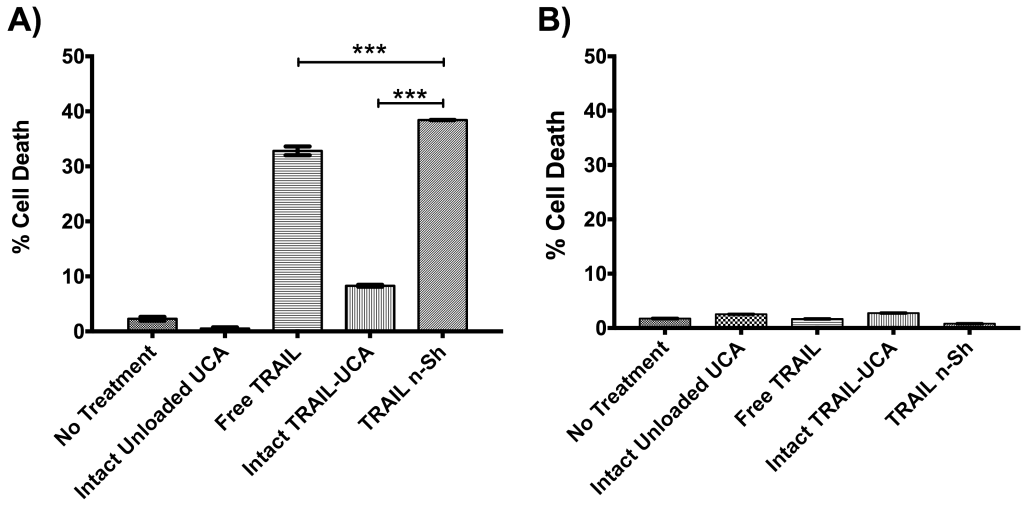

Figure 4.6: Cytotoxicity of TRAIL-ligated treatments and controls against cells of interest. A) MDA-MB-231 breast cancer cell cytotoxicity results, B) 3T3 fibroblast cytotoxicity results. ***$p<0.0001$, error bars = SEAM, n=2.

There was no significant difference between any of the fibroblast groups, which all showed little to no cell death, as expected since these cells are known to be insensitive to the apoptotic activity of TRAIL [156]. We also saw significant cell death in the MDA-MB-231 cells when they were exposed to TRAIL, a trend which has been observed in numerous studies [44, 150, 151, 157]. Interestingly, the TRAIL-ligated n-Sh showed significantly higher cell death than the intact TRAIL-ligated UCA ($p<0.0001$). This suggests that the full surface area of the UCA was utilized, as the n-Sh more effectively covered and treated the cells than only a portion of each UCA at its contact point with the cell surface. Overall, these studies demonstrated the selective efficacy of TRAIL against susceptible breast cancer cells, but not resistant or normal cells, that doxorubicin sensitized the resistant cells and that ligation to the UCA surface and subsequent UCA shattering did not negatively impact TRAIL apoptotic activity.

4.1.4 TRAIL Ligation Conclusions

In conclusion, ligation using maleimide chemistry was an effective method for attaching TRAIL directly to the surface of UCA, and these modified UCA maintained both acoustic properties and apoptotic activity towards susceptible cancer cells but not toward a healthy cell model. Additionally, MDA-MB-231 breast cancer cells treated with n-Sh generated by US treatment of ligated TRAIL-UCA showed the greatest extent of apoptosis/cell death among test groups ($p<0.0001$). Ultrasound-generated particles had a more extensive effect on the sensitive cells, suggesting that the treatment generated a greater number of particles that could interact with a larger number of cells. Ligation did not significantly affect UCA size or morphology, resulting in spherical agents that can easily pass through the vasculature to reach the target tumor tissue.

4.2 Development and Characterization of UCA with Reduced Immunogenicity

Two different techniques have been developed for incorporating PEG into our PLA UCA in an effort to inhibit opsonization and immunogenicity to the circulating agent and n-Sh while retaining the acoustic behavior of the UCA. Our initial loading technique consisted of incorporating small proportions of PEG-PLA copolymers combined with PLA during the double emulsion fabrication process, where the PEG molecule is a part of the UCA shell. The second incorporation method involved the use of small proportions of functionalized PEG phospholipids, where the phospholipid head embeds itself into the PLA shell and the PEG chains extend out from the surface to create a physical brush surrounding the UCA. Loading methods were optimized to provide UCA with strong acoustic enhancement, tight size distribution preferably in the 1-2μm range, smooth surface morphology, and reduced immunogenicity for future targeting and drug delivery applications. Formulation selection and optimization are discussed in terms of these properties over the remainder of the subsection.

4.2.1 Loading Efficiency of LipidPEG Molecules

A primary concern with the LipidPEG method of UCA PEGylation was the amount of surface coverage using PEG phospholipids, since previously this had only been attempted with lipid microcapsules where phospholipid incorporation is more straightforward [140, 147, 154]. PEG lipid fluorescently-tagged with carboxyfluorescein (CF) was loaded into the LipidPEG-type UCA during the organic phase at a 1 wt% ratio to the PLA, chosen based on the favorable characteristics for this formulation. Readings of the resulting microbubbles indicate 97.77% PEG lipid loading efficiency, with 13.97

µg PEG lipid per mg of UCA, based on the standard curve of known amounts of CF-tagged LipidPEG in DMSO (Figure A.1).

This high degree of loading is in line with loading efficiency observed with lipid-based microbubbles [140, 147, 154], which is surprising given the lack of studies investigating this method with polymeric microbubbles. Loading was confirmed visually with confocal microscopy (Figure 4.7), where the CF tag on the LipidPEG molecule fluoresces green within the UCA shell.

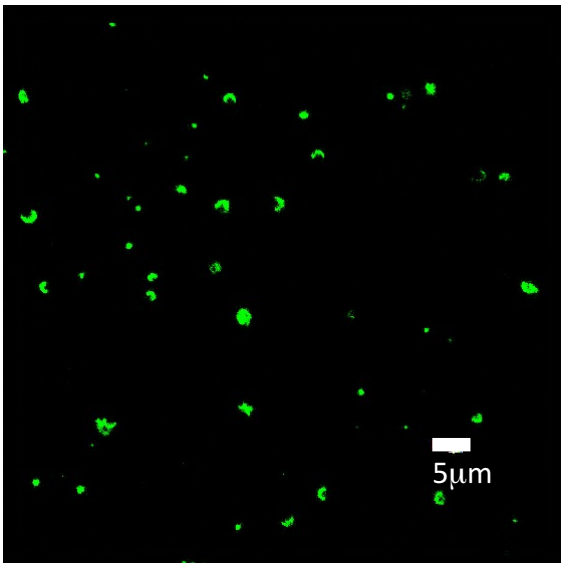

Figure 4.7: Confocal microscopy image of UCA loaded with CF-tagged LipidPEG molecules. Size bar = 5µm, , λ_{ex} =495nm, , λ_{em} = 517nm.

Understanding the level of PEG incorporation is important when assessing whether the agents elicit an immune response, as higher expression of PEG groups on the UCA surface should translate into higher degrees of immune shielding [137, 138, 140, 147, 154]. The results indicate that the expected loading of LipidPEG in the resulting

UCA is very close to the initial loading, suggesting an efficient PEGylation method for polymeric UCA.

4.2.2 Effects of PEGylation on UCA Quantity

Concentration of each UCA sample was determined by counting the number of microbubbles present in a known weight using a flow cytometer (Figure 4.8).

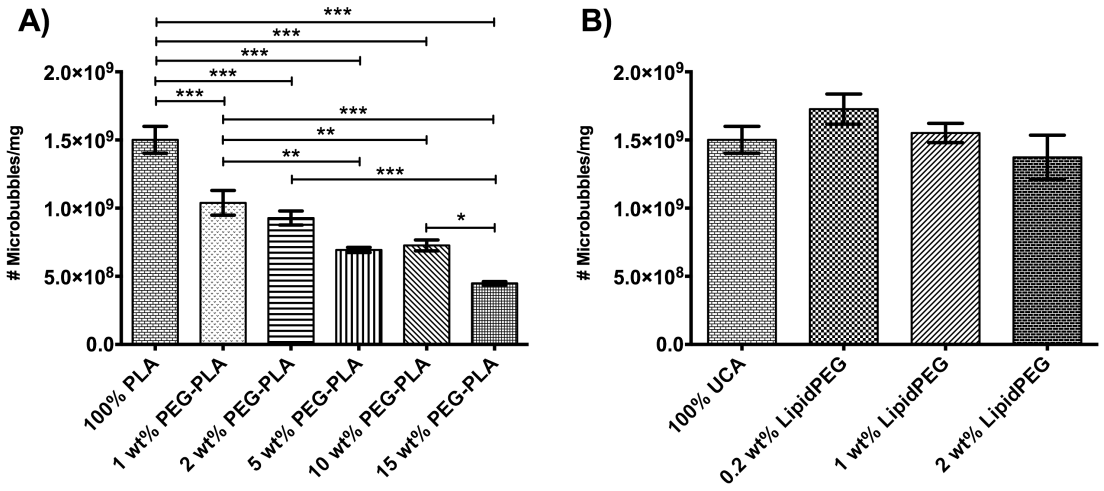

Figure 4.8: Concentration of UCA by weight. A) PEG-PLA groups, B) LipidPEG groups. Error bars = SEAM, n=3, *p=0.0284, **p=0.0031 for 1 wt% PEG-PLA to 5 wt% PEG-PLA, **p=0.0095 for 1 wt% PEG-PLA to 10 wt% PEG-PLA, ***p<0.0001.

There is a somewhat linear trend (R^2=0.7023) between increasing proportions of PEG-PLA and reduction in concentration of UCA per milligram, and all PEG-PLA formulations resulted in less UCA/mg than 100% PLA UCA (p<0.0001, Figure 4.8A). There was no significant different between the concentration of 1 wt% and 2 wt% PEG-PLA UCA, nor between 5 wt% and 10 wt% PEG-PLA UCA. Compared to 1 wt% PEG-PLA, there are significantly less 5 wt% PEG-PLA UCA (p=0.0031), 10 wt% PEG-PLA

UCA ($p=0.0095$), and 15 wt% PEG-PLA UCA ($p<0.0001$). There was also a significant reduction in UCA concentration between 2 wt% and 15 wt% PEG-PLA groups ($p<0.0001$). The 15 wt% PEG-PLA group was also significantly less than the 10 wt% group ($p=0.0284$), with this group comprising approximately half an order of magnitude less microbubbles/mg than 100% PLA ($p<0.0001$). This trend could be due, in part, to the interaction of co-polymer end groups within the shell, making the UCA shells thicker and heavier as more PEG-PLA is added to the formulation [158, 159]. Additionally, formulations including 5 wt% PEG-PLA and higher exhibited a bimodal distribution of intact microspheres and non-spherical debris which could skew the measurement of spheres in this method. There were no significant differences in concentration of UCA/mg in the LipidPEG group, both when compared to 100% PLA UCA and among all three formulation proportions (Figure 4.8B). This suggests that the lipid anchoring does not influence the double emulsion process, and produces similar populations to the 100% PLA native group.

We demonstrated a dose-dependent reduction in UCA quantity with increasing PEG-PLA proportions, suggesting structural changes within the polymeric shell in response to the additional co-block-polymer groups since this trend was not observed in the LipidPEG group. These results are important for proper preparation of future functionalized agents for treatment groups, to help standardize the number of microbubbles and subsequently co-encapsulated drug administered with each treatment.

4.2.3 Effects of PEGylation on Acoustic Enhancement and Stability

Microbubbles at resonance undergo inertial cavitation and shatter. Incorporation of PEGylated species will affect the material properties of the shell and hence behavior

within an US beam. Therefore, the PEGylated UCA were tested acoustically to determine the degree to which they can still interact with the US beam.

Previous studies were performed in our lab to evaluate a series of incorporations between 100 wt% PLA and 100 wt% PEG-PLA together with 25 and 50 wt% PEG-PLA to determine the relative proportions of PEGylated and non-PEGylated polymer upon which to focus [160]. Agents with 100 wt% PEG-PLA were not echogenic above background, and higher proportions of PLA resulted in increasingly improved acoustic performance. Figure 4.9 displays the linear trend between wt% PEG-PLA and reduction in echogenicity observed in these preliminary studies, which informed our decision to study the formulation range 1, 2, 5, 10, and 15 wt% PEG-PLA in detail. The linear regression line plotted from the preliminary study data (blue diamonds -◆-) was used to predict the echogenicity values for our ratios of interest (orange squares -■-). The actual echogenicity data collected in this study is plotted to show correlation with the trend (purple circles -●-).

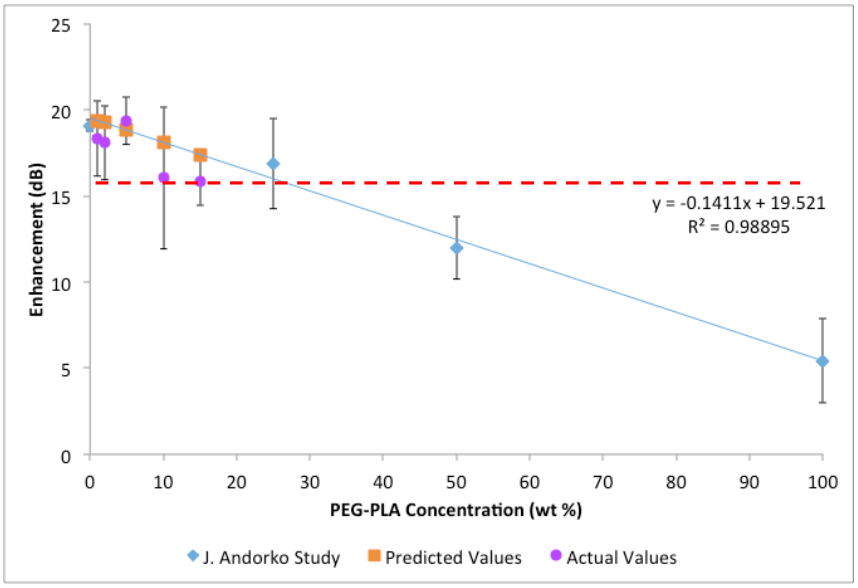

Figure 4.9: Effect of PEG-PLA incorporation on echogenicity. -◆- Average maximum echogenicity data from preliminary study performed previously. -■- Predicted maximum echogenicity for PEG-PLA ratios of interest. -●- Actual maximum echogenicity data from PEG-PLA ratios of interest in this study. Error bars represent SEAM, n=3. Linear trend with R^2=0.98895. Dotted line represents 16dB cutoff for effective interaction with US [5, 150, 160].

As expected, shell modification had a demonstrated effect on acoustic response (proportions of interest shown in Figure 4.10 and summarized in Table 4.3). The dose needed to achieve maximum enhancement nearly doubled with the addition of 1 wt% PEG-PLA, requiring 13.5µg/mL UCA compared to 7.5µg/mL UCA for the unmodified 100% PLA UCA, and above 5 wt% PEG-PLA at least 15µg/mL was needed. With 10 wt% PEG-PLA, there was also a significant decrease in the maximum enhancement compared to the 100% PLA UCA ($p=0.0214$). Similar losses of echogenic response were observed with LipidPEG incorporation, with a higher dose needed for maximum enhancement (9µg/mL for 0.2 wt%, and 13.5µg/mL for both 1 and 2 wt%). Incorporation of 2 wt% LipidPEG significantly reduced echogenicity ($p<0.0001$), possibly by inhibiting cavitation among fewer intact UCA

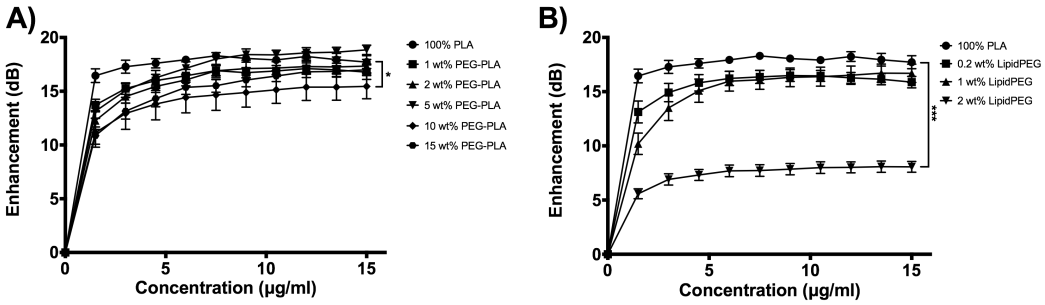

Figure 4.10: Acoustic results plotted as dose response curves. A) PEG-PLA formulations, B) LipidPEG formulations. Error bars = SEAM, n=5, *p=0.0214, ***p<0.0001.

Table 4.3: Acoustic properties of PLA, PEG-PLA, and LipidPEG UCA groups.

	Initial dB Enhancement (Dose in μg/ml)	Maximum dB Enhancement (Dose in μg/ml)	US Half-life at Lower MI (min)	US Half-life at Higher MI (min)
100% PLA UCA	16.45±0.63 (1.5 μg/ml)	18.30±0.25 (7.5 μg/ml)	>15	3
1 wt% PEG-PLA UCA	13.63±0.67 (1.5 μg/ml)	18.35±0.58 (13.5 μg/ml)	>15	4
2 wt% PEG-PLA UCA	12.67±1.00 (1.5 μg/ml)	18.09±0.56 (13.5 μg/ml)	>15	3
5 wt% PEG-PLA UCA	13.14±0.67 (1.5 μg/ml)	18.85±0.44 (15 μg/ml)	>15	4
10 wt% PEG-PLA UCA	11.15±1.36 (1.5 μg/ml)	15.46±1.15 (15 μg/ml)	13	3
15 wt% PEG-PLA UCA	10.88±0.81 (1.5 μg/ml)	17.00±0.54 (15 μg/ml)	7	3
0.2 wt% LipidPEG UCA	13.13±1.01 (1.5 μg/ml)	16.49±0.54 (9 μg/ml)	>15	3
1 wt% LipidPEG UCA	10.19±0.98 (1.5 μg/ml)	16.71±0.83 (13.5 μg/ml)	4	2
2 wt% LipidPEG UCA	5.58±0.46 (1.5 μg/ml)	8.08±0.50 (13.5 μg/ml)	1	1

In terms of instability within an US beam (loss of echogenicity with time, Figure 4.11) at a lower mechanical index (MI) useful for imaging (0.152 at peak positive pressure (PPP) of 0.7 MPa), UCA with low proportions of PEG-PLA showed similar stability to unmodified 100% PLA UCA (acoustic half-life, $t_{1/2}$, >15 min). At the higher PEG-PLA ratios (10 wt% and 15 wt% PEG-PLA), the agents lost echogenicity faster than the native PLA agent (10 wt% acoustic $t_{1/2}$ = 13 min, p=0.0018; 15 wt% acoustic $t_{1/2}$ = 7 min, p<0.0001) indicating that the shells were more easily disrupted. Both 1 and 2 wt% LipidPEG lost echogenicity more rapidly at the lower MI than 100% PLA UCA (1 wt% acoustic $t_{1/2}$ = 4 min, p<0.0001; 2 wt% acoustic $t_{1/2}$ = 1 min, p<0.0001). The 0.2 wt% LipidPEG agents exhibited similar stability to the 100% PLA UCA, with an acoustic $t_{1/2}$ of greater than 15 minutes.

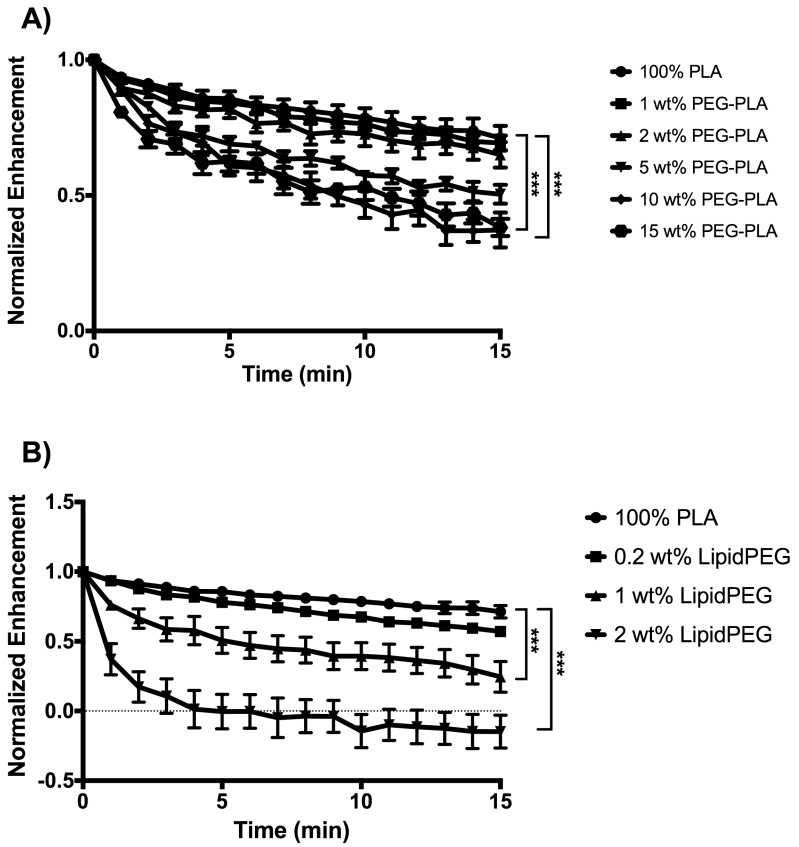

Figure 4.11: Acoustic results plotted as time response curves. . A) PEG-PLA formulations, B) LipidPEG formulations. Error bars = SEAM, n=5, ***p<0.0001.

These findings demonstrate that while echogenic response is diminished by incorporating PEGylated species in the shell in a dose-dependent manner, at low incorporation levels (<10 wt% PEG-PLA and <2 wt% LipidPEG) these PEGylated UCA are capable of interacting with US under conditions similar to those in a clinical imaging setting. The size of the doses is small compared to doses of contrast agent approved for use in the clinic (0.03 and 0.3mL/kg, SonoVue) [161]. Maximal enhancement at lower doses is the more desirable outcome. The majority of studies on influences of shell properties on acoustic behavior of UCA involve phospholipid shells [162-165], but there

are some that deal with polymer-shelled UCA. Sanna et al. reported obtaining *in vitro* US images with the use of 100% PLGA-PEG conjugated to a targeting ligand [166]; however, in our hands, the use of 100% PLA-PEG produced only background [160]. In the case of insertion of LipidPEG, the acoustic properties ranged from close to the control at 0.2 wt% to complete elimination of echogenicity at 2 wt% LipidPEG. Our study demonstrates that the anchoring of small percentages of lipid chain PEG molecules into the polymer shell is a viable method of PEGylation that can be further explored for functionalization with bioactive molecules for drug delivery applications.

Comparison of these two PEGylation methods has yielded valuable information that will inform our decisions toward achieving our long-term goals of developing "stealth" UCA for drug delivery and targeting. We have demonstrated the ability to generate PEGylated UCA capable of reflecting a focused US beam, establishing the upper limits of PEGylation for consistently reflective agents as 5 wt% PEG-PLA and 1 wt% LipidPEG, respectively.

4.2.4 *In vitro* Visualization of PEGylated UCA

In conjunction with the *in vitro* acoustic testing performed in our laboratory, the UCA were also visualized in a tissue mimicking flow phantom with an US scanner used for clinical imaging at Thomas Jefferson University Hospital with the help of Dr. John Eisenbrey and Dr. Flemming Forsberg. Using a linear US transducer, images were collected in both fundamental B-mode grayscale mode (right) and nonlinear contrast mode with gold tint (left). A baseline, pre-injection image is shown in Figure 4.12A.

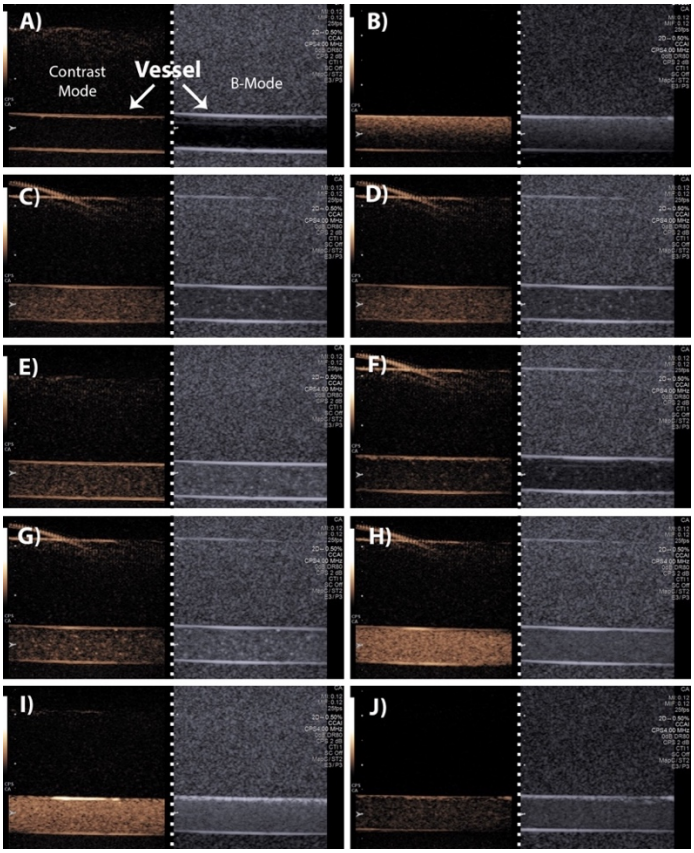

Figure 4.12: Images from ultrasound visualization of UCA in a tissue mimicking flow phantom. Each image was taken at a focal length of 4cm, in both non-linear contrast mode (left, orange) and fundamental B-mode (right, gray). A) Pre-injection empty vessel baseline image, B) 100% PLA, C) 1 wt% PEG-PLA, D) 2 wt% PEG-PLA, E) 5 wt% PEG-PLA, F) 10 wt% PEG-PLA, G) 15 wt% PEG-PLA, H) 0.2 wt% LipidPEG, I) 1 wt% LipidPEG, J) 2 wt% LipidPEG.

Strong enhancement is visible for the 100% PLA (Figure 4.12B), 1 wt% PEG-PLA (Figure 4.12C), 2 wt% PEG-PLA (Figure 4.12D), 5 wt% PEG-PLA (Figure 4.12E), 0.2 wt% LipidPEG (Figure 4.12H), and 1 wt% LipidPEG (Figure 4.12I) UCA. This is expected since these agents also showed high echogenicity in our custom acoustic setup, and confirms that these modified microbubbles are still functional as UCA. Inconsistent enhancement was observed for the 15 wt% PEG-PLA agents (Figure 4.12G), with low stability and visualization time. This is likely due to the bimodal distribution of intact UCA and non-spherical fragments present in this sample, contributing to the inconsistent

nature of the visible enhancement. Little to no enhancement was observed for the 10 wt% PEG-PLA (Figure 4.12F) and 2 wt% LipidPEG (Figure 4.12J), as expected due to the low echogenicity observed in previous experiments. Our visual evaluation of UCA with lower proportions of PEG-PLA indicate that 10 wt% appears to be the upper limit to maintain visibility and function within the US beam, with 1 wt% being the upper limit for LipidPEG incorporation. These results together with our dose response curves support the upper limits for PEGylation at 5 wt% PEG-PLA and 1 wt% LipidPEG, respectively.

4.2.5 Effects of PEGylation on Resonant Frequency

Acoustic backscattering from UCA is greatly improved when the agents are insonated in the same frequency range as their resonant frequency. By definition, the resonant frequency is the US frequency at which the UCA resonate and cavitate most. Therefore, it was important to understand whether the modifications to the UCA shell during PEGylation had any effect on the resonance of the resulting agents.

The resonant frequency of each PEGylated UCA and the 100% PLA UCA was determined experimentally, taking the minimum point from the graph plotting attenuation vs. frequency curves (Table 4.4, Figure 4.13 and Figure 4.14).

Results indicate that the resonant frequency of the 100% PLA UCA is 4.56MHz, which is well within the bandwidth range of the 5MHz transducer used for the acoustic evaluations discussed previously. The 1 wt% and 2 wt% PEG-PLA UCA also had a resonant frequency of approximately 4.5MHz, suggesting that these low proportions of PEG-PLA did not significantly affect the shell properties enough to shift the resonant frequency of the resulting UCA. A similar resonant frequency was observed for the 15 wt% PEG-PLA UCA (4.24MHz). This was surprising in light of the low echogenicity

from this sample, but is likely the signal received from the smaller intact microspheres that are present among the non-spherical debris produced in this sample. Both the 0.2 wt% and 1 wt% LipidPEG UCA had a resonant frequency of approximately 5MHz as well, suggesting that the anchoring of lipid-PEG chains into the PLA shell at low proportions does not cause significant changes to the shell resonance and cavitation. No clear resonant frequency was observed for the 2 wt% LipidPEG formulation, which can be expected based on the lack of echogenicity for this sample.

Table 4.4: Resonant frequency values for 100% PLA and PEGylated UCA, taken from attenuation vs. frequency curves.

	Resonant Frequency (MHz)
100% PLA	4.56
1 wt% PEG-PLA	4.48
2 wt% PEG-PLA	4.52
5 wt% PEG-PLA	7.84
10 wt% PEG-PLA	7.76
15 wt% PEG-PLA	4.24
0.2 wt% LipidPEG	5.24
1 wt% LipidPEG	4.96
2 wt% LipidPEG	N/A

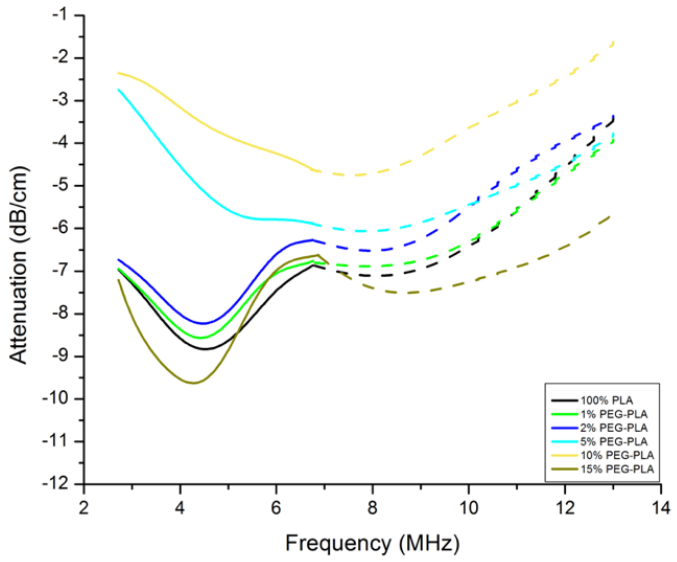

Figure 4.13: Attenuation (dB/cm) vs. frequency (MHz) curves for 100% PLA and PEG-PLA UCA. Solid line represents measurements taken with 5MHz unfocused transducer (bandwidth = 91%), and dotted line represents measurements taken with 10MHz unfocused transducer (bandwidth = 65%). PRF = 100Hz, Energy = 1, Damping Level = 3, Gain = 0.

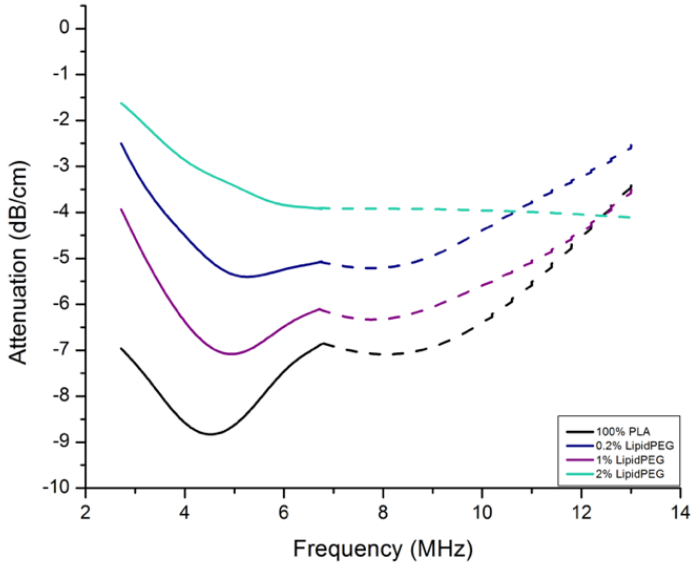

Figure 4.14: Attenuation (dB/cm) vs. frequency (MHz) curves for 100% PLA and LipidPEG UCA. Solid line represents measurements taken with 5MHz unfocused transducer (bandwidth = 91%), and dotted line represents measurements taken with 10MHz unfocused transducer (bandwidth = 65%). PRF = 100Hz, Energy = 1, Damping Level = 3, Gain = 0.

Both the 5 wt% and 10 wt% PEG-PLA UCA exhibited a shift in resonant frequency to approximately 7.8MHz. Based on the resonant frequency models developed by de Jong and Hoff, we believe the the higher proportions of PEG-PLA increased shell thickness and decreased shell elasticity, thus leading to an increase in the resonant frequency magnitude [153, 167]. These higher proportioned PEG-PLA UCA also had reduced average diameters, contributing to the observed increase in resonant frequency due to the inverse relationship these characteristics [153, 167]. Therefore, insonation frequency must be increased when insonating these agents to achieve maximum cavitation and drug delivery potential. Here we demonstrated that modifications to the UCA shell through PEGylation leads to structural changes affecting the oscillation of the encapsulated air core. These effects can potentially be mitigated by insonating the agents with a transducer with a center frequency similar to the resonant frequency of the modified UCA to allow for maximum oscillation.

4.2.6 Effects of PEGylation on UCA Size, Zeta Potential, and Surface Morphology

Acoustic behavior is also influenced by the physical properties of the UCA, particularly the size and morphology in relation to backscattering and resonance [168]. The strength of acoustic signal reflected from a UCA is largely influenced by the scattering cross-section and shell elasticity, both functions of the diameter of the agent [153, 169, 170]. As such, evaluation of the physical characteristics of our agents was crucial to fully understanding the observed trends in acoustic activity.

All UCA formulations had an average diameter between 1-3μm (Figure 4.15), well within the acceptable range for clear passage through the vasculature and resonance in the clinical frequency range. Most PEG-PLA modifications decreased the UCA

diameter. Average diameters ranged from 1.67±0.13 to 2.17±0.11μm compared to unmodified 100% PLA UCA (2.41±0.10μm), except for 15 wt% PEG-PLA at 2.46±0.15μm. However, only 1 wt% PEG-PLA ($p<0.0001$), 5 wt% PEG-PLA ($p=0.0003$), and 10 wt% PEG-PLA ($p=0.0498$) were significantly smaller than the unmodified 100% PLA UCA. Addition of PEG-PLA also caused less uniformity in size distribution, increasing the polydispersity index (PDI) from 0.184 for unmodified 100% PLA UCA to 0.308 for 1 wt% PEG-PLA. Similar degrees of uniformity were observed for the 2 wt% (PDI = 0.232) and 5 wt% (PDI = 0.293) groups, but both 10 wt% (PDI = 0.357) and 15 wt% (PDI = 0.501) groups were even less uniform in size distribution. Addition of LipidPEG produced UCA with average diameters ranging from 1.06±0.31 to 1.79±0.84μm, and all were significantly smaller than unmodified 100% PLA UCA ($p<0.0001$). LipidPEG incorporation also increased population size distribution compared to unmodified 100% PLA UCA, with 0.2 wt% measuring a PDI of 0.279, 1 wt% measuring a PDI of 0.275, and 2 wt% was highly non-uniform with a PDI of 0.594. Both 15 wt% PEG-PLA and 2 wt% LipidPEG exhibited an unacceptable degree of non-uniformity and would not be considered viable for use.

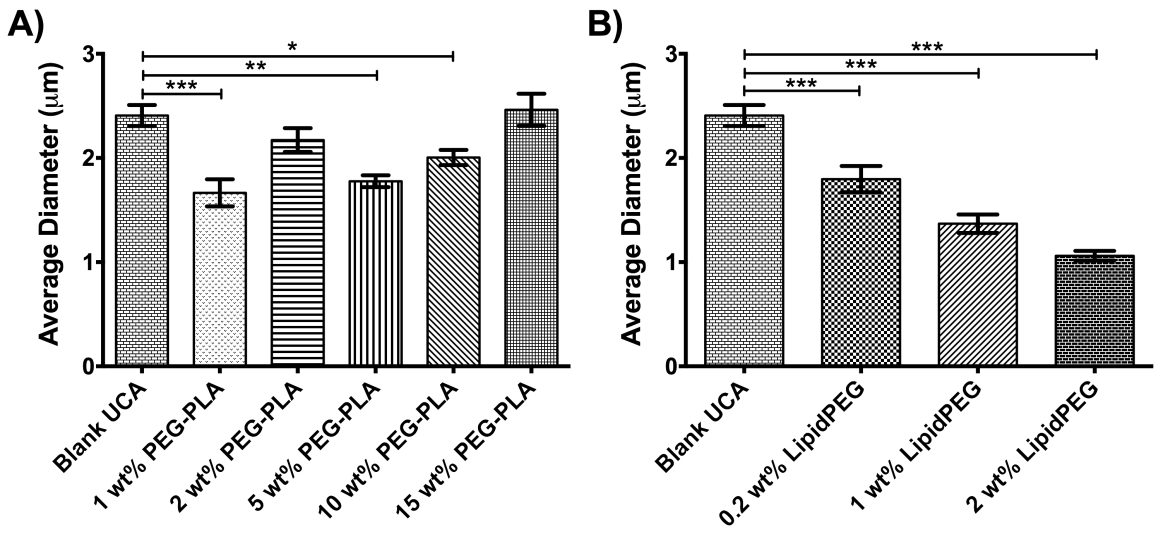

Figure 4.15: Average particle size of UCA. Error bars represent SEAM, n=5, *p=0.0498, **p=0.0003 ***p<0.0001. A) Measurements of the PEG-PLA copolymer group, B) Measurements of the LipidPEG lipid group.

The somewhat linear trend (R^2=0.7529) between wt% LipidPEG and reduction in UCA diameter could be due in part to the orientation of the lipid molecules within the UCA shell [137, 171]. As more LipidPEG molecules are added to the polymer shell, the shell likely becomes thicker and smaller to support the anchoring of these molecules.

Size is not only important for acoustics, but also an important consideration for US-driven deposition of particles, as forces pushing them toward the vascular wall are more effective on the micron scale than on the nano scale [108, 168, 172]. With an average diameter between 1-3μm, the PEGylated agents are highly susceptible to radiation forces pushing them toward the vascular wall for easier extravasation once shattered into n-Sh.

All UCA groups maintained a negative zeta potential (ζ) mV (Figure 4.16), reflective of the carboxylate end group of PLA, which helps inhibit aggregation and clumping in suspension, a key property for injectables to prevent forming a vascular

blockage during administration. FDA regulations mandate that zeta potential must have a magnitude of 20mV or greater to provide sufficient stabilization and aggregation inhibition in suspension [173]. All UCA groups met this requirement, with the exception of the 0.2 wt% LipidPEG group with an average zeta potential of -18.39±10.45mV.

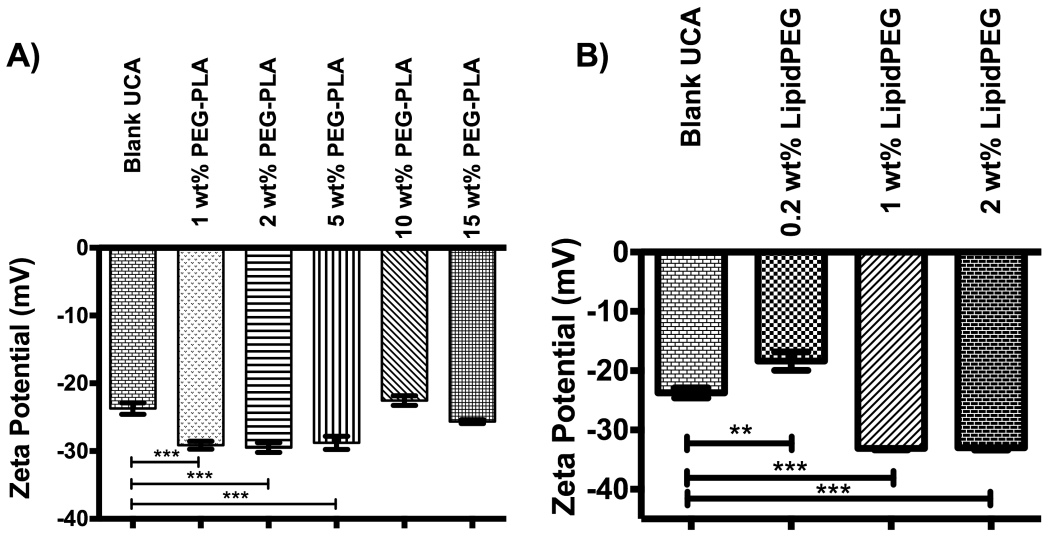

Figure 4.16: Average zeta potential of UCA. A) Measurements of the PEG-PLA copolymer group, B) Measurements of the LipidPEG group. Error bars represent SEAM, n=5, **p=0.0002, ***p<0.0001.

Unmodified 100% PLA UCA exhibited a ζ of -23.75±5.69mV. Addition of low percentages of PEG-PLA to the agent formulation increased the intensity of the negative charge to -29.14±0.58mV, -29.48±0.72mV, and -28.79±0.97mV for 1, 2, and 5 wt% respectively ($p<0.0001$ for all three groups compared to 100% PLA). At 10 and 15 wt%, proportions that had resulted in lower maximum enhancement, zeta potential values of -22.56±0.71mV and -25.65±0.28mV were recorded, closer to 100% PLA values. This is

likely due to the morphological changes to these agents altering the surface group expression and PEG conformation on the UCA surface. The majority of ζs reported for PEGylated PLA nanoparticles show similar results. For example, Yao et al. reported ζ of -27.50±1.15mV for PEG-PLA nanoparticles [174]. For 0.2 wt% LipidPEG incorporation we measured a less negative ζ of -18.39±10.45mV ($p=0.0002$), while 1 and 2 wt% LipidPEG produced agents with increased negative magnitudes at -33.10±1.77mV and -33.01±2.51mV, respectively ($p<0.0001$), again showing the dramatic difference in properties going from 0.2 to 1 wt% LipidPEG. This, again, is likely due to the arrangement of lipids and polymeric functional groups on the UCA surface, and given the reduction in echogenicity for these bubbles, suggests increased expression of –COO- groups on the UCA surface. Recalling that zeta potential is pH-dependent, it is important to note that these measurements were taken in a suspension with DI water (pH 7.0), which closely mimics physiological pH conditions (pH 7.4) but does not appropriately simulate the blood environment. PBS, however, cannot be used for these measurements because it shields the surface charge.

Scanning electron microscopy (SEM) images showed that increasing the proportion of PEG-PLA resulted in less uniform morphology, eventually leading to non-spherical, broken particles (Figure 4.17).

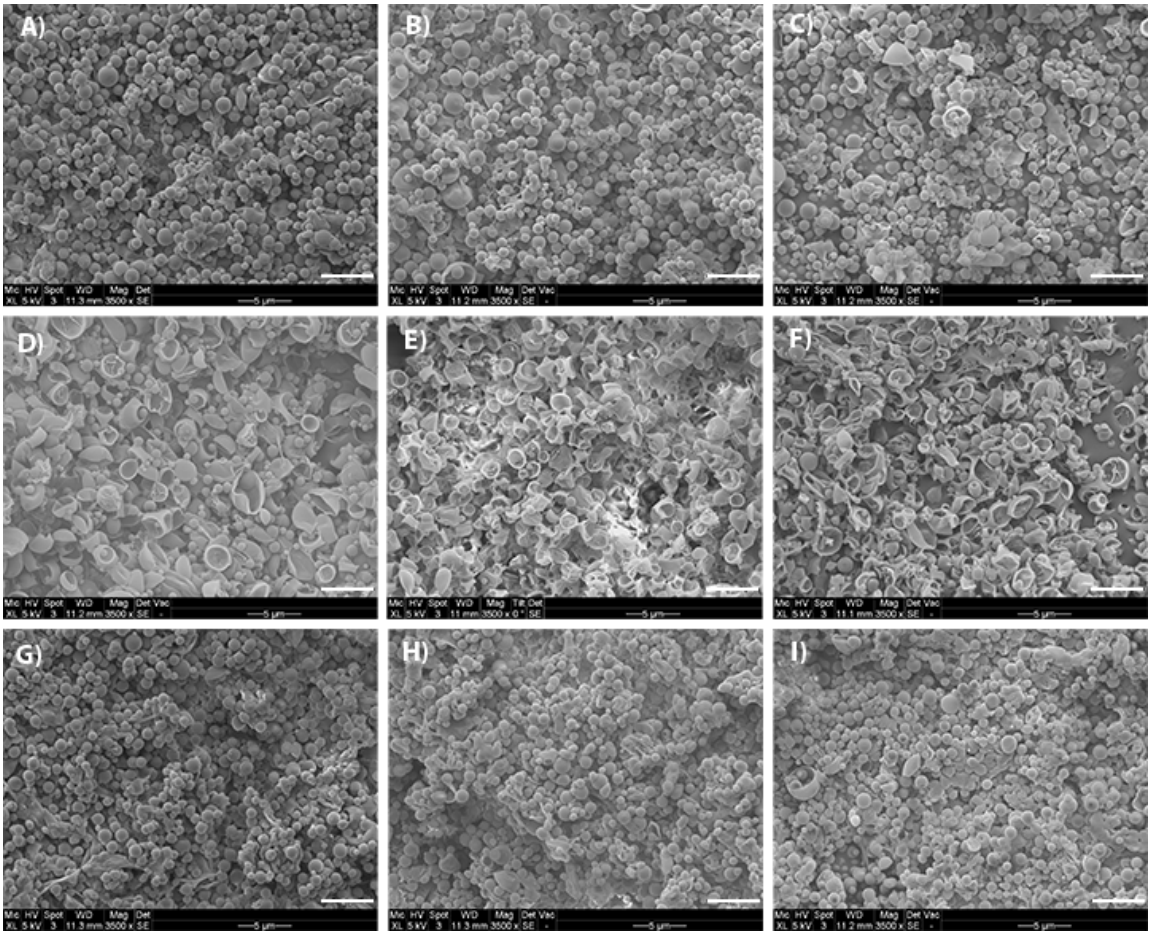

Figure 4.17: SEM images of UCA. Magnification 3500x, size bar 5μm. A) 100% PLA UCA, B) 1 wt% PEG-PLA UCA, C) 2 wt% PEG-PLA UCA, D) 5 wt% PEG-PLA UCA, E) 10 wt% PEG-PLA UCA, F) 15 wt% PEG-PLA UCA, G) 0.2 wt% LipidPEG UCA, H) 1 wt% LipidPEG UCA, I) 2 wt% LipidPEG UCA.

Passing from unmodified 100% PLA UCA through 15 wt% PEG-PLA (Figure 4.17A-F), there is a clear morphological shift from smooth and spherical to larger collapsed spheres. Similar morphological changes have been observed in studies investigating agent PEGylation and the effect of molecular weight and surface group expression [159, 166]. However, this trend was not observed in the LipidPEG UCA groups in which all maintained a generally smooth, spherical morphology (Figure 4.17G-

I). While Chen and Borden observed this smooth morphology with their lipid microbubbles [140, 147], it is interesting to observe similar behavior from these polymeric UCA. Considering the reduced echogenicity and visualization observed from the 2 wt% LipidPEG, we believe that the PEG chains oriented inward toward the microbubble core during the w/o emulsion, forming an inverted micelle inside of the polymer shell and limiting the cavitation ability of the resulting UCA by creating steric hindrance from PEG chain incompressibility [175].

These results indicate that PEGylation can have a significant effect on the physical characteristics of polymeric UCA. We have demonstrated that spherical morphology is lost in a dose-dependent manner with increasing proportions of PEG-PLA co-polymer added to the emulsion, suggesting undesirable interactions between the co-polymer end groups that cannot support the double emulsion process. These morphological changes likely contribute to the observed changes in UCA diameter and zeta potential, as the average particle size can be skewed by larger non-spherical particles and differences in surface area exposure with non-spherical particles can lead to fluctuations in zeta potential measurements. Again, our findings suggest that 5 wt% PEG-PLA represents an upper limit for PEGylation based on observed morphology, while 1 wt% LipidPEG represents the upper limit for PEGylation in this method based on average diameter.

4.2.7 Ultrasound-triggered n-Sh Production from PEGylated UCA

Native and PEGylated UCA were screened in our custom acoustic setup to determine the potential to undergo inertial cavitation and burst into n-Sh in the presence of a focused US. Agents were insonated with a 5MHz transducer set for high mechanical index (approximately 0.193, peak positive pressure 0.94MPa measured with a needle

hydrophone) for 15 minutes, with backscatter measurements taken every minute. As shown in Figure 4.18 for the PEG-PLA UCA and Figure 4.19 for the LipidPEG UCA, all agents lost echogenicity rapidly (reaching their acoustic half-life in 4 minutes or less, $p<0.0001$ compared to time to reach acoustic half-life under US at a lower MI) in the presence of this clinically-relevant US beam. The loss of signal signifies that the agents are shattering into fragments, and therefore can no longer reflect the signal from the encapsulated air core [176, 177].

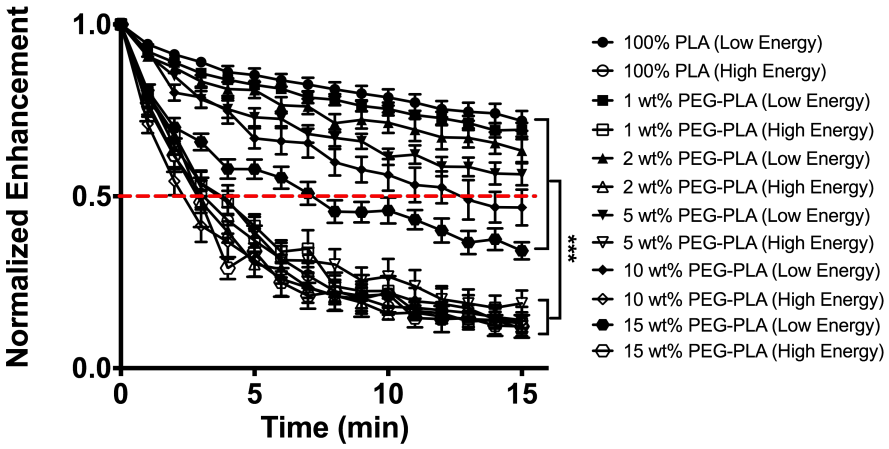

Figure 4.18: Acoustic time response curves for 100% PLA and PEG-PLA UCA insonated at low energy (MI 0.152, peak positive pressure 0.7 MPa) and high energy (MI 0.193, peak positive pressure 0.94 MPa). Dotted line represents acoustic half-life. Error bars = SEAM, n=5, ***$p<0.0001$.

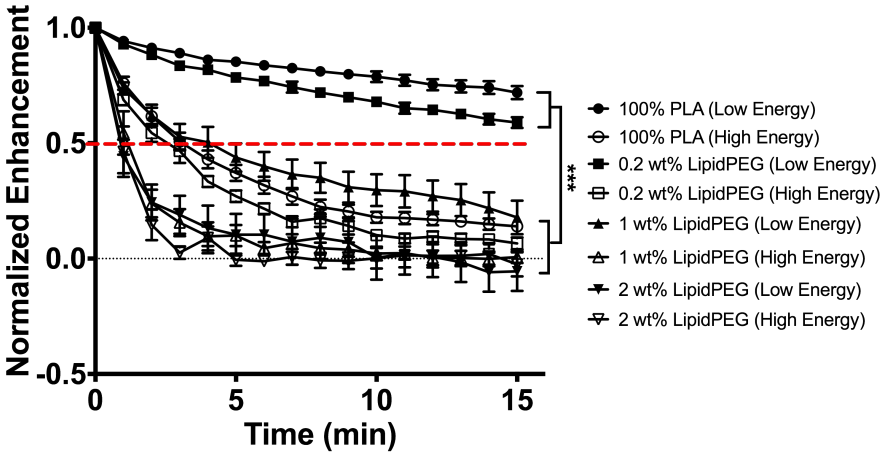

Figure 4.19: Acoustic time response curves for 100% PLA and LipidPEG UCA insonated at low energy (MI 0.152, peak positive pressure 0.7 MPa) and high energy (MI 0.193, peak positive pressure 0.94 MPa). Dotted line represents acoustic half-life. Error bars = SEAM, n=5, ***p<0.0001.

Based on these reductions in acoustic half-life, PEGylated agents were evaluated for average particle size after insonation, to determine whether US-triggered cavitation caused significant particle diameter decrease to within the desired range for extravasation (between 400-700nm), as denoted by the dotted lines and red region (Figure 4.20). The 100% PLA and all PEG-PLA agents, with the exception of 15 wt% PEG-PLA, exhibited n-Sh production with the resulting fragments having an average size within the desired range (Figure 4.20A). The LipidPEG (Figure 4.20B) mirrored the effect observed on echogenicity; the 0.2 wt% resembled the unmodified 100% PLA UCA and the 1 wt% and 2 wt% showed very little size reduction. PDI for the 100% PLA n-Sh was 0.662, ranged from 0.444 to 0.787 for the PEG-PLA n-Sh, and from 0.579 to 0.914 for the LipidPEG n-Sh. These findings indicate that US-triggered size reduction results in particles with highly non-uniform size distributions, suggesting that cavitation may burst the UCA into fragments of various sizes and shapes.

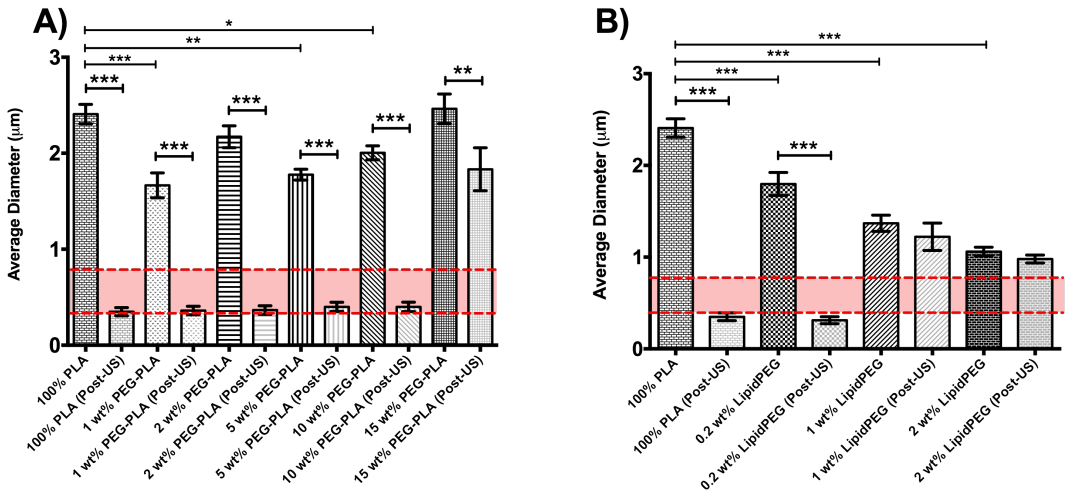

Figure 4.20: Average particle size of UCA pre-insonation and post-insonation (MI 0.193 at 0.94MPa PPP). A) Measurements of the PEG-PLA copolymer group, B) Measurements of the LipidPEG group. Dotted lines represent 400-700nm range for extravasation of n-Sh. Error bars represent SEAM, n=5, *p=0.0498, **p=0.0003 for 100% PLA to 5 wt% PEG-PLA, **p=0.0002 for 15 wt% PEG-PLA to 15 wt% PEG-PLA (post-US), ***p<0.0001.

The US-generated size reduction was significant in the unmodified 100% PLA UCA ($p<0.0001$) and all PEG-PLA groups (1 wt% through 10 wt% PEG-PLA $p<0.0001$, 15 wt% PEG-PLA $p=0.0002$), suggesting that PEGylation with PEG-PLA does not prevent shattering into n-Sh under the influence of US. The trend observed in the LipidPEG groups ($p<0.0001$) would be expected given the reduction in acoustic enhancement observed with the 1 and 2 wt% LipidPEG UCA, which cannot effectively interact with US to undergo cavitation. These results suggest that lipid-PEG chain arrangement and polymer shell conformations influence these acoustic interactions [175]. Generation of n-Sh of 400nm or less is an important aspect of our novel US-triggered drug delivery system, as the loaded n-Sh would be of an appropriate size to pass through

the pores in the leaky tumor vasculature (400-780nm) and reach the targeted tissue for effective therapy. We have demonstrated the ability of our PEGylated agents to shatter into nano-sized fragments upon exposure to a focused US beam, within the size range necessary for vascular escape through the leaky pores in the tumor vessel walls.

4.2.8 Immunogenic Characterization of PEGylated UCA

To determine the effect of PEGylation on the immune response triggered by the UCA, C3a activation in human serum incubated *ex vivo* with suspended UCA was measured with a specific ELISA assay (Figure 4.21).

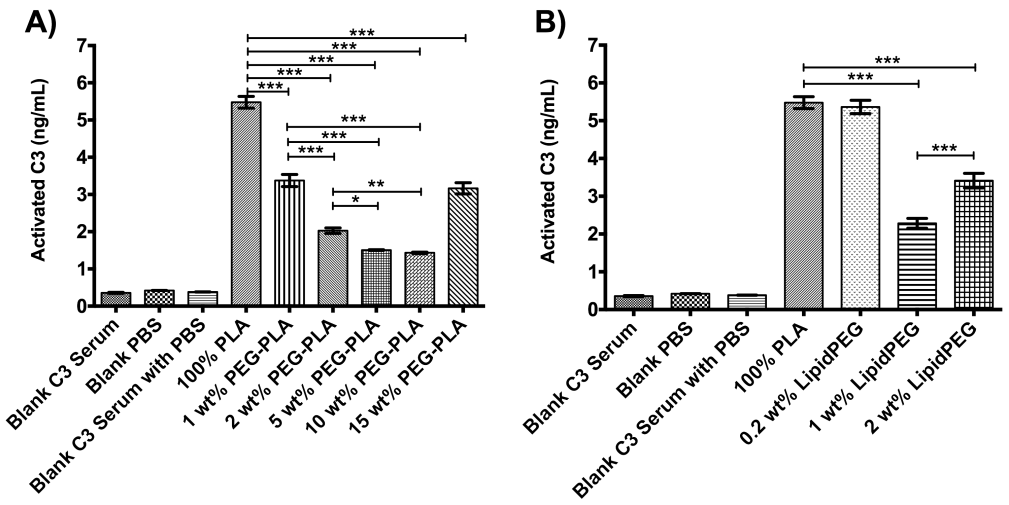

Figure 4.21: C3 complement activation assay results. Error bars represent SEAM, n=2. A) Results from the PEG-PLA copolymer group ***p<0.0001, **p=0.0077, *p=0.0371, B) Results from the LipidPEG lipid group ***p<0.0001.

In all cases except 0.2 wt% LipidPEG (5.36±0.18ng activated C3/mL serum), the addition of PEG into the UCA shell effectively led to a reduction in C3 activation over unmodified 100% PLA UCA (5.48±0.16ng activated C3/mL serum). The amount of

activated C3 in the serum decreased with increased proportions of PEG-PLA, with the exception of 15 wt% PEG-PLA which rose back to the same level as 1 wt% PEG-PLA (Figure 4.21A). All of the PEG-PLA groups exhibited lower C3 activation than the unPEGylated 100% PLA UCA ($p<0.0001$), suggesting diminished immune activation. Both the 1 wt% (2.28±0.13ng activated C3/mL serum) and 2 wt% (3.41±0.19ng activated C3/mL serum) LipidPEG UCA had reduced C3 activation compared to the unmodified 100% PLA UCA ($p<0.0001$).

Unfortunately, only small amounts of activated C3 protein are needed to initiate a cascade of immune pathway activations [178-181]. Significant interleukin-1 production is observed in human monocytes with the addition of just 0.1μg C3a/well in culture, demonstrating the potency of this protein to accelerate immune response [178]. Our assay indicated that 1mg unPEGylated 100% PLA UCA/1mL human complement-preserved serum activated approximately 5.5ng of C3a protein, while the 5 and 10 wt% PEGylated UCA reduced that activation to ~1.5ng activated C3a protein/1mL serum (reduction of 73%), which was within 1ng/mL of baseline assay controls.

The unPEGylated 100% PLA UCA exhibited a high C3a activation rate, consistent with our *in vivo* observations with Dox-loaded UCA [2]. An explanation for this immunogenic activity is the interaction between the PLA carboxylic acid end groups on the UCA surface and the unstable thioester bond in the C3 protein, which facilitates binding of the C3 protein to the UCA surface therefore activating the immune response [133, 182, 183]. C3 activation increased in the 2 wt% LipidPEG group compared to the 1 wt% LipidPEG group, as was also seen with the higher (15 wt%) PEG-PLA UCA (3.16±0.15ng activated C3/mL serum) compared to the 10 wt% PEG-PLA UCA

(1.43±0.02ng activated C3/mL serum). Studies on PEGylated nanocapsules identify the importance of molecular weight and distance between PEG chains for effective shielding of the underlying PLA surface from complement binding [125]. Since the 15 wt% PEG-PLA formulation resulted in mostly non-spherical particles, surface expression of PEG groups is likely affected, accounting for the observed increase in C3 activation. Additionally, Owens and Peppas showed that hydrophilic PEG chains can orient themselves toward the aqueous phase during fabrication [126]. In our case, it is possible then that the LipidPEG chains in the 2 wt% LipidPEG UCA oriented inward toward the initial aqueous core and are therefore not expressed on the UCA surface, accounting for the observed increase in C3 activation compared to the 1 wt% LipidPEG UCA. Chen and Borden also showed that there is a linear correlation between the number of exposed reactive (carbonyl and amino) groups and the degree of C3b activation [140]. This relationship was not seen when the reactive groups were masked within a PEG brush on a lipid microbubble surface, supporting the use of PEG for immune shielding in drug delivery. These studies showed that C3 activation decreased in the presence of the surface PEG brush, and vascular circulation time was greatly increased for PEGylated agents compared to unPEGylated agents [184].

We specifically wanted to investigate the differences between the use of a PEG co-polymer where the PEG molecules are incorporated into the polymer shell and the use of a lipid chain PEG molecule where the lipid chain anchors into the polymer shell allowing the PEG molecule to extend from the UCA surface and create a physical brush around the agent, determining which method resulted in the best balance between decreasing immunogenicity and retaining acoustic properties for future drug loading,

drug delivery, and targeting applications. We have demonstrated the efficacy of both PEGylation methods in reducing C3 activation in human complement-preserved serum, representing an expected reduction in immunogenic response when introduced to the physiological environment during patient treatment. Our results suggest that 10 wt% PEG-PLA and 1 wt% LipidPEG are the most effective proportions for reducing immune recognition and activation.

4.2.9 UCA PEGylation Conclusions

In an effort to determine the best formulation to achieve a balance between stealth and acoustic activity, we compared two PEGylation techniques; addition of increasing amounts of PEG-PLA copolymer and employing incorporation of LipidPEG into the shell. We have shown that adding PEG-PLA to the shell has a dose-dependent deleterious effect on acoustic properties, and inserting LipidPEG lipids has an even more dramatic effect at much lower proportions.

We showed that there exists a limit to the amount of PEG that can be incorporated into the UCA to maintain the balance between favorable acoustic properties and immune shielding. For the more traditional co-polymer method of PEGylation, our results indicate that this balance is achieved using 5 wt% PEG-PLA copolymer formulation for producing "stealth" UCA, (18.85dB enhancement at 15μg/mL, $t_{1/2}$ >15min at the lower MI and 4min at the higher MI, 1.78μm diameter, ζ -28.70mV, and C3a reduction by 73%). In comparison, our investigations into anchoring lipid chain PEG molecules into the polymer shell show that the 1 wt% LipidPEG formulation best maintains the acoustic-immunogenic balance (16.70dB enhancement at 13.5μg/mL, $t_{1/2}$ 5min at the lower MI and 2min at the higher MI, 1.24μm diameter, ζ -22.43mV, and C3a reduction by 58%).

Importantly, these results indicate that UCA rupture occurs at an MI of approximately 0.2, which is well below the clinical limit of 1.9 and indicative of shells that can easily shatter into fragments for drug delivery in the presence of a clinically-relevant US beam. This study has revealed that both PEGylation methods led to development of successful acoustic UCA that exhibited significantly reduced immunogenicity in our *ex vivo* model, and has served as a crucial step in developing and optimizing these PEGylated UCA for functionalization with targeting ligands and co-encapsulated drug for applications in targeted drug delivery.

4.3 Effects of Shell Functionalization and Drug Loading on PEGylated UCA for Targeted Cancer Therapy

Following the development of effective "stealth" UCA, we found that the 5 wt% PEG-PLA and 1 wt% LipidPEG formulations were the most appropriate for continued study. These agents were then functionalized for the purpose of targeted treatment and drug delivery. Two different modifications were performed, singularly and in tandem. One method was to decorate the PEGylated UCA surface with TRAIL protein, which serves as both a targeting and apoptotic agent to cancer cells. The other method was to encapsulate Doxorubicin (Dox) with the polymeric UCA shell, which would undergo sustained release as the PLA hydrolyzes and provide prolonged localized treatment. Agents were also produced that employed both of these modifications, expressing TRAIL on the UCA surface that also contains co-encapsulated Dox in an attempt to sensitize TRAIL-resistant cancer cells. Modification methods were optimized to provide UCA with strong acoustic enhancement, tight size distribution preferably in the 1-2μm range, smooth surface morphology, effective ligand activity, and sustained drug release for

targeting and drug delivery applications. Efficacy of these modifications is discussed in terms of these properties over the remainder of the subsection.

4.3.1 Encapsulation Efficiency of Doxorubicin

One of the modifications employed in these experiments was the encapsulation of 3 wt% (15mg) Dox within the polymeric shell of the UCA, both TRAIL-ligated and native UCA. Both final drug payload and encapsulation efficiency were measured for each type of drug-loaded agents, based on a standard curve to determine the relationship between amount of free Dox in DMSO and fluorescence intensity after encapsulation (Figure A.2) and the encapsulation efficiency equation (Eq. 20).

$$Encaspulation\ Efficiency = \frac{Final\ Dox\ Concentration}{Loading\ Dox\ Concentration}\ x\ 100\% \qquad \text{(Eq. 20)}$$

The resulting drug payload and encapsulation efficiency results are summarized in Table 4.5 and shown in Figure 4.22. An encapsulation efficiency of 35.09% (5.26mg) was achieved for the 100% PLA UCA (non-PEGylated), which represents an increase of approximately 15% from our previous Dox-loaded UCA [2, 3, 5, 87, 184, 185]. This loading increase could be due to a change in aqueous core materials from ammonium carbonate to ammonium carbamate or a change in PLA provider which could have made slight modifications to the shell that increased drug loading and retention. There was a significant decrease in drug payload and encapsulation efficiency with the post-fabrication TRAIL ligation for both the 100% PLA TRAIL UCA (23.28%, 3.49mg) and the 5 wt% PEG-PLA TRAIL UCA (21.26%, 3.19mg) compared to their native Dox-loaded counterparts ($p<0.0001$). The Dox-loaded native agents likely experience a burst

release when introduced to the aqueous environment during maleimide ligation, accounting for this loss of Dox. We also observed a significant decrease in Dox loading and encapsulation efficiency between the 1 wt% LipidPEG Dox UCA (17.82%, 2.76mg) and the 1 wt% LipidPEG Dox TRAIL UCA (12.51%, 1.88mg) ($p=0.0007$). These agents are not re-exposed to an aqueous environment after fabrication, as the TRAIL ligation to the LipidPEG molecule is performed separately, and these complexes are then incorporated into the UCA during the initial fabrication process. Coupled with the observation that both 1 wt% LipidPEG Dox UCA and 1 wt% LipidPEG Dox TRAIL UCA exhibit significantly less Dox encapsulation and payload than the 100% PLA and 5 wt% PEG-PLA agents ($p<0.0001$), these results suggest that the presence of the lipids in the organic phase during UCA fabrication creates a lipophilic environment that cannot support higher levels of Dox encapsulation within the polymeric shell, with the hydrophilic Dox collecting in the aqueous core and being sublimated from the agents during lyophilization [186]. Additional studies have shown that Dox exhibits lipophilic behavior with anionic lipids, suggesting that Dox could have statically bound to the LipidPEG tails instead of the copolymer groups and could have subsequently been lost during lyophilization [187].

Table 4.5: Total drug payload and encapsulation efficiency for Dox-loaded UCA.

	Total Dox Loading (total mg Dox/total mg UCA)	Final UCA Weight (mg)	Encapsulation Efficiency
100% PLA Dox	5.26±0.23	385±4	35.09±1.51%
100% PLA Dox TRAIL	3.49±0.11	352±20	23.28±0.72%
5 wt% PEG-PLA Dox	4.13±0.03	342±16	27.52±0.22%
5 wt% PEG-PLA Dox TRAIL	3.19±0.06	313±24	21.26±0.40%
1 wt% LipidPEG Dox	2.67±0.19	379±13	17.82±1.27%
1 wt% LipidPEG Dox TRAIL	1.88±0.04	376±19	12.51±0.30%

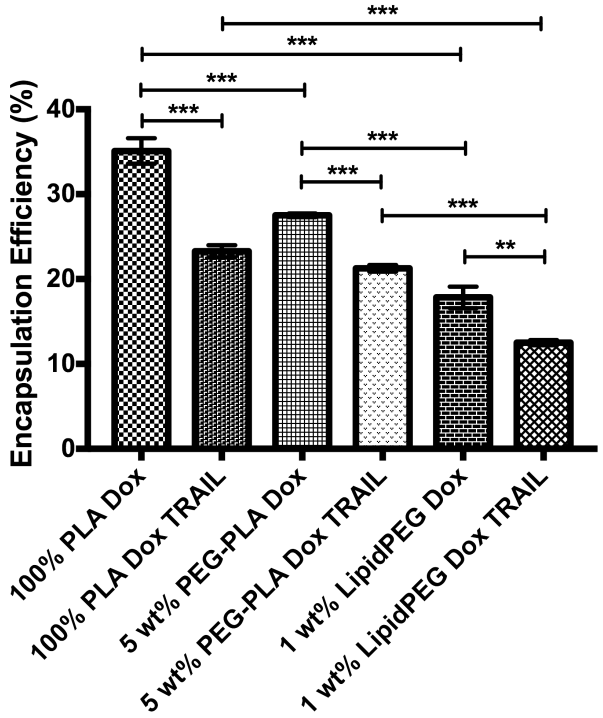

Figure 4.22: Effect of shell composition on Dox encapsulation efficiency.

Confocal microscopy was used to confirm that Dox was encapsulated within the UCA polymeric shell, as shown in Figure 4.23. For all three shell compositions with and without TRAIL ligation, Dox was visible as red fluorescence within the polymeric shell of the UCA.

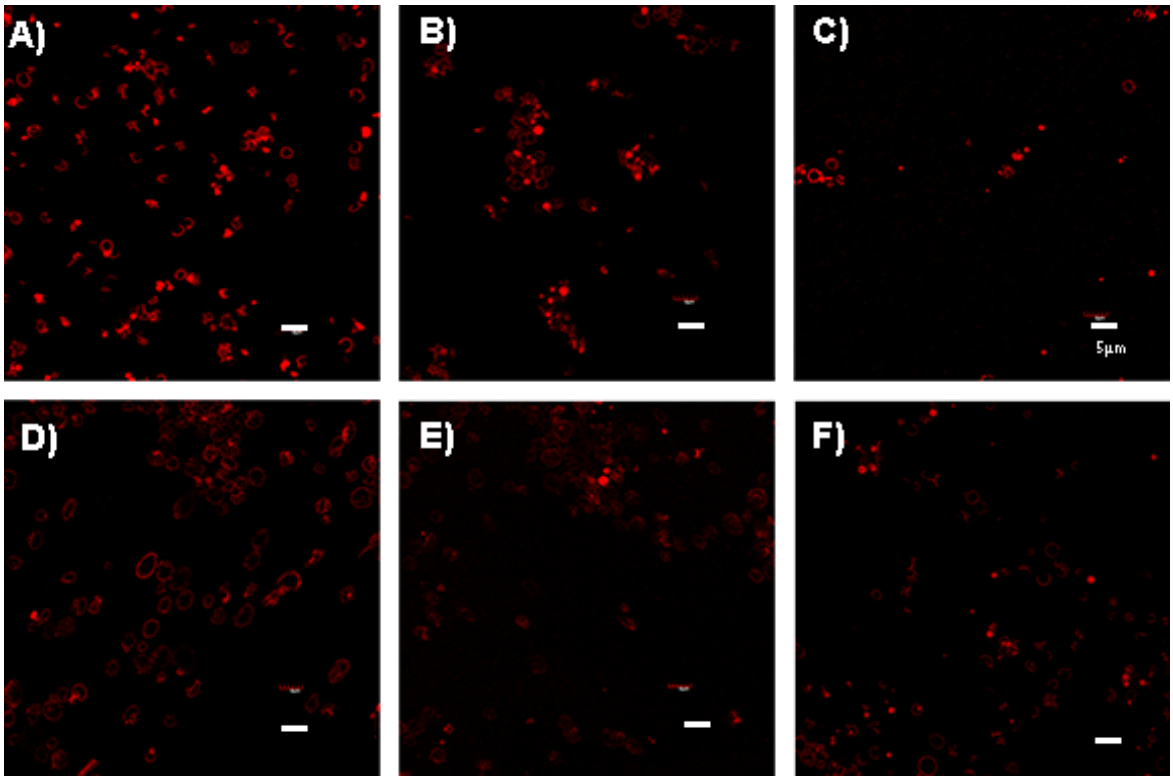

Figure 4.23: Confocal images of Dox-loaded UCA, with Dox appearing as red fluorescence, magnification 100x, size bar = 5µm. A) 100% PLA Dox UCA, B) 5 wt% PEG-PLA Dox UCA, C) 1 wt% LipidPEG Dox UCA, D) 100% PLA Dox TRAIL UCA, E) 5 wt% PEG-PLA Dox TRAIL UCA, F) 1 wt% LipidPEG Dox TRAIL UCA.

There was a visible reduction in fluorescence intensity and fluorescent UCA with the TRAIL-ligated agents (Figure 4.23D-F). The same weight of UCA was used in each test, with the sampled being vortexed before a sample was taken and a drop was placed

onto the slide and covered with a coverslip. We later found that the quantity of UCA per mg was different for each shell composition, accounting for the comparable reduction in visible UCA for the agents with PEGylated shells. Nonetheless, all Dox-loaded functionalized UCA exhibited encapsulation of drug within the polymeric shell. The reduction in Dox encapsulation observed in the TRAIL-ligated 100% PLA and 5 wt% PEG-PLA groups compared to their non-ligated counterparts suggests a loss of encapsulated Dox during the post-fabrication ligation process. We investigated the short-term and long-term release profiles of Dox from these agents to determine if Dox was lost upon introduction to an aqueous environment.

4.3.2 *In vitro* Doxorubicin Release

To investigate the release profile of Dox from the functionalized agents, UCA were suspended in 50mL PBS at 37°C, both with and without the presence of ultrasound. Agents were evaluated for burst release of Dox upon introduction to the aqueous environment for 20 minutes, and also for sustained release over a period of seven days. Prior to determining the extent of drug release during ultrasound-triggered cavitation and subsequent PLA hydrolysis, a standard curve was constructed to determine the relationship between amount of free Dox in PBS and fluorescence intensity (Figure A.3).

All of the Dox-loaded agents exhibited a burst of drug release upon suspension in the aqueous release buffer (37°C PBS) (Figure 4.24). Since the agents were washed extensively prior to lyophilization, this observation is not due to any residual Dox adsorbed to the UCA exterior and must be caused by movement of the encapsulated drug toward the UCA surface during sublimation of the aqueous components during freeze drying. Both the 100% PLA Dox UCA (Figure 4.24A) and 100% PLA Dox TRAIL UCA

(Figure 4.24B) showed an immediate burst of approximately 35% of the total encapsulated Dox with little to no further release detected over the 20 minute testing duration. The 5 wt% PEG-PLA Dox UCA exhibited an immediate burst of roughly 10% of encapsulated Dox (significantly lower than that unPEGylated 100% PLA Dox UCA, $p<0.0001$), while 5 wt% PEG-PLA Dox TRAIL UCA showed a burst release of approximately 16% of the total Dox loaded. Studies have shown that hydrophilic drugs encapsulated within PEG-PLA polymersomes exhibit a strong interaction with the copolymer, increasing drug retention [188]. This is an extremely encouraging result, since previous attempts in our lab at reducing the initial burst effect had not been successful. However, the 1 wt% LipidPEG Dox UCA showed significantly higher burst (approximately 45%, $p=0.0003$), as well as 1 wt% LipidPEG Dox TRAIL UCA (approximately 48%, $p<0.0001$). Actual drug release values are reported in Table 4.6.

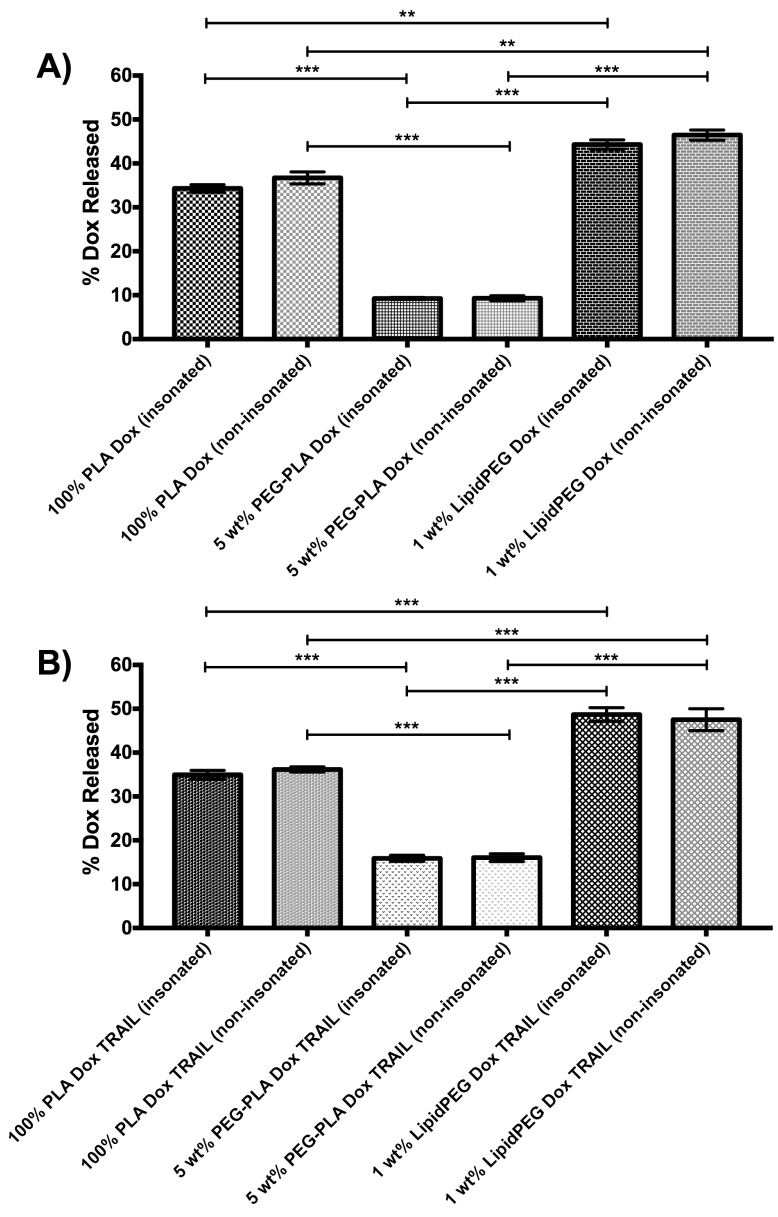

Figure 4.24: Burst release (% of total loading) of Dox from functionalized UCA (n=3, error bars = SEAM). A) Results from the Dox-loaded UCA group, **p=0.0002 for 100% PLA (insonated) to 5 wt% PEG-PLA (insonated), **p=0.0003 for 100% PLA (non-insonated) to 5 wt% PEG-PLA (non-insonated), ***p<0.0001. B) Results from the Dox-loaded, TRAIL-ligated group, ***p<0.0001.

Table 4.6: Dox burst release amounts and percentage of total encapsulated drug released.

	Amount of Dox released (μg)/mg UCA	Percent of Total Dox Released
100% PLA Dox UCA (non-insonated)	5.08±0.24	36.70±1.36%
100% PLA Dox UCA (insonated)	4.75±0.15	34.31±0.85%
100% PLA Dox TRAIL UCA (non-insonated)	3.32±0.12	36.17±0.58%
100% PLA Dox TRAIL UCA (insonated)	3.21±0.20	34.95±1.01%
5 wt% PEG-PLA Dox UCA (non-insonated)	1.01±0.06	9.32±0.57%
5 wt% PEG-PLA Dox UCA (insonated)	1.01±0.02	9.26±0.22%
5 wt% PEG-PLA Dox TRAIL UCA (non-insonated)	1.35±0.13	16.04±0.90%
5 wt% PEG-PLA Dox TRAIL UCA (insonated)	1.33±0.10	15.89±0.70%
1 wt% LipidPEG Dox UCA (non-insonated)	3.26±0.20	46.45±1.14%
1 wt% LipidPEG Dox UCA (insonated)	3.11±0.18	44.31±1.06%
1 wt% LipidPEG Dox TRAIL UCA (non-insonated)	3.60±0.33	47.53±2.49%
1 wt% LipidPEG Dox TRAIL UCA (insonated)	3.69±0.21	48.67±1.58%

For all three shell types there was significantly less Dox burst release from the Dox-loaded, TRAIL-ligated agents than from their Dox-loaded native counterparts ($p<0.0001$). All samples were standardized to evaluate the same number of UCA (based

on #UCA/mg determinations described in a later section). For the 100% PLA (Figure 4.25A) and 5 wt% PEG-PLA (Figure 4.25B) agents, this trend is likely due to the initial burst release of Dox when the agents are exposed to an aqueous environment during TRAIL ligation. For the LipidPEG agents, Dox release increased slightly over the 20 minute testing duration, as shown in Figure 4.25C. Again, since the agents were washed extensively during fabrication, this release is likely due to the movement of Dox toward the UCA surface during lyophilization coupled with the hydrophobic nature of the PEG lipids disrupting the polymeric shell and allowing more interaction with the hydrophilic Dox. There was no statistical significance in the amount of Dox released during n-Sh production compared to the non-insonated controls for all agents evaluated ($p>0.05$).

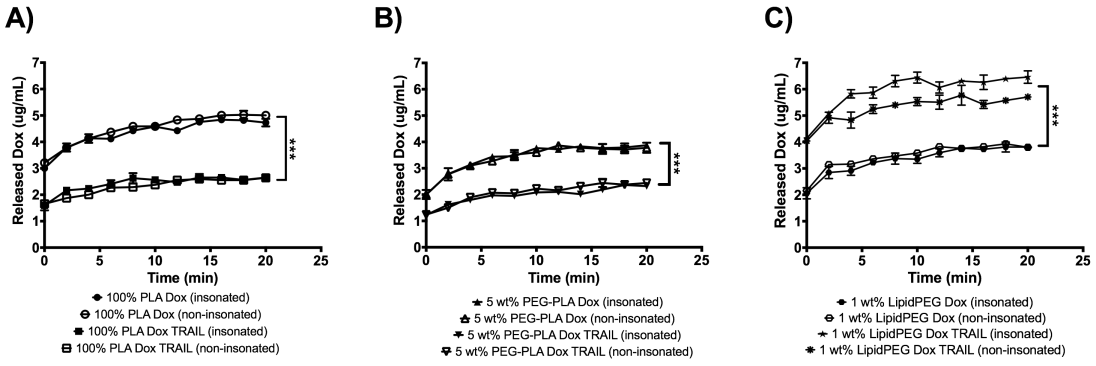

Figure 4.25: Burst release profiles of Dox from functionalized UCA (n=3, error bars = SEAM). A) Results from the 100% PLA UCA group, ***$p<0.0001$. B) Results from the 5 wt% PEG-PLA group, ***$p<0.0001$. C) Results from the 1 wt% LipidPEG UCA group, ***$p<0.0001$.

It was surprising to observe a similar trend in the 1 wt% LipidPEG UCA, since they do not undergo a second aqueous immersion for TRAIL ligation. As described before, electrostatic reactions between the LipidPEG tails and Dox molecules could prevent encapsulation within the UCA shell, with these interactions being interrupted upon introduction to an aqueous environment [187]. It is also possible that the relative weight of the PEG-TRAIL complex creates shear stresses and additional pores in the polymeric shell, causing increased and more rapid release of the encapsulated drug.

Once the burst release profile was determined, the long-term sustained release profile could be calculated in a similar way using data points collected at several intervals over a period of 7 days. Despite the initial higher burst release of Dox from the 1 wt% LipidPEG UCA, the release profile for these agents appeared to level off after 72 hours (Figure 4.26) and their final drug payload at the end of the 7-day release study was similar to that of the 5 wt% PEG-PLA UCA (Figure 4.27). As shown in Figure 4.27 and Figure 4.26, the insonated 100% PLA Dox UCA exhibited significantly more Dox release than any of the other agents ($p<0.0001$), releasing roughly 96% (88μg Dox/mg UCA) of its total encapsulated drug load by the end of 168 hours (7 days).

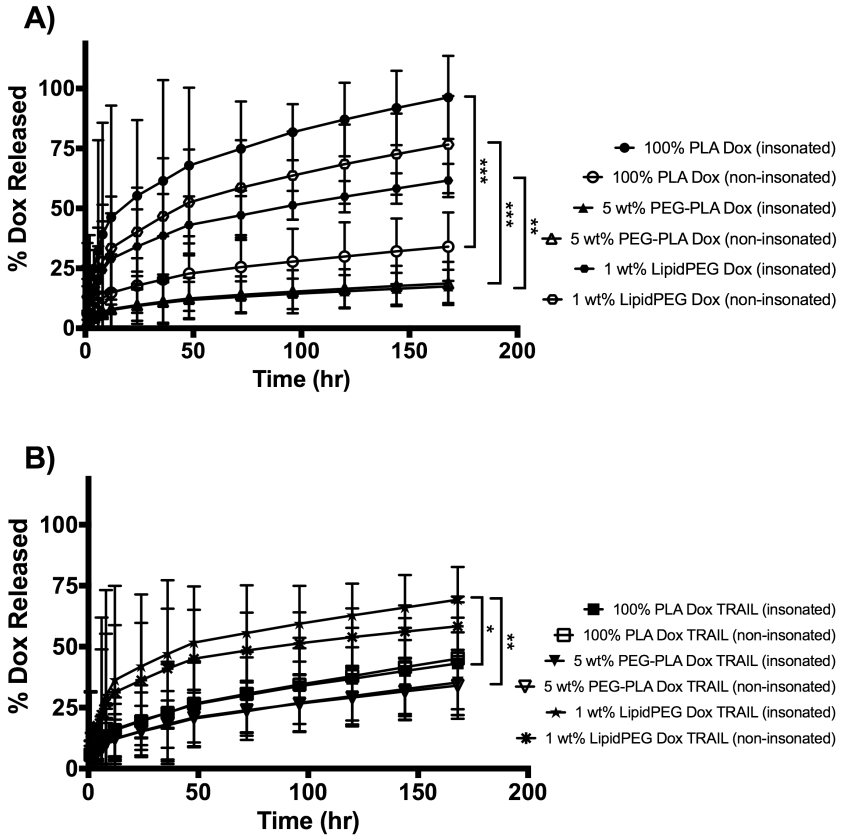

Figure 4.26: Effect of shell components on sustained Dox release (n=3, error bars = SEAM). A) Results from the Dox-loaded UCA group, **p=0.0011, ***p<0.0001. B) Results from the Dox-loaded TRAIL-ligated group, *p=0.0395, **p=0.0025.

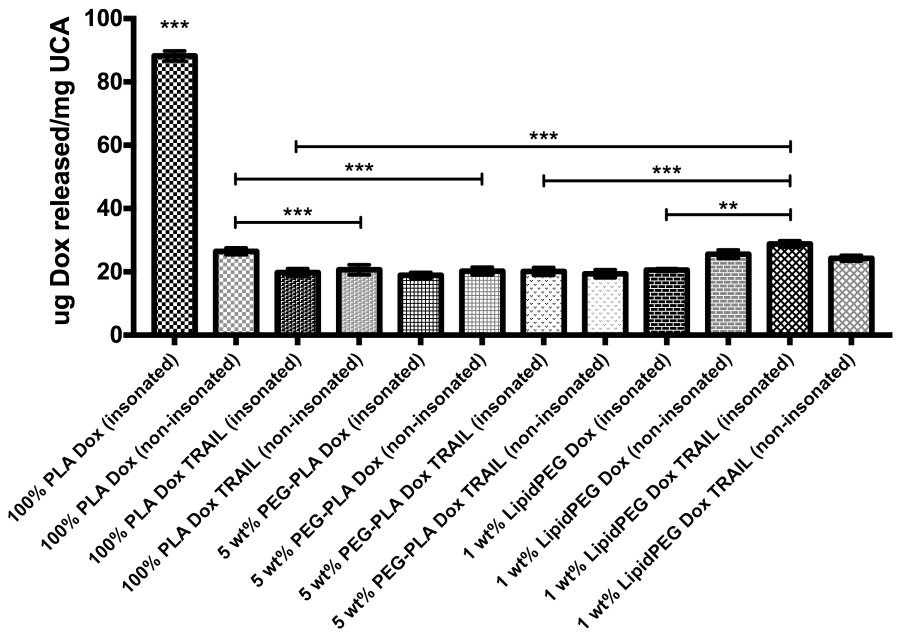

Figure 4.27: Total drug release after 7 days for Dox-loaded UCA (n=3, error bars = SEAM), **p=0.0001, ***p<0.0001.

Other than the 100 wt% PLA Dox UCA, the functionalized UCA exhibited a sustained release of roughly 20-30µg Dox/mg UCA over the duration of the 7-day measurement period (Figure 4.26). Of note, the insonated 1 wt% LipidPEG Dox TRAIL UCA had significantly more release (28.82µg Dox/mg UCA, $p<0.0001$) than both the insonated 100% PLA Dox TRAIL UCA (19.76 µg Dox/mg UCA) and the insonated 5 wt% PEG-PLA Dox TRAIL UCA (20.12µg Dox/mg UCA) (Figure 4.27). This is likely due to the rapid and higher burst release from the 1 wt% LipidPEG agents. Additionally, the percent release curves (Figure 4.26B) show that the release profile for the 1 wt% LipidPEG Dox TRAIL UCA to be significantly different than those for the 100% PLA Dox TRAIL ($p=0.0395$) and 5 wt% PEG-PLA Dox TRAIL UCA ($p=0.0025$).

In addition to the low initial burst release exhibited by the 5 wt% Dox TRAIL UCA, the sustained drug release from these agents (20.12μg Dox/mg UCA insonated, 19.38μg Dox/mg UCA non-insonated) was not significantly different from that of the 100% PLA Dox TRAIL UCA (19.76μg Dox/mg UCA insonated, 20.66μg Dox/mg UCA non-insonated) ($p>0.05$). Figure 4.26 shows that all of the agents exhibited increasing prolonged Dox release, presumably as a function of PLA hydrolysis [2-4, 87, 185].

One of the most interesting findings in this study was the burst release of Dox from all agents upon introduction to an aqueous environment, especially the 100% PLA Dox TRAIL UCA and 5 wt% PEG-PLA Dox TRAIL UCA since these agents had already been reintroduced to an aqueous solution during ligation. Additionally, there was no difference between the agents that were exposed to US and those not exposed, further supporting the release of Dox in response to the aqueous environment. The observed burst release from the non-TRAIL-ligated UCA explains the loss of Dox observed in the TRAIL-ligated counterparts, having been lost during ligation. Our studies also show drastic differences in the amount of Dox released during this initial burst with each shell type, with 5 wt% PEG-PLA exhibiting significantly less release than 100% PLA and 1 wt% LipidPEG UCA. These findings have important implications for both short-term effects when administered intravenously (less systemic exposure) and also long-term for sustained release of Dox during polymer hydrolysis. Long-term release profiling revealed similar trends, where Dox release amounts varied between shell types.

4.3.3 Effects of Shell Modification on UCA Quantity

As discussed previously, concentration of each modified UCA type was determined by counting the number of microbubbles present in a known weight using a flow cytometer (Figure 4.28).

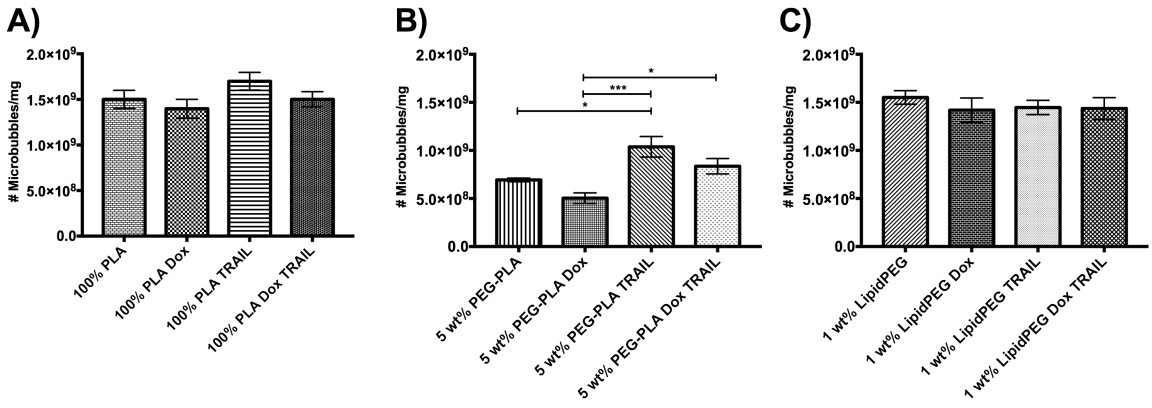

Figure 4.28: Concentration of UCA by weight, error bars = SEAM, n=3. A) 100% PLA functionalized UCA, B) 5 wt% PEG-PLA functionalized UCA, *p=0.0106 for 5 wt% PEG-PLA UCA to 5 wt% PEG-PLA TRAIL UCA, *p=0.0143 for 5 wt% PEG-PLA Dox to 5 wt% PEG-PLA Dox TRAIL, ***p<0.0001, C) 1 wt% LipidPEG groups.

For both the 100% PLA and 1 wt% LipidPEG groups, no significant difference was observed between any of the functionalized agents and the unmodified native agents ($p>0.05$). This finding demonstrates that functionalization modifications to these agents does not have deleterious effects to the concentration of agents produced, producing similar populations. For the 5 wt% PEG-PLA group, UCA concentration increased with TRAIL ligation for both TRAIL-ligated without Dox (1.04×10^9 UCA/mg) compared to unmodified 5 wt% PEG-PLA UCA (6.94×10^8 UCA/mg, $p=0.0106$) and also for the 5 wt% PEG-PLA Dox TRAIL UCA (8.35×10^8 UCA/mg) compared to its Dox-loaded

counterpart (5.03×10^8 UCA/mg, p=0.0143). This could be due to the ligation process, as UCA can appear more concentrated if the TRAIL molecules are counted as events passing through the cytometer beam. Addition of the PEG-PLA co-polymer yielded less UCA per mg, likely due to thicker polymeric shells. Microbubble concentration by weight is a critical factor in standardizing treatment groups for number of UCA delivered and also standardizing drug delivery to regions of interest.

4.3.4 Effects of Shell Modification on Acoustic Enhancement and Stability

The effects of TRAIL ligation and drug loading on the *in vitro* acoustic properties of the resulting UCA were examined. As expected, all of these manipulations had a demonstrated effect on acoustic response (shown in Figure 4.29, Figure 4.30, and also summarized in Table 4.7).

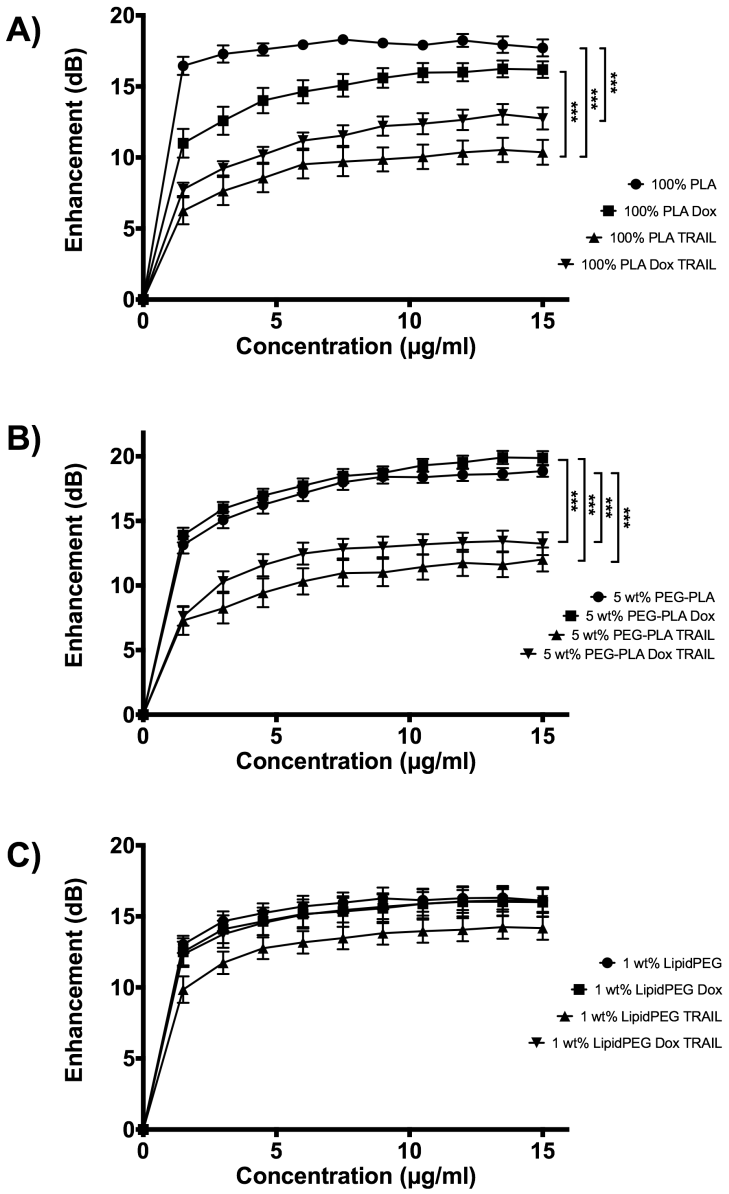

Figure 4.29: Acoustic results plotted as cumulative dose response curves. A) 100% PLA UCA functionalization group, B) 5 wt% PEG-PLA functionalization group, C) 1 wt% LipidPEG functionalization group. Error bars = SEAM, n=5, ***p<0.0001.

The dose needed to achieve maximum enhancement nearly doubled in response to all modifications of 100% PLA UCA, requiring at least 13.5µg/mL UCA compared to 7.5µg/mL UCA for the unmodified 100% PLA UCA (Figure 4.29A). Additionally, the

maximum enhancement from the 100% PLA TRAIL UCA (10.53±0.85 dB) and 100% PLA Dox TRAIL UCA (13.04±0.73 dB) were significantly reduced ($p<0.0001$) compared to that of the unmodified 100% PLA UCA (18.30±0.25 dB), suggesting that shell modifications during ligation have deleterious effects on the cavitation, resonance, and/or size of these microbubbles. Drug loading and TRAIL ligation of the 5 wt% PEG-PLA UCA (Figure 4.29B) did not significantly affect the dosage needed to reach maximum enhancement, remaining at 13.5μg/mL or increasing slightly to 15μg/mL. No significant difference in maximum enhancement was observed between 5 wt% PEG-PLA Dox UCA (19.91±0.51 dB) and 5 wt% PEG-PLA UCA (18.85±0.44 dB), suggesting that Dox encapsulation within these agents does not disrupt the polymer shell and allows for cavitation and resonance at 5MHz. Additionally, there was no significant difference ($p>0.05$) between the 5 wt% PEG-PLA TRAIL UCA (12.02±0.93 dB) and the 5 wt% PEG-PLA Dox TRAIL UCA (13.44±0.81 dB); however, both of these agents suffered significant loss in echogenicity compared to their non-ligated counterparts ($p<0.0001$). As explained previously, this finding supports that TRAIL ligation by reintroduction to an aqueous environment is detrimental to the shell properties in terms of resonance, cavitation, and backscattering. There were no significant changes to maximum enhancement for the 1 wt% LipidPEG UCA when functionalized (Figure 4.29C), suggesting that this platform is the most versatile for modifications.

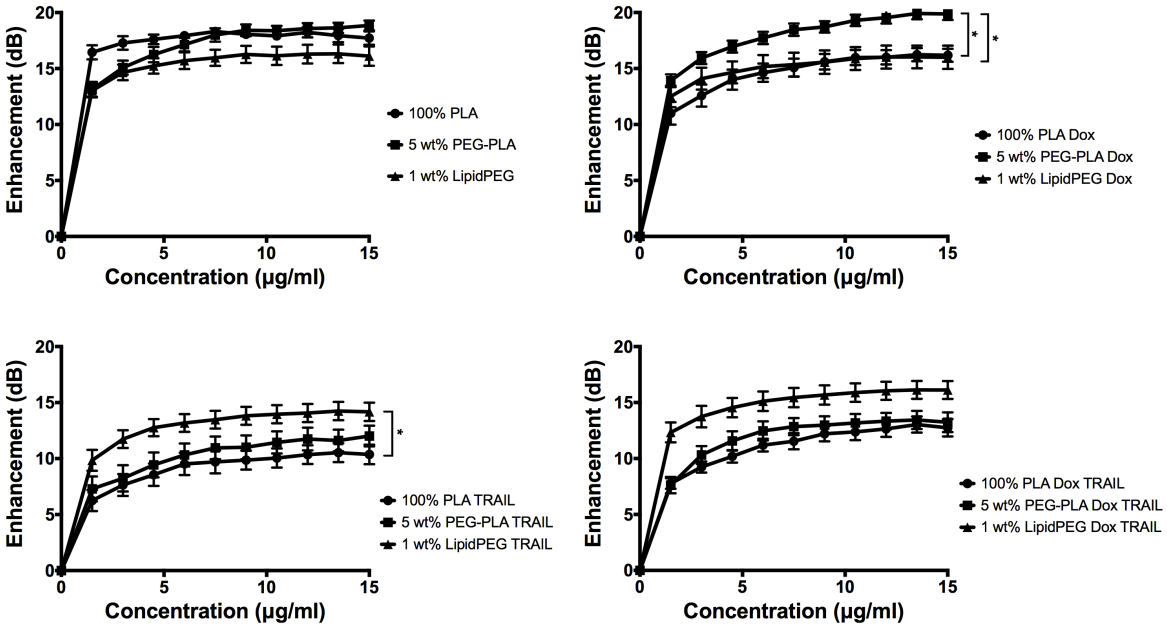

Figure 4.30: Acoustic results plotted as cumulative dose response curves, error bars = SEAM, n=5. A) Unmodified native UCA group, B) Dox-loaded functionalization group, *p=C) TRAIL-ligated functionalization group, D) Dox-loaded and TRAIL-ligated functionalization group.

We also investigated each shell manipulation to determine any advantages or significant issues between the different shell types. There were no significant differences in maximum enhancement between any of the unmodified native UCA (Figure 4.30A), establishing a good baseline for comparison. When UCA were modified to encapsulate Dox within the polymer shell (Figure 4.30B), 5 wt% PEG-PLA Dox UCA clearly exhibited the best acoustic enhancement (19.91±0.51 dB), and was significantly better than both 100% PLA Dox UCA (16.23±0.59 dB, p=0.0292) and 1 wt% LipidPEG Dox UCA (16.03±1.01 dB, p=0.0158). TRAIL ligation (Figure 4.30C) resulted in 1 wt% LipidPEG TRAIL UCA having the highest maximum cumulative enhancement (14.25±0.82 dB), which was significantly higher than 100% PLA TRAIL UCA

(10.53±0.85 dB, p=0.0259). This is likely due to the fabrication methods, since TRAIL is pre-ligated to the LipidPEG molecule before the double emulsion process while the 100% PLA and 5 wt% PEG-PLA agents must be reintroduced to an aqueous environment for TRAIL ligation. 1 wt% LipidPEG Dox TRAIL UCA also showed the highest maximum cumulative enhancement (16.13±0.80 dB) for the Dox and TRAIL functionalization group (Figure 4.30D), however there was no statistical difference between the three shell types ($p>0.05$).

Table 4.7: Acoustic properties of PEG-PLA co-polymer and LipidPEG UCA groups.

	Initial dB Enhancement (Dose in μg/ml)	Maximum dB Enhancement (Dose in μg/ml)	US Half-life at Lower MI (min)	US Half-life at Higher MI (min)
100% PLA UCA	16.45±0.63 (1.5 μg/ml)	18.30±0.25 (7.5 μg/ml)	>15	3
100% PLA Dox UCA	8.85±0.58 (1.5 μg/ml)	16.23±0.59 (13.5 μg/ml)	8	2
100% PLA TRAIL UCA	6.25±0.95 (1.5 μg/ml)	10.53±0.85 (13.5 μg/ml)	>15	2
100% PLA Dox TRAIL UCA	7.76±0.47 (1.5 μg/ml)	13.04±0.73 (13.5 μg/ml)	>15	2
5 wt% PEG-PLA UCA	13.14±0.67 (1.5 μg/ml)	18.85±0.44 (15 μg/ml)	>15	4
5 wt% PEG-PLA Dox UCA	13.91±0.57 (1.5 μg/ml)	19.91±0.51 (13.5 μg/ml)	10	2
5 wt% PEG-PLA TRAIL UCA	7.29±1.12 (1.5 μg/ml)	12.02±0.93 (15 μg/ml)	>15	2
5 wt% PEG-PLA Dox TRAIL UCA	7.62±0.73 (1.5 μg/ml)	13.44±0.81 (13.5 μg/ml)	14	2
1 wt% LipidPEG UCA	13.03±0.61 (1.5 μg/ml)	16.31±0.83 (13.5 μg/ml)	8	2
1 wt% LipidPEG Dox UCA	12.50±0.96 (1.5 μg/ml)	16.03±1.01 (13.5 μg/ml)	6	2
1 wt% LipidPEG TRAIL UCA	9,85±0.93 (1.5 μg/ml)	14.25±0.82 (13.5 μg/ml)	8	2
1 wt% LipidPEG Dox TRAIL UCA	12.33±0.89 (1.5 μg/ml)	16.13±0.80 (13.5 μg/ml)	8	1

In terms of instability within an US beam (loss of echogenicity with time, Figure 4.31 and Figure 4.32) at a lower MI useful for imaging (0.152 at peak positive pressure (PPP) of 0.7 MPa), both the 100% PLA UCA and 5 wt% PEG-PLA UCA groups retained

their stability (acoustic half-life, $t_{1/2}$, >15 min) with the exception of 100% PLA Dox UCA ($t_{1/2}$=8min) and 5 wt% PEG-PLA Dox UCA ($t_{1/2}$=10min). In fact, 100% PLA Dox UCA were less stable than all other UCA in the 100% PLA group (Figure 4.31A, p=0.0497 compared to 100% PLA TRAIL UCA, p=0.0014 compared to 100% PLA Dox TRAIL UCA, and p<0.0001 compared to 100% PLA UCA), suggesting that Dox encapsulation disrupts the shell structure making it more flexible to still allow for oscillations but with less stability [189]. No significant differences in stability were observed within the 5 wt% PEG-PLA ($t_{1/2}$ between 10-15min, Figure 4.31B) and 1 wt% LipidPEG ($t_{1/2}$ between 6-8min, Figure 4.31C) shell type groups (p>0.05).

While the both the 5 wt% PEG-PLA and 1 wt% LipidPEG unmodified UCA are significantly less stable than unmodified 100% PLA UCA (p=0.0129 compared to 5 wt% PEG-PLA UCA, p<0.0001 compared to 1 wt% LipidPEG UCA, Figure 4.32A), their stability is relatively unchanged in response to shell modification, while the 100% PLA agents experience a loss of stability when modified as explained above. This is likely due to the fact that 5 wt% PEG-PLA UCA and 1 wt% LipidPEG UCA already represent modifications to the native 100% PLA shell, and therefore further modifications (i.e. drug loading and surface ligation) do not have as significant of an impact on these agents.

When comparing the types of modification individually for each shell type, we found that there was no significant change in stability (p>0.05) when UCA were loaded with Dox (Figure 4.32B) or ligated with TRAIL (Figure 4.32C). When both loaded with Dox and ligated with TRAIL (Figure 4.32D), 1 wt% LipidPEG Dox TRAIL UCA were less stable than 100% PLA Dox TRAIL UCA (p=0.0008), suggesting that these shells are

more easily disrupted likely due to the shear stresses of the long molecules extending from the UCA surface and shell instability at the point of lipid tail incorporation.

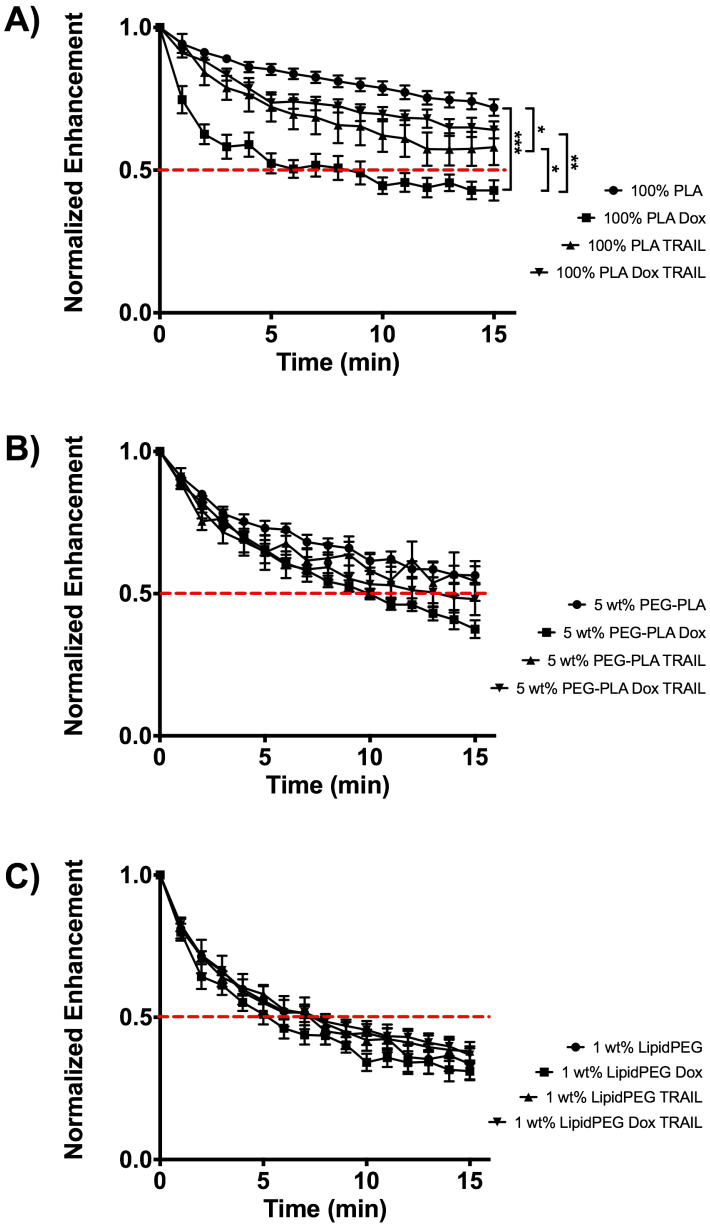

Figure 4.31: Acoustic results plotted as time response curves, error bars = SEAM, n=5, dotted line represents acoustic half-life. A) 100% PLA UCA group, *p=0.0439 for 100% PLA UCA to 100% PLA TRAIL UCA, *p=0.0497 for 100% PLA Dox UCA to 100% PLA TRAIL UCA, **p=0.0014, ***p<0.0001, B) 5 wt% PEG-PLA group, C) 1 wt% LipidPEG group.

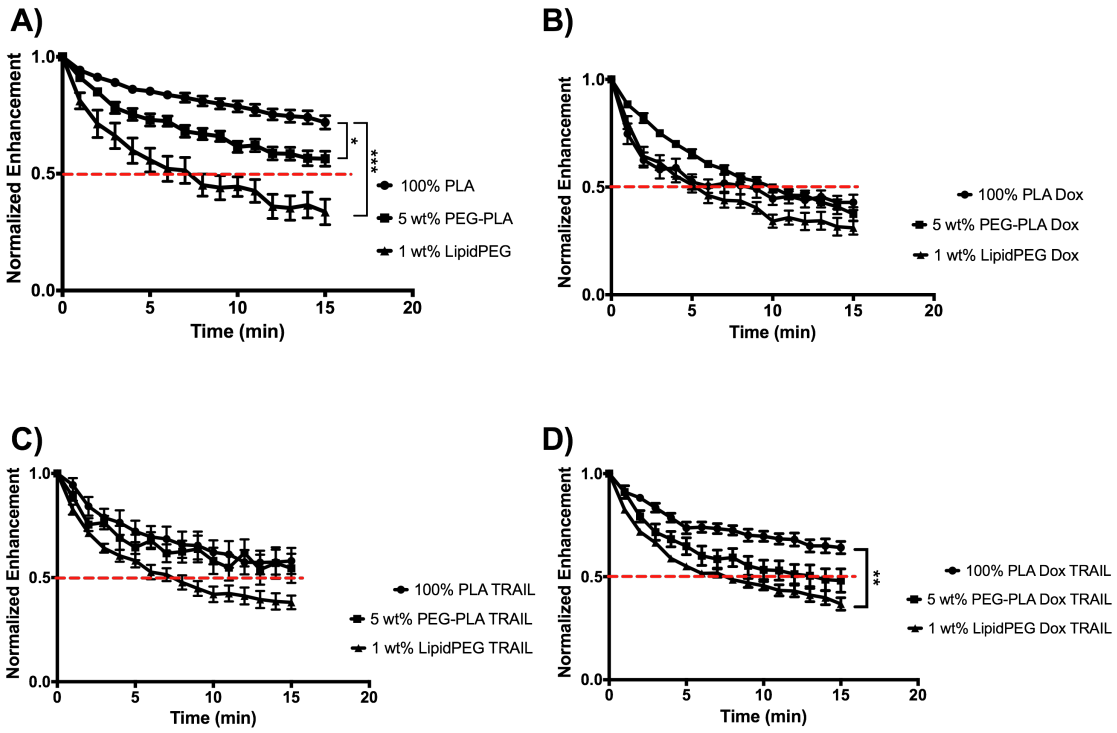

Figure 4.32: Acoustic results plotted as time response curves, error bars = SEAM, n=5, dotted line represents acoustic half-life. A) Unmodified native UCA group, *p=0.0129, ***p<0.0001, B) Dox-loaded group, C) TRAIL-ligated group, D) Dox-loaded and TRAIL-ligated group, **p=0.0008.

These findings demonstrate that while echogenic response is diminished by functionalization in most cases, the resulting functionalized UCA are still capable of interacting with US under conditions similar to those used in a clinical setting. As discussed previously, the acoustic enhancement observed at these comparatively low doses is desirable, when compared to the clinical doses of UCA such as SonoVue (0.03-0.3mL/kg) [161].

Results suggest that 1 wt% LipidPEG shell type is the most versatile for adaptation via TRAIL-ligation (native or Dox-loaded), while 5 wt% PEG-PLA best retains acoustic behavior for Dox loading without addition of TRAIL.

4.3.5 *In vitro* Visualization of Functionalized UCA

In conjunction with the *in vitro* acoustic testing performed in our laboratory, the UCA were also visualized in a tissue mimicking flow phantom with a clinical US scanner at Thomas Jefferson University Hospital. Using a linear US transducer, images were collected in both fundamental B-mode grayscale mode (right) and nonlinear contrast mode with gold tint (left). Images of the 100% PLA group are shown in Figure 4.33, the 5 wt% PEG-PLA group in Figure 4.34, and the 1 wt% LipidPEG group in Figure 4.35. A baseline, pre-injection image with these labels is shown in all these figures.

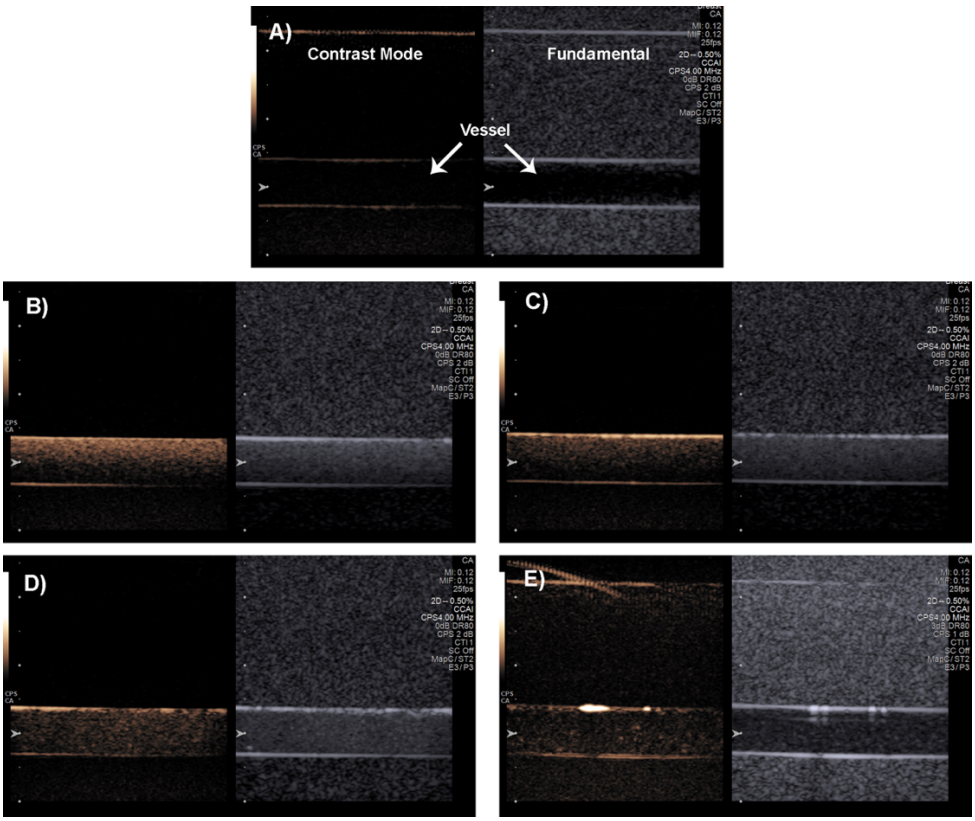

Figure 4.33: Images from ultrasound visualization of the 100% PLA UCA group in a tissue mimicking flow phantom. Each image was taken at a focal length of 4cm, in both non-linear contrast mode (left, orange) and fundamental B-mode (right, gray). A) Pre-injection empty vessel baseline image, B) 100% PLA, C) 100% PLA Dox, D) 100% PLA TRAIL, E) 100% PLA Dox TRAIL.

The strongest enhancement is visible for the unmodified 100% PLA UCA (Figure 4.33B), with visible acoustic shadowing caused by the strength of signal from the UCA blocking US transmission through the entire sample. Diminished enhancement is visible for the 100% PLA Dox (Figure 4.33C) and 100% PLA TRAIL (Figure 4.33D), which corresponds to the reduction in echogenicity observed in our custom acoustic setup. Nonetheless, the flow phantom images confirm that these modified microbubbles are still functional as UCA. The least enhancement was observed for the 100% PLA Dox TRAIL UCA (Figure 4.33E), which were barely visible with low stability and viability. However, these agents were still visible under conditions similar to those used in a clinical setting, and may require a higher dosage concentration for increased visualization.

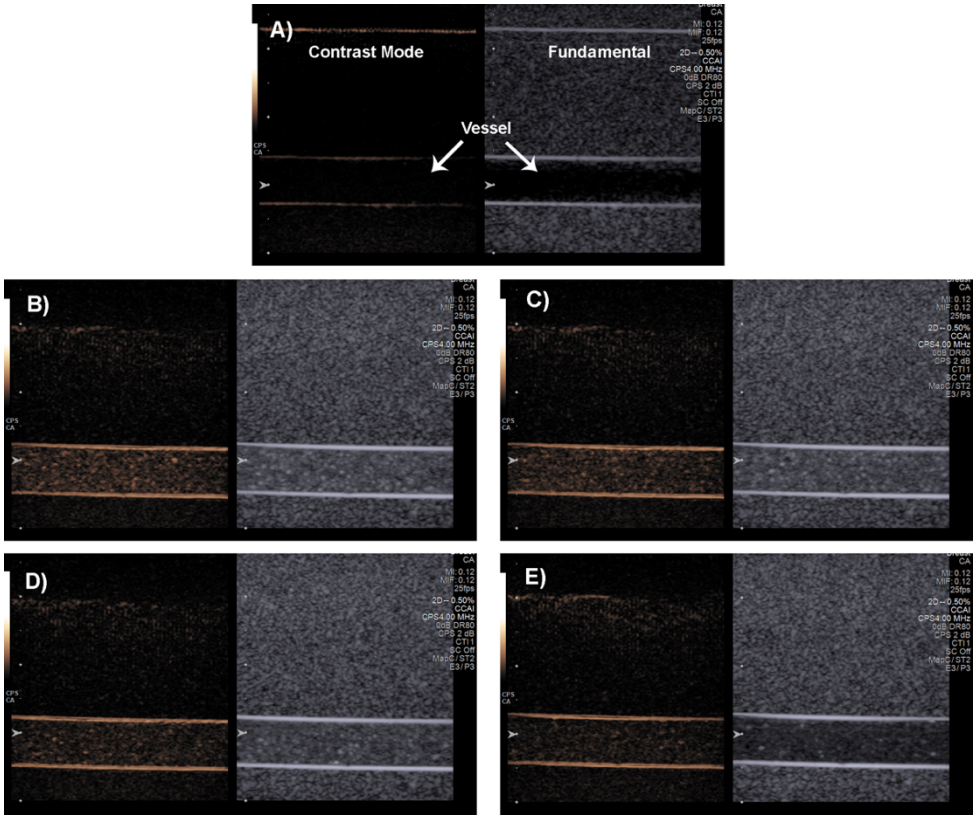

Figure 4.34: Images from ultrasound visualization of the 5 wt% PEG-PLA UCA group in a tissue mimicking flow phantom, focal length 4cm. Each image was taken in both non-linear contrast mode (left, orange) and fundamental B-mode (right, gray). A) Pre-injection empty vessel baseline image, B) 5 wt% PEG-PLA, C) 5 wt% PEG-PLA Dox, D) 5 wt% PEG-PLA TRAIL, E) 5 wt% PEG-PLA Dox TRAIL.

The 5 wt% PEG-PLA group behaved similarly to the 100% PLA group under these visualization conditions, but with diminished overall enhancement. Since samples were standardized to UCA concentration per milligram so that the same number of bubbles were passing through the phantom in each test, these images suggest that the strength of the enhancement is lost as a function of the shell material. Enhancement is visible for the unmodified 5 wt% PEG-PLA UCA (Figure 4.34B) and the 5 wt% PEG-PLA Dox UCA (Figure 4.34C), while the enhancement is further diminished with the 5

wt% PEG-PLA TRAIL UCA (Figure 4.34D). Again, this corresponds with their acoustic performance in our custom acoustic setup. Enhancement was even further diminished for the 5 wt% PEG-PLA Dox TRAIL UCA (Figure 4.34E), with low stability and visualization time while passing through the focused US beam. Despite the diminished enhancement, these agents were still visible under clinical conditions, and can still be considered viable as functionalized UCA for targeted drug delivery.

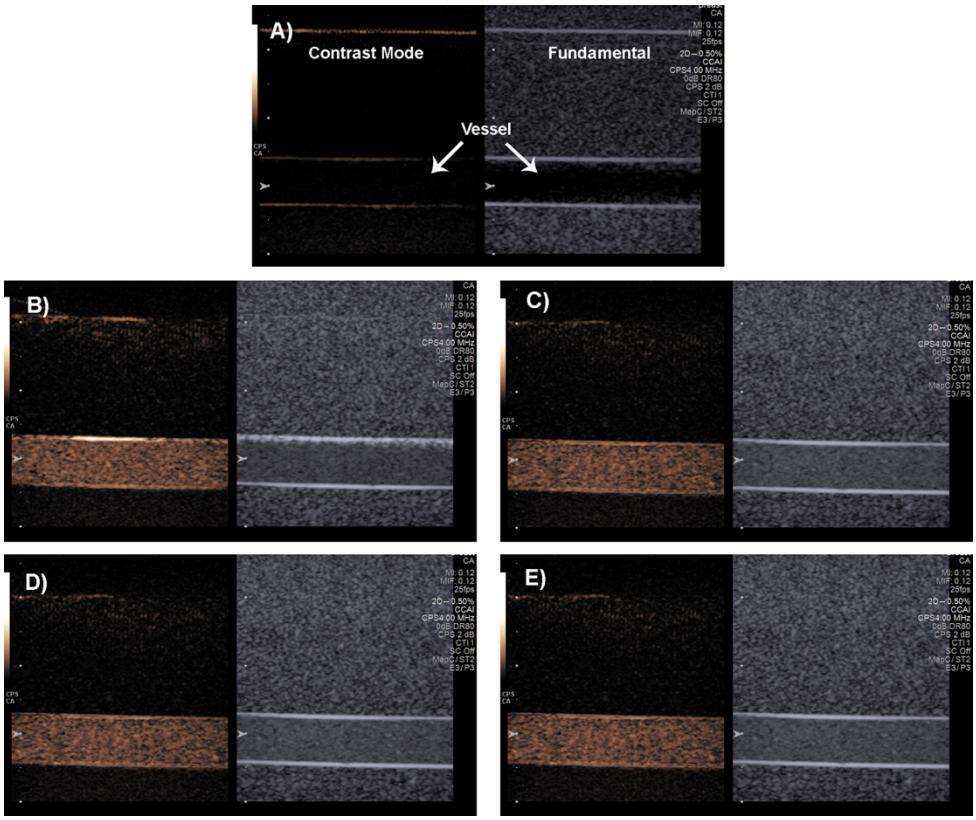

Figure 4.35: Images from ultrasound visualization of the 1 wt% LipidPEG UCA group in a tissue mimicking flow phantom. Each image was taken at a focal length of 4cm, in both non-linear contrast mode (left, orange) and fundamental B-mode (right, gray). A) Pre-injection empty vessel baseline image, B) 1 wt% LipidPEG, C) 1 wt% LipidPEG Dox, D) 1 wt% LipidPEG TRAIL, E) 1 wt% LipidPEG Dox TRAIL.

Unlike the trends observed in the 100% PLA and 5 wt% PEG-PLA groups, there was no discernible loss of enhancement from the unmodified 1 wt% LipidPEG UCA with any of the modifications (i.e. Dox loading and TRAIL ligation). Strong enhancement is visible for the unmodified 1 wt% LipidPEG UCA (Figure 4.35B), 1 wt% LipidPEG Dox UCA (Figure 4.35C), 1 wt% LipidPEG TRAIL UCA (Figure 4.35D), and 1 wt% LipidPEG Dox TRAIL UCA (Figure 4.35E). Again, this is in agreement with our custom backscatter measurements, and these images confirm that these modified agents retain their functionality as UCA when adapted for targeted therapy. Taken together with the backscatter measurements, these images further support the use of the 1 wt% LipidPEG shell material for TRAIL ligation, and the use of the 5 wt% PEG-PLA shell material for Dox encapsulation (without TRAIL).

4.3.6 Effects of Functionalization on Resonant Frequency

The resonant frequency of each functionalized UCA and their corresponding unmodified UCA was determined experimentally, taking the minimum point from the graph plotting attenuation vs. frequency curves (Figure 4.36).

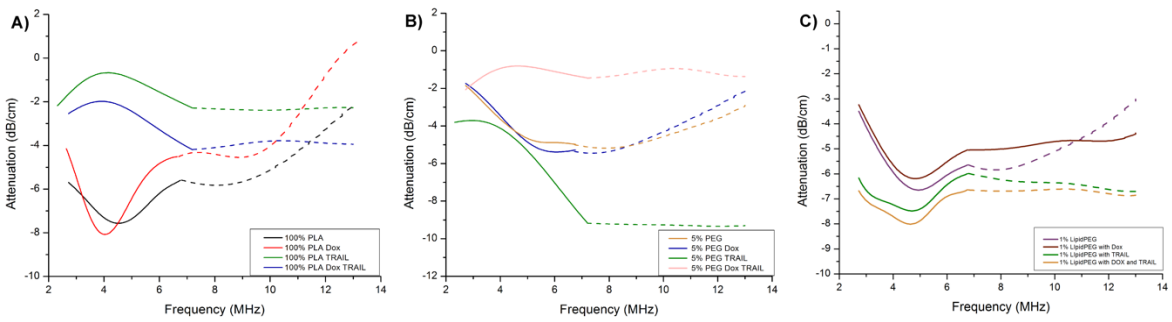

Figure 4.36: Attenuation (dB/cm) vs. frequency (MHz) resonance curves. Solid line represents measurements taken with 5MHz unfocused transducer (bandwidth = 91%), and dotted line represents measurements taken with 10MHz unfocused transducer (bandwidth = 65%). PRF = 100Hz, Energy = 1, Damping Level = 3, Gain = 0. A) Measurements of the 100% PLA group, B) Measurements of the 5 wt% PEG-PLA group, C) Measurements of the 1 wt% LipidPEG group.

As shown previously, the resonant frequency of the 100% PLA UCA is 4.56MHz. Dox-loading of the 100% PLA UCA caused a slight shift in resonance to 4.04MHz, which is well within the bandwidth range of the 5MHz transducer used for the acoustic evaluations discussed in previous subsections. Both 100% PLA TRAIL UCA and 100% PLA Dox TRAIL UCA showed a shift in resonant frequency to approximately 7.2MHz, suggesting that TRAIL ligation induces changes to the shell elasticity and stiffness that affect its ability to cavitate and resonate within the US beam [169, 170, 190, 191]. These TRAIL-ligated UCA also had reduced average diameters, which is another factor that inversely influences resonant frequency. Such a shift in resonance frequency could explain the reduced echogenicity observed in our acoustic evaluations, as the bandwidth of the transducer may not effectively insonate the UCA at their new resonant frequency resulting in reduced oscillations and cavitation. There were no major shifts in resonant frequency in response to modifications in the 5 wt% PEG-PLA group (range: 6.02-7.84MHz) and the 1 wt% LipidPEG group (range: 4.68-4.96MHz). However, the 5 wt%

PEG-PLA group showed large fluctuations in attenuation following ligation with TRAIL, suggesting a non-uniform population consisting of microspheres and other particles. The 1 wt% LipidPEG group showed the most stability in resonant frequency in response to modification, suggesting that this platform is most versatile for modification to desired applications. These findings suggest that post-fabrication TRAIL ligation in the 100% PLA and 5 wt% PEG-PLA UCA leads to structural changes in the shell that inhibit the oscillation of the encapsulated gas core in the presence of a focused US beam. Since these changes are not observed in the 1 wt% LipidPEG group, this shell material appears to be the best for generating UCA decorated with TRAIL.

4.3.7 Effects of Drug Loading and TRAIL Ligation on UCA Size, Zeta Potential, and Surface Morphology

As described previously, size and morphology play a crucial role in determining microbubble acoustic behavior [153, 168-170]. All UCA formulations had an average diameter between 1-3μm (Figure 4.37), well within the acceptable range (<6μm) for clear passage through the vasculature, resonance in the clinical frequency range, and susceptibility to radiation forces [108, 109].

Dox and TRAIL loading in the 100% PLA group (Figure 4.37A) resulted in decreased UCA diameter for all three types of modification ($p<0.0001$). Average diameters ranged from 1.43±0.04 to 1.71±0.06μm compared to unmodified 100% PLA UCA (2.41±0.10μm). Particle size distribution, measured by polydispersity index (PDI) was not significantly different for any of the 100% PLA groups, ranging from 0.184 to 0.214, indicating a tight size distribution for all 100% PLA UCA groups.

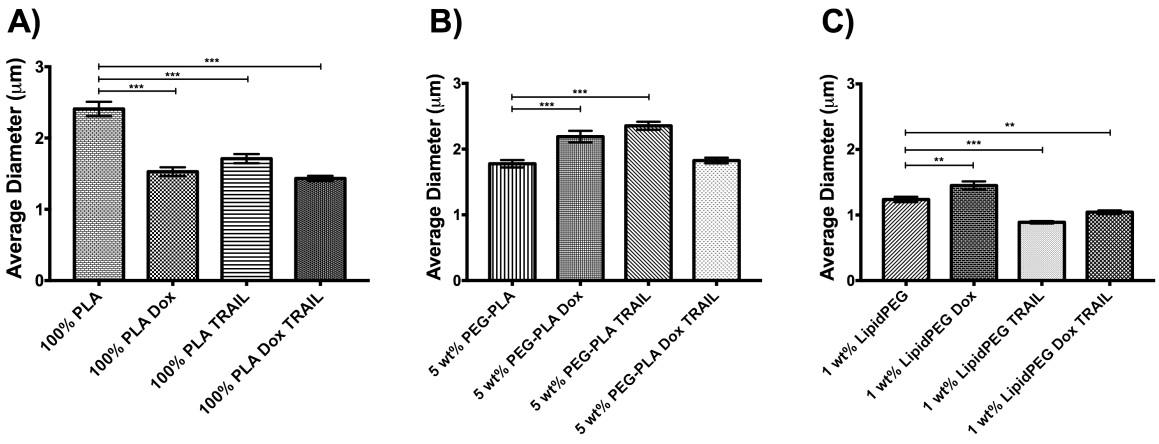

Figure 4.37: Average particle size of UCA. Error bars = SEAM, n=5, ***p<0.0001. A) Measurements of the 100% PLA UCA group, B) Measurements of the 5 wt% PEG-PLA UCA group, C) Measurements of the 1 wt% LipidPEG UCA group, **p=0.0009 for 1wt% LipidPEG to 1 wt% LipidPEG Dox, **p=0.0029 for 1 wt% LipidPEG to 1 wt% LipidPEG Dox TRAIL.

For the 5 wt% PEG-PLA group (Figure 4.37B), average UCA diameter increased from unmodified 5 wt% PEG-PLA (1.78±0.06μm) to 5 wt% PEG-PLA Dox UCA (2.24±0.07μm) ($p<0.0001$). Taken together with the changes in echogenicity and #UCA/mg, this change is likely due to interaction between the polymer groups while accommodating Dox loading, ultimately leading to thicker, larger polymeric shells. UCA diameter further increased with TRAIL ligation (2.35±0.06μm, $p<0.0001$), likely due to swelling during the maleimide ligation in an aqueous solution. Our lab previously showed an increase in UCA size immediately upon introduction to an aqueous environment, supporting this theory [4]. All 5 wt% PEG-PLA UCA had a wider size distribution than 100% PLA UCA, with PDI ranging from 0.258 to 0.346, indicating that these agents are less uniform in distribution.

Similarly, 1 wt% LipidPEG Dox UCA (1.45±0.06μm) were larger than unmodified 1 wt% LipidPEG UCA (1.24±0.04μm, $p=0.0009$) (Figure 4.37C). This is likely due to rearrangement of polymer chains and lipid tail groups to accommodate Dox encapsulation. Average particle size decreased with TRAIL ligation, both for 1 wt% LipidPEG TRAIL UCA (0.89±0.02μm, $p<0.0001$) and 1 wt% LipidPEG Dox TRAIL UCA (1.04±0.03μm, $p=0.0029$) compared to their unmodified counterpart. This is likely due to steric hindrance introduced by the TRAIL molecules preventing PEG folding into the mushroom formation. Similar to the 5 wt% PEG-PLA group, all 1 wt% LipidPEG UCA exhibited an increased PDI (0.262-0.352), suggesting that these agents have a wider, less uniform size distribution.

All UCA groups maintained a negative zeta potential (ζ) mV (Figure 4.38); however, the magnitude of this potential decreased dramatically ($p<0.0001$) in response to functionalization in the 100% PLA (Figure 4.38A) and 5 wt% PEG-PLA (Figure 4.38B) groups. Similar reduction in ζ magnitude was observed for the 1 wt% LipidPEG Dox UCA ($p<0.0001$). In all 5 of these cases, the magnitude of the zeta potential was decreased below 20mV, which would be in violation of the FDA regulation for injectables and also suggests that these agents are susceptible to aggregation and vascular blockage when administered intravenously [173].

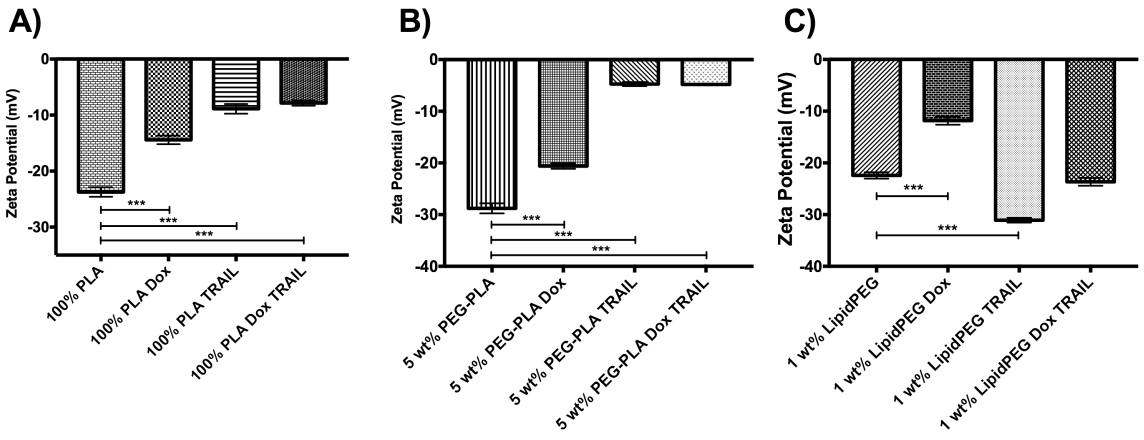

Figure 4.38: Average zeta potential of functionalized UCA, error bars = SEAM, n=5, ***p<0.0001. A) Measurements of the 100% PLA UCA group, B) Measurements of the 5 wt% PEG-PLA UCA group, C) Measurements of the 1 wt% LipidPEG UCA group.

For the 100% PLA group, all functionalized agents exhibited a significantly decreased magnitude in zeta potential ($p<0.0001$) compared to the unmodified 100% PLA UCA ($\zeta = -23.75\pm5.69$mV). The same trend is observed in the 5 wt% PEG-PLA group, with all functionalized agents becoming less negatively charged ($p<0.0001$) than the unmodified 5 wt% PEG-PLA UCA ($\zeta = -28.79\pm6.49$mV). While addition of Dox caused both the 100% PLA Dox UCA ($\zeta = -14.43\pm5.10$mV) and 1 wt% LipidPEG Dox UCA ($\zeta = -11.84\pm5.26$mV) to drop below the 20mV safety cutoff, Dox-loading of the 5 wt% PEG-PLA Dox UCA resulted in agents that could still be considered safe by FDA standards with an average ζ of -20.62 ± 3.54mV. Since Dox is a hydrophilic, positively-charged molecule, it stands to reason that its incorporation into the UCA shell would alter the arrangement of charged groups within the shell, leading to these changes in zeta potential.

Zeta potential was also significantly reduced ($p<0.0001$) in response to ligation of TRAIL to the surface of the 100% PLA TRAIL UCA ($\zeta = -8.89\pm5.76$mV), 100% PLA Dox TRAIL UCA ($\zeta = -7.86\pm3.18$mV), 5 wt% PEG-PLA TRAIL UCA ($\zeta = -4.74\pm2.69$mV), and 5 wt% PEG-PLA Dox TRAIL UCA ($\zeta = -4.82\pm1.14$mV) compared to their unmodified counterparts. Again, these agents cannot be considered viable as they do not meet the FDA cutoff of -20mV to prevent aggregation. TRAIL is a positively-charged protein, and it is reasonable to assume that decorating the surface of the UCA with TRAIL would shield the COOH on the UCA surface from detection and contribute to a significant dipole, ultimately altering the overall surface charge of the agent as a whole. However, there is no significant reduction in zeta potential magnitude when 1 wt% LipidPEG UCA are functionalized with TRAIL. Ligation of TRAIL to the LipidPEG molecule is optimized such that a larger proportion of LipidPEG remains unligated in order to reduce immunogenicity. Since the LipidPEG molecules are capped with a carboxyl group, they contribute to the overall negative zeta potential of the UCA and mitigate the charge effects of the ligated TRAIL molecules.

Scanning electron microscopy (SEM) images were taken to assess surface morphology of the functionalized agents, showing the 100% PLA group in Figure 4.39, the 5 wt% PEG-PLA group in Figure 4.40, and the 1 wt% LipidPEG group in Figure 4.41. In all cases, modification did not result in any changes to surface morphology compared to the unmodified native agent (A). UCA retained smooth, spherical morphology in both the 100% PLA and 1 wt% LipidPEG groups, while the bimodal distribution of spheres and collapsed particles remained in the 5 wt% PEG-PLA group. Despite the collapsed appearance observed in the 5 wt% PEG-PLA group, these agents

were still acoustically active, suggesting alterations to the shell making them overly sensitive to the vacuum conditions for SEM imaging.

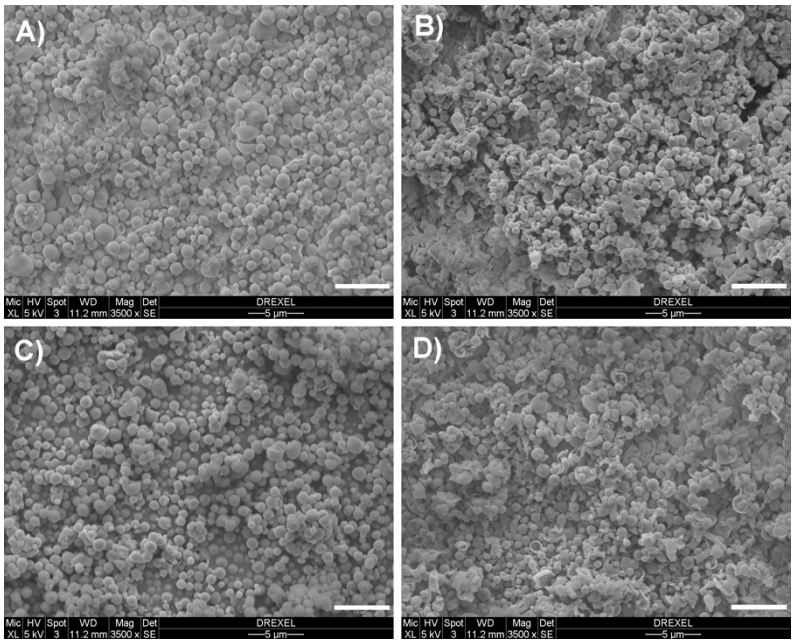

Figure 4.39: SEM images of 100% PLA UCA. Magnification 3500x, size bar 5μm. A) 100% PLA UCA, B) 100% PLA Dox UCA, C) 100% PLA TRAIL UCA, D) 100% PLA Dox TRAIL UCA.

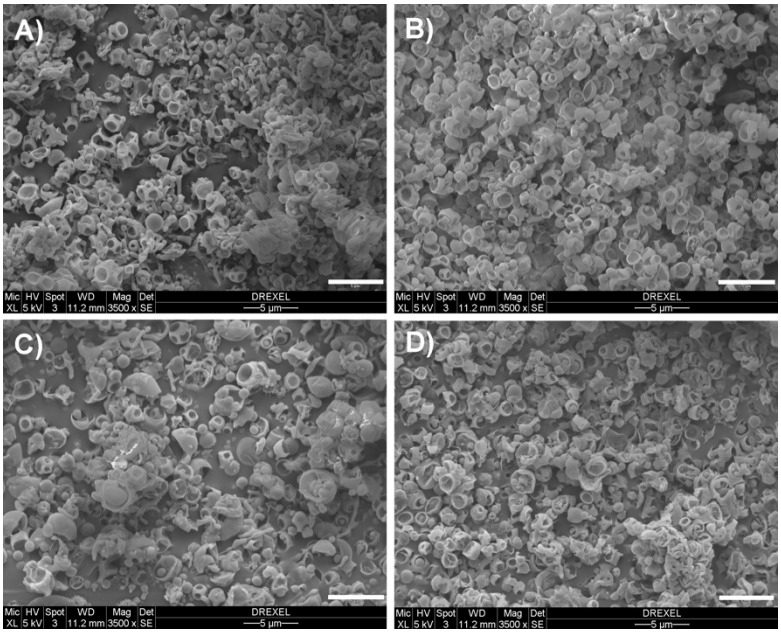

Figure 4.40: SEM images of 5 wt% PEG-PLA UCA. Magnification 3500x, size bar 5µm. A) 5 wt% PEG-PLA UCA, B) 5 wt% PEG-PLA Dox UCA, C) 5 wt% PEG-PLA TRAIL UCA, D) 5 wt% PEG-PLA Dox TRAIL UCA.

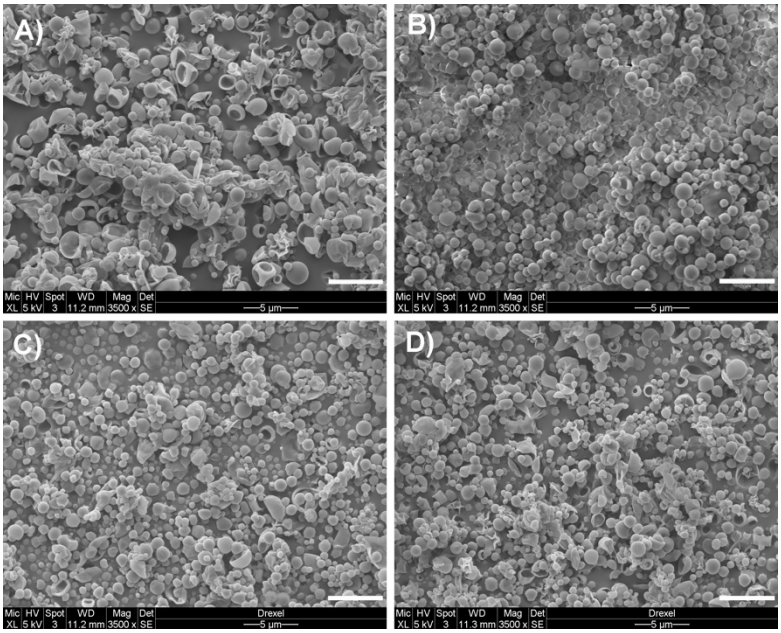

Figure 4.41: SEM images of 1 wt% LipidPEG UCA. Magnification 3500x, size bar 5µm. A) 1 wt% LipidPEG UCA, B) 1 wt% LipidPEG Dox UCA, C) 1 wt% LipidPEG TRAIL UCA, D) 1 wt% LipidPEG Dox TRAIL UCA.

In summary, shell modification led to changes in average UCA diameter, which can have an effect on acoustic backscatter and cavitation. Dox loading and TRAIL ligation also led to increased PDI measurements for modified UCA, indicating that these processes modify the agents such that they become less uniform in population. Zeta potential was significantly altered in response to modification. When ligated with TRAIL, 100% PLA and 5 wt% PEG-PLA exhibit a reduction in zeta potential magnitude, to such a high degree that they would be considered unsafe and susceptible to aggregation by FDA standards. 1 wt% LipidPEG TRAIL UCA and Dox TRAIL UCA do not experience this reduction, and represent viable TRAIL-ligated agents. However, 1 wt% LipidPEG Dox UCA reduced in zeta potential enough to fall below the FDA cutoff, while 5 wt% PEG-PLA Dox UCA retained enough zeta potential magnitude for viability and stability in solution. Modification did not cause any visible changes to UCA surface morphology compared to the unmodified native agents, further suggesting that any changes to UCA behavior are due to changes in interior shell structure (stiffness and thickness) when considered in conjunction with the resonant frequency results.

4.3.8 Ultrasound-triggered n-Sh Production from UCA with Shell Modifications

Native and modified UCA were screened in our custom acoustic setup to determine the potential to undergo bursting into n-Sh in the presence of focused US. Agents were insonated with a 5MHz transducer set for a higher mechanical index (approximately 0.193, peak positive pressure 0.94MPa) for 15 minutes, with backscatter measurements taken every minute. As shown in Figure 4.42, all functionalized agents lost echogenicity rapidly (reaching their acoustic half-life in 4 minutes or less, $p<0.0001$ compared to time to reach acoustic half-life under US at a lower MI) in the presence of a

clinically-relevant US beam. The loss of signal signifies that the agents can no longer reflect the signal from the formerly encapsulated air core, which could be lost due to shattering or shell rupture and subsequent shrinkage due to the gas loss [176, 177].

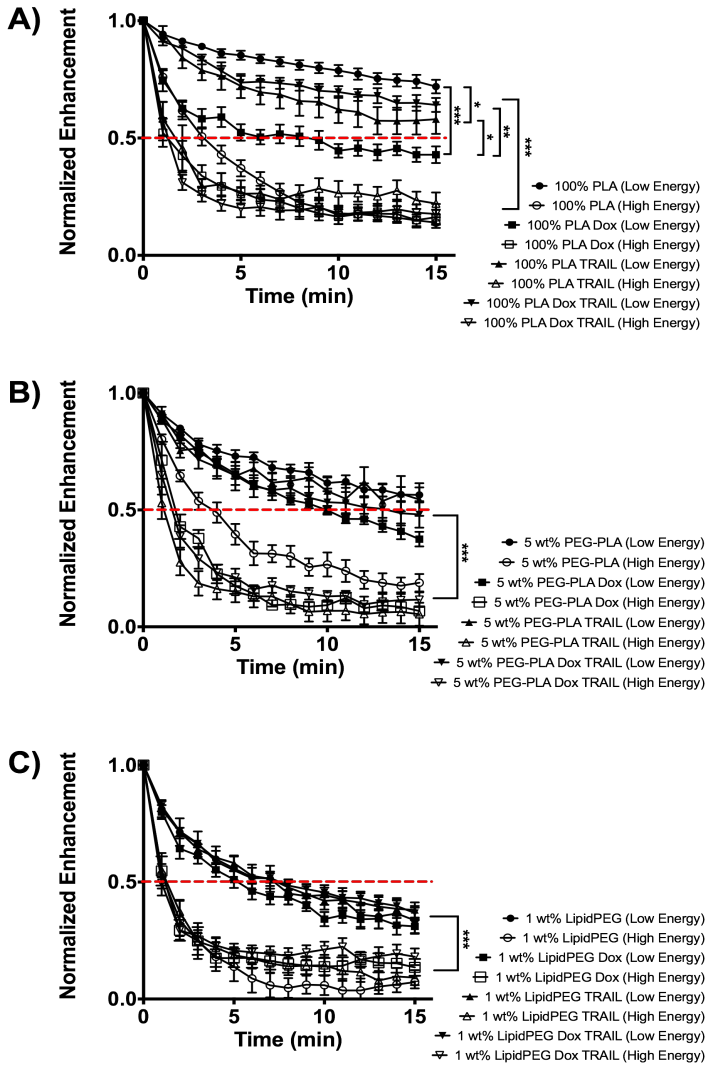

Figure 4.42: Acoustic time response curves for modified UCA insonated at low energy (MI 0.152, peak positive pressure 0.7 MPa) and high energy (MI 0.193, peak positive pressure 0.94 MPa). Dotted line represents acoustic half-life. Error bars = SEAM, n=5. A) Results from the 100% PLA group, *p=0.0439 for 100% PLA (low energy) to 100% PLA TRAIL (low energy), *p=0.0497 for 100% PLA Dox (low energy) to 100% PLA TRAIL (low energy), **p=0.0014, ***p<0.0001, B) Results from the 5 wt% PEG-PLA group, ***p<0.0001, C) Results from the 1 wt% LipidPEG group, ***p<0.0001.

For the 100% PLA group (Figure 4.42A), the Dox-loaded UCA ($p<0.0001$) and TRAIL-ligated UCA ($p=0.0439$) are significantly less stable than the unmodified 100% PLA UCA under US with a lower MI and pressure. The 100% PLA Dox UCA, which reach their acoustic half-life after approximately 9 minutes, are also significantly less stable that 100% PLA TRAIL UCA ($p=0.0497$) and 100% PLA Dox TRAIL UCA ($p=0.0014$) under low-powered US insonation. This is likely due to disruptions in the UCA shell caused by introduction of Dox and its probable movement through the shell during lyophilization. No statistical differences in stability under US with a lower MI were observed in the 5 wt% PEG-PLA group (Figure 4.42) or the 1 wt% LipidPEG group (Figure 4.42), suggesting that the PEGylation may contribute to stabilizing the UCA shell.

Based on these reductions in acoustic half-life, modified agents were evaluated for average particle size after insonation, to determine whether US exposure caused significant particle diameter decrease to within the desired range for extravasation (between 400-700nm), as denoted by the dotted lines and red region (Figure 4.43).

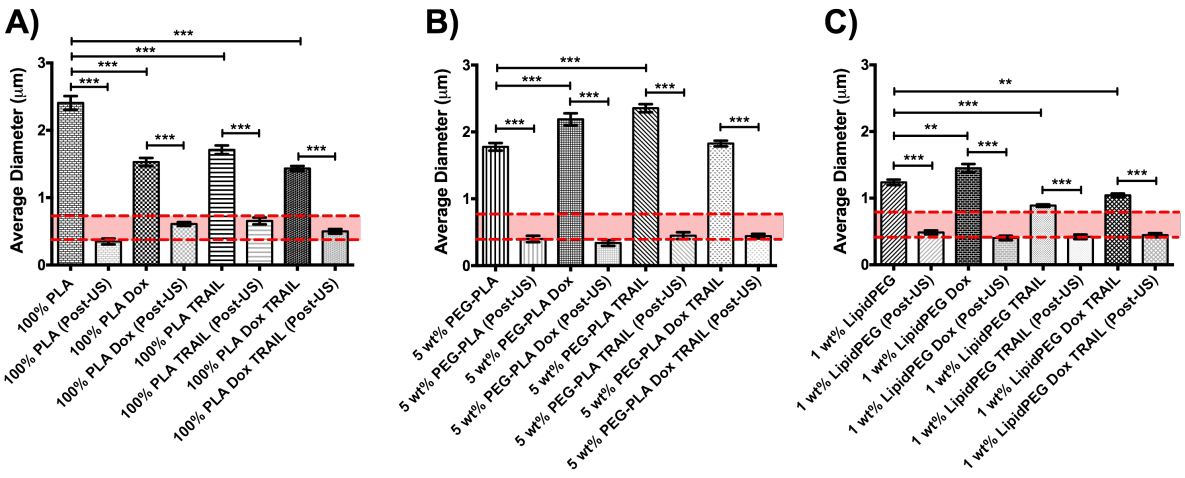

Figure 4.43: Average particle size of UCA pre-insonation and post-insonation (MI 0.193 at 0.94 MPa PPP). A) Measurements of the 100% PLA group, ***p<0.0001, B) Measurements of the 5 wt% PEG-PLA group, ***p<0.0001, C) Measurements of the 1 wt% LipidPEG group, **p=0.0009 for 1 wt% LipidPEG to 1 wt% LipidPEG Dox, **p=0.0029 for 1 wt% LipidPEG to 1 wt% LipidPEG Dox TRAIL, ***p<0.0001. Dotted lines represent 400-700nm range, the desired range for extravasation and n-Sh production. Error bars represent SEAM, n=5.

US-triggered size reduction was significant (p<0.0001) for each tested agent, and the n-Sh produced by shattering the UCA with US all have an average size within the desired range for extravasation. These findings suggest that shell modification with Dox, TRAIL, and a combination of both does not prevent shattering into n-Sh under the influence of US. Generation of appropriately-sized n-Sh is an important aspect of our novel US-triggered drug delivery system. The n-Sh from the modified shells would be of small enough to pass through the pores in the leaky tumor vasculature (400-780nm) and reach the targeted tissue for effective therapy. Therefore, we have demonstrated that our modified UCA are capable of oscillating and shattering into nano-sized fragments in response to exposure to a focused US beam, supporting their potential as targeted drug delivery agents.

4.3.9 Immunogenic Characterization of Functionalized UCA

Experiments were performed to determine the effect of shell modification on the immune response triggered by the UCA using a C3a activation ELISA assay (Figure 4.44 and Figure 4.45), as well as whether the agents exhibited contamination by bacteria using a limulus amebocyte lysate (LAL) chromogenic endotoxin quantification assay (Figure 4.46).

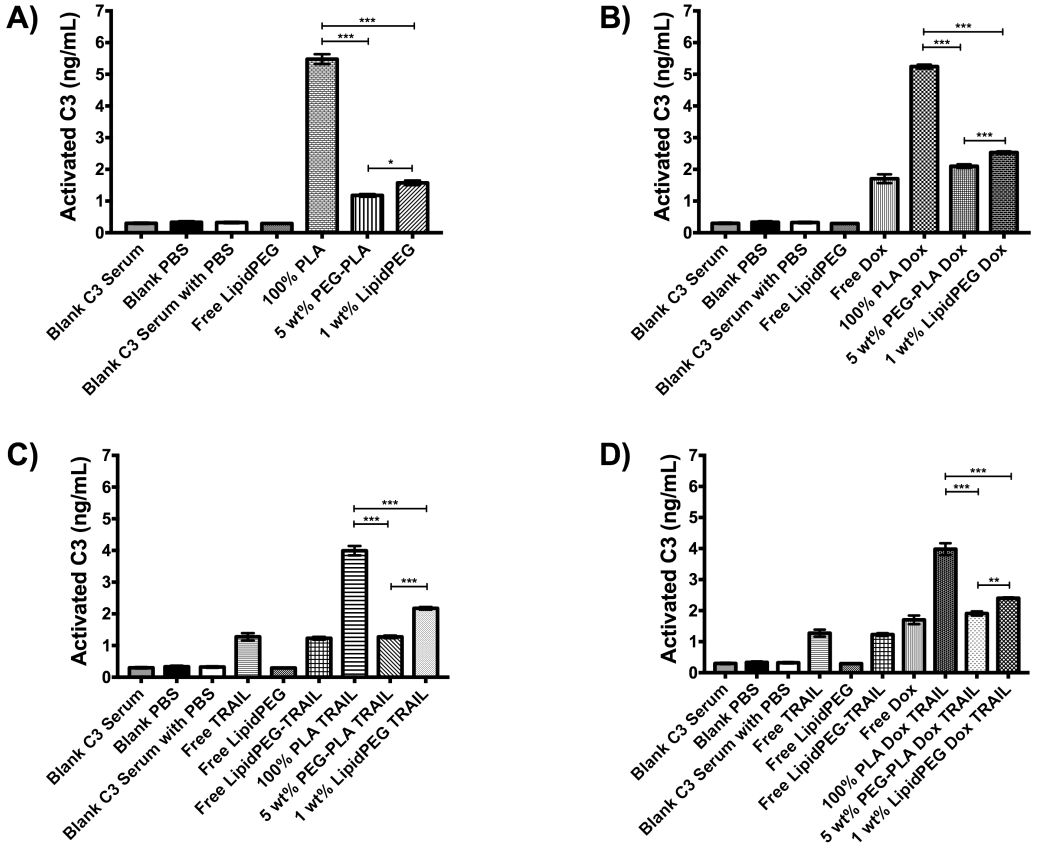

Figure 4.44: C3 complement activation assay results. Error bars represent SEAM, n=2. A) Results from the unmodified UCA group, *p=0.0143, ***p<0.0001, B) Results from the Dox-loaded UCA group ***p<0.0001, C) Results from the TRAIL-ligated UCA group ***p<0.0001, D) Results from the Dox-loaded and TRAIL-ligated UCA group **p=0.0072, ***p<0.0001.

In all three modification groups and in the unmodified control group, both PEGylated forms of UCA were significantly less immunogenic than the 100% PLA UCA ($p<0.0001$). Additionally, the 5 wt% PEG-PLA UCA was less immunogenic than the 1 wt% LipidPEG UCA for all three functional groups (Dox only $p<0.0001$, TRAIL only $p<0.0001$, and Dox TRAIL combined $p=0.0072$) and the unmodified control group ($p=0.0143$).

For the 100% PLA group (Figure 4.45A), no significant difference in immunogenicity was observed between the unmodified 100% PLA UCA (5.48±0.16ng activated C3/mL serum) and the 100% PLA Dox UCA (5.24±0.06ng activated C3/mL serum) ($p=0.6797$). Immunogenicity was significantly reduced when TRAIL was ligated to the 100% PLA shell, for both unmodified 100% PLA UCA to 100% PLA TRAIL UCA (3.99±0.15ng activated C3/mL serum, $p<0.0001$) and for 100% PLA Dox UCA to 100% PLA Dox TRAIL UCA (3.98±0.19ng activated C3/mL serum, $p<0.0001$). No significant difference was observed between the 100% PLA TRAIL UCA and 100% PLA Dox TRAIL UCA ($p>0.9999$).

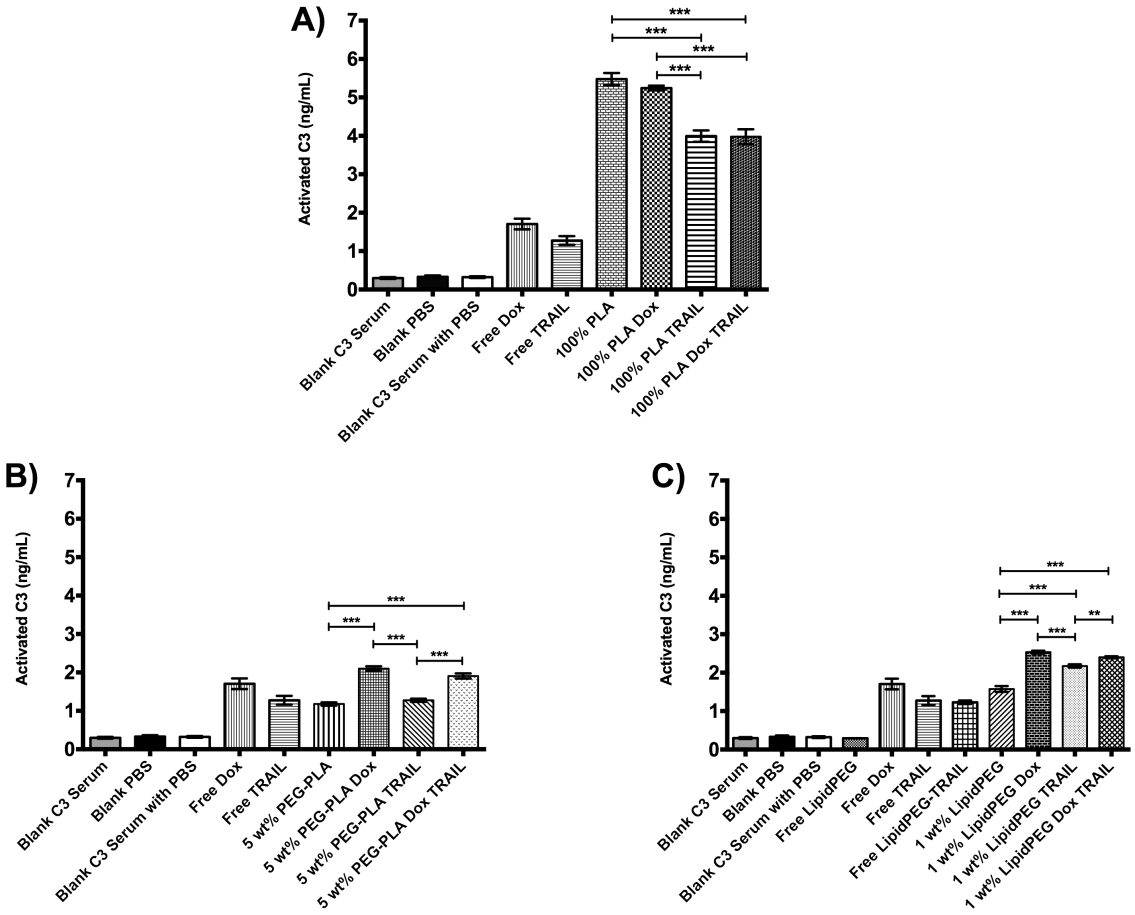

Figure 4.45: C3 complement activation assay results. Error bars represent SEAM, n=2. A) Results from the 100% PLA group ***p<0.0001, B) Results from the 5 wt% PEG-PLA group ***p<0.0001, C) Results from the 1 wt% LipidPEG group **p=0.0093 ***p<0.0001.

Unlike the 100% PLA group, there was no significant decrease in C3 activation with the addition of TRAIL to the 5 wt% PEG-PLA UCA (Figure 4.45B) for unmodified (1.18±0.04ng activated C3/mL serum) to TRAIL-ligated (1.27±0.04ng activated C3/mL serum (p=0.5938) and for Dox-loaded (2.10±0.06ng activated C3/mL serum) to Dox TRAIL UCA (1.91±0.07ng activated C3/mL serum) (p=0.0685). This is likely due to the fact that immunogenicity is already significantly reduced due the the PEG groups

exposed on the UCA surface, compared to the 100% PLA UCA ($p<0.0001$). Encapsulation of Dox resulted in a significant increase in immunogenicity for both 5 wt% PEG-PLA Dox UCA compared to unloaded 5 wt% PEG-PLA UCA ($p<0.0001$) and for 5 wt% PEG-PLA TRAIL UCA compared to 5 wt% PEG-PLA Dox TRAIL UCA ($p<0.0001$).

This trend was also observed in the 1 wt% LipidPEG group (Figure 4.45C), with the 1 wt% LipidPEG Dox UCA (2.53±0.04ng activated C3/mL serum) significantly more immunogenic than unloaded 1 wt% LipidPEG UCA (1.58±0.07ng activated C3/mL serum) ($p<0.0001$) as well as 1 wt% LipidPEG Dox TRAIL UCA (2.40±0.03ng activated C3/mL serum) compared to 1 wt% LipidPEG TRAIL UCA (2.17±0.04ng activated C3/mL serum) ($p=0.0093$). Interestingly for the 1 wt% LipidPEG group, all modified agents exhibited significantly more C3 activation than the unmodified 1 wt% LipidPEG UCA ($p<0.0001$). This suggests that the modifications made to the agents during modification may influence the orientation and expression of the PEG molecule brush on the UCA surface, allowing for more interaction with the C3 protein. In both the 5 wt% PEG-PLA and 1 wt% LipidPEG groups, C3 activation significantly increased when Dox was encapsulated within the agents ($p<0.0001$); however, this was not observed for the 100% PLA group despite the higher Dox encapsulation efficiency of these agents. These observations suggest that the modifications to the shell material may increase the expression of Dox closer to the UCA surface, allowing the serum to interact with the toxic drug and become activated.

Our observation of reduced C3 activation in the presence of TRAIL supports the emerging belief that TRAIL plays a role in immune regulation [192-194]. Briefly, TRAIL

is a member of the tumor necrosis factor (TNF) family, of which ligands and their receptors have critical influence on the immune system through apoptosis in active lymph cells [192, 193]. Specifically, TRAIL has been demonstrated to be a regulator of $CD8^+$ T-cell activation as well as a preventative mechanism to autoimmune disease [192, 195, 196]. As explained previously, C3 could also be activated through interaction of the unstable thioester bonds in the C3 protein and the carboxylic end groups on the PLA shell surface [133, 140, 182, 183]. The ligation of TRAIL to the UCA surface may provide some steric hindrance that reduces these interactions by blocking access to the UCA surface, and therefore reducing immunogenicity similar to the action of the LipidPEG molecules that extend from the UCA surface in the LipidPEG group.

Based on the fabrication process, another immunogenic concern with these agents was the presence of endotoxins that could contaminate the agent and skew the C3 assay results. Endotoxin quantification assay results, shown in Figure 4.46, indicate that all of the experimental UCA (unmodified and functionalized) were well below the FDA limit of 0.2 EU/mL ($p<0.0001$) while still exhibiting a small amount of activation (average 0.06 EU/mL) that can trigger the immune-regulated apoptosis cascade [41, 197].

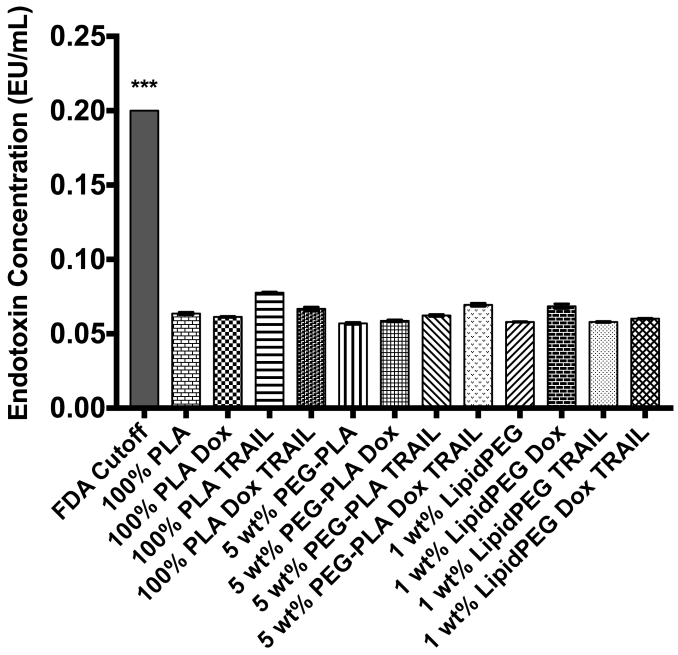

Figure 4.46: Endotoxin quantification assay results. Error bars represent SEAM, n=3, ***p<0.0001.

Overall, UCA shell modification yielded UCA that retained the ability to reduce immune activation through the complement system, having a low bio-burden, and also retaining base levels of endotoxin to support immune-regulated apoptosis. Both 5 wt% PEG-PLA and 1 wt% LipidPEG groups exhibited reduced complement activation compared to the 100% PLA group, indicating that the addition of Dox and TRAIL to the UCA was not deleterious to the immunogenic protection of PEGylation. Low levels of endotoxin were detected across all groups, indicating that the UCA were not contaminated with bacteria. As such, these drug-loaded and ligated agents represent a great potential for use as targeted drug delivery agents.

4.3.10 *In vitro* Tumoricidal Activity of Dox-loaded and TRAIL-ligated UCA

To determine the effectiveness of these agents against breast cancer tumors, we performed *in vitro* cell studies against two breast cancer cell lines. The first, MDA-MB-231 breast adenocarcinoma cells, is known to be sensitive to TRAIL by having abundant DR4 and DR5 receptors expressed on the surface. We also have extensive experience with these cells. The second cell line, MCF7 breast adenocarcinoma cells, was selected as a TRAIL-resistant population. These cells represent breast cancers that are less responsive to TRAIL treatments, resulting from cell-specific combinations of reduced expression of DR4/DR5 receptors, increased expression of decoy receptors, and intracellular resistance mechanisms [198]. Studies evaluated whether co-administration of Dox helps overcome resistance to TRAIL treatments. Dox-loaded UCA and n-Sh were introduced to the cells in a standardized amount based on encapsulation efficiency. A third cell line, MCF-12A breast epithelial cells, were evaluated as a healthy control group. All cells were grown in 6-well plates, incubated with each treatment for 24 hours, and read via flow cytometry. Cells were stained with green-fluorescent Alexa Fluor 488 Annexin V to detect the externalization of phosphatidylserine in apoptotic cells, red-fluorescent propidium iodide to detect nucleic acids of necrotic/dead cells, and blue-fluorescent Hoescht blue nuclear stain to visualize live cells.

4.3.10.1 MDA-MB-231 Cells

MDA-MB-231 cells were first exposed to negative and positive control treatments for comparison with the experimental agents. Negative control consisted of incubation with pure cell media, with no additives. Positive controls were free Dox, free TRAIL and a combination of both free Dox and free TRAIL. Flow cytometry results are shown in

Figure 4.47, and cell fate percentages are summarized in Table 4.8. Negative control of no treatment resulted in 98.52±0.38% live cells, indicating that no environmental conditions caused observed cell death. All three positive controls exhibited significant reduction in cell survival ($p<0.0001$). Incubation with free Dox resulted in 60.64±5.32% cell death and 16.95±2.81% apoptosis, leaving only 19.59±6.36% cells alive. Free TRAIL exposure led to 57.65±9.74% apoptosis and 26.44±10.35% cell death, with only 15.29±1.14% cells remaining alive. The combination of free Dox and free TRAIL resulted in only 8.73±1.17% living cells, with 43.43±8.61% apoptotic cells and 46.79±7.47% necrotic/dead cells. These control results will form the basis for determining effectiveness of the experimental agents.

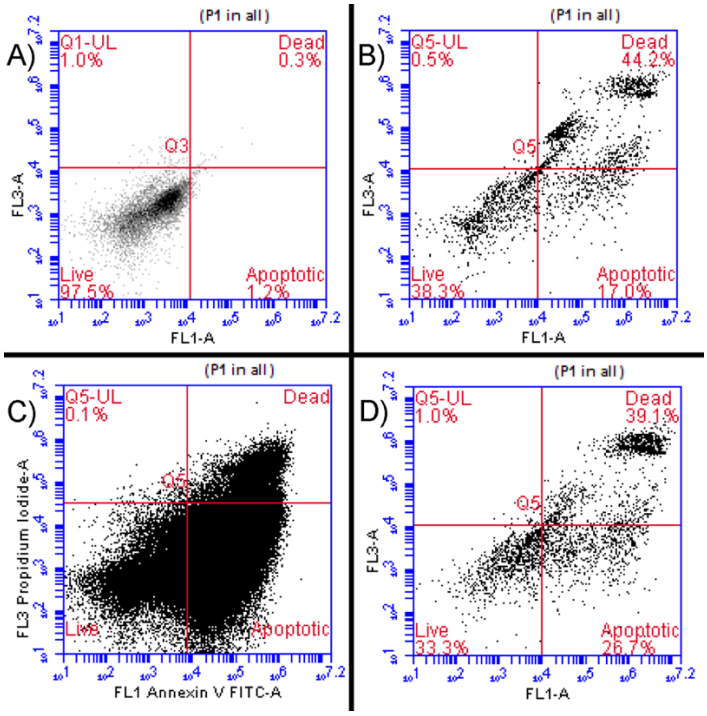

Figure 4.47: Representative flow cytometry plots for MDA-MB-231 breast cancer cells. A) No treatment, B) Dox Only, C) TRAIL Only, D) Dox and TRAIL Only.

Table 4.8: Average cell fate percentages from flow cytometry results for MDA-MB-231 cell control groups, n=3.

	Live Cells (%)	Apoptotic Cells (%)	Dead Cells (%)
No Treatment	98.52 ± 0.38	0.87 ± 0.18	0.28 ± 0.13
Free Dox Only	19.59 ± 6.36	16.95 ± 2.81	60.64 ± 5.32
Free TRAIL Only	15.29 ± 1.14	57.65 ± 9.74	26.44 ± 10.35
Free Dox and TRAIL Only	8.73 ± 1.17	43.43 ± 8.61	46.79 ± 7.47

For the 100% PLA shell type group (summarized in Table 4.9, flow results shown in Figure 4.48), negative controls of unmodified, native 100% PLA UCA (99.03±0.66% live cells) and 100% PLA n-Sh (92.87±2.48% live cells) were evaluated to verify that the polymeric shell or its hydrolytic byproducts did not cause any cell death or disruption. These high levels of cell survival (statistically similar to No Treatment control, $p>0.9999$) indicate that the polymeric shell is not detrimental to cell survival, and any cell death or apoptosis observed in the experimental groups is due to the loaded Dox or ligated TRAIL.

Cell survival was decreased when MDA-MB-231 cells were exposed to the experimental Dox-loaded and TRAIL-ligated agents compared to their unloaded native UCA and n-Sh counterparts. Dox-loaded UCA resulted in 65.36±12.23% cell survival ($p=0.0056$ to 100% PLA UCA), while Dox-loaded n-Sh resulted in 53.75±16.52% cell survival ($p=0.0004$ to 100% PLA n-Sh). There was no statistical difference in cell survival between the Dox-loaded UCA and Dox-loaded n-Sh ($p=0.9993$), likely due to exposure to similar amounts of Dox based the burst release of Dox upon suspension in the cell media in addition to the similar 24-hour release profiles observed in the *in vitro* release study. The combination Dox-loaded and TRAIL-ligated UCA (64.56±6.50% live)

and n-Sh (41.43±0.43% live) also resulted in significantly less cell survival than their native counterparts (p=0.0038 and p=0.0144, respectively).

Table 4.9: Average cell fate percentages from flow cytometry results for MDA-MB-231 cells treated with 100% PLA group of agents, n=3.

	Live Cells (%)	Apoptotic Cells (%)	Dead Cells (%)
100% PLA UCA	99.03 ± 0.66	0.57 ± 0.36	0.39 ± 0.30
100% PLA n-Sh	92.87 ± 2.48	4.61 ± 1.74	2.46 ± 1.01
100% PLA Dox UCA	65.36 ± 12.23	0.76 ± 0.05	33.11 ± 11.96
100% PLA Dox n-Sh	53.75 ± 16.52	6.50 ± 3.17	39.49 ± 14.45
100% PLA TRAIL UCA	86.71 ± 2.72	10.25 ± 3.42	2.39 ± 0.29
100% PLA TRAIL n-Sh	52.84 ± 11.65	36.44 ± 13.17	11.21 ± 6.32
100% PLA TRAIL UCA + Free Dox	78.67 ± 5.26	12.35 ± 4.34	9.50 ± 0.99
100% PLA TRAIL n-Sh + Free Dox	20.32 ± 6.91	42.55 ± 3.47	35.59 ± 4.38
100% PLA Dox TRAIL UCA	64.56 ± 6.50	20.50 ± 4.64	14.69 ± 1.92
100% PLA Dox TRAIL n-Sh	41.43 ± 0.43	24.94 ± 0.38	33.50 ± 0.30

While the cell survival rates for the Dox-loaded UCA/n-Sh and TRAIL-ligated UCA/n-Sh were similar (p=0.4847 for UCA, p>0.9999 for n-Sh), the cell death mechanisms were very different for these two groups. Dox-loaded UCA resulted in 33.11±11.96% dead/necrotic cells and only 0.76±0.05% apoptotic cells, while Dox-

loaded n-Sh resulted in 39.49±14.45% dead/necrotic cells with 6.50±3.17% apoptotic cells. Conversely, TRAIL-ligated UCA resulted in only 2.39±0.29% dead/necrotic cells ($p=0.0152$) and 10.25±3.42% apoptotic cells ($p=0.0500$), while TRAIL-ligated n-Sh resulted in 11.21±6.32% dead/necrotic cells ($p=0.0436$) and 36.44±13.17% apoptotic cells ($p=0.0022$). Since the mechanism of cell death for Dox includes early activation of p53 in tumor cells leading to DNA fragmentation and death, and TRAIL induces apoptosis via transmembrane signaling, this shift in cell death mechanism between these two treatments type can be expected [43, 44, 199]. Additionally, the TRAIL n-Sh resulted in a greater degree of apoptosis (36.44±13.17%) compared to TRAIL UCA (10.25±3.42%, $p=0.0178$), as well as decreased overall cell survival (52.84±11.65% live n-Sh to 86.71±2.72% live UCA, $p=0.0051$). This same trend was observed with the TRAIL UCA + free Dox (78.67±5.26% live; 12.35±4.34% apoptotic) and TRAIL n-Sh + free Dox (20.32±6.91% live, $p=0.0095$; 42.55±3.47% apoptotic, $p=0.0019$). The increased apoptosis observed with the n-Sh comes from an increased availability of TRAIL molecules to bind to the cells, utilizing the entire UCA surface as n-Sh spread across the cell plate surface instead of a single contact point at the UCA-cell surface interface [4, 200].

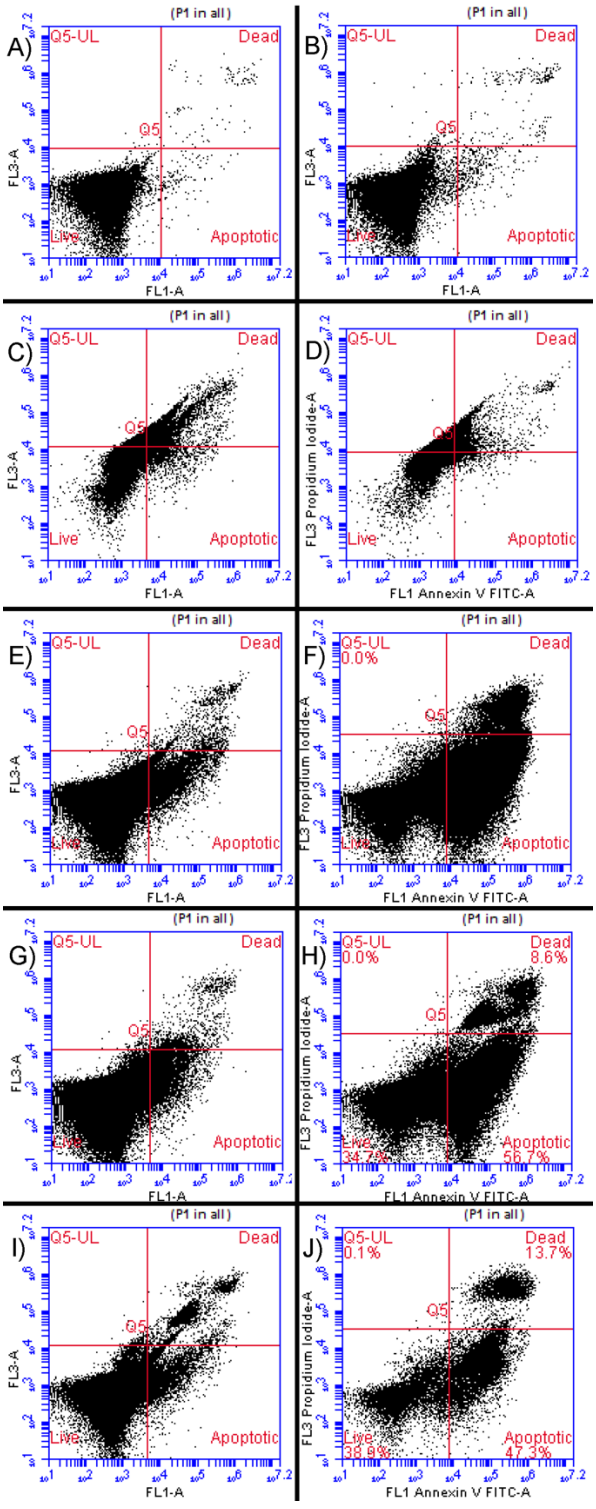

Figure 4.48: Representative flow cytometry plots for MDA-MB-231 breast cancer cells treated with the 100% PLA group. A) 100% PLA UCA, B) 100% PLA n-Sh, C) 100% PLA Dox UCA, D) 100% PLA Dox n-Sh, E) 100% PLA TRAIL UCA, F) 100% PLA TRAIL n-Sh, G) 100% PLA TRAIL UCA + Free Dox, H) 100% PLA TRAIL n-Sh + Free Dox, I) 100% PLA Dox TRAIL UCA, J) 100% PLA Dox TRAIL n-Sh.

Cell survival results for the 5 wt% PEG-PLA shell type group (summarized in Table 4.10, flow results shown in Figure 4.49) showed that negative controls of unmodified, native 5 wt% PEG-PLA UCA (98.80±0.13% live cells) and 5 wt% PEG-PLA n-Sh (96.90±0.42% live cells) exhibited high levels of cell survival ($p>0.9999$ compared to No Treatment control), again indicating that the shell material is non-toxic to the cell environment.

Similar to the trend observed with the 100% PLA group, cell survival was decreased when these cells were exposed to the experimental Dox-loaded and TRAIL-ligated agents compared to their unloaded native UCA and n-Sh counterparts. Dox-loaded UCA resulted in 75.50±2.94% cell survival ($p=0.0004$), while Dox-loaded n-Sh resulted in 71.00±0.30% cell survival ($p=0.0005$). Again, no statistical difference in cell survival was observed between the Dox-loaded UCA and Dox-loaded n-Sh ($p=0.9993$), with correlation to the experimental Dox release profile. Both the TRAIL-ligated UCA (80.93±1.31% live, $p=0.0030$) and TRAIL-ligated UCA co-administered with free Dox (59.43±3.78% live, $p<0.0001$) significantly reduced cell survival rates compared to the native UCA. Similar trends were observed with the TRAIL-ligated n-Sh (67.53±3.35% live, $p=0.0002$) and TRAIL-ligated n-Sh together with free Dox (61.33±5.26% live, $p<0.0001$). However, neither of these groups exhibited significant differences between the intact UCA and post-US n-Sh. This is likely due to the shift in resonant frequency observed with these agents, suggesting an inefficient US-driven production of n-Sh. The combination Dox-loaded and TRAIL-ligated UCA (63.21±3.19% live) and n-Sh (64.19±2.68% live) also resulted in significantly less cell survival than their native counterparts ($p<0.0001$ for both). Again, these agents exhibited a shift in resonant

frequency, likely accounting for the lack of significance between the intact UCA and post-US n-Sh treatments.

Table 4.10: Average cell fate percentages from flow cytometry results for MDA-MB-231 cells treated with 5 wt% PEG-PLA group of agents, n=3.

	Live Cells (%)	Apoptotic Cells (%)	Dead Cells (%)
5 wt% PEG-PLA UCA	98.80 ± 0.13	0.77 ± 0.17	0.27 ± 0.03
5 wt% PEG-PLA n-Sh	96.90 ± 0.42	2.04 ± 0.31	0.81 ± 0.44
5 wt% PEG-PLA Dox UCA	75.50 ± 2.94	1.75 ± 0.89	22.21 ± 3.91
5 wt% PEG-PLA Dox n-Sh	71.00 ± 0.30	2.17 ± 1.01	26.82 ± 1.29
5 wt% PEG-PLA TRAIL UCA	80.93 ± 1.31	3.92 ± 0.97	15.79 ± 1.98
5 wt% PEG-PLA TRAIL n-Sh	67.53 ± 3.35	19.93 ± 6.53	12.35 ± 5.06
5 wt% PEG-PLA TRAIL UCA + Free Dox	59.43 ± 3.78	17.44 ± 2.44	24.12 ± 1.35
5 wt% PEG-PLA TRAIL n-Sh + Free Dox	61.33 ± 5.26	19.73 ± 6.15	19.06 ± 5.91
5 wt% PEG-PLA Dox TRAIL UCA	63.21 ± 3.19	19.48 ± 0.66	18.45 ± 1.20
5 wt% PEG-PLA Dox TRAIL n-Sh	64.19 ± 2.68	11.55 ± 1.92	24.60 ± 2.07

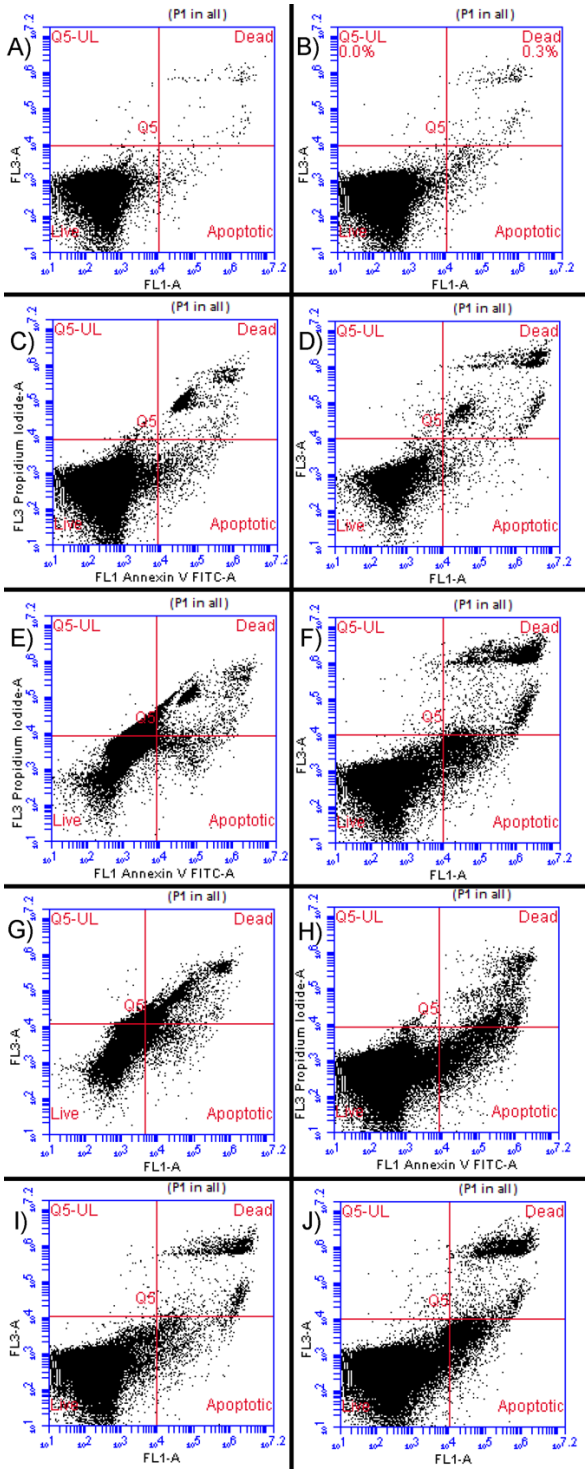

Figure 4.49: Representative flow cytometry plots for MDA-MB-231 breast cancer cells treated with the 5 wt% PEG-PLA group. A) 5 wt% PEG-PLA UCA, B) 5 wt% PEG-PLA n-Sh, C) 5 wt% PEG-PLA Dox UCA, D) 5 wt% PEG-PLA Dox n-Sh, E) 5 wt% PEG-PLA TRAIL UCA, F) 5 wt% PEG-PLA TRAIL n-Sh, G) 5 wt% PEG-PLA TRAIL UCA + Free Dox, H) 5 wt% PEG-PLA TRAIL n-Sh + Free Dox, I) 5 wt% PEG-PLA Dox TRAIL UCA, J) 5 wt% PEG-PLA Dox TRAIL n-Sh.

Interestingly, there were no statistical differences between the intact UCA and post-US n-Sh for any of the treatment types. As discussed above, the TRAIL-ligated agents suffered a loss of echogenicity and a shift in resonant frequency after ligation, possibly hindering the ability of these agents to form n-Sh in response to insonation. One other explanation for this finding is the reduced quantity of 5 wt% PEG-PLA UCA per mg, which led to a large amount of UCA and n-Sh to the added to each well for standardization of Dox concentration among treatment groups. This could have an effect on the PLA hydrolysis, as well as the Dox release along a potentially altered concentration gradient. Another possible explanation for the TRAIL-ligated agents is that TRAIL ligation was less effective with this polymeric shell type. Studies have shown that TRAIL encapsulation within a PEGylated polymeric microsphere exhibited reduced burst response, higher encapsulation efficiency, and also a longer sustained release than unPEGylated polymeric microspheres, suggesting that the PEG helps to retain the TRAIL and may prevent all of the ligated molecules from binding to the cell surface [149].

As observed with the 100% PLA and 5 wt% PEG-PLA groups, the polymeric shell material of the 1 wt% LipidPEG group (Table 4.11, Figure 4.50) was non-cytotoxic ($p>0.9999$ compared to No Treatment) with the intact UCA group exhibiting 95.69±0.84% cell survival and the post-US n-Sh group exhibiting 95.59±1.04% cell survival. Since all three shell types are mainly comprised of PLA, it is not surprising that all of the native agents exhibited similar high rates of cell survival. Dox-loaded UCA resulted in 80.34±2.83% cell survival ($p=0.0011$), while Dox-loaded n-Sh resulted in 81.01±5.05% cell survival ($p=0.0262$). Again, no statistical difference in cell survival was observed between the Dox-loaded UCA and Dox-loaded n-Sh ($p>0.9999$), likely due

to the low encapsulation efficiency, inefficient release, and reduction in echogenicity which could hinder n-Sh production. Both the TRAIL-ligated UCA (83.38±1.65% live, $p=0.0056$) and TRAIL-ligated UCA co-administered with free Dox (74.65±2.12% live, $p<0.0001$) significantly reduced cell survival rates compared to the native UCA. Similar trends were observed with the TRAIL-ligated n-Sh (76.34±3.25% live, $p=0.0045$) and TRAIL-ligated n-Sh together with free Dox (50.81±1.53% live, $p<0.0001$). However, neither of these groups exhibited significant differences between the intact UCA and post-US n-Sh. This could be due to steric hindrance from the surrounding PEG chains preventing the TRAIL from binding to the DR4/5 receptors efficiently. The combination Dox-loaded and TRAIL-ligated UCA (76.42±1.97% live, $p=0.0002$) and n-Sh (52.66±2.45% live, $p<0.0001$) also resulted in significantly less cell survival than their native counterparts. Cell death was significantly increased when free Dox was co-administered with TRAIL-ligated n-Sh (35.54±3.53% dead/necrotic cells) compared to TRAIL-ligated n-Sh alone (4.51±1.78% dead/necrotic cells, $p=0.0131$). Such an observation is expected, since free Dox induces significant cell death when incubated with MDA-MB-231 cells.

Table 4.11: Average cell fate percentages from flow cytometry results for MDA-MB-231 cells treated with 1 wt% LipidPEG group of agents, n=3.

	Live Cells (%)	Apoptotic Cells (%)	Dead Cells (%)
1 wt% LipidPEG UCA	95.69 ± 0.84	2.95 ± 0.62	1.32 ± 0.32
1 wt% LipidPEG n-Sh	95.59 ± 1.04	3.34 ± 0.83	1.04 ± 0.31
1 wt% LipidPEG Dox UCA	80.34 ± 2.83	1.85 ± 0.81	17.44 ± 3.10
1 wt% LipidPEG Dox n-Sh	81.01 ± 5.05	0.94 ± 0.34	17.95 ± 4.78
1 wt% LipidPEG TRAIL UCA	83.38 ± 1.65	15.64 ± 1.14	1.05 ± 0.13
1 wt% LipidPEG TRAIL n-Sh	76.34 ± 3.25	18.74 ± 3.52	4.51 ± 1.78
1 wt% LipidPEG TRAIL UCA + Free Dox	74.65 ± 2.12	9.14 ± 0.76	16.00 ± 2.96
1 wt% LipidPEG TRAIL n-Sh + Free Dox	50.81 ± 1.53	12.99 ± 5.11	35.54 ± 3.53
1 wt% LipidPEG Dox TRAIL UCA	76.42 ± 1.97	10.26 ± 1.48	12.86 ± 0.73
1 wt% LipidPEG Dox TRAIL n-Sh	52.66 ± 2.45	16.97 ± 8.50	29.53 ± 8.23

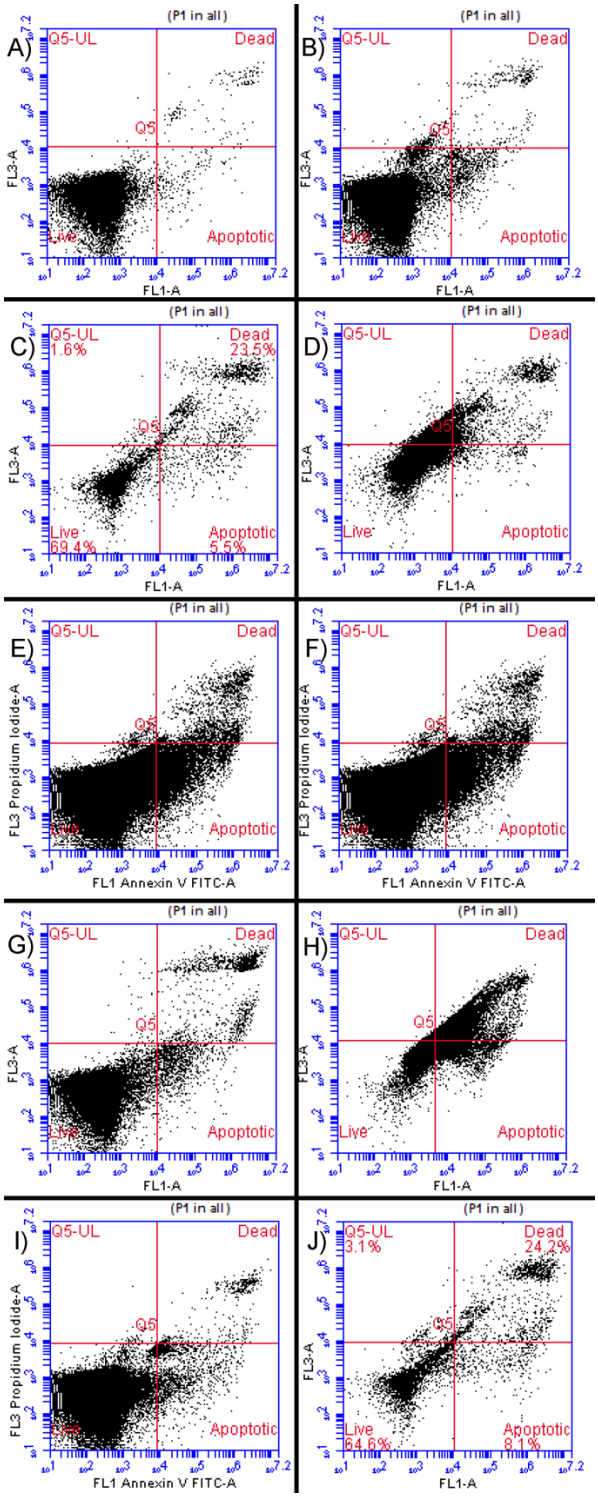

Figure 4.50: Representative flow cytometry plots for MDA-MB-231 breast cancer cells treated with the 1 wt% LipidPEG group. A) 1 wt% LipidPEG UCA, B) 1 wt% LipidPEG n-Sh, C) 1 wt% LipidPEG Dox UCA, D) 1 wt% LipidPEG Dox n-Sh, E) 1 wt% LipidPEG TRAIL UCA, F) 1 wt% LipidPEG TRAIL n-Sh, G) 1 wt% LipidPEG TRAIL UCA + Free Dox, H) 1 wt% LipidPEG TRAIL n-Sh + Free Dox, I) 1 wt% LipidPEG Dox TRAIL UCA, J) 1 wt% LipidPEG Dox TRAIL n-Sh.

Across the shell type groups, 100% PLA TRAIL n-Sh with free Dox resulted in significantly reduced cell survival (20.32±6.91% live) compared to both 5 wt% PEG-PLA TRAIL n-Sh with free Dox (61.33±5.26% live, p=0.0001) and 1 wt% LipidPEG TRAIL n-Sh with free Dox (50.81±1.53% live, p=0.0233). This can be accounted for by the significantly greater degree of apoptosis induced by the 100% PLA TRAIL n-Sh with free Dox (42.55±3.47% apoptotic) compared to both 5 wt% PEG-PLA TRAIL n-Sh with free Dox (19.73±6.15% apoptotic, p=0.0012) and 1 wt% LipidPEG TRAIL n-Sh with free Dox (12.99±5.11% apoptotic, p=0.0028). These differences in apoptosis could be in relation to the amount of TRAIL ligated to the UCA surface for each shell type, especially for the LipidPEG group as the PEG groups may prevent the TRAIL from effectively binding to the DR4/5 receptors through steric hindrance. Borden and Chen have demonstrated that small bioactive molecules, such as streptavidin, can be hidden within the PEG brush on the surface of a phospholipid microbubble [140, 147, 154]. Overall, we observed reductions in cell viability in response to incubation with the modified UCA across all three shell types, supporting the potential of these agents as drug delivery vehicles.

4.3.10.2 MCF7 Cells

Similar to the MDA-MB-231 cells, TRAIL-resistant MCF7 cells were exposed to the negative and positive control treatments for comparison with the experimental agents. Flow cytometry results are shown in Figure 4.51, and average cell fate percentages are summarized in Table 4.12. Negative control of no treatment resulted in 95.36±1.09% live cells, indicating that environmental conditions did not have an effect on cell death. Both free Dox (23.27±3.57% live) and the combination of both free Dox and free TRAIL

(31.28±4.99% live) resulted in significant reduction in cell survival ($p<0.0001$), while free TRAIL did not cause significant cell apoptosis or death (84.74±5.70% live, $p>0.9999$). However, when administered in the presence of Dox, cell survival was significantly decreased ($p<0.0001$), and the percentage of apoptotic cells significantly increased from 8.73±1.50% for free TRAIL to 20.20±1.86% for free Dox and TRAIL ($p=0.0086$). This finding confirms that Dox acts synergistically with TRAIL to overcome the inherent resistance to TRAIL-induced apoptosis expressed by these cells [45, 49, 50, 52, 157, 201].

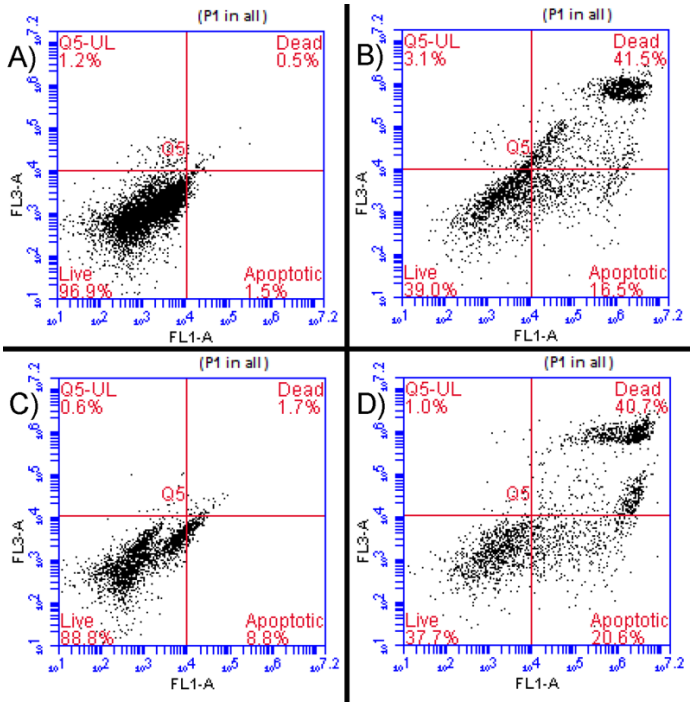

Figure 4.51: Representative flow cytometry plots for MCF7 breast cancer cells. A) No treatment, B) Dox Only, C) TRAIL Only, D) Dox and TRAIL Only.

Table 4.12: Average cell fate percentages from flow cytometry results for MCF7 cell control groups, n=3.

	Live Cells (%)	Apoptotic Cells (%)	Dead Cells (%)
No Treatment	95.36 ± 1.09	3.06 ± 1.02	0.56 ± 0.12
Free Dox Only	23.27 ± 3.57	7.51 ± 1.67	67.70 ± 3.23
Free TRAIL Only	84.74 ± 5.70	8.73 ± 1.50	5.87 ± 4.47
Free Dox and TRAIL Only	31.28 ± 4.99	20.20 ± 1.86	47.20 ± 6.31

Average cell fate percentages for the 100% PLA shell type group are summarized in Table 4.13, and flow cytometry plots are shown in Figure 4.52. Exposure to the Dox-loaded experimental agents as well as the TRAIL-ligated agents with Dox co-administration resulted in reduced MCF7 cell survival. For the intact UCA, both TRAIL-ligated UCA + free Dox (49.96±7.80% live, $p=0.0011$) and Dox TRAIL UCA (69.77±9.02% live, $p=0.0493$) caused significant reduction in cell survival compared to the native UCA (94.92±1.26% live). Considering the treatments with post-US n-Sh, incubation with the Dox-loaded n-Sh (52.61±10.82% live, $p=0.0011$), TRAIL-ligated n-Sh co-administered with free Dox (37.37±5.39% live, $p<0.0001$), and Dox-loaded TRAIL-ligated n-Sh (67.78±3.98% live, $p=0.0206$) led to reduced cell survival compared to the native n-Sh (96.51±0.50% live).

Cell survival is also significantly reduced when TRAIL-ligated UCA and n-Sh are incubated together with free Dox, compared to incubation alone in cell media. For the intact UCA groups, cell survival rates decrease from an average of 94.65±1.65% live cells for TRAIL UCA to an average of only 49.96±7.80% live cells for TRAIL UCA with free Dox ($p=0.0001$). Co-administration of Dox led to significant increases in both apoptotic cells ($p=0.0862$) and dead/necrotic cells ($p=0.0347$), accounting for the

decreased overall cell survival. Similarly, increased apoptosis ($p=0.0246$) and necrosis ($p=0.0051$) account for the significant cell survival reduction ($p<0.0001$) observed when Dox is co-administered with TRAIL-ligated n-Sh (98.11±0.44% to 37.37±5.39% live).

Table 4.13: Average cell fate percentages from flow cytometry results for MCF7 cells treated with 100% PLA group of agents, n=3.

	Live Cells (%)	Apoptotic Cells (%)	Dead Cells (%)
100% PLA UCA	94.92 ± 1.26	2.33 ± 0.60	2.66 ± 0.67
100% PLA n-Sh	96.51 ± 0.50	1.67 ± 0.17	1.77 ± 0.40
100% PLA Dox UCA	79.31 ± 4.89	3.46 ± 1.48	17.08 ± 3.02
100% PLA Dox n-Sh	52.61 ± 10.82	3.11 ± 1.66	44.44 ± 11.82
100% PLA TRAIL UCA	94.65 ± 1.65	2.97 ± 0.10	2.68 ± 1.04
100% PLA TRAIL n-Sh	98.11 ± 0.44	0.94 ± 0.12	0.87 ± 0.31
100% PLA TRAIL UCA + Free Dox	49.96 ± 7.80	15.86 ± 4.08	32.79 ± 6.76
100% PLA TRAIL n-Sh + Free Dox	37.37 ± 5.39	19.26 ± 2.97	42.38 ± 6.77
100% PLA Dox TRAIL UCA	69.77 ± 9.02	14.63 ± 4.65	15.48 ± 4.39
100% PLA Dox TRAIL n-Sh	67.78 ± 3.98	12.62 ± 1.77	18.88 ± 2.33

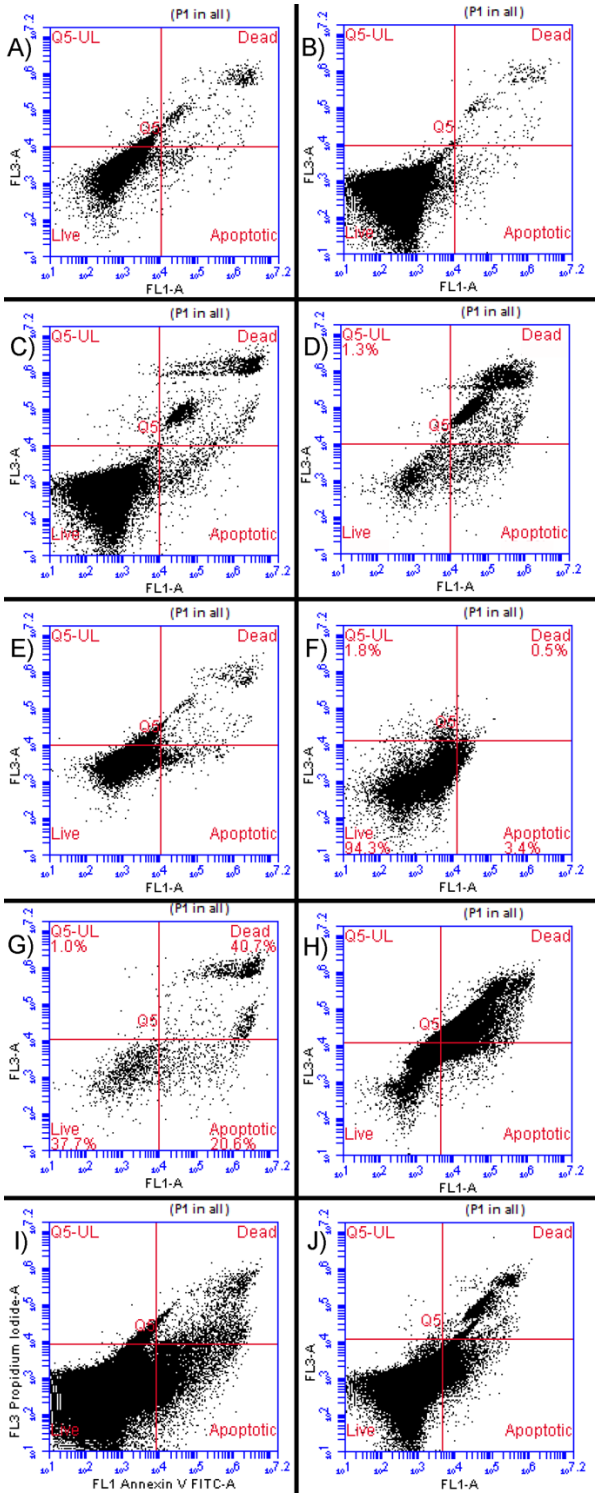

Figure 4.52: Representative flow cytometry plots for MCF7 breast cancer cells treated with the 100% PLA group. A) 100% PLA UCA, B) 100% PLA n-Sh, C) 100% PLA Dox UCA, D) 100% PLA Dox n-Sh, E) 100% PLA TRAIL UCA, F) 100% PLA TRAIL n-Sh, G) 100% PLA TRAIL UCA + Free Dox, H) 100% PLA TRAIL n-Sh + Free Dox, I) 100% PLA Dox TRAIL UCA, J) 100% PLA Dox TRAIL n-Sh.

Similar to the trend observed with the 100% PLA group, cell survival was decreased when these cells were exposed to the experimental 5 wt% PEG-PLA agents compared to their unloaded native UCA and n-Sh counterparts, with the exception of the TRAIL-ligated UCA and n-Sh ($p<0.0001$).

Cell survival is again significantly reduced when TRAIL-ligated UCA and n-Sh are incubated together with free Dox and when Dox is co-encapsulated within the polymeric shell, compared to incubation alone in cell media. For the intact UCA groups, cell survival rates decrease from an average of 98.83±0.42% live cells for TRAIL UCA to an average of only 26.59±5.51% live cells for TRAIL UCA with free Dox ($p<0.0001$) and an average of 58.58±5.16% live cells for Dox TRAIL UCA ($p=0.0009$). Co-administration of Dox led to significant increases in both apoptotic cells ($p=0.0665$ for TRAIL UCA + free Dox) and dead/necrotic cells ($p<0.0001$ for both TRAIL UCA + free Dox and Dox TRAIL UCA), accounting for the decreased overall cell survival.

Similarly, increased apoptosis ($p=0.0086$ for TRAIL n-Sh + free Dox) and necrosis ($p<0.0001$ for TRAIL n-Sh + free Dox) account for the significant cell survival reduction ($p<0.0001$) observed when either free Dox is co-administered with TRAIL-ligated n-Sh (26.59±5.51% live) or Dox is co-encapsulated within the polymeric shell (48.37±5.04% live) compared to TRAIL-ligated n-Sh alone (98.18±1.04% live). These results suggest that the 5 wt% PEG-PLA shell allows for effective localized Dox release to help sensitize TRAIL-resistant cells to therapeutic treatment while limiting systemic exposure to the toxic chemotherapeutic.

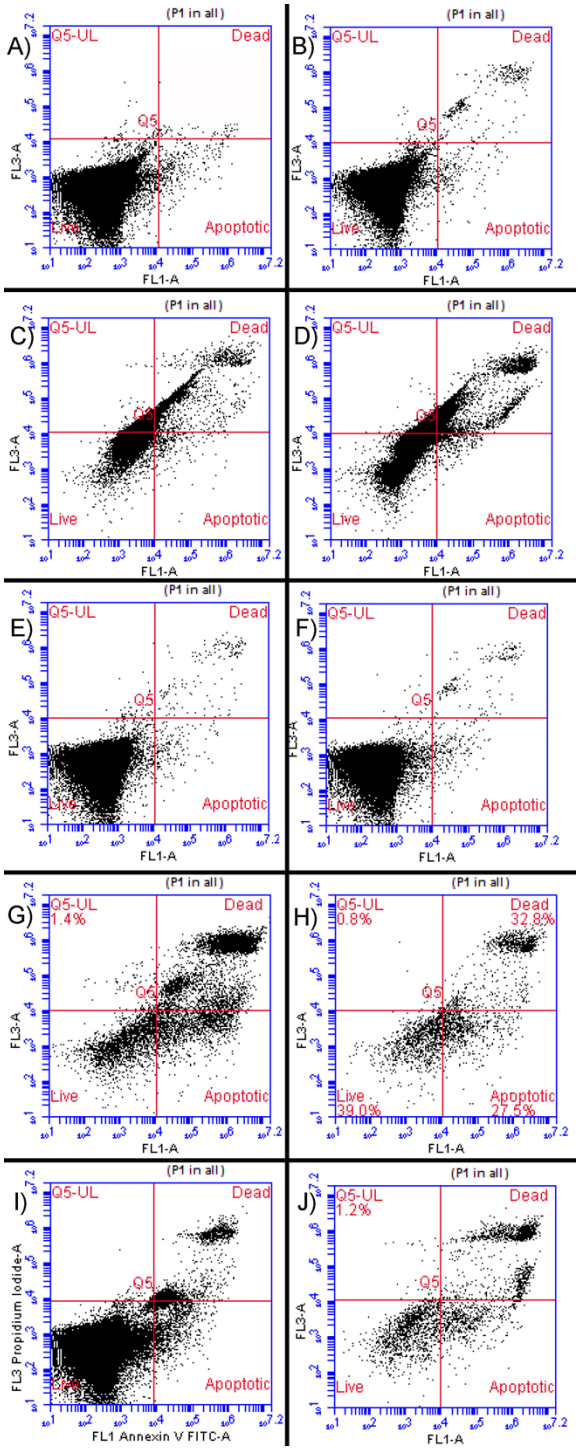

Figure 4.53: Representative flow cytometry plots for MCF7 breast cancer cells treated with the 5 wt% PEG-PLA group. A) 5 wt% PEG-PLA UCA, B) 5 wt% PEG-PLA n-Sh, C) 5 wt% PEG-PLA Dox UCA, D) 5 wt% PEG-PLA Dox n-Sh, E) 5 wt% PEG-PLA TRAIL UCA, F) 5 wt% PEG-PLA TRAIL n-Sh, G) 5 wt% PEG-PLA TRAIL UCA + Free Dox, H) 5 wt% PEG-PLA TRAIL n-Sh + Free Dox, I) 5 wt% PEG-PLA Dox TRAIL UCA, J) 5 wt% PEG-PLA Dox TRAIL n-Sh.

Table 4.14: Average cell fate percentages from flow cytometry results for MCF7 cells treated with 5 wt% PEG-PLA group of agents, n=3.

	Live Cells (%)	Apoptotic Cells (%)	Dead Cells (%)
5 wt% PEG-PLA UCA	98.99 ± 0.22	0.62 ± 0.15	0.29 ± 0.08
5 wt% PEG-PLA n-Sh	97.04 ± 0.86	1.14 ± 0.46	1.25 ± 0.48
5 wt% PEG-PLA Dox UCA	57.70 ± 2.65	4.01 ± 1.21	38.03 ± 3.45
5 wt% PEG-PLA Dox n-Sh	58.73 ± 1.24	3.37 ± 0.93	38.31 ± 0.60
5 wt% PEG-PLA TRAIL UCA	98.83 ± 0.42	0.59 ± 0.15	0.48 ± 0.24
5 wt% PEG-PLA TRAIL n-Sh	98.18 ± 1.04	0.69 ± 0.33	1.41 ± 1.07
5 wt% PEG-PLA TRAIL UCA + Free Dox	26.59 ± 5.51	54.74 ± 9.79	17.17 ± 4.36
5 wt% PEG-PLA TRAIL n-Sh + Free Dox	39.97 ± 1.94	24.62 ± 2.76	34.76 ± 3.31
5 wt% PEG-PLA Dox TRAIL UCA	58.58 ± 5.16	21.15 ± 3.79	20.31 ± 1.72
5 wt% PEG-PLA Dox TRAIL n-Sh	48.37 ± 5.04	16.60 ±1.83	34.42 ± 5.32

Within the 1 wt% LipidPEG shell type group (Figure 4.54, Table 4.15), cell survival was decreased when these cells were exposed to the experimental agents compared to their unloaded native n-Sh counterparts, with the exception of the TRAIL-ligated n-Sh. Dox-loaded n-Sh resulted in 54.72±15.23% live cells (p=0.0086), while TRAIL-ligated n-Sh + free Dox resulted in 28.05±4.40% live cells (p=0.0002) and Dox-loaded TRAIL-ligated n-Sh resulted in 24.48±1.79% live cells (p=0.0001). Only the 1 wt% LipidPEG TRAIL UCA + free Dox produced significant reduction in cell survival (51.83±12.07% live cells) compared to the native UCA (97.20±0.91% live cells,

p=0.0045). While the other experimental intact UCA, with the exception of TRAIL-ligated UCA, exhibited some reduction in cell survival, these reductions were not statistically significant within the entire group.

Cell survival is again significantly reduced when TRAIL-ligated UCA and n-Sh are incubated together with free Dox and when Dox is co-encapsulated within the polymeric shell, compared to incubation alone in cell media. For the intact UCA groups, cell survival rates decrease from an average of 97.86±0.70% live cells for TRAIL UCA to an average of only 51.83±12.07% live cells for TRAIL UCA with free Dox ($p<0.0001$). Similarly, increased apoptosis ($p<0.0001$ for TRAIL n-Sh + free Dox) and necrosis ($p<0.0001$ for Dox TRAIL n-Sh) account for the significant cell survival reduction ($p<0.0001$) observed when either free Dox is co-administered with TRAIL-ligated n-Sh (28.05±4.40% live) or Dox is co-encapsulated within the polymeric shell (24.48±1.79% live) compared to TRAIL-ligated n-Sh alone (93.44±2.88% live). Similar to the 5 wt% PEG-PLA group, these results suggest that the 1 wt% LipidPEG shell can allow for effective localized Dox release to help sensitize TRAIL-resistant cells.

Unlike the other shell type groups, significant differences were observed between some of the TRAIL-ligated intact UCA and their corresponding n-Sh. Apoptosis was significantly increased in response to TRAIL-ligated n-Sh + free Dox (36.61±19.18% apoptotic) compared to the TRAIL-ligated UCA + free Dox (13.05±1.65% apoptotic, $p=0.0246$). This increase in apoptosis is likely due to the combination of Dox sensitization of the cells, as well as increased binding of ligated TRAIL molecules since n-Sh allow for utilization of the entire surface area of the UCA instead of the few contact points between the UCA spherical surface and the cell plate. Necrosis and cell death

increased (p=0.0034) when cells were incubated with Dox TRAIL n-Sh (57.28±3.63% dead/necrotic) compared to Dox TRAIL UCA (21.01±6.73% dead/necrotic). Dox is released from the polymeric shell via PLA hydrolysis; therefore, n-Sh may hydrolyze more rapidly than intact UCA based on amount of polymer resulting in an increased Dox concentration released from the n-Sh than intact UCA. Based on these results, the 1 wt% LipidPEG shell type seems to be most effective for US-triggered therapy to MCF7 cells, resulting in the best sensitization and n-Sh treatment efficacy.

Table 4.15: Average cell fate percentages from flow cytometry results for MCF7 cells treated with 1 wt% LipidPEG group of agents, n=3.

	Live Cells (%)	Apoptotic Cells (%)	Dead Cells (%)
1 wt% LipidPEG UCA	97.20 ± 0.91	1.36 ± 0.26	1.30 ± 0.69
1 wt% LipidPEG n-Sh	96.87 ± 1.19	1.58 ± 0.64	1.49 ± 0.58
1 wt% LipidPEG Dox UCA	71.09 ± 7.04	5.61 ± 1.95	23.14 ± 7.04
1 wt% LipidPEG Dox n-Sh	54.72 ± 15.23	8.60 ± 1.66	37.23 ± 13.78
1 wt% LipidPEG TRAIL UCA	97.86 ± 0.70	1.16 ± 0.22	1.44 ± 0.44
1 wt% LipidPEG TRAIL n-Sh	93.44 ± 2.88	2.96 ± 1.24	3.43 ± 1.66
1 wt% LipidPEG TRAIL UCA + Free Dox	51.83 ± 12.07	13.05 ± 1.65	35.64 ± 12.77
1 wt% LipidPEG TRAIL n-Sh + Free Dox	28.05 ± 4.40	36.61 ± 19.18	35.25 ± 18.46
1 wt% LipidPEG Dox TRAIL UCA	72.77 ± 7.48	7.25 ± 1.00	21.01 ± 6.73
1 wt% LipidPEG Dox TRAIL n-Sh	24.48 ± 1.79	17.67 ± 2.15	57.28 ± 3.63

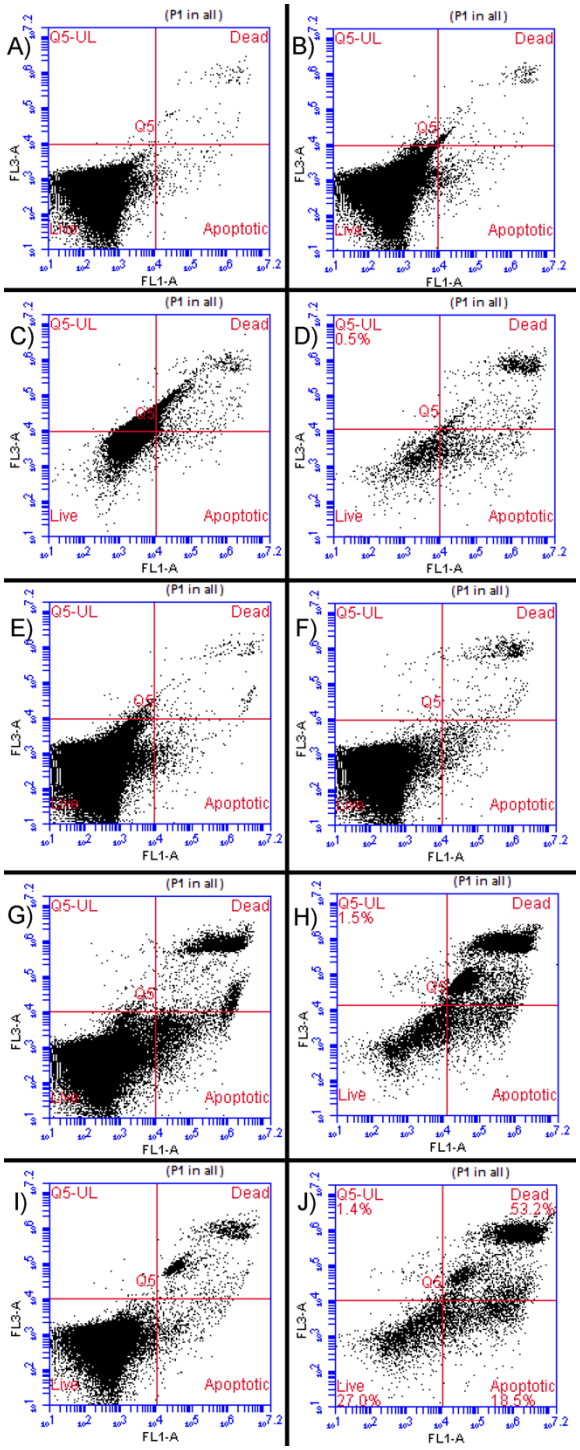

Figure 4.54: Representative flow cytometry plots for MCF7 breast cancer cells treated with the 1 wt% LipidPEG group. A) 1 wt% LipidPEG UCA, B) 1 wt% LipidPEG n-Sh, C) 1 wt% LipidPEG Dox UCA, D) 1 wt% LipidPEG Dox n-Sh, E) 1 wt% LipidPEG TRAIL UCA, F) 1 wt% LipidPEG TRAIL n-Sh, G) 1 wt% LipidPEG TRAIL UCA + Free Dox, H) 1 wt% LipidPEG TRAIL n-Sh + Free Dox, I) 1 wt% LipidPEG Dox TRAIL UCA, J) 1 wt% LipidPEG Dox TRAIL n-Sh.

Results confirmed that all three native shell materials were not cytotoxic to the MCF7 cells, since incubation with intact UCA and post-US n-Sh resulted in cell survival similar to that of the negative No Treatment control group ($p>0.9999$) for each shell type group. Again, this confirms that any cell death or apoptosis observed in the experimental groups is due to the therapeutic element. Since all three shell types are mainly comprised of PLA, which biodegrades into lactic acid, it is not surprising that all of the native agents exhibited similar high rates of cell survival.

MCF7 cell survival was unaffected by incubation with TRAIL UCA and n-Sh across all three shell types, with cell survival similar to those of the native agents as well as the No Treatment control ($p>0.9999$). This outcome is expected based on the knowledge that MCF7 cells are intrinsically resistant to TRAIL-induced apoptosis due to reduced expression of DR4/5 receptors on the cell surface and upregulation of the cyclooxygenase-2/prostaglandin E2 (COX-2/PGE_2) pathway [45, 202]. As an alternative to administration of free Dox or co-encapsulation of the chemotherapeutic, administration of a COX-2 inhibitor to the tumor cells could help reverse the intrinsic TRAIL resistance and improve treatment efficacy [202].

Across the shell type groups, 1 wt% LipidPEG Dox TRAIL n-Sh resulted in significantly reduced cell survival (24.48±1.79% live) compared to 100% PLA Dox TRAIL n-Sh (67.78±3.98% live, $p=0.0002$). This can be accounted for by the significantly greater degree of cell death induced by the 1 wt% LipidPEG Dox TRAIL n-Sh (57.28±3.63% dead/necrotic) compared to its 100% PLA counterpart (18.88±2.33% dead/necrotic, $p=0.0162$). Since the 1 wt% LipidPEG agents exhibit a higher Dox burst release than 100% PLA agents, these cells could have been exposed to a greater

concentration of Dox resulting in the observed cell death increase. Across all groups, we observed a reduction in cell viability when Dox was co-administered with TRAIL, supporting the hypothesis that cells that are intrinsically resistant to TRAIL can be sensitized to the apoptotic activity with use of a secondary treatment to increase death receptor expression and affinity to improve cell death signaling.

4.3.10.3 MCF-12A Cells

MCF-12A breast epithelial cells represent the healthy cells surrounding tumor tissue that could be susceptible to tumor treatments. These cells express the decoy TRAIL receptors (DcR1/DcR2) that do not signal apoptosis upon binding, and were evaluated as a control to investigate the effects of the experimental agents on healthy tissue surrounding the area of interest.

As with the two breast cancer cell groups, MCF-12A cells were exposed to the negative and positive control treatments (Table 4.16, Figure 4.55). Negative control of no treatment resulted in 93.07±1.77% live cells, and incubation with free TRAIL resulted in 90.40±2.21% live cells, confirming that these cells are non-reactive to TRAIL. However, MCF-12A are highly susceptible to Dox, resulting in only 6.08±1.42% live cells with 88.83±1.90% dead/necrotic cells. These findings are very important when considering treatment regimes, as the surrounding epithelial cells experience significant necrosis when exposed to Dox ($p<0.0001$).

Table 4.16: Average cell fate percentages from flow cytometry results for MCF-12A cell control groups, n=3.

	Live Cells (%)	Apoptotic Cells (%)	Dead Cells (%)
No Treatment	93.07 ± 1.77	3.84 ± 1.55	2.65 ± 1.286
Free Dox Only	6.08 ± 1.42	4.22 ± 1.20	88.83 ± 1.90
Free TRAIL Only	90.40 ± 2.21	5.84 ± 1.15	3.52 ± 3.13
Free Dox and TRAIL Only	5.31 ± 0.64	12.11 ± 1.94	81.86 ± 2.15

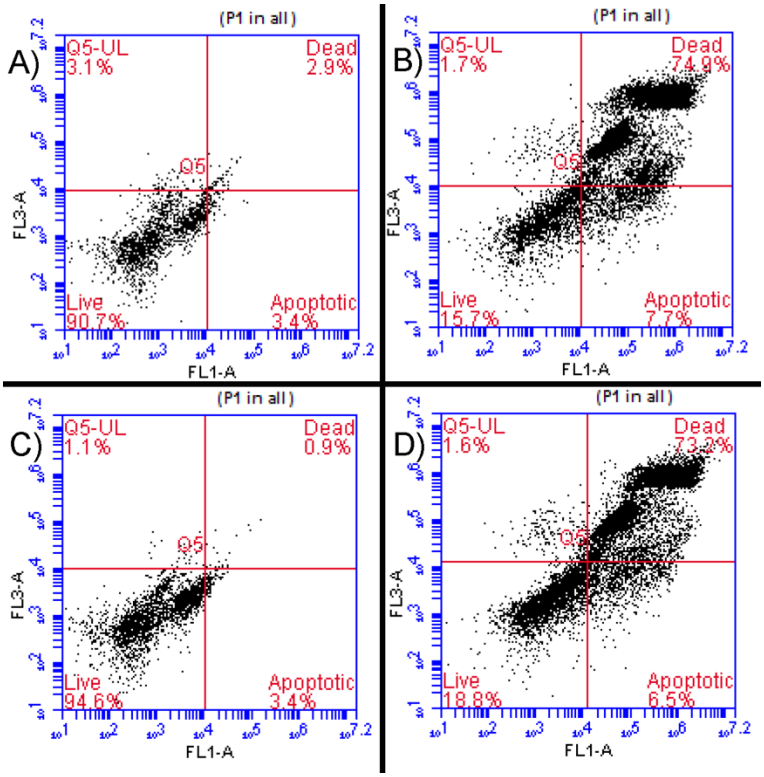

Figure 4.55: Representative flow cytometry plots for MCF-12 breast epithelial cells. A) No treatment, B) Dox Only, C) TRAIL Only, D) Dox and TRAIL Only.

For all three shell materials, significant reductions in cell survival with corresponding increases in dead/necrotic cells were observed for all of the Dox-loaded groups compared to the native agents ($p<0.0001$ for all necrotic comparisons). Significance values compared to the corresponding native agent (UCA or n-Sh) are listed below the cell fate percentage in Table 4.17 - Table 4.19 for cell survival.

Table 4.17: Average cell fate percentages from flow cytometry results for MCF-12A cells treated with 100% PLA group of agents, n=3.

	Live Cells (%)	Apoptotic Cells (%)	Dead Cells (%)
100% PLA UCA	95.99 ± 1.78	1.53 ± 0.57	2.32 ± 1.16
100% PLA n-Sh	95.94 ± 1.58	1.04 ± 0.26	2.93 ± 1.49
100% PLA Dox UCA	72.71 ± 2.59 (p=0.0423)	1.64 ± 0.19	25.50 ± 2.85
100% PLA Dox n-Sh	58.15 ± 1.45 (p<0.0001)	4.10 ± 1.24	37.22 ± 1.26
100% PLA TRAIL UCA	91.84 ± 1.68	2.61 ± 0.72	4.57 ± 0.94
100% PLA TRAIL n-Sh	95.53 ± 1.01	1.07 ± 0.40	3.28 ± 0.63
100% PLA TRAIL UCA + Free Dox	73.91 ± 1.36 (p=0.0487)	1.39 ± 0.31	14.57 ± 1.50
100% PLA TRAIL n-Sh + Free Dox	58.15 ± 1.27 (p<0.0001)	3.34 ± 1.06	38.39 ± 0.52
100% PLA Dox TRAIL UCA	66.39 ± 8.60 (p=0.0022)	5.03 ± 1.80	28.49 ± 6.79
100% PLA Dox TRAIL n-Sh	68.79 ± 6.89 (p=0.0007)	5.92 ± 2.25	25.93 ± 4.91

Table 4.18: Average cell fate percentages from flow cytometry results for MCF-12A cells treated with 5 wt% PEG-PLA group of agents, n=3.

	Live Cells (%)	Apoptotic Cells (%)	Dead Cells (%)
5 wt% PEG-PLA UCA	95.52 ± 1.64	2.15 ± 0.73	2.22 ± 0.98
5 wt% PEG-PLA n-Sh	93.27 ± 1.43	0.98 ± 0.21	5.41 ± 1.27
5 wt% PEG-PLA Dox UCA	60.69 ± 7.91 (p=0.0089)	1.80 ± 0.95	38.42 ± 7.42
5 wt% PEG-PLA Dox n-Sh	60.03 ± 4.11 (p=0.0164)	2.47 ± 0.71	38.70 ± 3.94
5 wt% PEG-PLA TRAIL UCA	95.81 ± 1.20	1.59 ± 0.44	2.50 ± 0.79
5 wt% PEG-PLA TRAIL n-Sh	97.46 ± 0.62	0.90 ± 0.18	1.51 ± 0.42
5 wt% PEG-PLA TRAIL UCA + Free Dox	71.46 ± 4.98 (p=0.0484)	5.31 ± 1.02	23.26 ± 5.13
5 wt% PEG-PLA TRAIL n-Sh + Free Dox	40.13 ± 12.37 (p=0.0006)	6.10 ± 1.72	53.27 ± 10.74
5 wt% PEG-PLA Dox TRAIL UCA	69.03 ± 9.54 (p=0.0451)	8.57 ± 1.88	22.01 ± 7.03
5 wt% PEG-PLA Dox TRAIL n-Sh	50.58 ± 5.42 (p=0.0031)	5.03 ± 1.89	45.27 ± 7.23

Table 4.19: Average cell fate percentages from flow cytometry results for MCF-12A cells treated with 1 wt% LipidPEG group of agents, n=3.

	Live Cells (%)	Apoptotic Cells (%)	Dead Cells (%)
1 wt% LipidPEG UCA	96.87 ± 0.09	1.47 ± 0.19	1.59 ± 0.22
1 wt% LipidPEG n-Sh	92.59 ± 0.71	2.68 ± 0.26	4.57 ± 0.44
1 wt% LipidPEG Dox UCA	79.30 ± 3.87 (p=0.0492)	1.62 ± 0.01	18.42 ± 3.78
1 wt% LipidPEG Dox n-Sh	54.49 ± 3.84 (p=0.0160)	2.20 ± 0.67	43.36 ± 4.40
1 wt% LipidPEG TRAIL UCA	95.90 ± 1.86	1.62 ± 0.68	2.33 ± 1.17
1 wt% LipidPEG TRAIL n-Sh	90.64 ± 2.54	1.83 ± 0.13	7.42 ± 2.54
1 wt% LipidPEG TRAIL UCA + Free Dox	56.35 ± 8.45 (p=0.0003)	4.15 ± 0.23	39.14 ± 8.63
1 wt% LipidPEG TRAIL n-Sh + Free Dox	44.73 ± 15.26 (p=0.0035)	5.59 ± 2.53	49.18 ± 12.61
1 wt% LipidPEG Dox TRAIL UCA	74.55 ± 2.36 (p=0.0189)	7.12 ± 3.13	18.09 ± 1.29
1 wt% LipidPEG Dox TRAIL n-Sh	59.60 ± 2.86 (p=0.0369)	2.06 ± 0.79	38.86 ± 1.21

4.3.11 UCA Modification for Cancer Therapy Conclusions

The work discussed here presents an innovative, dual-functioning platform to create a "theranostic" modality to overcome many of the challenges surrounding *in vivo* delivery of nanoparticles. The UCA provide valuable diagnostic information during administration, and we have shown that shell modifications for therapeutic applications do not compromise the ability to obtain this diagnostic information.

Three UCA modification strategies for targeted therapy were evaluated, loading the UCA shell with Dox, decorating the surface of the UCA shell with TRAIL, and combining these two strategies in the same UCA. Based on the results discussed here, the 5 wt% PEG-PLA UCA shell composition seems to be the best for encapsulation of Dox, as it reduces immunogenicity compared to native PLA, exhibits higher drug encapsulation efficiency (27.5%) than the 1 wt% LipidPEG UCA, exhibits sustained release of Dox without a large initial burst release, and also retains its acoustic behavior for function as a targeted drug delivery agent. On the other hand, the 1 wt% LipidPEG shell composition emerges as the better option for functionalization with TRAIL, as these agents exhibit better acoustic behavior than the 5 wt% PEG-PLA TRAIL UCA, retain their immunogenic reduction, retain a zeta potential of greater magnitude than -20mV to prevent aggregation in suspension, and are still capable of supporting co-encapsulation of Dox (~12% encapsulation efficiency).

Cell studies demonstrated that all three polymeric shell types, 100% PLA, 5 wt% PEG-PLA, and 1 wt% LipidPEG and their hydrolytic byproducts were not cytotoxic to any of the three breast cell lines, indicating that any cell death observed in the experimental groups was in response to the therapeutic element. MDA-MB-231 cells were highly responsive to the therapeutic agents, exhibited significantly reduced cell survival in response to incubation with Dox-loaded, TRAIL-ligated, and combination therapy UCA and their resulting n-Sh. Results also showed that TRAIL-resistant MCF7 breast cancer cells can be sensitized to treatment with TRAIL by co-administration of Dox, which led to significant reduction in cell viability for both intact UCA and n-Sh across all three polymeric shell types. Finally, we demonstrated that MCF-12A breast

epithelial cells, which represent the healthy cells surrounding the tumor, are insensitive to TRAIL-induced apoptosis. However, these cells are susceptible to Dox-induced necrosis, which is an important consideration when determining treatment regimes.

In terms of clinical relevance, we calculated the amount of Dox that would be delivered from one injected dose of loaded UCA based on the maximum dose of UCA (20mg/mL) determined in previous animal studies (rat model) and scaled to adult humans (factor of 7 for body mass) [5, 90]. Considering a dose of 140mg loaded UCA, 100% PLA Dox UCA would deliver 1.94mg Dox, and 100% PLA Dox TRAIL UCA would deliver 1.29mg Dox per injection. Similarly, 140mg of 5 wt% PEG-PLA Dox UCA delivers 1.52mg Dox, and its TRAIL-ligated counterpart delivers 1.18mg Dox per injected dose. For the 1 wt% LipidPEG group, the Dox-loaded UCA deliver 0.99mg Dox per dose, while the TRAIL-ligated, Dox-loaded UCA deliver 0.69mg Dox per dose. The maximum therapeutic dose for Dox in humans is reported to be 1.62mg/kg, or approximately 97mg in a single systemic dose [203]. A single injected dose of our loaded UCA would represent ~1-2% of this amount, and therefore would be considered safe in terms of therapeutic index. Even taking into consideration the sustained release and subsequent treatments, the cumulative dose would still be below the maximum tolerated dose. Studies have shown high tolerance of TRAIL in humans at doses up to 30mg/kg, with the maximum dose delivered with our agents falling far below this therapeutic index threshold and still effective against susceptible cancer cells [204]. Based on the results presented here, our UCA represent effective cancer treatment agents that fall well below the therapeutic index cutoff dosage for each treatment modality while retaining efficacy. Dose escalation *in vivo* studies would be needed to determine the maximum tolerated

dose of loaded UCA and the maximum deliverable therapeutic doses of the loaded treatments.

This study also provides a basis for investigation of encapsulation of other drugs, possibly hydrophobic drugs such as paclitaxel and docetaxel, or ligation of other ligands or proteins, such as other members of the TNF family and malaria protein VAR2CSA [205], to the UCA surface.

5. CONCLUSIONS AND FUTURE RECOMMENDATIONS

5.1 Conclusions and Contributions to Science

The overall objective of this thesis was the development and characterization of non-immunogenic, PEGylated functionalized UCA capable of locally delivering encapsulated drug to cancerous cells while also inducing cancer cell death through specific ligand binding.

Initially, PLA UCA were ligated with TRAIL protein to determine the efficacy of this platform to induce cytotoxicity in susceptible breast cancer cells while retaining its acoustic properties. Ligation using maleimide chemistry was an effective method for attaching TRAIL to UCA, and these modified UCA maintained apoptotic activity towards susceptible breast cancer cells. Additionally, cells treated with n-Sh generated by US treatment of ligated TRAIL-UCA showed the greatest extent of apoptosis/cell death among test groups ($p<0.0001$), suggesting that these agents were still able to cavitate and shatter when exposed to therapeutic US.

Two PEGylation techniques were investigated in an effort to reduce the immunogenicity of our UCA: addition of increasing amounts of PEG-PLA copolymer and employing incorporation of LipidPEG into the shell. Addition of PEG-PLA showed dose-dependent reductions in acoustic enhancement, while insertion of LipidPEG molecules was deleterious to acoustic properties at low proportions. Results indicated that the 5 wt% PEG-PLA and 1 wt% LipidPEG formulations best achieved a balance between retention of acoustic interaction, appropriate physical properties, and reduction in immune activation.

PEGylated UCA were then modified for targeted cancer therapies with two different modalities, resulting in the fabrication of three different classes of modified agents. Fluctuations in acoustic behavior and physical properties were observed in the modified agents, suggesting the chemical process of ligation negatively affects the shell's ability to cavitate. Dox release profiles were determined for drug-loaded PLA, showing sustained release of Dox over the 7-day testing period. *In vitro* testing showed that cancer cells were susceptible to modified agents, while healthy cells are shielded from TRAIL-induced apoptosis but remain highly susceptible to Dox-induced cell death. Additionally, these studies demonstrated the ability to use co-administration of Dox to overcome cancer cell resistance to TRAIL-mediated apoptosis. We determined that the 5 wt% PEG-PLA formulation was optimal for creation of non-immunogenic, Dox-loaded UCA. However, the 1 wt% LipidPEG shell formulation appeared to perform better as non-immunogenic, TRAIL-ligated UCA in addition to the dual-functionalized Dox-loaded, TRAIL-ligated UCA.

These results represent important advances in the field of US-triggered drug delivery and cancer therapy with great potential for improvement over current standard treatments. The platforms presented here demonstrate how PEGylated polymeric UCA can be utilized, and modified, for localized, US-driven cancer therapy.

We demonstrated that PEGylation of our native agents reduces immunogenicity through reduction of C3a complement component activation. The results presented here expand on the work of Mosquiera and Chen regarding PEG coatings to mask capsules [125, 140]. Mosquiera previously demonstrated that polymeric nanocapsules decorated with PEG chains resulted in base levels of C3 activation, with nanocapsules displaying

longer PEG chains and/or a higher surface density of PEG chains activating C3 to a lesser degree than other formulations [125]. Chen performed similar evaluations of PEGylated phospholipid microbubbles, demonstrating that longer PEG chains (5kDa) extending from the bubble surface can better mask the underlying surface and therapeutic agent, reducing immune recognition by C3b tagging protein [140]. Our work expands upon these studies by evaluating two different PEGylation methods for polymeric microbubbles, and determining the efficacy of these methods to mask Dox-loaded, TRAIL-ligated UCA from C3a complement component activation.

Considering the sustained release of encapsulated Dox during PLA hydrolysis of n-Sh embedded within the tumor tissue following cavitation and extravasation, these agents present an opportunity for increased local treatment potency, allowing for a higher drug payload to be delivered directly to the target tumor tissue while significantly limiting systemic exposure. Furthermore, sustained release from the agents produced in this study represents the potential for the desirable metronomic treatment mechanism. Several studies have shown metronomic, or consistent release over time, treatment to be more effective in cancer therapy than traditional bolus dose administration [206-210]. Specifically, Klement and colleagues demonstrated tumor regression and antiangiogenic activity when neuroblastoma cells were exposed to continuous low-dose treatment with vinblastine, a neutralizing antibody that targets VEGF receptors, and VEGF receptor-2 antibody over a period of 6 months with no evidence of collateral damage to the host [210]. Fontana et al. observed similar effects in response to metronomic treatment of patients with advanced pancreatic cancer with an oral low-dose combination of cyclophosphamide, celecoxib, and dexamethasone, with patients exhibiting reduced

plasma VEGF levels together with reduced prostate-specific antigen levels [208]. More recently, Bhatt et al. showed that continuous infusion of a low-dose of paclitaxel with oral celecoxib resulted in disease stabilization by acting as an antiangiogenic agent in a phase-II clinical trial involving patients with metastatic melanoma [206]. We have demonstrated a continuous low-dose release of Dox from the agents created in this study, representing the potential to improve treatment efficacy by subjecting tumor cells to constant, localized drug delivery as opposed to a bolus systemic injection.

Moreover, adaptation of the UCA to carry both Dox and TRAIL represents an attractive two-fold treatment mechanism with the potential to greatly improve treatment efficacy. The study presented here expands on the work of Wu et al. evaluating the synergistic relationship between Dox and TRAIL in prostate cancer [211]. The prostate study showed a synergistic cytotoxic effect on LNCaP, LNCaP-Bcl-2, PC-3, and PC93 prostate cancer cells in as short as 2 hours, with Dox significantly activating caspase-8, caspase-6, and caspase-3 which is a major player in the apoptosis cascade [44, 56, 211]. Our work expands upon these studies by investigating TRAIL-sensitive and TRAIL-resistant human breast cancer cell lines, demonstrating the synergistic effects of Dox in sensitizing the resistant cells to TRAIL-mediated apoptosis.

To our knowledge, this study is the first to combine PEGylation, Dox encapsulation, and TRAIL ligation into a single polymeric UCA population that can be used for US-driven targeted drug delivery. The results presented here demonstrate the influence of shell materials, particularly block co-polymers and lipid tails, on acoustic behavior, morphology and physical characteristics, drug loading capacities, and drug release profiles of the resulting agents. Taken together, these results can be used to

develop finely-tuned treatments, with specific drug release profiles or acoustic behaviors, customizing the treatment to the needs of the patient and physician. Future work is expected to investigate alternative ligands and drugs for broader applications of this platform.

5.2 Future Recommendations

While the work presented here represents improvements and refinements over previous studies, there are several areas for future improvement and expansion. The following are some suggestions and recommendations to help guide this research further.

The platform discussed here has proven to significantly reduce immunogenicity over traditional PLA microbubbles. However, the ratios and incorporations of PEG into the PLA shell can be further optimized. In specific aim 2, there was a noticeable shift in UCA resonant frequency between the 2 wt% and 5 wt% PEG-PLA agents, suggesting a change in the shell properties occurs between these ratios. Future work examining the shell properties resulting from 3 wt% and 4 wt% PEG-PLA incorporation may prove important for understanding this shift and better anticipating the changes in echogenicity associated with PEGylation.

Within specific aims 1 and 3, investigating TRAIL ligation before the initial lyophilization may be beneficial. It may be found that by suspending the microbubble pellet in MES buffer and continuing with the TRAIL ligation without the intermediate lyophilization following initial UCA formation helps mitigate the loss of echogenicity resulting from the ligation process. Future experimentation should also be done to develop a quantification assay to determine the amount of active TRAIL ligated to the UCA surface.

An *in vivo* study of the agents produced in this study would provide valuable information and perspective, since the experiments in this thesis only represent *in vitro* testing in a well plate. There are several limitations associated with *in vitro* studies, especially inefficient modeling of physiological conditions such as blood circulation, lack of 3D tumor structure, extravasation to reach tumor tissue. Biodistribution studies *in vivo* would help determine if PEGylation effectively reduces collection of intact and shattered particles in the spleen and healthy liver, and if increased delivery is seen in the target tissue. A long-term survival study would also shed light on the treatment efficacy, especially that of the co-encapsulated Dox with TRAIL to determine the effectiveness of sensitizing resistant cells to this therapy. These agents could also be evaluated in Opticell® cartridges in an *in vitro* setup to better understand the cavitation and uptake effects of US in this therapeutic method.

Another area that could benefit from future experimentation is increasing the drug loading within the UCA shell. Methods that could be explored include addition of drug-loaded nanoparticles to the UCA shell, loading within the agent core, and drug layering. Generation of an agent with a higher drug payload that still retains its acoustic and immunogenic properties would be an improvement to the current agent.

Finally, the UCA fabrication process may benefit from adaptation to a microfluidics approach. Such a process would reduce the variability from user to user, better standardizing the resulting UCA from batch to batch. The microfluidics process could also be optimized to each type of agent desired, allowing for fine-tuned changes to UCA diameter, shell thickness, and so forth [212]. Production of a more monodisperse UCA population would improve echogenicity as well, allowing all UCA to cavitate at the

desired frequency, resulting in more effective US-triggered drug delivery. Microfluidics may also help increase the overall drug loading and encapsulation efficiency, which as discussed previously would be a substantial improvement to the current agents.

List of References

1. *Cancer Facts & Figures 2016*. 2016, American Cancer Society: Atlanta, GA.

2. Cochran, M.C., et al., *Doxorubicin and paclitaxel loaded microbubbles for ultrasound triggered drug delivery.* International Journal of Pharmaceutics, 2011. **414**(1-2): p. 161-170.

3. Eisenbrey, J., et al., *Development and optimization of a doxorubicin loaded poly (lactic acid) contrast agent for ultrasound directed drug delivery.* Journal of Controlled Release, 2010. **143**(1): p. 38-44.

4. Eisenbrey, J., M. Soulen, and M. Wheatley, *Delivery of encapsulated Doxorubicin by ultrasound-mediated size reduction of drug-loaded polymer contrast agents.* IEEE Transactions on Biomedical Engineering, 2010. **57**: p. 24-8.

5. Cochran, M.C., et al., *Disposition of ultrasound sensitive polymeric drug carrier in a rat hepatocellular carcinoma model.* Academic radiology, 2011. **18**(11): p. 1341-1348.

6. Hobbs, S.K., et al., *Regulation of transport pathways in tumor vessels: role of tumor type and microenvironment.* Proceedings of the National Academy of Sciences, 1998. **95**(8): p. 4607-4612.

7. Jain, R.K., *Delivery of molecular and cellular medicine to solid tumors.* Advanced drug delivery reviews, 1997.

8. Maeda, H., *The enhanced permeability and retention (EPR) effect in tumor vasculature: the key role of tumor-selective macromolecular drug targeting.* Advances in enzyme regulation, 2001. **41**(1): p. 189-207.

9. Maeda, H., et al., *Tumor vascular permeability and the EPR effect in macromolecular therapeutics: a review.* Journal of Controlled Release, 2000. **65**(1): p. 271-284.

10. Iyer, A.K., et al., *Exploiting the enhanced permeability and retention effect for tumor targeting.* Drug discovery today, 2006. **11**(17): p. 812-818.

11. Jain, R.K., *Barriers to drug-delivery in solid tumors.* Scientific American, 1994. **271**: p. 58-65.

12. Group, E.B.C.T.C., *Effects of chemotherapy and hormonal therapy for early breast cancer on recurrence and 15-year survival: an overview of the randomised trials.* The Lancet, 2005. **365**(9472): p. 1687-1717.

13. von Minckwitz, G., *Docetaxel/anthracycline combinations for breast cancer treatment.* Expert opinion on pharmacotherapy, 2007. **8**(4): p. 485-495.

14. Jain, R.K., *Delivery of molecular medicine to solid tumors: lessons from in vivo imaging of gene expression and function.* Journal of controlled release, 2001. **74**(1): p. 7-25.

15. Fearon, E.R. and B. Vogelstein, *A genetic model for colorectal tumorigenesis.* Cell, 1990. **61**(5): p. 759-767.

16. Bergers, G. and L.E. Benjamin, *Tumorigenesis and the angiogenic switch.* Nature reviews cancer, 2003. **3**(6): p. 401-410.

17. Papetti, M. and I.M. Herman, *Mechanisms of normal and tumor-derived angiogenesis.* American Journal of Physiology-Cell Physiology, 2002. **282**(5): p. C947-C970.

18. Moeller, B.J., et al. *The relationship between hypoxia and angiogenesis*. in *Seminars in radiation oncology*. 2004. Elsevier.

19. Volpert, O., J. Lawler, and N. Bouck, *A human fibrosarcoma inhibits systemic angiogenesis and the growth of experimental metastases via thrombospondin-1.* Proc Natl Acad Sci, 1998. **11**: p. 6343-6348.

20. Carmeliet, P. and R.K. Jain, *Angiogenesis in cancer and other diseases.* nature, 2000. **407**(6801): p. 249-257.

21. Li, W., *Tumor angiogenesis: Molecular pathology, therapeutic targeting, and imaging.* Acad Radiol, 2000. **7**: p. 800-811.

22. Pasqualini, R., W. Arap, and D.M. McDonald, *Probing the structural and molecular diversity of tumor vasculature.* Trends in molecular medicine, 2002. **8**(12): p. 563-571.

23. Jang, S.H., et al., *Drug delivery and transport to solid tumors.* Pharmaceutical research, 2003. **20**: p. 1337-50.

24. Yuan, F., et al., *Vascular permeability in a human tumor xenograft: molecular size dependence and cutoff size.* Cancer research, 1995. **55**(17): p. 3752-3756.

25. Monsky, W.L., et al., *Augmentation of transvascular transport of macromolecules and nanoparticles in tumors using vascular endothelial growth factor.* Cancer Research, 1999. **59**(16): p. 4129-4135.

26. Heldin, C.-H., et al., *High interstitial fluid pressure—an obstacle in cancer therapy.* Nature Reviews Cancer, 2004. **4**(10): p. 806-813.

27. Alitalo, K. and P. Carmeliet, *Molecular mechanisms of lymphangiogenesis in health and disease.* Cancer cell, 2002. **1**(3): p. 219-227.

28. Jain, R.K., *Vascular and interstitial barriers to delivery of therapeutic agents in tumors.* Cancer and Metastasis Reviews, 1990. **9**(3): p. 253-266.

29. Mitra, S., et al., *Tumour targeted delivery of encapsulated dextran–doxorubicin conjugate using chitosan nanoparticles as carrier.* Journal of Controlled Release, 2001. **74**(1): p. 317-323.

30. Jain, R., A.W. Cook, and E.L. Steele, *Haemodynamic and transport barriers to the treatment of solid tumours.* International journal of radiation biology, 1991. **60**(1-2): p. 85-100.

31. *Cancer Facts & Figures 2013*. 2013, American Cancer Society: Atlanta, GA.

32. Abdalla, E.K., et al., *Recurrence and outcomes following hepatic resection, radiofrequency ablation, and combined resection/ablation for colorectal liver metastases.* Annals of surgery, 2004. **239**(6): p. 818-827.

33. Wood, B.J., et al., *Percutaneous tumor ablation with radiofrequency.* Cancer, 2002. **94**(2): p. 443-451.

34. Fisher, B., et al., *Twenty-year follow-up of a randomized trial comparing total mastectomy, lumpectomy, and lumpectomy plus irradiation for the treatment of invasive breast cancer.* New England Journal of Medicine, 2002. **347**(16): p. 1233-1241.

35. Kinsella, T.J., J. Sohn, and B. Wessels, *Principles of radiation oncology*, in *Oncology*. 2006, Springer. p. 41-57.

36. Hortobagyi, G., *Anthracyclines in the treatment of cancer.* Drugs, 1997. **54**(4): p. 1-7.

37. Minotti, G., et al., *Anthracyclines: molecular advances and pharmacologic developments in antitumor activity and cardiotoxicity.* Pharmacological reviews, 2004. **56**(2): p. 185-229.

38. Murphy, G., W. Lawrence, and R. Lenhard, *American Cancer Society Textbook of Clincal Oncology*. 2nd ed. 1995, Atlanta, GA: American Cancer Society.

39. Gewirtz, D., *A critical evaluation of the mechanisms of action proposed for the antitumor effects of the anthracycline antibiotics adriamycin and daunorubicin.* Biochemical pharmacology, 1999. **57**(7): p. 727-741.

40. Singal, P.K. and N. Iliskovic, *Doxorubicin-induced cardiomyopathy.* New England Journal of Medicine, 1998. **339**(13): p. 900-905.

41. Dai, X., et al., *Targeting TNF-related apoptosis-inducing ligand (TRAIL) receptor by natural products as a potential therapeutic approach for cancer therapy.* Experimental Biology and Medicine, 2015. **240**(6): p. 760-773.

42. French, L.E. and J. Tschopp, *The TRAIL to selective tumor death.* Nature medicine, 1999. **5**(2): p. 146-147.

43. Mitsiades, C.S., et al., *TRAIL/Apo2L ligand selectively induces apoptosis and overcomes drug resistance in multiple myeloma: therapeutic applications.* Blood, 2001. **98**(3): p. 795-804.

44. Wang, S. and W.S. El-Deiry, *TRAIL and apoptosis induction by TNF-family death receptors.* Oncogene, 2003. **22**: p. 8628-8633.

45. Sanlioglu, A., et al., *Surface TRAIL decoy receptor-4 expression is correlated with TRAIL resistance in MCF7 breast cancer cells.* BMC Cancer, 2005. **5**.

46. Truneh, A., et al., *Temperature-sensitive Differential Affinity of TRAIL for Its Receptors: DR5 IS THE HIGHEST AFFINITY RECEPTOR.* Journal of Biological Chemistry, 2000. **275**(30): p. 23319-23325.

47. Mahalingam, D., et al., *TRAIL receptor signalling and modulation: Are we on the right TRAIL?* Cancer Treatment Reviews, 2009. **35**(3): p. 280-288.

48. Kuijlen, J.M., et al., *The efficacy of alginate encapsulated CHO-K1 single chain-TRAIL producer cells in the treatment of brain tumors.* Journal of neuro-oncology, 2006. **78**(1): p. 31-39.

49. Cuello, M., et al., *Synergistic induction of apoptosis by the combination of TRAIL and chemotherapy in chemoresistant ovarian cancer cells.* Gynecologic oncology, 2001. **81**: p. 380-90.

50. Lashinger, L.M., et al., *Bortezomib abolishes tumor necrosis factor–related apoptosis-inducing ligand resistance via a p21-dependent mechanism in human bladder and prostate cancer cells.* Cancer research, 2005. **65**(11): p. 4902-4908.

51. Thorburn, A., K. Behbakht, and H. Ford, *TRAIL receptor-targeted therapeutics: resistance mechanisms and strategies to avoid them.* Drug Resistance Updates, 2008. **11**(1): p. 17-24.

52. Tomek, S., et al., *Resistance to TRAIL-induced apoptosis in ovarian cancer cell lines is overcome by co-treatment with cytotoxic drugs.* Gynecologic oncology, 2004. **94**: p. 107-14.

53. Wahl, H., et al., *Curcumin enhances Apo2L/TRAIL-induced apoptosis in chemoresistant ovarian cancer cells.* Gynecologic oncology, 2007. **105**(1): p. 104-112.

54. You, M., et al., *The combination of ADI-PEG20 and TRAIL effectively increases cell death in melanoma cell lines.* Biochemical and biophysical research communications, 2010. **394**: p. 760-6.

55. Huang, X., et al., *Novel targeted pro-apoptotic agents for the treatment of prostate cancer.* The Journal of urology, 2007. **178**(5): p. 1846-1854.

56. MacFarlane, M. and A.C. Williams, *Apoptosis and disease: a life or death decision.* EMBO reports, 2004. **5**(7): p. 674-678.

57. Bae, Y.H. and K. Park, *Targeted drug delivery to tumors: myths, reality and possibility.* Journal of Controlled Release, 2011. **153**(3): p. 198.

58. Safari, J. and Z. Zarnegar, *Advanced drug delivery systems: Nanotechnology of health design A review.* Journal of Saudi Chemical Society, 2014. **18**(2): p. 85-99.

59. Mishra, B., B.B. Patel, and S. Tiwari, *Colloidal nanocarriers: a review on formulation technology, types and applications toward targeted drug delivery.* Nanomedicine: Nanotechnology, biology and medicine, 2010. **6**(1): p. 9-24.

60. Mura, S., J. Nicolas, and P. Couvreur, *Stimuli-responsive nanocarriers for drug delivery.* Nature materials, 2013. **12**(11): p. 991-1003.

61. Zhu, L. and V.P. Torchilin, *Stimulus-responsive nanopreparations for tumor targeting.* Integrative Biology, 2013. **5**(1): p. 96-107.

62. Oborotova, N., *Liposomal Medicinal Forms of Antitumor Drugs (A Review).* Pharmaceutical Chemistry Journal, 2001. **35**(4): p. 209-215.

63. Hauff, P., M. Reinhardt, and S. Foster, *Ultrasound basics*, in *Molecular Imaging I*. 2008, Springer. p. 91-107.

64. Nelson, T.R., et al., *Ultrasound biosafety considerations for the practicing sonographer and sonologist.* Journal of Ultrasound in Medicine, 2009. **28**(2): p. 139-150.

65. Bigelow, T.A., et al., *The thermal index its strengths, weaknesses, and proposed improvements.* Journal of Ultrasound in Medicine, 2011. **30**(5): p. 714-734.

66. Szabo, T.L., *Diagnostic ultrasound imaging: inside out*. 2004: Academic Press.

67. Gramiak, R. and P.M. Shah, *Echocardiography of the aortic root.* Investigative radiology, 1968. **3**(5): p. 356-366.

68. Palma, L. and M. Bertolotto, *Introduction to ultrasound contrast agents: physics overview.* Eur Radiol, 1999. **9**: p. S338-342.

69. Stride, E. and N. Saffari, *Microbubble ultrasound contrast agents: a review.* Proceedings of the Institution of Mechanical Engineers, Part H: Journal of Engineering in Medicine, 2003. **217**(6): p. 429-447.

70. Kinsler, L., et al., *Fundamentals of Acoustics*. 2000, Hoboken, NJ: John Wiley & Sons, Inc. .

71. Calliada, F., et al., *Ultrasound contrast agents: basic principles.* European journal of radiology, 1998. **27**: p. S157-S160.

72. Borden, M.A. and M.L. Longo, *Dissolution behavior of lipid monolayer-coated, air-filled microbubbles: Effect of lipid hydrophobic chain length.* Langmuir, 2002. **18**(24): p. 9225-9233.

73. Epstein, P. and M.S. Plesset, *On the Stability of Gas Bubbles in Liquid-Gas Solutions.* The Journal of Chemical Physics, 1950. **18**(11): p. 1505-1509.

74. Hoff, L., *Acoustic characterization of contrast agents for medical ultrasound imaging*. 2001: Springer Science & Business Media.

75. Leighton, T., *The acoustic bubble*. 1994, London: Academic Press.

76. Marmottant, P., et al., *A model for large amplitude oscillations of coated bubbles accounting for buckling and rupture.* The Journal of the Acoustical Society of America, 2005. **118**(6): p. 3499-3505.

77. Katiyar, A. and K. Sarkar, *Excitation threshold for subharmonic generation from contrast microbubbles.* The Journal of the Acoustical Society of America, 2011. **130**(5): p. 3137-3147.

78. Anderson, A.L. and L.D. Hampton, *Acoustics of gas-bearing sediments I. Background.* The Journal of the Acoustical Society of America, 1980. **67**(6): p. 1865-1889.

79. Correas, J.-M., et al., *Ultrasound contrast agents: properties, principles of action, tolerance, and artifacts.* European radiology, 2001. **11**(8): p. 1316-1328.

80. Ferrara, K., R. Pollard, and M. Borden, *Ultrasound Microbubble Contrast Agents: Fundamentals and Application to Gene and Drug Delivery.* Annual Review of Biomedical Engineering, 2007. **9**(1): p. 415-447.

81. Goldberg, B., J. Raichlen, and F. Forsberg, *Ultrasound Contrast Agents: Basic Principles and Clinical Applications*. 2nd ed. 2001, London: Martin Dunitz.

82. Wheatley, M.A. and M.C. Cochran, *Ultrasound contrast agents.* Journal of Drug Delivery Science and Technology, 2013. **23**(1): p. 57-72.

83. Ophir, J., et al., *Ultrasonic Backscatter from Contrast Producing Collagen Microspheres.* Ultrasonic Imaging, 1980. **2**(1): p. 67-77.

84. Straub, J.A., et al., *Porous PLGA microparticles: AI-700, an intravenously administered ultrasound contrast agent for use in echocardiography.* Journal of controlled release, 2005. **108**(1): p. 21-32.

85. Straub, J.A., et al., *Method for making porous microparticles by spray drying*. 1998, Google Patents.

86. Wheatley, M.A., B. Schrope, and P. Shen, *Contrast agents for diagnostic ultrasound: development and evaluation of polymer-coated microbubbles.* Biomaterials, 1990. **11**(9): p. 713-717.

87. Eisenbrey, J., *Ultrasound sensitive polymeric drug carriers for treatment of solid tumors*. 2010, Drexel University School of Biomedical Engineering, Science & Health Systems: Philadelphia, PA.

88. El-Sherif, D.M. and M.A. Wheatley, *Development of a novel method for synthesis of a polymeric ultrasound contrast agent.* Journal of Biomedical Materials Research Part A, 2003. **66**(2): p. 347-355.

89. Wheatley, M.A., et al., *Comparison of in vitro and in vivo acoustic response of a novel 50: 50 PLGA contrast agent.* Ultrasonics, 2006. **44**(4): p. 360-367.

90. Cochran, M.C., *Polymer Ultrasound Contrast Agents for Targeted Drug and Gene Delivery*, in *Biomedical Engineering*. 2012, Drexel University: Philadelphia, PA.

91. Forsberg, F., et al., *Effect of shell type on the in vivo backscatter from polymer-encapsulated microbubbles.* Ultrasound in medicine & biology, 2004. **30**(10): p. 1281-1287.

92. Brophy, B., *Biodegradable polyester polymers as drug carriers*, in *Encyclopedia of Pharmaceutical Technology*, I. Swarbrick and J. Boylan, Editors. 1990, Marcel Dekker: New York. p. 21-32.

93. Bloch, S.H., et al., *Optical observation of lipid-and polymer-shelled ultrasound microbubble contrast agents.* Applied Physics Letters, 2004. **84**(4): p. 631-633.

94. Postema, M., et al., *Ultrasound-induced encapsulated microbubble phenomena.* Ultrasound in medicine & biology, 2004. **30**(6): p. 827-840.

95. Chomas, J.E., et al., *Optical observation of contrast agent destruction.* Applied Physics Letters, 2000. **77**(7): p. 1056-1058.

96. Newman, C. and T. Bettinger, *Gene therapy progress and prospects: ultrasound for gene transfer.* Gene therapy, 2007. **14**(6): p. 465-475.

97. Forbes, M., R. Steinberg, and W. O'Brien Jr., *Examination of Inertial Cavitation of Optison in Producing Sonoporation of Chinese Hamster Ovary Cells.* Ultrasound in medicine & biology, 2008. **34**: p. 2009-2018.

98. Postema, M., et al., *High-speed photography during ultrasound illustrates potential therapeutic applications of microbubbles.* Medical physics, 2005. **32**(12): p. 3707-3711.

99. Prentice, P., et al., *Membrane disruption by optically controlled microbubble cavitation.* Nature Physics, 2005. **1**(2): p. 107-110.

100. Brayman, A.A., L.M. Lizotte, and M.W. Miller, *Erosion of artificial endothelia in vitro by pulsed ultrasound: acoustic pressure, frequency, membrane orientation and microbubble contrast agent dependence.* Ultrasound in medicine & biology, 1999. **25**(8): p. 1305-1320.

101. Song, J., et al., *Influence of injection site, microvascular pressureand ultrasound variables on microbubble-mediated delivery of microspheres to muscle.* Journal of the American College of Cardiology, 2002. **39**(4): p. 726-731.

102. Skyba, D.M., et al., *Direct in vivo visualization of intravascular destruction of microbubbles by ultrasound and its local effects on tissue.* Circulation, 1998. **98**(4): p. 290-293.

103. Price, R.J., et al., *Delivery of colloidal particles and red blood cells to tissue through microvessel ruptures created by targeted microbubble destruction with ultrasound.* Circulation, 1998. **98**(13): p. 1264-1267.

104. Bekeredjian, R., et al., *Ultrasound targeted microbubble destruction increases capillary permeability in hepatomas.* Ultrasound in medicine & biology, 2007. **33**(10): p. 1592-1598.

105. Böhmer, M., et al., *Focused ultrasound and microbubbles for enhanced extravasation.* Journal of Controlled Release, 2010. **148**(1): p. 18-24.

106. Rychak, J.J., A.L. Klibanov, and J.A. Hossack, *Acoustic radiation force enhances targeted delivery of ultrasound contrast microbubbles: in vitro verification.* Ultrasonics, Ferroelectrics, and Frequency Control, IEEE Transactions on, 2005. **52**(3): p. 421-433.

107. Dayton, P.A., et al., *A preliminary evaluation of the effects of primary and secondary radiation forces on acoustic contrast agents.* Ultrasonics, Ferroelectrics, and Frequency Control, IEEE Transactions on, 1997. **44**(6): p. 1264-1277.

108. Dayton, P.A., J.S. Allen, and K.W. Ferrara, *The magnitude of radiation force on ultrasound contrast agents.* The Journal of the Acoustical Society of America, 2002. **112**: p. 2183.

109. Lum, A.F., et al., *Ultrasound radiation force enables targeted deposition of model drug carriers loaded on microbubbles.* Journal of Controlled Release, 2006. **111**(1): p. 128-134.

110. Yasuda, K. and T. Kamakura, *Acoustic radiation force on micrometer-size particles.* Applied physics letters, 1997. **71**(13): p. 1771-1773.

111. Harrison, G., E. Balcer-Kubiczek, and H. Eddy, *Potentiation of chemotherapy by low-level ultrasound.* International journal of radiation biology, 1991. **59**(6): p. 1453-1466.

112. Saad, A.H. and G.M. Hahn, *Ultrasound enhanced drug toxicity on Chinese hamster ovary cells in vitro.* Cancer research, 1989. **49**(21): p. 5931-5934.

113. Escoffre, J., et al., *Doxorubicin delivery into tumor cells with ultrasound and microbubbles.* Molecular pharmaceutics, 2011. **8**(3): p. 799-806.

114. Sonoda, S., et al., *Inhibition of melanoma by ultrasound-microbubble-aided drug delivery suggests membrane permeabilization.* Cancer biology & therapy, 2007. **6**(8): p. 1282-1289.

115. Bekeredjian, R., H. Katus, and H. Kuecherer, *Therapeutic use of ultrasound targeted microbubble destruction: a review of non-cardiac applications.* Ultraschall in der Medizin (Stuttgart, Germany: 1980), 2006. **27**(2): p. 134-140.

116. Kinoshita, M. and K. Hynynen, *Intracellular delivery of Bak BH3 peptide by microbubble-enhanced ultrasound.* Pharmaceutical research, 2005. **22**(5): p. 716-720.

117. Miao, C.H., et al., *Ultrasound enhances gene delivery of human factor IX plasmid.* Human gene therapy, 2005. **16**(7): p. 893-905.

118. Lentacker, I., et al., *Design and evaluation of doxorubicin-containing microbubbles for ultrasound-triggered doxorubicin delivery: cytotoxicity and mechanisms involved.* Molecular therapy, 2010. **18**: p. 101-8.

119. Huang, S.-L. and R.C. MacDonald, *Acoustically active liposomes for drug encapsulation and ultrasound-triggered release.* Biochimica et Biophysica Acta (BBA)-Biomembranes, 2004. **1665**(1): p. 134-141.

120. Kooiman, K., et al., *Oil-filled polymer microcapsules for ultrasound-mediated delivery of lipophilic drugs.* Journal of Controlled Release, 2009. **133**(2): p. 109-118.

121. Eisenbrey, J., et al., *Ultrasound triggered cell death in vitro with doxorubicin loaded poly lactic-acid contrast agents.* Ultrasonics, 2009. **49**(8): p. 628-633.

122. Lathia, J.D., et al., *Surface Modification of Polymeric Contrast Agents for Cancer Targeting.* Pharmaceutical Engineering, 2004. **24**(1): p. 92-103.

123. AlléAaemann, E., et al., *Kinetics of blood component adsorption on poly(D,L-lactic acid) nanoparticles: Evidence of complement C3 component involvement.* Journal of Biomedical Materials Research, 1997. **37**(2): p. 229-234.

124. Lim, A.K., et al., *Evidence for Spleen-specific Uptake of a Microbubble Contrast Agent: A Quantitative Study in Healthy Volunteers1.* Radiology, 2004. **231**(3): p. 785-788.

125. Mosqueira, V.C.F., et al., *Relationship between complement activation, cellular uptake and surface physicochemical aspects of novel PEG-modified nanocapsules.* Biomaterials, 2001. **22**(22): p. 2967-2979.

126. Owens Iii, D.E. and N.A. Peppas, *Opsonization, biodistribution, and pharmacokinetics of polymeric nanoparticles.* International Journal of Pharmaceutics, 2006. **307**(1): p. 93-102.

127. Ricklin, D., et al., *Complement: a key system for immune surveillance and homeostasis.* Nat Immunol, 2010. **11**(9): p. 785-797.

128. Van Furth, R., et al., *The mononuclear phagocyte system: a new classification of macrophages, monocytes, and their precursor cells.* Bulletin of the World Health Organization, 1972. **46**(6): p. 845.

129. Kazatchkine, M. and M. Carreno, *Activation of the complement system at the interface between blood and artificial surfaces.* Biomaterials, 1988. **9**(1): p. 30-35.

130. Papahadjopoulos, D., et al., *Sterically stabilized liposomes: improvements in pharmacokinetics and antitumor therapeutic efficacy.* Proceedings of the National Academy of Sciences, 1991. **88**(24): p. 11460-11464.

131. Stolnik, S., L. Illum, and S. Davis, *Long circulating microparticulate drug carriers.* Advanced Drug Delivery Reviews, 1995. **16**(2): p. 195-214.

132. Alexis, F., et al., *Factors affecting the clearance and biodistribution of polymeric nanoparticles.* Molecular pharmaceutics, 2008. **5**(4): p. 505-515.

133. Vonarbourg, A., et al., *Parameters influencing the stealthiness of colloidal drug delivery systems.* Biomaterials, 2006. **27**(24): p. 4356-4373.

134. Rother, K., G.O. Till, and G.M. Hänsch, *The complement system*. 1998: Springer.

135. Sarma, J.V. and P.A. Ward, *The complement system.* Cell and tissue research, 2011. **343**(1): p. 227-235.

136. Sahu, A. and J.D. Lambris, *Structure and biology of complement protein C3, a connecting link between innate and acquired immunity.* Immunological reviews, 2001. **180**(1): p. 35-48.

137. Gref, R., et al., *'Stealth'corona-core nanoparticles surface modified by polyethylene glycol (PEG): influences of the corona (PEG chain length and surface density) and of the core composition on phagocytic uptake and plasma protein adsorption.* Colloids and Surfaces B: Biointerfaces, 2000. **18**(3): p. 301-313.

138. Amoozgar, Z. and Y. Yeo, *Recent advances in stealth coating of nanoparticle drug delivery systems.* Wiley Interdisciplinary Reviews: Nanomedicine and Nanobiotechnology, 2012. **4**(2): p. 219-233.

139. Avgoustakis, K., *Pegylated poly (lactide) and poly (lactide-co-glycolide) nanoparticles: preparation, properties and possible applications in drug delivery.* Current Drug Delivery, 2004. **1**(4): p. 321-333.

140. Chen, C.C. and M.a. Borden, *The role of poly(ethylene glycol) brush architecture in complement activation on targeted microbubble surfaces.* Biomaterials, 2011. **32**: p. 6579-87.

141. Lim, S.M., et al., *Improved biological half-life and anti-tumor activity of TNF-related apoptosis-inducing ligand (TRAIL) using PEG-exposed nanoparticles.* Biomaterials, 2011. **32**: p. 3538-46.

142. Pisani, E., et al., *Tuning microcapsules surface morphology using blends of homo- and copolymers of PLGA and PLGA-PEG.* Soft Matter, 2009. **5**: p. 3054-3060.

143. Storm, G., et al., *Surface modification of nanoparticles to oppose uptake by the mononuclear phagocyte system.* Advanced Drug Delivery Reviews, 1995. **17**(1): p. 31-48.

144. Xiao, R.Z., et al., *Recent advances in PEG–PLA block copolymer nanoparticles.* International journal of nanomedicine, 2010. **5**: p. 1057.

145. Gref, R., et al., *The controlled intravenous delivery of drugs using PEG-coated sterically stabilized nanospheres.* Advanced Drug Delivery Reviews, 1995. **16**(2): p. 215-233.

146. Ishida, T., et al., *PEGylated liposomes elicit an anti-PEG IgM response in a T cell-independent manner.* Journal of Controlled Release, 2007. **122**(3): p. 349-355.

147. Chen, C.C. and M.a. Borden, *Ligand conjugation to bimodal poly(ethylene glycol) brush layers on microbubbles.* Langmuir, 2010. **26**: p. 13183-94.

148. Youn, Y.S., et al., *Biological and physicochemical evaluation of the conformational stability of tumor necrosis factor-related apoptosis-inducing ligand (TRAIL).* Biotechnology letters, 2007. **29**(5): p. 713-721.

149. Kim, T.H., et al., *PEGylated TNF-related apoptosis-inducing ligand (TRAIL)-loaded sustained release PLGA microspheres for enhanced stability and antitumor activity.* Journal of controlled release : official journal of the Controlled Release Society, 2011. **150**: p. 63-9.

150. Oum, K., *Therapeutic and diagnostic applications of ultrasound contrast media for breast, ovarian and skin cancers*. 2008, Drexel University School of Biomedical Engineering, Science & Health Systems: Philadelphia, PA.

151. Wheatley, M.A., et al., *Cellular signal transduction can be induced by TRAIL conjugated to microcapsules.* Journal of Biomedical Materials Research Part A, 2012. **100**(10): p. 2602-2611.

152. de Jong, N. and L. Hoff, *Ultrasound scattering properties of Albunex microspheres.* Ultrasonics, 1993. **31**(3): p. 175-181.

153. de Jong, N., et al., *Absorption and scatter of encapsulated gas filled microspheres: Theoretical considerations and some measurements.* Ultrasonics, 1992. **30**(2): p. 95-103.

154. Borden, M.A., et al., *A stimulus-responsive contrast agent for ultrasound molecular imaging.* Biomaterials, 2008. **29**(5): p. 597-606.

155. Proikakis, C.S., et al., *Swelling and hydrolytic degradation of poly(d,l-lactic acid) in aqueous solutions.* Polymer Degradation and Stability, 2006. **91**(3): p. 614-619.

156. Shetty, S., et al., *Transcription Factor NF-κB Differentially Regulates Death Receptor 5 Expression Involving Histone Deacetylase 1.* Molecular and Cellular Biology, 2005. **25**(13): p. 5404-5416.

157. Keane, M.M., et al., *Chemotherapy augments TRAIL-induced apoptosis in breast cell lines.* Cancer research, 1999. **59**(3): p. 734-741.

158. Diou, O., et al., *PEGylated nanocapsules of PFOB as ultrasound contrast agents : mechanism of formation , influence of polymer concentration on morphology and mechanical properties.* Langmuir, 2013.

159. Eisenbrey, J.R., O.M. Burstein, and M.A. Wheatley, *Effect of molecular weight and end capping on poly(lactic-co-glycolic acid) ultrasound contrast agents.* Polymer Engineering & Science, 2008. **48**(9): p. 1785-1792.

160. Andorko, J., *Formulation, fabrication, and drug loading of PEGylated ultrasound contrast agents*. 2012, Drexel University School of Biomedical Engineering, Science & Health Systems: Philadelphia, PA.

161. Morel, D.R., et al., *Human Pharmacokinetics and Safety Evaluation of SonoVue™, a New Contrast Agent for Ultrasound Imaging.* Investigative Radiology, 2000. **35**(1).

162. Poehlmann, M., et al., *On the interplay of shell structure with low-and high-frequency mechanics of multifunctional magnetic microbubbles.* Soft matter, 2014. **10**(1): p. 214-226.

163. Sboros, V., et al., *Probing microbubble targeting with atomic force microscopy.* Colloids and Surfaces B: Biointerfaces, 2010. **80**(1): p. 12-17.

164. Stride, E., M. Tang, and R.J. Eckersley, *Physical phenomena affecting quantitative imaging of ultrasound contrast agents.* Applied Acoustics, 2009. **70**(10): p. 1352-1362.

165. Wrenn, S.P., M. Mleczko, and G. Schmitz, *Phospholipid-stabilized microbubbles: Influence of shell chemistry on cavitation threshold and binding to giant uni-lamellar vesicles.* Applied Acoustics, 2009. **70**(10): p. 1313-1322.

166. Sanna, V., et al., *Development of Polymeric Microbubbles Targeted to Prostate-Specific Membrane Antigen as Prototype of Novel Ultrasound Contrast Agents.* Molecular Pharmaceutics, 2011. **8**(3): p. 748-757.

167. Hoff, L., P.C. Sontum, and J.M. Hovem, *Oscillations of polymeric microbubbles: Effect of the encapsulating shell.* The Journal of the Acoustical Society of America, 2000. **107**(4): p. 2272-2280.

168. Azmin, M., et al., *How do microbubbles and ultrasound interact? Basic physical, dynamic and engineering principles.* Current pharmaceutical design, 2012. **18**: p. 2118-34.

169. de Jong, N., et al., *Ultrasonic characterization of ultrasound contrast agents.* Medical & Biological Engineering & Computing, 2009. **47**(8): p. 861-873.

170. Morse, P.M. and K.U. Ingard, *Theoretical acoustics*. 1968: Princeton university press.

171. Lindén, M.V., et al., *Characterization of phosphatidylcholine/polyethylene glycol-lipid aggregates and their use as coatings and carriers in capillary electrophoresis.* Electrophoresis, 2008. **29**: p. 852-62.

172. Neppiras, E.A., *Subharmonic and Other Low-Frequency Emission from Bubbles in Sound-Irradiated Liquids.* The Journal of the Acoustical Society of America, 1969. **46**(3B): p. 587-601.

173. Honary, S. and F. Zahir, *Effect of zeta potential on the properties of nano-drug delivery systems-a review (Part 1).* Tropical Journal of Pharmaceutical Research, 2013. **12**(2): p. 255-264.

174. Yao, L., et al., *Facilitated brain delivery of poly (ethylene glycol)–poly (lactic acid) nanoparticles by microbubble-enhanced unfocused ultrasound.* Biomaterials, 2014. **35**(10): p. 3384-3395.

175. Marsh, D., R. Bartucci, and L. Sportelli, *Lipid membranes with grafted polymers: physicochemical aspects.* Biochimica et Biophysica Acta (BBA) - Biomembranes, 2003. **1615**(1–2): p. 33-59.

176. Chen, W.-S., et al., *A comparison of the fragmentation thresholds and inertial cavitation doses of different ultrasound contrast agents.* The Journal of the Acoustical Society of America, 2003. **113**(1): p. 643-651.

177. Tinkov, S., et al., *Characterization of ultrasound-mediated destruction of drug-loaded microbubbles using an improved in vitro model.* Applied Acoustics, 2009. **70**(10): p. 1323-1329.

178. Haeffner-Cavaillon, N., et al., *C3a(C3adesArg) induces production and release of interleukin 1 by cultured human monocytes.* The Journal of Immunology, 1987. **139**(3): p. 794-9.

179. Janeway, C.A., et al., *Immunobiology: The Immune System in Health and Disease*. 5th ed. 2001, New York: Garland Science.

180. Morgan, E.L., W.O. Weigle, and T.E. Hugli, *Anaphylatoxin-mediated regulation of the immune response. I. C3a-mediated suppression of human and murine humoral immune responses.* The Journal of Experimental Medicine, 1982. **155**(5): p. 1412-1426.

181. Tedder, T.F., M. Inaoki, and S. Sato, *The CD19–CD21 Complex Regulates Signal Transduction Thresholds Governing Humoral Immunity and Autoimmunity.* Immunity, 1997. **6**(2): p. 107-118.

182. Janssen, B.J.C., et al., *Structures of complement component C3 provide insights into the function and evolution of immunity.* Nature, 2005. **437**(7058): p. 505-511.

183. Sperling, C., et al., *In vitro blood reactivity to hydroxylated and non-hydroxylated polymer surfaces.* Biomaterials, 2007. **28**(25): p. 3617-3625.

184. Borden, M.A., et al., *In vivo demonstration of cancer molecular imaging with ultrasound radiation force and buried-ligand microbubbles.* Mol Imaging, 2013. **12**(6): p. 357-363.

185. Eisenbrey, J., et al., *Doxorubicin loaded contrast agents for ultrasound triggered drug delivery: importance of process parameters.* Pharmaceutical Engineering, 2008. **28**: p. 70-78.

186. Abraham, S.A., et al., *The Liposomal Formulation of Doxorubicin*, in *Methods in Enzymology*. 2005, Academic Press. p. 71-97.

187. de Wolf, F.A., et al., *Comparable interaction of doxorubicin with various acidic phospholipids results in changes of lipid order and dynamics.* Biochimica et Biophysica Acta (BBA) - Molecular Basis of Disease, 1990. **1096**(1): p. 67-80.

188. Danafar, H., et al., *PLA-PEG-PLA copolymer-based polymersomes as nanocarriers for delivery of hydrophilic and hydrophobic drugs: preparation and evaluation with atorvastatin and lisinopril.* Drug Development and Industrial Pharmacy, 2014. **40**(10): p. 1411-1420.

189. Gorce, J.-M., M. Arditi, and M. Schneider, *Influence of bubble size distribution on the echogenicity of ultrasound contrast agents: a study of Sonovue™.* Investigative radiology, 2000. **35**(11): p. 661-671.

190. Geers, B., et al., *Crucial factors and emerging concepts in ultrasound-triggered drug delivery.* Journal of Controlled Release, 2012. **164**: p. 248-255.

191. Husseini, G.A., et al., *The role of cavitation in acoustically activated drug delivery.* Journal of controlled release, 2005. **107**(2): p. 253-261.

192. Anel, A., et al., *Apo2L/TRAIL and immune regulation.* Front Biosci, 2007. **12**(1): p. 2074-2084.

193. Droin, N.M., et al., *Egr Family Members Regulate Nonlymphoid Expression of Fas Ligand, TRAIL, and Tumor Necrosis Factor during Immune Responses.* Molecular and Cellular Biology, 2003. **23**(21): p. 7638-7647.

194. Pellicoro, A., et al., *Liver fibrosis and repair: immune regulation of wound healing in a solid organ.* Nat Rev Immunol, 2014. **14**(3): p. 181-194.

195. Bosque, A., et al., *Human CD8+ T cell blasts are more sensitive than CD4+ T cell blasts to regulation by APO2L/TRAIL.* European journal of immunology, 2005. **35**(6): p. 1812-1821.

196. Marsters, S.A., et al., *Activation of apoptosis by Apo-2 ligand is independent of FADD but blocked by CrmA.* Current Biology, 1996. **6**(6): p. 750-752.

197. Carswell, E.A., et al., *An endotoxin-induced serum factor that causes necrosis of tumors.* Proceedings of the National Academy of Sciences, 1975. **72**(9): p. 3666-3670.

198. Kim, Y., et al., *An inducible pathway for degradation of FLIP protein sensitizes tumor cells to TRAIL-induced apoptosis.* Journal of Biological Chemistry, 2002. **277**(25): p. 22320-22329.

199. Wang, S., et al., *Doxorubicin Induces Apoptosis in Normal and Tumor Cells via Distinctly Different Mechanisms: INTERMEDIACY OF H2O2- AND p53-DEPENDENT PATHWAYS.* Journal of Biological Chemistry, 2004. **279**(24): p. 25535-25543.

200. Jablonowski, L., A. Palovcak, and M. Wheatley, *Induction of apoptosis by targeted ultrasound contrast agents in cancer therapy.* Pharmaceutical Engineering, 2014. **34**(4): p. 70-80.

201. Nagane, M., et al., *Increased death receptor 5 expression by chemotherapeutic agents in human gliomas causes synergistic cytotoxicity with tumor necrosis factor-related apoptosis-inducing ligand in vitro and in vivo.* Cancer research, 2000. **60**(4): p. 847-853.

202. Chandrasekaran, S., et al., *TRAIL-mediated apoptosis in breast cancer cells cultured as 3D spheroids.* PloS one, 2014. **9**(10): p. e111487.

203. Shanskij, Y.D., Y.A. Ershov, and V.M. Pechennikov, *A Method for Evaluation of Therapeutic Dose of Doxorubicin Hydrochloride Using Breast Tumor Cell Culture MCF-7.* Bulletin of Experimental Biology and Medicine, 2009. **148**(3): p. 464-467.

204. Herbst, R.S., et al., *Phase I Dose-Escalation Study of Recombinant Human Apo2L/TRAIL, a Dual Proapoptotic Receptor Agonist, in Patients With Advanced Cancer.* Journal of Clinical Oncology, 2010. **28**(17): p. 2839-2846.

205. Salanti, A., et al., *Targeting Human Cancer by a Glycosaminoglycan Binding Malaria Protein.* Cancer Cell, 2015. **28**(4): p. 500-514.

206. Bhatt, R.S., et al., *A phase 2 pilot trial of low-dose, continuous infusion, or "metronomic" paclitaxel and oral celecoxib in patients with metastatic melanoma.* Cancer, 2010. **116**(7): p. 1751-1756.

207. Hanahan, D., G. Bergers, and E. Bergsland, *Less is more, regularly: metronomic dosing of cytotoxic drugs can target tumor angiogenesis in mice.* The Journal of clinical investigation, 2000. **105**(8): p. 1045-1047.

208. Fontana, A., et al., *Clinical and pharmacodynamic evaluation of metronomic cyclophosphamide, celecoxib, and dexamethasone in advanced hormone-refractory prostate cancer.* Clinical Cancer Research, 2009. **15**(15): p. 4954-4962.

209. Browder, T., et al., *Antiangiogenic scheduling of chemotherapy improves efficacy against experimental drug-resistant cancer.* Cancer research, 2000. **60**(7): p. 1878-1886.

210. Klement, G., et al., *Continuous low-dose therapy with vinblastine and VEGF receptor-2 antibody induces sustained tumor regression without overt toxicity.* Journal of Clinical Investigation, 2000. **105**(8): p. R15.

211. Wu, X., et al., *Doxorubicin enhances TRAIL-induced apoptosis in prostate cancer.* International journal of oncology, 2002. **20**(5): p. 949-954.

212. Watanabe, T., Y. Kimura, and T. Ono, *Microfluidic Fabrication of Monodisperse Polylactide Microcapsules with Tunable Structures through Rapid Precipitation.* Langmuir, 2013. **29**(46): p. 14082-14088.

APPENDIX A: STANDARD CURVES

The following section includes the standard curves created and used to determine the results presented throughout this thesis.

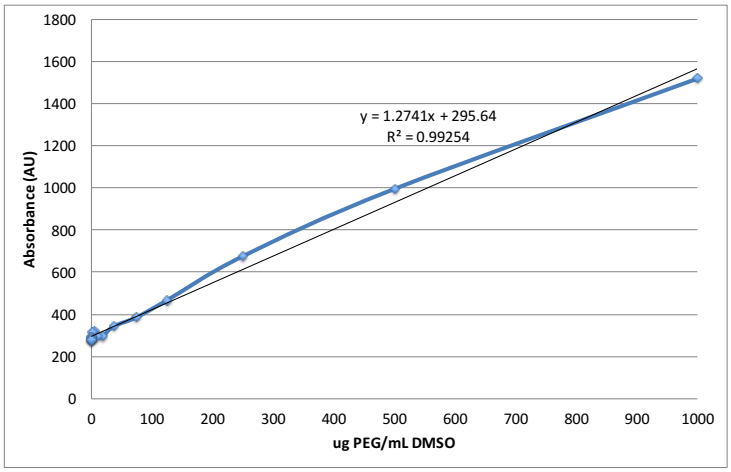

Figure A.1: Standard curve of CF-tagged LipidPEG in DMSO used to calculate loading efficiency. (n=3, error bars = SEAM, λ_{ex} = 495nm, , λ_{em} = 585nm, gain = 100).

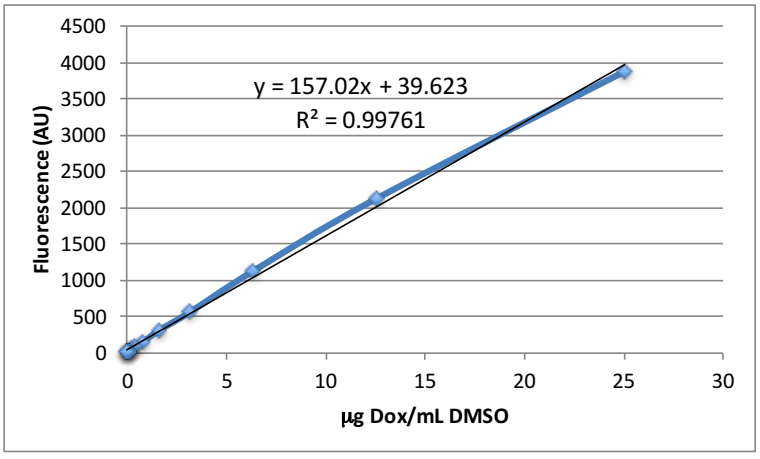

Figure A.2: Standard curve of Dox in DMSO used to calculate drug payload and encapsulation efficiency (n=3, error bars = SEAM, λ_{ex} = 495nm, λ_{em} = 585nm, gain = 100dB).

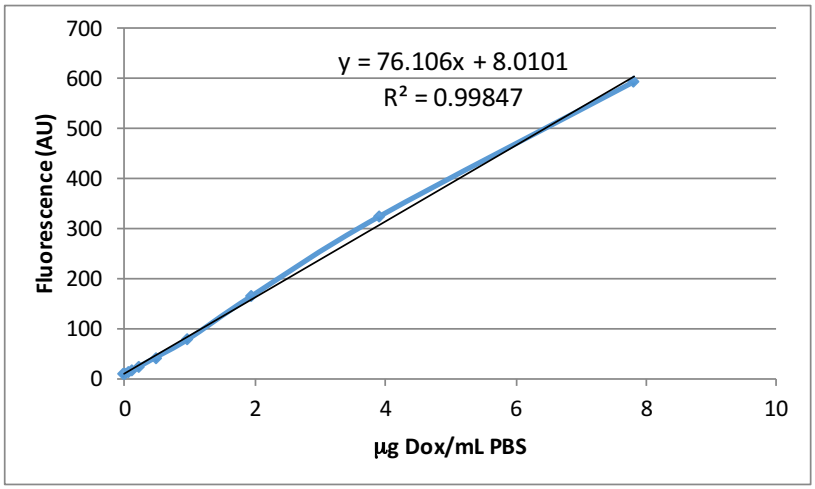

Figure A.3: Standard curve of Dox in PBS used to calculate drug burst and sustained release (n=3, error bars = SEAM, λ_{ex} = 495nm, λ_{em} = 585nm, gain = 100dB).

APPENDIX B: STANDARD OPERATING PROCEDURES

I. Protocol for Fabrication of PLA Ultrasound Contrast Agents

The following protocol is used to produce native PLA UCA. Preparing fresh microcapsules is essential for all studies and takes about three hours.

1. Weigh out the following chemicals: polymer (0.5g, record lot number as well), and porogens ammonium carbamate (0.78g) or ammonium carbonate (0.4g) and camphor (0.05g-if used)

    a. Note: Polymer should always be brought to room temp. before opening so that condensation does not form on the beads and cause degradation. For convenience you should take ~5g out of the stock solution and place it in a sealed vial in the freezer.

2. Combine the polymer and 10ml of methylene chloride in a beaker (40ml max volume) with a stir bar and stir on a magnetic stir plate, cover with a layer of wax paper topped by a layer of parafilm, until camphor and polymer are dissolved (~15min).

    a. Note: The ratio of polymer to solvent should is important. If the cover opens during stirring, some methylene chloride may evaporate. You should be careful, but if needed you can add more methylene chloride to bring the level to 10ml after stirring. Also, remember to wear gloves when using methylene chloride.

3. Combine porogen with 10ml of deionized water in a beaker (40ml max volume) with a stir bar and stir on a magnetic stir plate.

4. Measure out 50ml of 5% poly vinyl alcohol (PVA) and put it in a beaker (600ml max volume) and place it in the refrigerator.

5. Measure out 100ml of 2% isopropyl alcohol (IPA) and keep it in the graduated cylinder.

6. When the camphor and polymer are dissolved, remove stir bar and add 1ml of the porogen solution and sonicate with Misonix probe sonicator at 110W for 30 seconds. Sonicate in an ice bath 3 seconds on 1 second off.

7. After sonication, pour the solution into the cold PVA and homogenize with Brinkmann PT 3100 homogenizer with attached Polytron PT-DA 3020/2 generator for 5 minutes at 9,500 rpm.

8. After homogenization, pour the 100ml of IPA in the solution, add a larger stir bar, and stir on a magnetic stir plate (~375 setting) for 90 minutes. Make sure the vortex spans the diameter of the beaker so the solvent can fully evaporate.

    a. After homogenization remove the blade and pour the IPA over it into the beaker to prevent the loss of yield.

9. After 90 minutes, combine the solution in at least 4 centrifuge tubes (50ml max volume) and then centrifuge for 5 minutes at 5,000 rpm (the equivalent of approximately 5,000 g).

10. Decant the liquid and combine the microcapsules into 1 tube and recentrifuge for 5 minutes at 5,000 rpm.

11. Decant the liquid and wash the microcapsules three times with hexane. Lay the centrifuge tube under the hood and let excess solvent evaporate for about 20 min.

12. When the microcapsules appear to be thick and pasty, add DI water and recentrifuge for 5 minutes at 5,000 rpm.

13. Decant the water, mix (fluff) the microcapsules so they are mostly in solution, put a kimwipe on top of the tube with a rubber band, and flash freeze using nitrogen (swirling the tube in nitrogen to create a cone shaped pellet and increase exposed surface area for lyophilization).

14. Put the frozen microcapsules in a freeze dryer vessel and on the freeze dryer for at least 48 hours.

II. Protocol for Conducting Dose and Time Responses

The purpose of the dose response is to find the optimum dose where the ultrasound enhancement is the maximum. The purpose of a time response is to measure acoustic stability of the contrast agent. The time response should be done following a dose response at a dose less than the maximum dose.

For Dose Response

1. Weigh out 3mg of contrast agent and suspend it in 200µl of Phosphate Buffered Saline (PBS pH 7.4). This is your stock solution.
2. Fill the sample vessel with 100 ml of PBS and a small stir bar, turn on the oscilloscope and pulser, and focus the sample vessel.
3. For each dose, starting with 0.003mg/ml, inject 20µl of stock solution into the sample vessel and begin the LabView computer program.
4. Run the program.
5. For the next dose, 0.006mg/ml, inject another 20µl of stock solution into the sample vessel. Do not remove the original contents if this is a cumulative dose response.
6. Continue dose response up to 0.03mg/ml or until shadowing is evident.

Computer Operation for Dose Response

1. Create a folder with appropriate subfolders.
2. Open up the Main Ultrasound Program from LabVIEW and then open up the Main Ultrasound Program.vi.

3. Using the open file program, choose a directory path in which the data should be saved by opening the folder path, selecting which folder to save the data in, and hitting select current directory.

4. To begin taking the dose response, push the Run button.

5. When completed, to view the results, first under the Analyze Data tab, push Export Calculated Data and choose a folder to save the data to.

6. To view results, open up the dose data file using Excel and the enhancement in will be displayed for each dose in mV and dB.

For Time Response

1. Choose dose on the dose response curve that is not the maximum (it should be on the linear part of the curve) and prepare a solution of that concentration, using procedure described above in the dose response section.

2. Fill the sample vessel with 100 ml of PBS and a small stir bar, turn on the oscilloscope and pulser, and focus the sample vessel.

3. Inject dose into the sample vessel and begin the LabView computer program (Main Ultrasound Program.vi).

4. Run the program for 15 minutes.

    a. For n-Sh production screening, repeat this test at Energy Level 4, turning the energy level back down to 1 while each measurement is being taken.

Computer Operation for Time Response

1. Create a folder with appropriate subfolders.

2. Open up the Main Ultrasound Program from LabVIEW and then open up the Main Ultrasound Program.vi.

3. Using the open file program, choose a directory path in which the data should be saved by opening the folder path, selecting which folder to save the data in, and hitting select current directory.

4. To active Time Response, select button next to “Capture waveform on set time interval” and set the interval and number of time points to acquire.

5. Hit run button to begin Time Response.

6. To view the results when completed, go to the Analyze Data tab, select Export Calculated Data and choose a folder to save the data to.

7. To view results, open up the time data file using Excel and for each minute the enhancement will be given in mV and dB.

III: Protocol for Measuring UCA Size and Zeta Potential

The following protocol is used to measure size distributions and zeta potential of UCA in solution using a Malvern ZetaSizer Nano ZS. Size distribution is important in understanding an UCA size and safety, while zeta potential is useful in understanding the agent's surface charge and tendency to flocculate in suspension

1. Ensure Malvern ZetaSizer is connected to CPU via USB cable, turn machine on and open software program DTS (Nano)
2. Create a new data file by selecting 'File -> New Measurement File'
3. Suspend 1mL of dry agent in 1mL of solution (PBS for size measurements, DI water or a low ionic strength buffer for zeta potential measurements)

<u>For Size Measurements</u>

1. Pipette 1mL of suspended UCA solution into clear plastic rectangular Malvern cuvette
2. Select measurement protocol by selecting Measure-> SOPs -> Size-> PLA Microspheres
3. Click "Start" in protocol window
4. Data will be saved in data measurement file and can be exported using File -> Export
5. Size cuvettes can be reused between samples, but are disposable and should be thrown away after several days of use (or become cloudy)

For Zeta Potential Measurements

1. Pipette 1mL of suspended UCA solution into clear plastic Malvern Zeta Potential Capillary cuvette

2. Select measurement protocol by selecting Measure-> SOPs -> Zeta-> PLA Microspheres

3. Click “Start” in protocol window

4. Data will be saved in data measurement file and can be exported using File -> Export

5. Zeta potential capillaries are reusable and can be rinsed with DI water for future use

IV: Protocol for Counting UCA by Flow Cytometry

The following protocol is used to measure UCA population concentration by weight using an BD Biosciences Accuri C6 Flow Cytometer. Concentration is an important consideration when determining treatment amounts and drug loading.

Materials Needed

- 100uL and 1000uL pipettes and tips
- 100mL graduated cylinder
- 2mL Eppendorf tubes (rounded bottom)
- 2 250mL beakers
- plastic waste cup (for tips and tubes)
- CountBright absolute counting beads

    Bring to room temperature before use; keep lights off while using (light sensitive); note bead concentration and lot number from label on the bottle; shake the counting beads EVERY TIME before pipetting from the bottle

Procedure

1. Turn on the Accuri Flow Cytometer by pressing the button on the front of the machine
2. Open the CFlow Sample software on the computer
3. Select 24-tube rack as plate type
4. Eject the plate and add DI water to the tube in the A01 position
5. Name the A01 position “Wash” and adjust the settings for a 5 minute run at fast fluidics. Load the plate and press run

6. While the starting wash is running, fill each of the 2 beakers with 100mL DI water for sample preparation
7. Prepare the "Beads Only" control by adding 500µL DI water and 10µL counting beads to a 2mL Eppendorf tube. **BE SURE TO SHAKE THE BEADS WITH EACH USE**
8. After the wash is complete, eject the plate, and place the beads control tube in the A02 position. Select A02 and name the sample "Beads Only" then adjust the settings for a 2 minute run at medium fluidics. Load the plate and press run
9. When the run is complete, zoom in on the line formed by the beads on the scatter plot (top middle of graph). Use the rectangle tool to draw a box around the beads - this area will be called R1 and represents those items counted that are the counting beads. A CV-SSC-A of approximately 10% is good
10. Click wash when A02 is completed running and you have set the R1 area
11. Wash the tip by selecting A01 ("Wash") and adjusting the settings for a 1 minute run at fast fluidics
12. While the wash is running, prepare the sample by mixing 2mg bubbles with 100mL DI water in the 250mL beaker. Ensure that any clumps are broken up by pipetting up and down several times. Pipette 500µL of the bubble solution into a 2mL Eppendorf tube and add 10µL counting beads (shake the bottle first!), mix well by shaking. Repeat twice to test sample in triplicate
13. When the wash is complete, eject the plate. Shake the sample to ensure even distribution and load into position A03 in the plate. Select A03 and name the

sample, then adjust the settings for a 2 minute run at medium fluidics. Load the plate and press run

14. Record the data at the end of the run, noting both "All" and "R1" values. Use the counting formula to calculate the number of bubbles (see bottom of document)
15. Once data has been recorded, press wash
16. Once wash is complete, select A01 and adjust settings for a 1 minute run at fast fluidics. Press "Add to A01" (it will no longer say "Run")
17. Repeat steps 12-16 for each sample, choosing the new position on the plate for each new tube. MAKE SURE THE WASH TUBE (A01) DOES NOT RUN OUT OF DI WATER!!
18. Once all samples have been tested and washes have been run, complete another 5-minute wash with A01 (as explained in step 5)
19. At the conclusion of the wash, eject the plate and remove all samples except the wash tube in A01
20. Load the plate and press the power button on the front of the Flow Cytometer. Close the CFlow software and log out of the computer.

Bubble Counting Formula

For example, if the bottle label gives a bead concentration of 0.51×10^5 beads/50µL:

$$\frac{\#\ beads}{10\mu L} = \frac{0.51 \times 10^5}{5} = \frac{10{,}200\ beads}{10\mu L}$$

then

$$\frac{\#\ UCA}{mg} = \frac{\#\ beads}{10\mu L} \frac{(Total\ Count\ "All" - Bead\ Count\ "R1")}{Bead\ Count\ "R1"} \frac{2mg \times 0.05\mu L}{100mL}$$

V: Protocol for Maleimide Conjugation of TRAIL

For Ligation to UCA Surface

1. Weigh out 60mg of freeze dried UCA into a 50mL centrifuge tube
2. Suspend the UCA in 4mL of MES buffer (pH 5.2)
3. Separately, prepare the cross linkers into Eppendorf tubes: 14.86mg BMPH (25mM), 19.17mg EDC (50mM), and 12mg sulfo-NHS (0.6 ratio to EDC)
4. Add 1mL DI water to each Eppendorf tube (BMPH, EDC, and NHS), mix well, then add 1mL of each crosslinking solution to the centrifuge tube holding the UCA suspension ****For controls without crosslinkers, omit these agents****
5. Shake end-over-end at room temperature for 30 minutes
6. Centrifuge the solution for 5 minutes at 5000rpm, wash with 5mL PBS, centrifuge again for 5 minutes, wash again with 5mL PBS, and centrifuge again to collect pellet
7. Resuspend pellet in 2mL PBS
8. Add 1.2ug TRAIL to resuspended pellet
9. Shake end-over-end at room temperature for 90 minutes
10. Add 50uL thioglycolic acid (5mM)* to the solution to stop the reaction
11. Shake end-over-end at room temperature for 10 minutes
12. Centrifuge the solution for 5 minutes at 5000rpm, wash with 5mL PBS, centrifuge again, repeat 3x for 3 washes
13. Flash freeze pellet by swirling in liquid nitrogen, then lyophilize for 48 hours
14. Store at -20C with desiccant

For Ligation to Carboxy-capped LipidPEG Molecule

1. Weigh out 5mg of carboxy-capped LipidPEG into a 50mL centrifuge tube
2. Suspend the LipidPEG in 4mL of MES buffer (pH 5.2)
3. Separately, prepare the cross linkers into Eppendorf tubes: 95.85mg EDC and 60mg sulfo-NHS (0.6 ratio to EDC)
4. Add 5mL DI water to each Eppendorf tube (EDC and NHS), mix well, then add 1mL of each crosslinking solution to the centrifuge tube holding the UCA suspension ****For controls without crosslinkers, omit these agents****
5. Shake end-over-end at room temperature for 30 minutes
6. Add 6ug TRAIL to the solution
7. Shake end-over-end at room temperature for 90 minutes
    a. During the 90 minutes, prepare the dialysis tubing by cutting ~6 inches of tubing for each sample and soaking the sections in DI water for at least 20 minutes
8. Add 250uL thioglycolic acid (5mM)* to the solution to stop the reaction
9. Shake end-over-end at room temperature for 10 minutes
10. Pour resulting solution into prepared length of dialysis tubing with weighted clip in place at the bottom of the tubing
11. Secure the top clip, then float in 3-4L DI water on a stir plate for at least 6 hours, changing the water every 2 hours
12. Freeze dialyzed solution overnight, then lyophilize frozen solution for 48 hours
13. Store at -20C with desiccant

***To make 5mM thioglycolic acid: Add 34.9µL thioglycolic acid to 100mL DI water**

V: Protocol for Measurement of UCA Resonant Frequency

These measurements will help determine the resonance of the UCA, providing important information about the acoustic backscattering behavior and necessary US parameters for appropriate UCA evaluation.

Collection of Attenuation Data

1. Connect the power supply cable to the back of the Agilent Technologies oscilloscope
2. Connect the "Ch 1" and "Ext" cables to their respective outlets on the oscilloscope ("Ch 1" is yellow on the front, and "Ext" is on the back)
3. Change the transducer to the desired unfocused transducer (1, 2.25, 5, 7.5, or 10 MHz) and submerge it in the water tank
4. Fill the metal-plated sample holder with 250 mL of 1x PBS and place it into the water tank
5. Turn on the magnetic stirrer to ~3 setting
6. Align the transducer to be in the center of the acoustic window of the sample holder
7. Turn on the pulser-receiver and adjust the settings (pulse repetition frequency: 100Hz, gain: 0dB, energy level: 1, damping level: 3)
8. Turn on the oscilloscope
9. Turn on Channel 1 (yellow) by pressing its button, adjust the waveform (similar to initial adjustment for dose/time response curves), then turn off Channel 1 by pressing its button again

10. Press the “Math” function button to get the options at the bottom of the screen for span, center, etc.
11. Adjust the span and center frequencies for the transducer being used
    a. For 5 MHz transducer, Span: 10 MHz, Center: 5 MHz
    b. For 10 MHz transducers, Span: 20 MHz, Center 10 MHz
12. For all transducers, FFT(Ch1), Window Hanning, Scale 20bB, Offset -82.5dBV
13. Press the “Save” function button
14. Go to “Save” > “Settings” > “Length” and adjust recording length to 250, then press back
15. Plug in your USB drive to the USB port on the front of the oscilloscope and select “Save to” USB drive
16. Change your “File Name” to your preference (turn knob to change letter, press knob to select letter)
17. Press “Press to Save” to record your data as the baseline
18. Change file name to your preference for the sample you are testing
19. Add your sample to the sample holder (0.06mg/mL), wait 10-15 seconds for the sample to be mixed in the holder, and record your data (3x for triplicate readings)
20. Remove the sample holder from the tank, rinse with DI water, and fill with 250 mL of fresh 1x PBS.
21. Repeat steps 15-19 for each sample to be tested.

Other Oscilloscope Settings (should be the same, but for reference):

Trigger: Sweep Mode Auto, Coup DC, Noise Rej Off, HF Rej Off, Holdoff 40.0ns, Mode Edge, Source Ch 1, Slope Rising, Level 0.0V

Horizontal: Mode Normal, Ref Center, Main Scale 1.000us, Main Delay 140us

Acquisition: Mode Averaging, # Avgs 512, Realtime On, Vectors On, Persistence Off

Attenuation Data Processing

1. Enter all data into Excel to generate average values for all samples
2. Copy averaged values into OriginPro8 software (available for PC Only)
3. Plot attenuation, **α** (dB/cm) on the y-axis vs. frequency (MHz) on the x-axis
4. Right click on plot and choose "layer contents"
5. Click "Analysis" > "Signal Processing" > "Smoothing"
    a. Input = y-axis data
    b. Method = Savitzky-Golay
    c. Points of Window = 20
    d. Click OK, this generates new "smoothed" column
    e. Repeat for each set of averaged data
6. Click "Plot" > "Symbol" > "Scatter"
7. Only plot the range for the bandwidth of each transducer
    a. 2.73 - 4.27 MHz for 3.5 MHz transducer
    b. 2.7 - 7.2 MHz for 5 MHz transducer
    c. 6.7 - 13 MHz for 10 MHz transducer
    d. Determine these values from the Excel file

8. Right click on the line in the graph, click “Edit Range” and input cell numbers determined from Excel *must change each line individually*
9. Change x-axis to MHz
    a. Double click on axis
    b. Change tick labels
    c. Divide by factor 10^6 for MHz
10. Offset y-axis data to create a smooth graph from the 2 transducer data sets (5 and 10MHz)

VITA

Lauren Jablonowski was born March 25, 1988 in Laurel Springs, New Jersey. She received her Bachelor's and Master of Science in Biomedical Engineering from Drexel University in 2011, as part of the accelerated BS/MS program. As an undergraduate, she worked in the Implant Research Center, which is affiliated with both Drexel University School of Biomedical Engineering and Exponent, Inc., under the guidance of Dr. Steven Kurtz and Dr. Marla Steinbeck. Here, she focused on analysis of tissue samples retrieved from patients with failed joint implants, correlating inflammation and osteolysis to the presence of implant debris.

Following her undergraduate, she pursued her doctoral degree within the School of Biomedical Engineering at Drexel University. Under the guidance of Dr. Margaret Wheatley, she worked in the microencapsulation laboratory where she focused on using polymer ultrasound contrast agents for targeted drug delivery and cancer therapy.

While at Drexel, Lauren had the opportunity to present at various scientific symposiums with both poster and podium presentations, and received several awards including the Delaware Valley International Society of Pharmaceutical Engineers (ISPE) poster award, National Academies Ford Foundation Dissertation Fellowship honorable mention, Drexel Graduate College Teaching Excellence Award, and selection to the NIH Clinical Center's Clinical and Translational Research Course. She also received the Allied Scientist Research Grant from the Society of Interventional Radiology Foundation.

Outside of research, Lauren was involved in a variety of activities. She was President and Vice President of the Drexel Biomedical Graduate Association (DBGA), and volunteered with the FIRST robotics program at her local elementary school.